Characterization of CNP-induced cGMP signaling in the gastrointestinal tract and its role in colonic smooth muscle relaxation

Dissertation

der Mathematisch-Naturwissenschaftlichen Fakultät

der Eberhard Karls Universität Tübingen

zur Erlangung des Grades eines

Doktors der Naturwissenschaften

(Dr. rer. nat.)

vorgelegt von

Michael Simon Krämer

aus Nürtingen

Tübingen

2022

Gedruckt mit Genehmigung der Mathematisch-Naturwissenschaftlichen Fakultät der Eberhard Karls Universität Tübingen.

Tag der mündlichen Qualifikation:	12.05.2022
Dekan:	Prof. Dr. Thilo Stehle
1. Berichterstatter:	Prof. Dr. Robert Feil
2. Berichterstatter:	PD Dr. Hannes Schmidt

Table of contents

List of abbreviations

ACh	Acetylcholine
Acta2	Actin alpha 2
AF488	Alexa Fluor 488
AMDM	Acromesomelic dysplasia Maroteaux type
ANP	A-type natriuretic peptide
APS	Ammonium persulfate
αSMA	Alpha smooth muscle actin
ATP	Adenosine triphosphate
B220	Protein tyrosine phosphatase, receptor type, C
β3Tub	Beta 3 Tubulin
βGal	Beta Galactosidase
BK channel	Large conductance calcium-activated potassium channel
BNP	B-type natriuretic peptide
CaM	Calmodulin
cAMP	3'-5' cyclic adenosine monophosphate
CCh	Carbachol
CD3	Cluster of differentiation 3
CD31	Cluster of differentiation 31 (also: PECAM - platelet endothelial cell adhesion molecule)
CFP	Cyan fluorescent protein
cGi500	cGMP indicator with an EC50 of 500 nmol/L
cGKI	cGMP-dependent protein kinase type I
cGKII	cGMP-dependent protein kinase type II
cGMP	3'-5' cyclic guanosine monophosphate
ch	Chicken
c-kit	Tyrosine-protein kinase kit
CNP	C-type natriuretic peptide
Cre	Cyclization recombination (Cre recombinase)
$CreER^{T2}$	Cre recombinase – estrogen receptor T2
CSML	Circular smooth muscle layer
Cy3	Cyanine 3
DAPI	4,6-Diamidine-2-phenylindole
ddH_2O	Double-distilled water
DEA-NO	2-(N,N-Diethylamino)-diazenoate-2-oxide
DMEM	Dulbecco's modified eagle medium
DNA	Desoxyribonucleic acid
dNTP	Desoxynucleotide triphosphate
do	Donkey
EC50	Half maximal effective concentration
ECL	Enhanced chemiluminescence
EMN	Excitatory motor neurons
ENS	Enteric nervous system
ER	Endoplasmic reticulum
F12	Ham's F-12 nutrient medium
F4/80	EGF-like module-containing mucin-like hormone receptor-like 1 (EMR1)
FBS	Fetal bovine serum
FLC	Fibroblast-like cell
flox / floxed	Flanked by 2 loxP sites
FPLC	Fast protein liquid chromatography
FRET	Förster resonance energy transfer
Fwd	Forward
GAPDH	Glycerinaldehyd-3-phosphat-dehydrogenase
GC	Guanylyl cyclase
GC-A	Guanylyl cyclase A
GC-B	Guanylyl cyclase B
GC-C	Guanylyl cyclase C
GC-D/E/F	Guanylyl cyclase D/E/F
GFAP	Glial fibrillary acidic protein
GFP	Green fluorescent protein
GI	Gastrointestinal
GIT	Gastrointestinal tract
go	Goat
HA	Haemaglutinin
HRP	Horse-radish peroxidase
HuC/D	ELAV-like protein 3 (HuC) and ELAV-like protein 4 (HuD)
ICC	Interstitial cell of Cajal
IF	Immunofluorescence
IFM	Isometric force measurement
IP_3	Inositol triphosphate
IP_3R	Inositol triphosphate receptor
IPAN	Intrinsic primary afferent neuron
IRAG	IP_3R-associated cGMP kinase substrate
K_D	Dissociation constant
KO	Knock-out
LEC	Lymphatic ECs
LOF	Loss-of-function
LSM	Laser scanning microscope
LSML	Longitudinal smooth muscle layer
Lyz	Lysozyme
M	Mesenteries
mcGi500	Membrane-tethered cGMP indicator with an EC50 of 500 nmol/L
MLCK	Myosin light chain kinase
MLCP	Myosin light chain phosphatase
MLN	Mesenteric lymph nodes
MMC	Migrating myoelectric complex
mo	Mouse
MP	Myenteric plexus

MP-IPAN	Myenteric plexus-localized intrinsic primary afferent neuron
NA	Not available
NEP	Neprilysin
NFR	Nuclear fast red
NGS	Normal goat serum
NLS	Nuclear localization sequence
nNOS	Neuronal nitric oxide synthase
NO	Nitric oxide
NO-GC	Nitric oxide-sensitive guanylyl cyclase
NOS	Nitric oxide synthase
NP	Natriuretic peptide
Nppc	Natriuretic peptide precursor C
Npr1	Natriuretic peptide receptor 1
Npr2	Natriuretic peptide receptor 2
Npr3	Natriuretic peptide receptor 3
PBS	Phosphate buffered saline
PCR	Polymerase chain reaction
PDE	Phosphodiesterase
PDGFRα	Platelet-derived growth factor receptor alpha
PFA	Paraformaldehyde
pGC	Particulate guanylyl cyclase
PGP9.5	Protein gene product 9.5
PK	Proteinase K
PLC	Phospholipase C
PMSF	Phenylmethylsulfonylfluoride
PNS	Parasympathetic nervous system
PVDF	Polyvinylidene fluoride
R26	ROSA26 (reverse oriented splice acceptor, clone 26)
rb	Rabbit
Rev	Reverse
RFP	Red fluorescent protein
ROI	Region of interest
RPM	Rounds per minute
RT	Room temperature
rt	Rat
S	Serosa
SDS-PAGE	Sodium dodecyl sulfate polyacrylamide gel electrophoresis
SE / SEM	Standard error of the mean
SK channel	Small conductance calcium-activated potassium channels
SMC	Smooth muscle cell
SML	Smooth muscle layer
SNS	Sympathetic nervous system
SP	Submucosal plexus
SP-IPAN	Submucosal plexus-localized intrinsic primary afferent neuron
Taq	*Thermophilus aquaticus*
TBS	Tris-buffered saline
TBS-T	Tris-buffered saline with Tween-20
TEMED	Tetramethyl ethylene diamine
TG / tg	Transgene
TLR	Toll-like receptor
TTX	Tetrodotoxin
UV	Ultra violet
VDCC	Voltage-gate calcium channel
vim	Vimentin
WB	Western blot
Wnt1 /Wnt11	Wingless-type MMTV integration site 1
WT	Wildtype
Xgal	5-bromo-4-chloro-3-indolyl-β-$_D$-galactoside
YFP	Yellow fluorescent protein

Abstract

Background: The 3'-5' cyclic guanosine monophosphate (cGMP) signaling pathway is known to regulate gastrointestinal (GI) functions like water and electrolyte secretion of GI epithelial cells and relaxation of the GI smooth muscle layer. Guanylyl cyclase B (GC-B), which generates cGMP upon binding of the C-type natriuretic peptide (CNP), has previously been shown to mediate smooth muscle relaxation in pylorus and colon. Furthermore, GC-B loss-of-function (LOF) mutation mice have been reported to suffer from pyloric stenosis and GI obstruction in ileum, cecum, and colon. However, the cell types mediating this smooth muscle-relaxing effect of CNP and the obstruction phenotype of GC-B LOF mutation mice have not been identified yet.

Aim: This study seeks to discover the cellular identity of CNP and GC-B expressing cells in the GI tract and investigates the role of CNP-induced cGMP signaling in colonic motility.

Materials and Methods: Global GC-B knock-out (KO) mice were generated to investigate GI dysfunction. Whole mount Xgal staining of GI segments from *lacZ* reporter mice was performed to identify regions with CNP and GC-B gene transcription. Immunofluorescence double staining was used to identify the involved cell types. Western blot was used to confirm GC-B expression. The colon of mice, expressing the cGMP biosensor cGi500 in neurons or smooth muscle cells (SMCs), was used to measure cGMP generation in response to CNP. Isometric force measurements were employed to investigate colonic contraction patterns in response to CNP with and without Tetrodotoxin.

Results: Young GC-B KO mice (<P20) showed a distension phenotype at the ileal-cecal-colonic region of the GI tract. A high number of *CNP* transcribing cells was found in esophagus, pylorus, small intestine, and large intestine. A high number of *GC-B* transcribing cells was found in esophagus, pylorus, ileum, large intestine, and mesenteric lymph nodes (MLN). The expression of GC-B was confirmed at the protein level in esophagus, pylorus, ileum, colon, and MLN. Regarding cell types, *CNP* transcription was observed in Paneth cells of the small intestine and *GC-B* transcription in lymphatic endothelial cells of the MLN. In colon, *CNP* and *GC-B* were both transcribed in nitrergic neurons of the mature enteric nervous system (ENS) and *GC-B* transcription was also found in SMCs. Colonic neurons and SMCs showed a CNP-induced elevation of intracellular cGMP levels *in vitro*. In CNP-stimulated SMCs, cGMP was degraded by the phosphodiesterases (PDEs) 2A and 5. Dose-response curves, assessing the colon circular smooth muscle relaxing effect of CNP, revealed an EC50 of about 15 nM CNP. The distal

colon showed a stronger reduction of the contraction amplitude than the proximal colon at higher concentrations of CNP (≥ 50 nM CNP). The application of 100 nM and 250 nM CNP led to complete relaxation of the distal colon from wildtype (WT) mice, whereas the distal colon from global GC-B KO mice did not respond to CNP. Interestingly, the distal colon from neuron-specific GC-B KO mice displayed a CNP-induced smooth muscle relaxation which was not significantly different from WT. The distal colon from SMC-specific GC-B KO mice, in turn, responded similar to the global GC-B KO and significantly different from WT.

Conclusion: *CNP* and *GC-B* are both transcribed by nitrergic neurons of the mature ENS in colon and *GC-B* is also transcribed in colonic SMCs. The GC-B that is expressed in distal colon SMCs, but not the GC-B on nitrergic neurons, leads to colonic circular smooth muscle relaxation in response to CNP. Upon CNP stimulation, colonic SMCs generate cGMP that is degraded by PDE2A and PDE5. These results imply that the CNP/GC-B/cGMP signaling pathway contributes to the tonic inhibition of the circular smooth muscle layer in distal colon.

Zusammenfassung

Hintergrund: Im Gastrointestinaltrakt (GIT) reguliert der Signalweg des cyclischen Guanosin-3‘,5‘-monophosphates (cGMP) die Wasser und Elektrolytsekretion in Epithelzellen, sowie die Relaxation der glatten Muskulatur. Vorhergehende Studien haben gezeigt, dass das C-Typ natriuretische Peptid (CNP), welches cGMP-Bildung durch die Guanylylzyklase B (GC-B) hervorruft, eine Glattmuskelrelaxation im Pylorus und Kolon auslöst. Weiterhin leiden Mäuse mit einer GC-B „loss-of-function“-Mutation unter einer Pylorusstenose und einem aufgeblähten Ileum, Coecum und Kolon. Jedoch sind die Zelltypen, welche diesen Glattmuskel relaxierenden Effekt von CNP sowie den Blähbauchphänotyp auslösen, noch nicht bekannt.

Ziel der Arbeit: Das Ziel dieser Arbeit ist es, die CNP- und GC-B-exprimierenden Zellen im GIT zu identifizieren und die Bedeutung der CNP-induzierten cGMP Signaltransduktion für die Kolonmotilität aufzuklären.

Material und Methoden: Es wurden globale GC-B Knockout (KO) Mäuse generiert, um potentielle Fehlfunktionen des GITs zu untersuchen. Die Transkription von *CNP* und *GC-B* in gastrointestinalen (GI) Segmenten wurde mittels Xgal Färbungen von *lacZ* Reportermäusen untersucht. Die *CNP*- und *GC-B*-transkribierenden Zelltypen wurden mithilfe von Immunfluoreszenz Doppelfärbungen identifiziert und die Expression von GC-B im Western Blot bestätigt. Die CNP-stimulierte Bildung von cGMP konnte, mithilfe von Mäusen die einen cGMP-Biosensor spezifisch in Glattmuskelzellen und Neuronen exprimieren, *in vitro* untersucht werden. Ferner wurden isometrische Kraftmessungen durchgeführt, um den Einfluss von CNP auf das Kontraktionsmuster von Kolonabschnitten, in der An- und Abwesenheit von Tetrodotoxin, zu untersuchen.

Ergebnisse: Bei jungen GC-B KO Mäusen (<P20) wurde ein Blähbauchphänotyp beobachtet, welcher mit dem Ileum, Coecum und Kolon assoziiert war. Eine hohe Anzahl *CNP* transkribierender Zellen wurde im Oesophagus, Pylorus, Dünndarm und Dickdarm gefunden. *GC-B* transkribierende Zellen dahingegen, wurden in hoher Anzahl im Oesophagus, Pylorus, Ileum, Dickdarm und den mesenterialen Lymphknoten (MLN) gefunden. Auf Proteinebene konnte die Expression von GC-B im Oesophagus, Pylorus, Ileum, Kolon und den MLN bestätigt werden. Identifiziert wurden folgende Zelltypen: Im Dünndarm transkribierten Paneth Zellen *CNP* und im MLN transkribierten lymphatische Endothelzellen *GC-B*. Im Kolon hingegen transkribierten nitrerge Neuronen des adulten enterischen Nervensystems (ENS) beide Gene (*CNP* und *GC-B*), während

Glattmuskelzellen nur *GC-B* transkribierten. Die durch CNP stimulierte, intrazelluläre Biosynthese von cGMP, wurde *in vitro* in beiden Zelltypen gezeigt. In Glattmuskelzellen wurde das dadurch gebildete cGMP durch die Phosphodiesterasen (PDE) 2A und 5 abgebaut. Dosis-Wirkungs-Kurven haben gezeigt, dass die CNP vermittelte Relaxation der glatten Muskulatur des Kolons konzentrationsabhängig ist (EC50 = 15 nM CNP). Bei Konzentrationen von ≥ 50 nM CNP zeigte die glatte Muskulatur des distalen Kolons eine stärkere Reduktion der Kontraktionsamplitude, als die glatte Muskulatur des proximalen Kolons. Interessanterweise führten 100 nM und 250 nM CNP, im distalen Kolon von Wildtyp (WT) Mäusen, zu vollständiger Relaxation der zirkularen glatten Muskulatur, währen dieselben CNP Konzentrationen im distalen Kolon von globalen GC-B KO Mäusen zu keinerlei Reaktion führten. Darüber hinaus relaxierte das distale Kolon von Neuronen-spezifischen GC-B KO Mäusen in gleichem Maße wie das distale Kolon von WT Mäusen. Der Glattmuskelzell-spezifische GC-B KO dahingegen, verhielt sich ähnlich wie der globale GC-B KO, aber signifikant verschieden vom WT.

Schlussfolgerung: Im Kolon werden *CNP* und *GC-B* von nitrergen Neuronen des adulten ENS transkribiert und GC-B darüber hinaus auch von Glattmuskelzellen. Das von Glattmuskelzellen exprimierte GC-B, aber nicht das GC-B in nitrergen Neuronen, vermittelt den relaxierenden Effekt von CNP auf die zirkuläre Glattmuskelschicht des Kolons. Des Weiteren stimuliert CNP auch die Bildung von cGMP in Glattmuskelzellen des Kolons. Dieses cGMP wird von PDE2A und PDE5 abgebaut. Die Ergebnisse dieser Arbeit implizieren, dass der CNP/GC-B/cGMP Signalweg zur basalen Hemmung der zirkulären Glattmuskelschicht des distalen Kolons beiträgt.

1. Introduction

Seeking to understand and influence physiological processes in health and pathogenesis is a fundamental motivation of live science researchers all around the world. To protect human life, mammalian physiology and behavior is investigated in small animals like mice or other rodents. Working with mice, as a mammalian model organism, provides many advantages such as easy and cheap housing, a short generation time (21 days pregnancy, 56 days until sexual maturity), and a broad toolbox of already existing genetically modified mice. This toolbox of transgenic mice contains reporter mice, which allow the detection of target protein expressing cells in their physiological and histological context, as well as knock-out (KO) mice that resemble disease models such as, for instance, dwarfism. The more conserved a signaling pathway is, the more likely it is to translate conclusions drawn from the respective mouse models to the corresponding human disease. As an example, a form of human dwarfism, the acromesomelic dysplasia type Maroteaux (AMDM), is a skeletal achondrodysplasia which affects 1 out of 1 000 000 people worldwide. These patients have short limbs due to a growth inhibition in long bones which is linked to a loss-of-function (LOF) mutation in the guanylyl cyclase B (GC-B; gene name: *natriuretic peptide receptor 2*, abbr.: *Npr2*) gene [6]. Global GC-B KO mice, which do not express a functional version of this gene, develop the same dwarfism phenotype as humans [141]. Research on those mice led to a deeper understanding of AMDM and the development of new drugs like Vosoritide which is a GC-B agonist that can help patients suffering from even the predominating form of human dwarfism: achondrodysplasia (1 out of 27 500 people) [11]. Intensive research on GC-B, unveiled its role in a great variety of physiological processes such as dwarfism [141], female fertility [4], axon bifurcation [122], and homeostasis of arterial blood pressure [134]. But, research about its role in the gastrointestinal tract (GIT) has not yet been conclusive and is the main objective of this thesis.

1.1. The gastrointestinal tract

Food digestion and nutrient absorption are the most vital processes in animal survival. The GIT supplies the organism with nutrients like carbohydrates, fats, amino acids, nucleotides, vitamins, dietary fibers, water, and electrolytes. Unprocessed food like plants or meat has to be broken down from nutrient polymers (e.g. polysaccharides, proteins, fats or DNA), in a complex arrangement of cells and tissue (e.g. cells embedded in an extracellular matrix), into nutrient monomers (e.g. monosaccharides, amino acids, fatty acids, phosphates and nucleobases) which can be taken up by the organism [56]. To facilitate this complicated

process, the GIT is subdivided into multiple specialized segments (**Figure 1 A**). The small intestine consists of the duodenum, jejunum, and ileum, whereas the large intestine harbors the colon and rectum. The different segments of the digestive tube, from the esophagus to the anal sphincter, all share a common microanatomy (**Figure 1 B**).

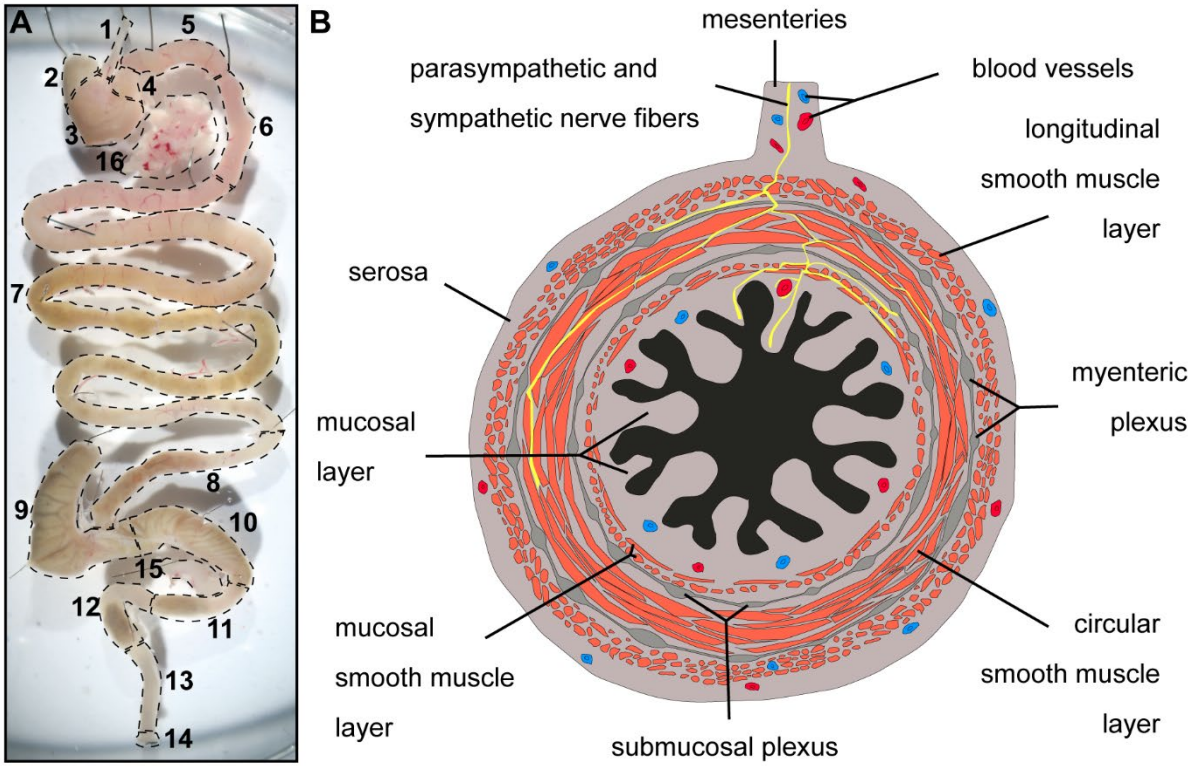

Figure 1: Segments of the GIT and their common microanatomy.

A) Specialized segments of the GIT: 1) esophagus, 2) forestomach, 3) glandular stomach, 4) pylorus, 5) proximal duodenum, 6) distal duodenum, 7) jejunum, 8) ileum, 9) cecum, 10) proximal colon (ascending colon in human), 11) median colon (transverse colon in human), 12) distal colon (descending colon in human), 13) rectum, 14) anal sphincter, 15) mesenteric lymph nodes, 16) mesenteries with pancreas. B) Common microanatomy of the digestive tube. The outermost layer is the serosa which is a combination of connective tissue, blood vessel, and the mesothelium (a thin squamous epithelial layer). Surrounding the digestive tube, the serosa fuses together on each side forming a supporting structure, the mesenteries. This structure holds the tube in place and supplies the other layers with aortic and venous blood vessels, lymphatic vessels as well as sympathetic and parasympathetic nerve fibers. The longitudinal and circular smooth muscle layers are spatially separated by the myenteric plexus which harbors neurons of the enteric nervous system. The endings of these neurons project deep into the two muscle layers which are arranged orthogonally to each other. Hence, they allow for complex movement patterns of the digestive tube. The endings of neurons from the submucosal plexus majorly project within the mucosal layer, herein, regulating a variety of processes like secretion, absorption, and the motility of a thin mucosal smooth muscle layer. The mucosal layer is the most changing of all layers. Morphology and cellular composition are different in the esophagus, stomach, small and large intestine. It consists of connective tissue, fibroblasts, and a columnar epithelial cell layer that is attached to a basal lamina. The mucosal layer is supplied with blood and lymphatic vessels, but also nerve endings from the submucosal plexus, the myenteric plexus, the sympathetic and parasympathetic nervous system.

1.1.1. Digestion, absorption, feces formation and defecation

Digestion starts already in the mouth where the teeth grind the food into small pieces and enrich the so formed food bolus with saliva. Enzymes present in the saliva (e.g. α-amylase) start digesting nutrient polymers in the mouth already. In the next step, the food bolus is

swallowed and travels through the esophagus into the stomach. The esophagus, hereby, serves as transport pipe with a lower esophageal sphincter that prevents the stomach contents from spilling back into the esophagus. The stomach of mice is split into the forestomach, the glandular stomach, and the pylorus. While the function of the forestomach is mainly the mixing of the stomach content, the glandular stomach secretes gastric juice which contains hydrochloric acid and acidic digestion enzymes. As soon as the food bolus is mixed with the gastric juice, it is called chyme. The pH of the chyme is typically between 1.5 to 2. The stomach is connected to the duodenum through the pyloric valve which gates the chyme into the duodenum in a process called gastric emptying. In this process, the pyloric antrum engulfs a small proportion of the chyme and releases it, through the now opened pyloric sphincter, into the duodenum. The gastric emptying rate is dependent on the viscosity and digestion state of the chyme which are sensed in the pylorus itself and the duodenum [56].

At next, in the duodenum, segmentation movements mix the chyme mechanically with juice from the pancreas and the gall bladder. The pancreatic juice contains alkaline digestion enzymes like glucosidases, proteases, lipases, and nucleases, but also bicarbonate to neutralize the acidic pH of the chyme. Bile juice, in turn, contains bile acids (steroid acids like cholic acid), phospholipids, cholesterol and other substances that aid in emulsifying the fatty component of the chyme [48]. After thorough mixing, the chyme is transported further aboral from the duodenum into the jejunum and ileum where the nutrient oligo- and monomers are then absorbed through epithelial enterocytes (**Figure 2**). Occasional segmentation movements, along the small intestine, triturate accumulated chyme adducts and distribute them over a larger area. After passing the ileum, the remaining chyme only contains a small amount of nutrients which are further processed by bacteria in the large intestine. To separate the small from the large intestine, the ileo-cecal sphincter gates the chyme into the next segment [56].

The cecum is the major place of microbial digestion. In this process, bacteria brake down the undigested parts of the chyme. Degradation products of bile acids like bilirubin make up for the characteristic brown color of the feces. Some bacteria even produce vitamins like vitamin K which are then taken up by the epithelial cells. The proximal colon, with its large mucosal folds, removes most water and electrolytes from the feces and enriches it with mucin instead. The mucin protects the epithelial layer from bacteria, glues together the fecal content, and colonic mass movements, in the transition zone between the proximal and median colon, then form fecal pellets. In addition, mucin also lubricates the epithelial surface

of the median colon, distal colon, and rectum, allowing for an unhindered transport of the fecal pellets towards the anal sphincter. Fecal pellets can be temporarily stored in the distal colon and rectum until a defecation reflex is provoked. During defecation the anal sphincter circular smooth muscle tone is weakened and peristaltic waves, which migrate through the rectum, push the fecal pellet outside [56].

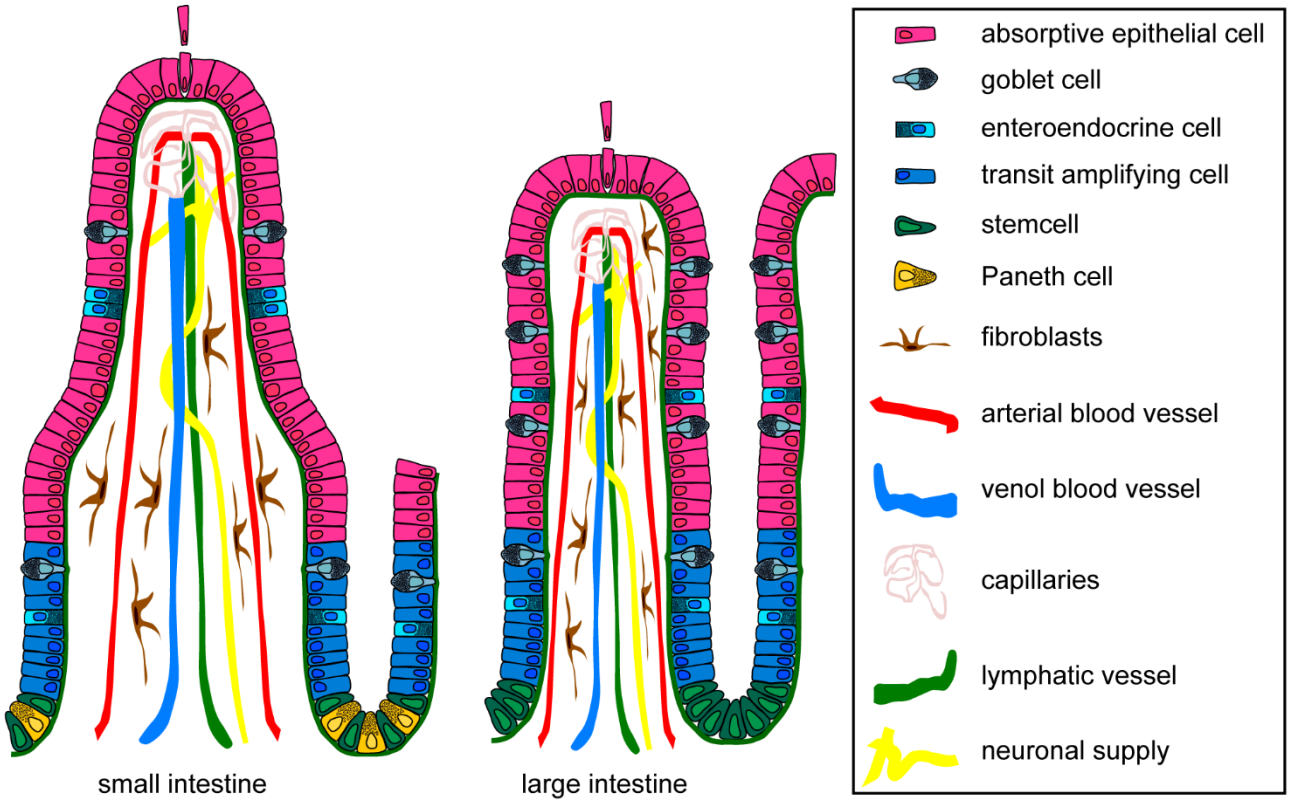

Figure 2: Microanatomy of the mucosal layer in small and large intestine.

The small intestinal mucosal layer consists of villi, microvilli and mucosal folds that enlarge the luminal surface drastically to about 1.3 m² in mice. In contrast, the large intestinal mucosal layer is only grooved with mucus producing crypts and, therefore, the luminal surface area amounts for 0.11 m² [19]. The large luminal surface area in small intestine is necessary for optimal nutrient absorption. Stem cells located at the crypt base differentiate into two cell types: Paneth cells (only in small intestine) reside at the crypt base, whereas the transit amplifying cells travel upwards out of the crypt. The Paneth cells are interspersed between the stem cells at the crypt base maintaining the small intestinal stem cell niche and secreting antimicrobial peptides [24]. Transit amplifying cells form a proliferation zone in which the epithelial cells proliferate and differentiate into mature epithelial cells. Most abundant are absorptive epithelial cells (enterocytes) which take up nutrients and secrete water and electrolytes [49, 125]. Goblet cells, which are more abundant in large intestine, secrete mucus and bicarbonate, while enteroendocrine cells regulate various functions of the mucosal layer. Maintenance of the epithelial layer is achieved by constant replacement of epithelial cells through cells from the proliferation zone leading to complete epithelial renewal within 4-7 days [49]. At the point where two epithelial layers meet (tip of a villus in small intestine and the point between two crypts in large intestine), the epithelial cells are shredded and released into the lumen of the intestine where they are digested themselves. The mucosa between two crypts harbors fibroblasts, blood and lymphatic vessels which transport blood and interstitial liquids back and forth, as well as neurons and neuronal projections which allow for communication with the enteric, sympathetic and parasympathetic nervous system. Adapted from [49, 125].

1.1.2. Surveillance of the microbiome: Paneth cells

To ensure that bacteria cannot compete with the host organism for the nutrient monomers, several defense mechanisms keep the number of bacteria low in the small intestine. These are the acidity in the stomach, the bile juice, Peyer patches, gastrointestinal (GI) motility, and Paneth cells [89].

The bile juice consists of agents which prevent the chyme from forming big aggregates and provide a hostile environment for bacteria. Peyer Patches, which are primarily localized in the ileum, are lymphatic organs that interact with bacteria and mediate an adapted immune response. They are connected with the mesenteric lymph node (MLN) through lymphatic vessels of the mesenteries. The MLN collects the lymph juice from the whole GIT, thereby, distributing the adaptive immune response, elicited at a specific GI segment, to the rest of the GIT. In addition to direct antipathogenic actions, complex movement patterns of the GIT also prevent bacteria from remaining in the small intestine. Peristaltic waves, which go through the small intestine even in absence of luminal content, constantly transport bacteria into the aboral direction (towards the large intestine). This mechanism is especially important in the ileum to keep bacteria away from the jejunum [56, 89].

Paneth cells have first been reported by Joseph Paneth in 1887. They are located between the stem cells at the crypts of Lieberkühn in the small intestine. Their two main functions are the maintenance of the stem cell niche and the secretion of antimicrobial peptides like lysozyme or defensins (e.g. defensinα6). The antimicrobial peptides are stored in large intracellular vesicles and are released into the lumen in response to different, endogenous and exogenous, stimuli like interstitial acetylcholine (ACh) release from neurons or the luminal presence of bacterial cell surface products like lipopolysaccharide. Paneth cells protect the small intestine from pathogens and help to shape the composition of the microbiome. A pathologic absence or malfunction of Paneth cells can lead to severe diseases like inflammatory bowel disease (colonization and attack of the mucosal layer by pathologic bacteria). In addition, Paneth cells provide essential signals for the stem cell niche. Without Paneth cells, the stem cells discontinue to maintain their function. In healthy individuals, Paneth cells are only found in small intestine, however, Paneth cells have also been found in the stomach and colon as metaplastic response to mucosal inflammation [24].

1.1.3. Internal sphincters and motility patterns

GI motility patterns control the movement of luminal content throughout the GIT, from the esophagus to the anus. These motility patterns are performed by the orthogonally arranged longitudinal and circular smooth muscle layers (LSML and CSML). Circumferential contraction of the CSML can close the luminal space completely. This is how GI sphincters separate the lumen of one GI segment from another one. The GIT has three permanent sphincters. The lower esophageal sphincter prevents chyme from spilling back to the esophagus, the pyloric sphincter separates the stomach from the duodenum and the ileo-cecal sphincter prevents content from the large intestine to enter the small intestine (**Figure 3 A & B**). Longitudinal contraction of the LSML, in turn, is used to shorten a GI segment. The combination of CSML and LSML contractions can, thereby, either lead to the development of a segmentation movement or a peristaltic wave (**Figure 3 C & D**) [56].

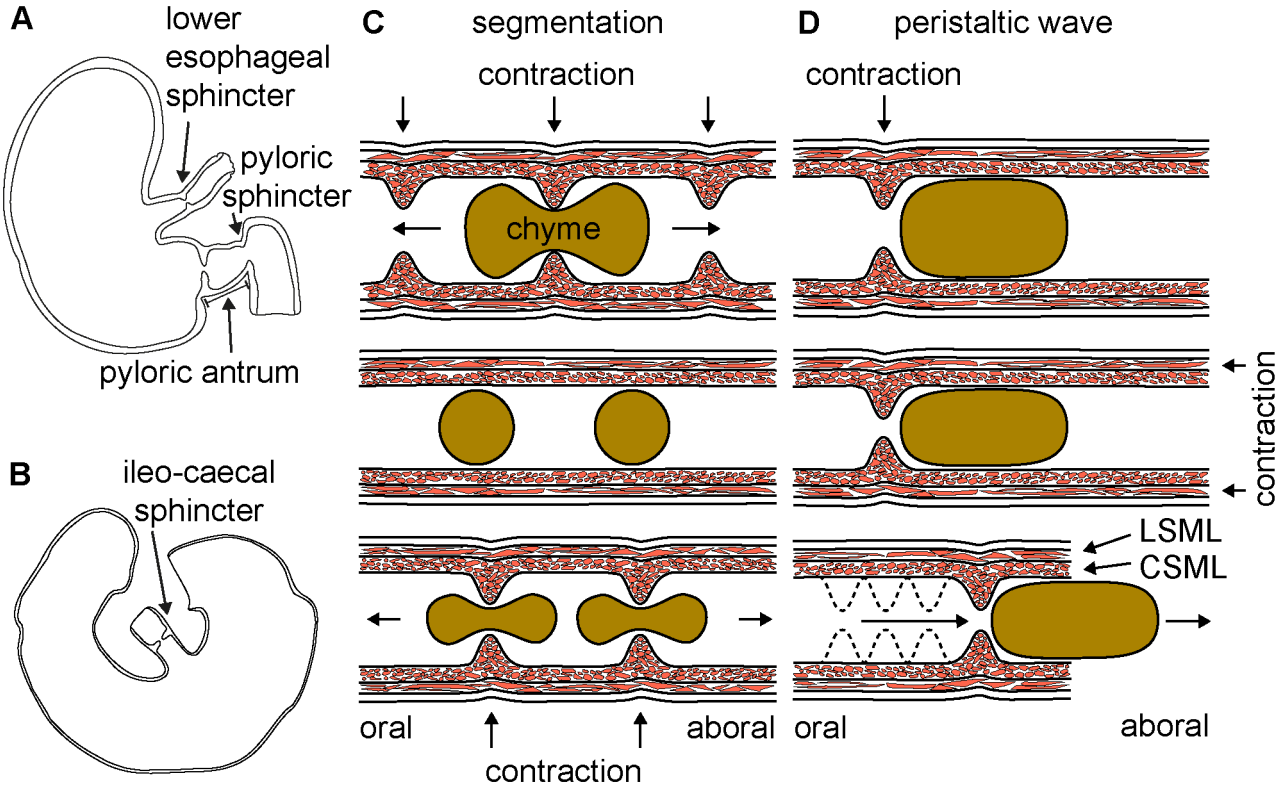

Figure 3: GI sphincters and motility patterns.

A) Position of the lower esophageal sphincter and the pyloric sphincter in stomach. B) Cecum with highlighted ileo-cecal sphincter. C) Segmentation movements are mainly found in the small intestine and proximal colon. Synchronized CSML and LSML contractions occur in regularly interspaced distances, thereby, grinding the chyme into smaller parts and distributing it over a large surface area. This allows a greater interaction of the chyme with the epithelial cells. D) In peristaltic waves, ascending interneurons mediate a CSML contraction and LSML relaxation, whereas descending interneurons mediate CSML relaxation and LSML contraction. This leads to a blocked passage in the oral direction which pushes the GI content into the aboral direction. Peristaltic waves are found throughout the whole GIT, transporting the chyme from the esophagus to the anus. Abbr.: circular smooth muscle layer (CSML), longitudinal smooth muscle layer (LSML).

The time between ingestion and first excretion of the food bolus is called gastrointestinal transit time. Peristaltic waves push the luminal content into the aboral direction and directly influence the transit time. In adult mice, the food bolus enters the stomach within seconds or minutes. Mixing of the food with stomach secretions results in chyme that stays in the stomach for several hours. Already 10 minutes after entering the stomach, small pieces of the chyme are gated into the small intestine. It can take up to 8 hours until the stomach is completely emptied. Despite the length of the small intestine, the chyme travels through it within 1 hour (30-60 minutes). The large intestine, in turn, is the part of the GIT where feces are located the longest time from 1 hour up to 8 hours. This sums up to a total gastrointestinal transit time of about 2-3 hours on average in adult mice [40, 99, 101].

Coordination of these complex motility patterns is performed by the enteric nervous system (ENS) which is one part of the functional syncytium of the smooth muscle layers (SML).

1.1.4. Innervation and motility control

The GIT is controlled by the ENS, parasympathetic nervous system (PNS) and the sympathetic nervous system (SNS). The PNS and SNS connect different GI segments with each other and stimulate (PNS) or inhibit (SNS) GI activity. The ENS, in turn, senses local stimuli (e.g. luminal content, stretch or inflammation) and elicits nerve reflexes within a GI region. The neuronal cell bodies of ENS neurons are located within the myenteric plexus (MP; **Figure 4 A**: neuron type 1-10) and the submucosal plexus (SP; **Figure 4 A**: neuron type 11-13), and project their axons and dendrites (harboring nerve varicosities) into the LSML and CSML (MP neurons), as well as the mucosal layer (mainly SP neurons). Thereby, MP neurons coordinate GI motility patterns, whereas SP neurons coordinate secretion, absorption, and blood supply of the mucosal layer [42]. The neuron composition of the ENS changes slightly from GI segment to segment. Therefore, this part of the introduction focuses on the different neuron types present in small and large intestine.

Overall, there are 13 neuron types which are differentiated by the location of their cell body (**Figure 4 A**: MP or SP), their primary and secondary neurotransmitters (**Table 1**), and their function in the ENS. Their activation state is characterized by the membrane potential and cytosolic Ca^{2+} levels. Elevated Ca^{2+} levels in the soma elicit a wave of membrane depolarization which propagates along neuronal projections as action potential. Reaching dendrites and neuroeffector junctions (varicosities), the action potential elevates cytosolic Ca^{2+} levels again leading to the release of neurotransmitters. Many different signaling pathways and neurotransmitters influence the activation state of enteric neurons. The major

excitatory neurotransmitter is ACh, whereas inhibitory neurotransmitters range from small molecules like nitric oxide (NO) and adenosine triphosphate (ATP), to signaling peptides like enkephalins and the vasoactive intestinal polypeptide (**Table 1**) [42].

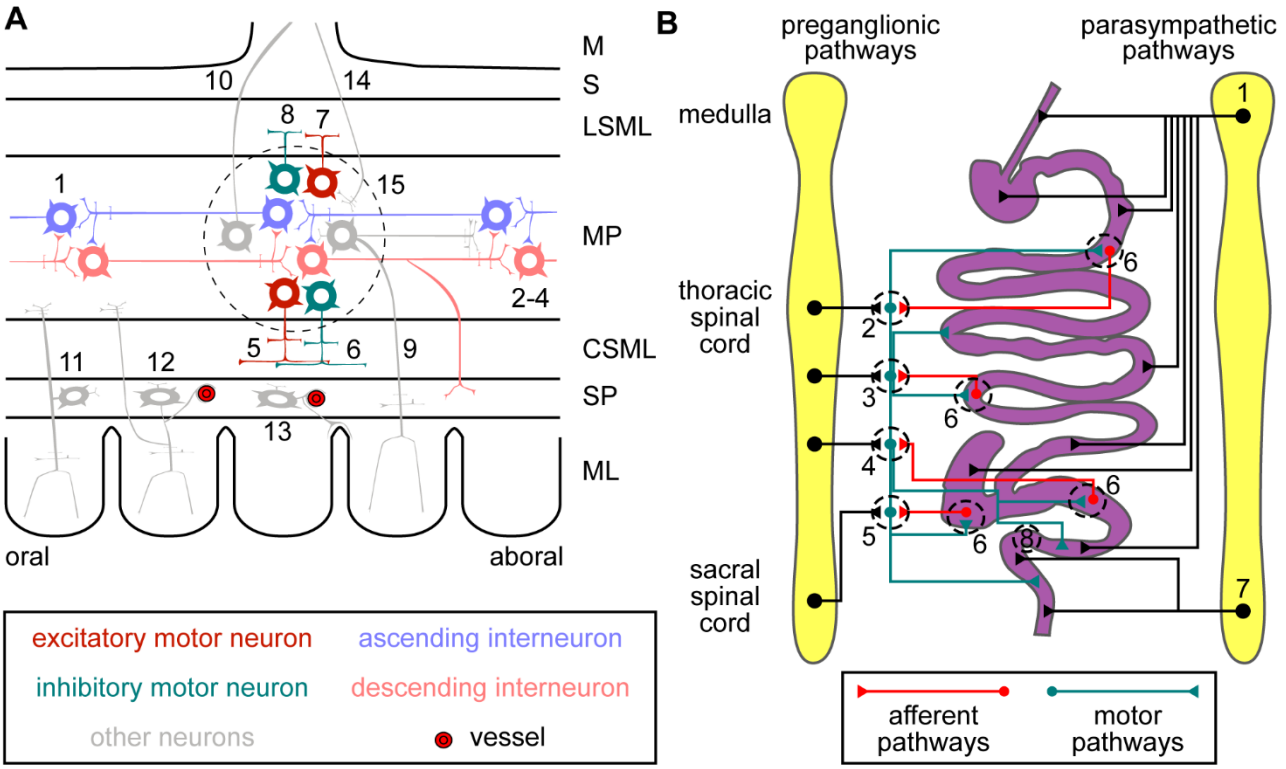

Figure 4: The ENS and extrinsic GI innervation.

A) Different neuron cell types of the ENS located in the MP and SP. Neurons in the MP are arranged in ganglia where the different neuron cell types are interconnected and form neuronal networks (15). The neurons of the MP are: Ascending interneurons transmitting local reflexes (1; 5 % of MP neurons). Descending interneurons transmitting local reflexes (2; 5 % of MP neurons). Descending interneurons transmitting secretomotor reflexes (3; 2 % of MP neurons). Descending interneurons transmitting the migrating myoelectric complex (4; 4 % of MP neurons). Excitatory circular smooth muscle motor neurons (5; 12 % of MP neurons) and inhibitory circular smooth muscle motor neurons (6; 16 % of MP neurons). Excitatory longitudinal smooth muscle motor neurons (7; 25 % of MP neurons) and inhibitory longitudinal smooth muscle motor neurons (8; 2 % of MP neurons). Myenteric intrinsic primary afferent neurons (MP-IPAN, 9; 26 % of MP neurons). Intestinofugal neurons which project to prevertebrate ganglia (10; < 1 % of MP neurons). The neurons of the SP are: Submucosal intrinsic primary afferent neurons (SP-IPAN, 11; 11 % of SP neurons). Cholinergic secretomotor / vasodilator neurons (12; 15 % of SP neurons). Non-cholinergic secretomotor / vasodilator neurons (13; 45 % of SP neurons). Ascending and descending interneurons communicate signals between MP ganglia which then elicit circular and longitudinal smooth muscle contraction (via excitatory motor neurons) or relaxation (via inhibitory motor neurons). In addition, nerve endings from PNS and SNS neurons (14) also contribute to ENS signaling. Abbr.: Mesenteries (M), serosa (S), longitudinal smooth muscle layer (LSML), myenteric plexus (MP), circular smooth muscle layer (CSML), submucosal plexus (SP) and mucosal layer (ML). Adapted from [42]. B) Extrinsic innervation of the GIT through the vagus nerve (1) and pelvic nerve (7) of the PNS, sympathetic nerve fibers from dorsal root ganglion neurons (2-4) and prevertebrate ganglia (2-5). Vagal nodose afferent pathways transmit signals from the esophagus and stomach to the spinal cord and elicit stomach motility responses through dorsomotor vagal efferent motor neurons (1). Coeliac ganglia (2), the superior mesenteric ganglion (3), and inferior mesenteric ganglion (4) interconnect afferent pathways and motor pathways from the GIT with sympathetic nerve fibers and the pelvic ganglia (5). Afferent pelvic nerve fibers sense stimuli from the rectum and the anal sphincter, and mediate a response via pelvic afferent nerve fibers to the pelvic ganglia (7). Intestinofugal afferent neurons (6) project into prevertebrate ganglia. This allows for fast communication between different segments of the GIT. The transition zone between vagal and pelvic innervation is called the Cannon-Böhm point (8). Adapted from [133, 142].

The two types of secretomotor / vasodilator neurons of the SP (**Figure 4 A**: neuron type 12 & 13) control the secretion and absorption of nutrients, water ,and electrolytes, as well as the constriction/dilation of vessels in the mucosal layer [42]. Their activity is coordinated by an active communication between the epithelial cells, the underlaying fibroblasts [45], signals from MP neurons and extrinsic nerve fibers [44].

The other 11 neurons are involved in sensing local stimuli (IPANs and interneurons) and transmitting those stimuli, via an action potential, to other neurons (interneurons and intestinofugal neurons) which then elicit a motility response (motor neurons).

A local stimulus can be luminal/circular smooth muscle stretch or the luminal chyme composition/viscosity. This is sensed by intrinsic primary afferent neurons (IPAN; **Figure 4 A**: neuron type 9 & 11) and interneurons (**Figure 4 A**: neuron type 1-4). Both integrate their activation state into the local ENS ganglion. The excitability of that ganglion then defines whether the signal from IPANs and interneurons leads to an activation of the ganglion neurons or not [42-44]. Ganglion excitability, which is the membrane polarization state of the neurons, is influenced by nerve endings from the PNS increasing excitability, nerve endings from the SNS inhibiting excitability, and IPANs/interneurons which mediate both. The activation of an excitable ganglion then leads to synchronized membrane depolarization, hence, activation of all neurons present (**Figure 4 A**: possible composition of an ENS ganglion). One of these neurons are the intestinofugal neurons (**Figure 4 A**: neuron type 10) that themselves project to prevertebral ganglia and integrate the activating signal into the SNS and PNS (**Figure 4 B**: ganglia 2-5). Other neurons in the activated ganglion are excitatory and inhibitory motor neurons which project with their axons and dendrites (containing nerve varicosities) into the CSML and LSML (**Figure 4 A**: neuron type 5-8). The release of excitatory (e.g. ACh) and inhibitory (e.g. NO) neurotransmitters (**Table 1**) from those motor neurons, in turn, excites/inhibits SMCs leading to a local smooth muscle contraction/relaxation. Inhibitory motor neurons (**Figure 4 A**: neuron type 7-8) are constitutively active, thereby, releasing inhibitory neurotransmitters. This process is called tonic inhibition and aims at the suppression of uncoordinated motility patterns [32]. Excitatory motor neurons of one ENS ganglion usually do not project to the whole circumference of the GI tube. Hence, complete contraction of the CSML requires the synchronized activation of multiple ganglia. This is achieved by interneurons which transmit the activation state of one ENS ganglion to adjacent ganglia around the GI tube as well as in the oral and aboral direction. In this way a chain reaction of activated neurons is triggered,

traveling through multiple ganglia (around the circumference and along the GI tube) as a so-called migrating myoelectric complex (MMC).

Table 1: Neuron types of the ENS, their neurotransmitters and marker proteins.

# in figure 5 A	neuron type	primary neurotransmitter	secondary neurotransmitter / modulator	other markers	neuron population in SCS
1	ascending interneuron	ACh	TK, ATP	Calretinin, ENK	PIN1-3 [31], ENC6,12 [88]
2	descending interneuron (local reflex)	ACh, ATP	-	nNOS, VIP	PIN1-3 [31], ENC10-11 [88]
3	descending interneuron (secretomotor reflex)	ACh	5-HT, ATP	-	PIN1-3 [31], ENC7 [88]
4	descending interneuron (MMC)	ACh	-	SOM	PIN1-3 [31], ENC5 [88]
5 & 7	excitatory motor neurons	ACh	TK, ENK	Calretinin,	PEMN1-5 [31], ENC1-4 [88]
6 & 8	inhibitory motor neurons	NO	VIP, ATP	PACAP, CART [88]	PIMN1-7 [31], ENC8-9 [88]
9 &11	IPAN (MP-IPAN & SP-IPAN)	ACh, CGRP, TK	-	Calbindin, Calretinin	PSN1-4 [31], ENC12 [88]
10	intestinofugal neurons	ACh	VIP	CCk	PSN3 [31], ENC7 [88]
12	cholinergic secretomotor	ACh	-	Calretinin	PSVN1-2 [31]
13	non-cholinergic secretomotor	VIP	PACAP	NPY	PSVN1-2 [31]
14	sympathetic neurons (motility inhibition)	NorAd	-	NPY	-
14	sympathetic neurons (secretion inhibition)	NorAd	SOM	-	-
14	sympathetic neurons (vasoconstriction)	NorAd, ATP	NPY	-	-
14	parasympathetic neurons	ACh	CCK	-	-

Footnote: Typical excitatory neurotransmitters are acetylcholine (ACh; marker protein: choline acetyltransferase - ChAT), serotonin (5-HT) and tachykinin (TK), cholecystokinin (CCk). Typical inhibitory neurotransmitters are NO (marker protein: nNOS), vasoactive intestinal polypeptide (VIP), adenosine triphosphate (ATP), pituitary adenylate cyclase-activating polypeptide (PACAP), enkephalin (ENK), calcitonin gene-related peptide (CGRP), somatostatin (SOM) and Noradrenaline (NorAd). The neuron types of this table were correlated with neuron types identified in recently published single cell mRNA studies (SCS). Other abbr.: putative interneuron (PIN), enteric neuron class (ENC), putative excitatory motor neuron (PEMN), putative inhibitory motor neuron (PIMN), putative sensory neuron (PSN) and putative secretomotor vasodilatory neuron (PSVN). Table was adapted from [43].

The distance the MMC can migrate through the ENS (i.e. from a few millimeters up to centimeters) is again depending on the individual ganglion excitability. Synchronized activation of multiple adjacent ganglia also activates excitatory motor neurons (**Figure 4 A**: neuron type 5-6). The here through coordinated release of neurotransmitters from all involved excitatory motor neurons at once leads to a coordinated and complete

circumferential contraction of the CSML (also called “spike burst”). In this way the MMC elicits a wave of CSML contraction on its way along the GI tube which can be observed as a segmentation movement or peristaltic wave [132].

Extrinsic innervation of the GIT via the PNS and SNS are depicted in **Figure 4 B**. The SNS delivers its inhibitory influence to the small and large intestine via prevertebral ganglia (**Figure 4 B**: 2-5). Vagal innervation ranges from the esophagus to the end of the median colon (**Figure 4 B**: 1). Pelvic innervation covers the distal colon, rectum, and anal sphincter (**Figure 4 B**: 7). The Cannon-Böhm point marks the transition zone between the median and distal colon (**Figure 4 B**: 8) where Vagal innervation stops and Pelvic innervation starts [18, 133]. In addition, there is also a change in sympathetic motor innervation from the inferior mesenteric ganglion (**Figure 4 B**: 4) to pelvic ganglia (**Figure 4 B**: 5) [133]. Due to those changes in innervation, high smooth muscle tension and luminal narrowing are frequently observed at the Cannon-Böhm point [85].

Communication of different GI segments via sympathetic and parasympathetic pathways are described as reflexes. Three different reflexes are discussed here: the gastro-colonic reflex, the duodenal-colonic reflex, and the defecation reflex. The gastro-colonic reflex is initiated by mechanical stretch of the stomach, whereas the duodenal-colonic reflex is sensed in the duodenum by stretch and luminal content. As a result of both reflexes, the colonic sympathetic inhibitory signals are dampened and parasympathetic excitatory signals elicit a peristaltic wave that pushes the fecal pellet towards the rectum. A filled rectum then triggers the defecation reflex simply via luminal stretch. During defecation, the anal sphincter circular smooth muscle tone is weakened and a peristaltic wave pushes the fecal pellet through the anal sphincter out of the GI tube [44, 56, 82].

1.1.5. The functional smooth muscle syncytium in colonic motility

The functional syncytium of the GI smooth muscle describes all cells directly involved in the coordinated contraction of the SMLs. It consists of motor neurons from the ENS which project into the CSML and LSML. Those projections are axons, dendrites, and varicosities which are intertwined with smooth muscle cells (SMC), interstitial cells of Cajal (ICC) and fibroblast-like cells (FLC). Similar to neurons of the ENS, the activation state of these cells is characterized by their membrane polarity and the cytosolic Ca^{2+} levels. SMCs contract in response to membrane depolarization which also leads to an increase in cytosolic Ca^{2+} levels. SMC relaxation, in turn, is triggered upon membrane repolarization and hyperpolarization which leads to a lowering of cytosolic Ca^{2+} levels. The ICCs and FLCs

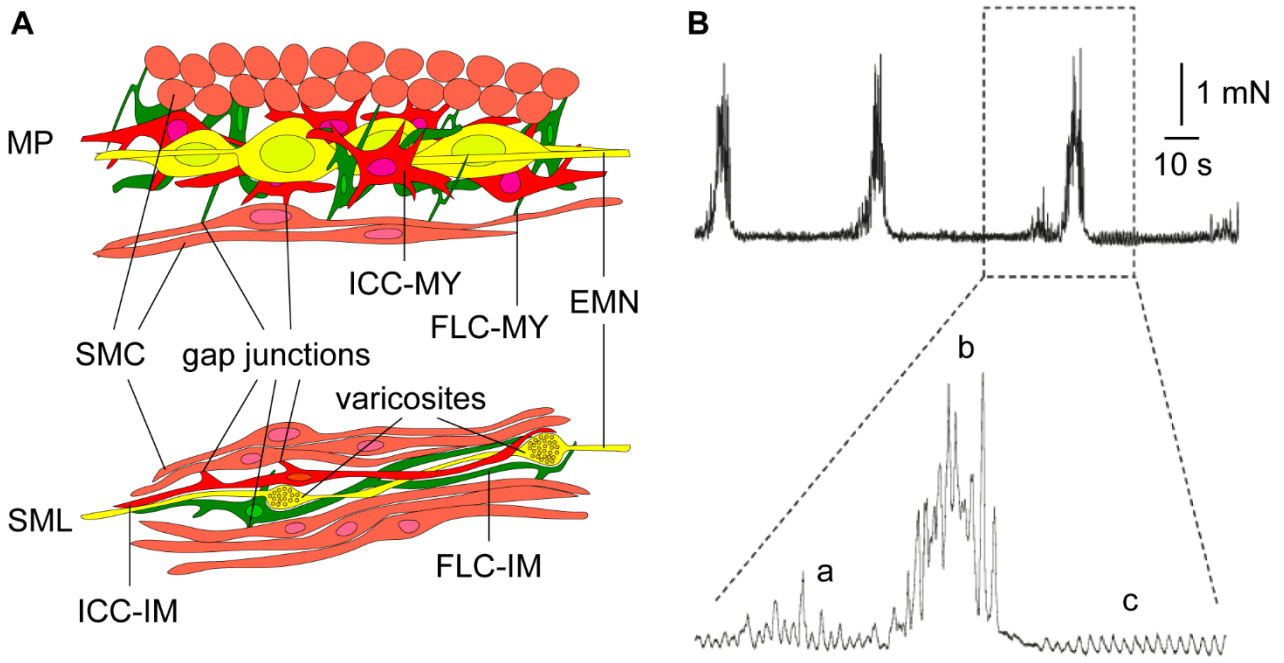

Figure 5: Functional syncytium of the MP/SML and composition of colonic contraction patterns.

A) The functional syncytium of the MP/SML consists of motor neurons, smooth muscle cells (SMC), interstitial cells of Cajal (ICC) and fibroblast-like cells (FLC). Motor neurons release neurotransmitters, which act on the other cell types. ICCs and FLCs are electrically coupled to SMCs via gap junctions that can transmit the membrane polarity. Thereby, ICCs and FLCs aid SMCs in membrane depolarization and repolarization, which allows for a rhythmic contraction pattern. ICCs and FLCs are further distinguished by their localization within the tissue. In the MP they are termed ICC-MY and FLC-MY whereas in the SML they are termed ICC-IM and FLC-IM respectively. Abbr.: Myenteric plexus (MP), smooth muscle layer (SML), enteric motor neuron (EMN), myentericus (MY), intramuscular (IM). Adapted from [115]. B) Contraction pattern of the colon CSML recorded by isometric force measurements *ex vivo* on colonic rings. The upper part shows regularly occurring contractions, which are under control of the ENS. The magnified area shows the three contraction patterns observed, the slow phasic contractions (a), the long-lasting large contractions (b) and the small high-frequency ripples. Adapted from [7].

are electrically coupled to SMCs via gap junctions. This means that they can conduct their membrane potential onto SMCs and, thereby, aid with membrane depolarization, repolarization, and hyperpolarization. ICCs are the pacemaker cells of the GIT. They form large networks along the MP, CSML, and LSML (**Figure 5**). The ICC-MY are intertwined with the ENS ganglion neurons and assist in propagating MMCs, whereas ICC-IM assist the SMCs with contraction and subsequent relaxation. SMC membrane repolarization has not been observed in mice lacking ICCs. Therefore, ICCs are suspected to assist SMCs in repolarization and hyperpolarization of the plasma membrane. ICCs exhibit a pacemaker activity which is characterized by a spontaneously occurring membrane depolarization that lasts from one to several seconds and ends with membrane repolarization. This so-called “slow wave” happens every few seconds in a highly coordinated rhythmic pattern. ICCs conduct the slow wave membrane polarity rhythm onto SMCs and, thereby, cause a rhythmic colonic contraction pattern [115]. Tonic inhibition, which is mediated by inhibitory

motor neurons, constantly suppresses the slow wave-induced rhythmic colonic contraction pattern. In colon, tonic inhibition is mediated primarily by NO, but also ATP [32]. The slow wave-induced rhythmic colonic contraction pattern can be observed as slow phasic contractions (**Figure 5 B**: a) which are present right before a long-lasting large contraction occurs (**Figure 5 B**: b). Directly after long-lasting large contractions, when the SMC membranes re-and hyperpolarize, small high-frequency ripples (**Figure 5 B**: c), which are of so far unknown origin, occur [7]. The exact function of FLCs in colonic contraction pattern generation has not been clarified yet, but it is suspected that FLCs transduce their membrane polarity onto SMCs in response to neurotransmitters (e.g. ATP) which are not known to act via ICCs [75]. The signaling pathways leading to SMC contraction and relaxation in colon are depicted in **Figure 6**.

The composition of the functional syncytium changes between different GI segments. The proximal colon is characterized by a higher density of ICCs and nitrergic neurons, but also fewer FLCs. This leads to a stronger nitrergic neurotransmission. The median and distal colon, in turn, harbor a higher density of FLCs, but less ICCs and nitrergic neurons, leading to stronger purinergic neurotransmission [80, 83]. With respect to contraction patterns, the slow phasic contractions, which originate from ICCs, are primarily observed in the proximal colon. The median and distal colon mainly exhibit long lasting large contractions [7, 80]. *Ex vivo* contraction measurements of the murine colon revealed two different types of MMCs. The first one propagates along the entire colon (complete MMCs), resulting in a continuous peristaltic wave that pushes fecal pellets towards the rectum. The second one is restricted to the proximal colon (incomplete MMC) and characterized by multiple, intermediate action potentials which yield in slow phasic contractions [26]. This matches with the function of the proximal colon where water and electrolyte absorption from the feces requires the distribution of the feces over the whole luminal surface area. The incomplete MMCs, which can be imagined as a type of segmentation movement, distribute the luminal content within the proximal colon. Complete MMCs, in turn, do not require slow phasic contractions in between the long-lasting large contractions, because the previously formed fecal pellets are not supposed to be distributed over a large surface area. Instead fecal pellets stay in a pellet-like shape and are stored or excreted whenever required [56].

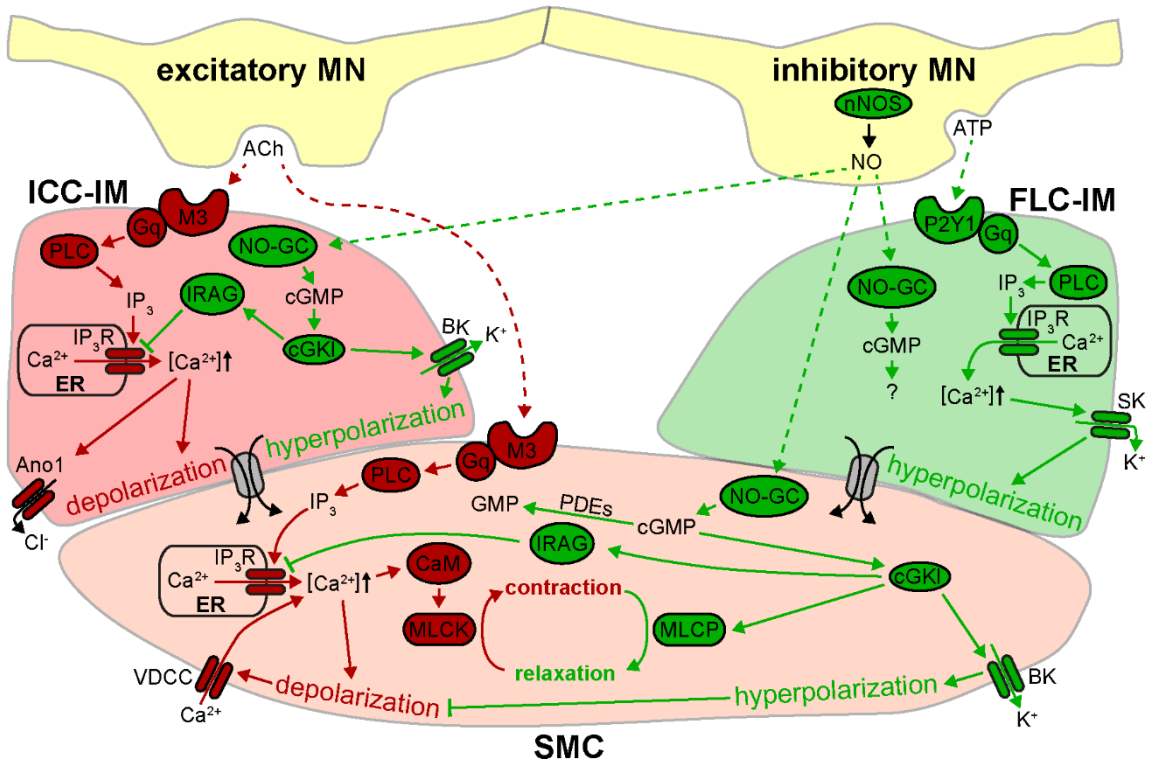

Figure 6: Schematic depiction of signaling pathways leading to colonic smooth muscle contraction and relaxation.

Excitatory motor neurons (excitatory MN) are activated by coordinated ENS activation and release ACh. ACh binds to the G-protein coupled muscarinic M3 receptor on ICC-IM and SMCs. The M3 receptor releases the $G_{\alpha q}$ subunit (Gq) and, thereby, activates the membrane bound beta-type phospholipase C (PLC). PLC, in turn, hydrolyzes phosphatidylinositol 4,5-bisphosphate to diacylglycerol and inositol trisphosphate (IP_3). IP_3, which is released into the cytosol, then activates the IP_3-receptor (IP_3R) which is a specialized Ca^{2+} channel in the membrane of the endoplasmic reticulum (ER). The subsequent increase in cytosolic Ca^{2+} leads to membrane depolarization. ICCs and FLCs, which are electrically coupled to SMCs, transmit their membrane potential onto SMCs, whereas the increased Ca^{2+} levels in SMCs itself lead to the opening of L-type voltage-dependent calcium channels (VDCC). VDCCs then allow for an influx of additional Ca^{2+}. Ca^{2+} associates with calmodulin (CaM) which then increases the myosin light chain kinase (MLCK) activity. This leads to SMC contraction. Reestablishment of the ICC-IM membrane potential is achieved using anoctamin-1 (Ano1) which is voltage-gated calcium-activated Cl^- channel. In contrast, the SMC relaxing signaling pathway is mediated via NO and ATP. NO binds to NO-GC in ICCs, SMCs and FLCs where 3'-5' cyclic guanosine monophosphate (cGMP) is generated. Subsequent activation of cGKI in ICCs and SMCs then activates the IP_3R-associated cGMP kinase substrate (IRAG) which in turn inhibits the IP_3R Ca^{2+} channel. This action blocks the efflux of Ca^{2+} from the ER and, thereby, prevents further depolarization of the cell membrane. In addition, large conductance calcium-activated potassium channels (BK), which are activated as soon as cytosolic Ca^{2+} levels reach a threshold, are phosphorylated by cGKI. This enhances the BK channel activity and leads to faster re-and hyperpolarization. In SMCs, cGKI also enhances the activity of the myosin light chain phosphatase (MLCP) which in turn leads to SMC relaxation. The cGMP is then degraded to guanosine monophosphate (GMP) by phosphodiesterases (PDEs) in SMCs. The hyperpolarized state of the ICC and SMC membrane is sustained by NO during tonic inhibition. FLCs are also hyperpolarized in this process, but rather by ATP than NO. FLCs, which express the G_{qa}-protein coupled P2Y1 ATP-receptor, also display a cytosolic increase in Ca^{2+} levels upon ATP binding. In contrast to ICCs and SMCs, FLCs express the small conductance calcium-activated potassium channels (SK channel) which are already activated at small increases of cytosolic Ca^{2+} levels. The SK channels then transport K^+ across the cell membrane to the extracellular space. Hence, leading to hyperpolarization of the FLC membrane. This hyperpolarization state is again conducted onto SMCs. Although SMCs also express the P2Y1 receptor membrane hyperpolarization, in response to ATP or other purines, was only observed on FLCs. Adapted from [7, 32, 33, 46, 75, 78, 114].

1.1.6. Development and maturation

The digestive system in juvenile mice is specialized on mother's milk which consists of sugars (e.g. lactose), fats, proteins, and electrolytes. All components are completely digestible and allow for optimal energy transmission from the mother to the pup. In consequence, mother's milk does not contain fibers like the food of adult mice [3, 144]. Thus, juvenile mice, which are still nursed, have another requirement for GI motility than adult mice. Lactose, which is cleaved by lactase (a βGal) into D-glucose and D-galactose, serves as glucose source. Lactase is expressed from duodenal and jejunal epithelial cells until weaning [69, 71, 102].

Although GI SMCs and the extrinsic innervation are present and functioning at birth, the ENS and glia cell network are not fully developed. Neurons of the ENS and glia cells mature until postnatal day 10 to 14 (P10-14) and glia cells expand even afterwards. Mature contraction patterns (including complete MMCs) and, thereby, full development of the ENS is observed between P10-14. Before that time, immature motility patterns take over rudimentary actions like segmentation movements and small, local peristaltic waves. Complete MMCs that propagate the chime from the beginning to the end of the colon are not observed in newborn mice until P10-14 [14, 142].

1.1.7. Pathology

The susceptibility for GI diseases changes during the lifetime and is dependent on general health, nutrition, and genetic prevalence. One of those diseases is chronic constipation in which defecation occurs three times less frequent as in healthy individuals over a long-time of up to 6 months in humans. It is caused by chronically narrowed or even constricted areas of the large intestine that block feces from moving further aboral (like at the Cannon-Böhm point [85]). In consequence, the bacteria continue to ferment the feces. Hence, gas is generated and distends the large intestine. Depending on the gas permeability of the constricted area this either leads to flatulence or a chronically inflated GIT [10]. Besides nutrient and health related issues, genetic prevalence can also cause constipation. In Hirschsprung disease, parts of the large intestine are not innervated by the ENS. These parts do not experience tonic inhibition of the SMLs which then results in chronically narrowed or constricted areas. In consequence, some patients develop a megacolon in which the colon is continuously filled with feces and expands drastically in size. In the final stages of megacolon, only surgical removal of the feces from the colon can save the patient from death by intestinal perforation [68].

1.2. The cGMP signaling pathway

The second messenger molecules, 3'-5' cyclic guanosine monophosphate (cGMP) and 3'-5' cyclic adenosine monophosphate (cAMP), are very important signaling molecules in mammals. Processes regulated by cGMP can be as diverse as phototransduction, cell growth and differentiation, axon bifurcation, homeostasis of arterial blood pressure, the secretion of water and electrolytes, and the relaxation of vascular and gastrointestinal SMCs [74, 118, 123], while cAMP signaling is involved in gene transcription, insulin secretion, glycogenolysis, and lipolysis [76, 116, 127]. Both pathways can be regulating the same

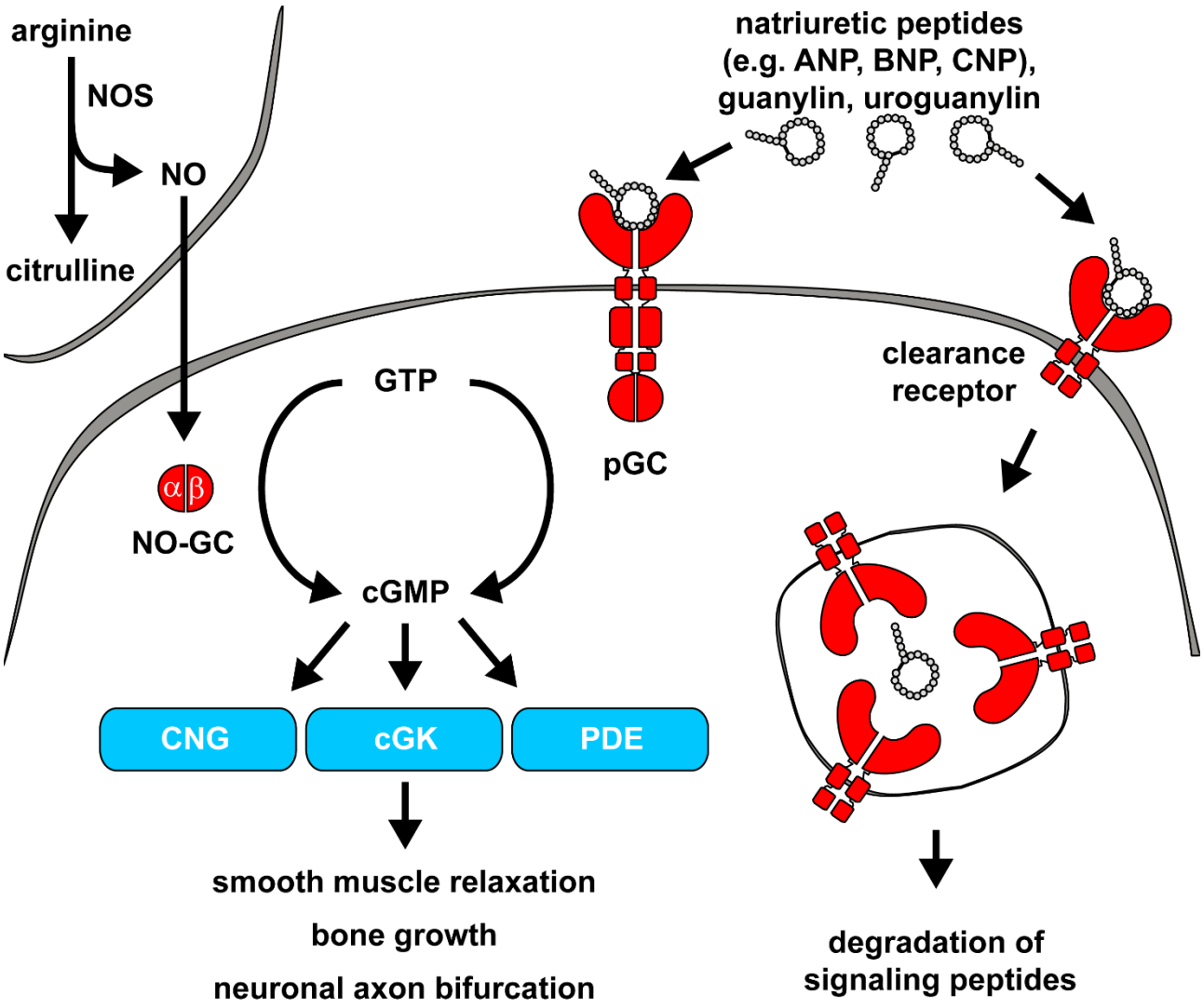

Figure 7: Components of the cGMP signaling pathway.

Inducer molecules like NO (generator: NO-GC), natriuretic peptides (generator: pGCs like GC-A and GC-B), guanylin and uroguanylin (generator: pGCs like GC-C and GC-D) activate the respective cGMP generating enzyme. NOS catalyzes the reaction from arginine to citrulline, thereby, releasing gaseous NO. The liberated NO travels through cells and their cell membranes to the target cell. Other inducer molecules, which are primarily peptide hormones like natriuretic peptides, guanylin or uroguanylin, are secreted by the cell of origin and bind to the extracellular ligand-binding domain of the respective pGCs or the clearance receptor. While pGCs generate cGMP, the clearance receptor is internalized with the respective peptide hormone as a cargo. The peptide hormone is then degraded, while the clearance receptor translocates back to the membrane. All abbreviations and processes are more closely introduced in (**1.2.1.**) and (**1.2.2**.).

process within an individual cell, but leading to a different or the same cellular response. For instance, both the cGMP and the cAMP signaling increase the chloride-ion secretion in intestinal epithelial cells. This chapter provides an overview of the cGMP signaling pathway in general, whereas the specific cGMP signaling components present in the GIT are described later (**1.3.**).

The cGMP signaling components (**Figure 7**) are divided into three groups, the inducers, generators, and effectors [36].

1.2.1. Inducers and generators

Inducer molecules are ligands that bind to a cGMP synthesizing enzyme, the guanylyl cyclase (GC; cGMP generators). Upon binding of the inducer, GCs catalyze the intramolecular cyclization of guanosine-5'-triphosphate to cGMP. The enzyme class of GCs is divided into two different types, the NO-induced guanylyl cyclases (NO-GCs; in literature also referred to as soluble guanylyl cyclase, sGC) and the membrane-bound particulate guanylyl cyclases (pGCs) [74].

The NO-GC type of GCs consists of two active isoenzymes which are assembled from two of the following subunits: the α1, α2 and β1 subunit. While the first isoenzyme termed NO-GC1 (α1β1 heterodimer) is expressed in most tissues, NO-GC2 (α2β1 heterodimer) expression is restricted to the brain, lung, colon, heart, spleen, uterus, and placenta [39]. Both isoenzymes are cytosolic, but NO-GC2 can also be localized to membrane proteins [110]. The inducer molecule of NO-GCs is NO. NO was historically identified in the cardiovascular system as an endothelial-derived relaxing factor of blood vessels. Ferid Murad, Robert F. Furchgott and Louis J. Ignarro, who got the Nobel prize for their discoveries in 1998, found that NO is generated by endothelial cells in response to ACh stimulation. The gaseous NO then diffuses to the adjacent smooth muscle layer leading to its relaxation [41, 58]. Today we know that NO is synthesized by NO synthases (NOS) from which three different isoforms are expressed in mammals. The endothelial NOS is expressed in the vascular endothelium and is the isoform responsible for NO-induced vascular smooth muscle relaxation. The inducible NOS is expressed in immune cells like macrophages and the neuronal NOS (nNOS) is expressed in neurons. The activity of the endothelial NOS and nNOS is regulated through intracellular Ca^{2+}/calmodulin levels (increased intracellular Ca^{2+} leads to NOS activation), while inducible NOS is constitutively active after expression [35, 106, 124]. Due to its size and lipophilic nature, NO can travel through multiple cell layers to

reach the NO-GC-expressing target cell. As a radical, its traveling distance is only limited by the amount of reaction partners which are encountered on the way.

There are seven different members of the pGC type of GCs known in rodents, named from GC-A to GC-G. All pGCs share the same domain composition consisting of an inducer-specific extracellular ligand binding domain, a transmembrane domain, and three intracellular domains (kinase-like domain, dimerization domain, and guanylyl cyclase domain). Functional pGCs are homodimers which assemble via the dimerization domain. The kinase-like domain allows GC-A and GC-B to be sensitized or desensitized (**1.2.3.**). Binding of the ligand to the extracellular domain induces a conformational change in GC-A, B, C and D which then leads to the intracellular activation of the guanylyl cyclase domain. GC-E, F and G are not activated by extracellular ligands, but rather through intracellular processes. GC-A (gene name: *natriuretic peptide receptor 1*, abbr.: *Npr1*), which is highly expressed in kidney, lung, vasculature, brain, liver, adrenal, endothelial, and adipose tissue, is activated by two small signaling peptides termed A-type natriuretic peptide (ANP; in the literature also referred to as atrial natriuretic peptide, gene name: *Nppa*) and B-type natriuretic peptide (BNP; in the literature also referred to as brain natriuretic peptide, gene name: *Nppb*). In the cardiovascular system, ANP and BNP are both secreted from cells of the heart as response to an increased blood pressure which then leads to vascular relaxation and natriuresis in the kidney. The second natriuretic peptide receptor, GC-B, is expressed in bone, brain, heart, kidney, liver, lung, uterus, vascular smooth muscle tissue, dorsal root ganglion neurons, and fibroblasts and is activated by a small signaling peptide termed C-type natriuretic peptide (CNP, gene name: *Nppc*) [105, 122]. GC-C and GC-D are both activated by the signaling peptides guanylin and uroguanylin, but, in addition, GC-D can also be activated by low concentrations of CO_2. While GC-D is expressed in the olfactory bulb, GC-C is expressed in the intestinal epithelium where it regulates the water and electrolyte secretion (**1.3.1.**). GC-E and GC-F are both expressed in retina and involved in phototransduction. GC-G is expressed in the olfactory bulb and responsible for thermo sensation in young rodents. In contrast to rodents, GC-D and GC-G are pseudogenes in human [74].

The last receptor mentioned is the clearance receptor (gene name: *natriuretic peptide receptor 3*, abbr.: *Npr3*) which harbors the same domain composition as pGCs, but without the intracellular guanylyl cyclase domain. Therefore, the clearance receptor cannot generate cGMP and is not considered a cGMP generator. The extracellular domain of the clearance receptor, however, binds ANP, BNP, CNP, uroguanylin, guanylin, and other signaling

peptides without triggering intracellular cGMP generation. Instead, the clearance receptor and its cargo are internalized and the cargo is targeted for intracellular degradation [94]. The main function is thought to be the removal and degradation of signaling peptides from the tissue, but other functions have also been discussed in recent years [2]. In the cardiovascular system, for instance, where CNP is produced by endothelial cells, CNP-induced vascular relaxation might be mediated mainly by the clearance receptor on vascular SMCs [90]. Expression of the clearance receptor was observed in brain, heart, kidney, lungs, mesenteries, adrenal, and vascular smooth muscle tissue [105].

1.2.2. Effector proteins

After cGMP generation, cGMP spreads out, from its origin of synthesis to the cellular periphery, modulating effector proteins on the way. Most effector proteins are activated by cGMP, but in some cases, cGMP can also reduce their activity (e.g. PDE3). Effector proteins can be divided into three major groups, the cGMP-dependent protein kinases (cGK), cyclic nucleotide gated (CNG) ion channels, and phosphodiesterases (PDE) [36].

The cGKs belong to the serine-threonine family of protein kinases. Upon cGMP binding and activation, cGKs transfer a phosphate group from ATP to the side chain hydroxyl group of serine or threonine on the substrate. The phosphorylated substrate then mediates the downstream function. In mammals, three different cGKs are encoded by two genes, *Prkg1* and *Prkg2* [59]. *Prkg1* codes for two cytosolic isoforms that only differ in their N-terminal domain, the cGMP-dependent protein kinase type Iα and type Iβ (cGKI) [98]. Although the different N-terminal domains define the substrate specificity *in vitro*, studies on SMC-specific rescue mice have shown that each isoform compensate for the other one *ex vivo* and *in vivo* [146]. The second gene, *Prkg2*, codes for the cGMP-dependent protein kinase type II (cGKII) which is myristoylated at the N-terminus and, therethrough, localized to the plasma membrane. Substrate specificity of cGKII is mediated by its subcellular localization [152]. Strong expression of cGKI is found in all smooth muscle tissues (especially vascular and gastrointestinal), platelets, cerebellum, hippocampus, dorsal root ganglia, kidney, and neuromuscular endplates. Lower expression of cGKI is found in cardiac muscle, vascular endothelium, granulocytes, chondrocytes, and osteoclasts. The expression of cGKII is confined to several brain nuclei, kidney, adrenal cortex, chondrocytes, lung, and the intestinal mucosa [59].

The gene family of CNG channels consists of six different genes coding for four α and two β subunits. Functional CNG ion channels are either homo tetramers of the α1, α2 or α3

subunits or hetero tetramers with the α4, β1 or β3 subunits. These nonselective cation channels are regulated in response to cyclic nucleotides like cGMP and cAMP and mediate the influx of Na^+ and Ca^{2+}. The cation influx leads to membrane depolarization. Hence, a neuronal action potential is formed. The expression of these ion channels is known in olfactory neurons and the retina [67].

The PDE gene family consists of eleven members and each member has several isoforms [25]. They cleave the cyclic 3'-5' phosphodiester bond of either cGMP or cAMP and convert them into guanosine-5'-monophosphate or adenosine-5'-monophosphate. PDEs degrade cGMP to confine excessive cGMP generation from spreading to other parts of the cell [8]. Although all PDEs cleave cyclic nucleotides, they differ in their substrate specificity for cAMP and cGMP. Therefore, PDEs are grouped into specifically cAMP cleaving PDEs (i.e. PDE4, 7, 8), specifically cGMP cleaving PDEs (i.e. PDE5, 6, 9) and dual specific, cAMP and cGMP cleaving PDEs (i.e. PDE1, 2, 3, 10, 11). Some PDEs are stimulated allosterically by cAMP, cGMP or calmodulin binding. Others are inhibited by competitive binding of cyclic nucleotides to the catalytic site [8, 25]. PDE1, for instance, is stimulated by Ca^{2+}/calmodulin [21, 97], PDE2 and PDE5 are stimulated by cGMP [84, 96, 112, 149], PDE3 is inhibited by cGMP [8, 28, 29] and PDE10 is inhibited by cAMP [8, 52]. In addition, cGKI phosphorylation of PDE5 enhances the affinity of cGMP to the allosteric binding site which then leads to a prolonged PDE5 activation [25, 111]. The PDEs that are mainly expressed in smooth muscle tissue are PDE1, 3, 4 and 5 and the PDEs mainly expressed in neuronal tissue are PDE1, 2, 4, 5, 6, 7, 9 and 10 [97]. Due to their broad range of isoforms, with individual expression patterns and relevance in different tissues, PDEs are very prominent drug targets. PDE5 inhibitors like sildenafil and tadalafil prevent the degradation of cGMP which, in turn, leads to a prolonged SMC relaxation. This is used to treat diseases like pulmonary hypertension (by prolonged bronchodilation) and erectile dysfunction (by prolonged relaxation of the vasculature in the penile corpora cavernosa) [8, 25].

1.2.3. CNP-induced cGMP signaling

The family of natriuretic peptide receptors consists of GC-A, GC-B, and the clearance receptor. All three are bound by natriuretic peptides, but with different affinities. GC-A is stronger bound by ANP (K_D = 1.9 pM) and BNP (K_D = 7.3 pM) than by CNP (K_D > 500 000 pM). GC-B is stronger bound by CNP (K_D = 7 pM) than by ANP (K_D = 5 400 pM) and BNP (K_D = 30 000 pM). And the clearance receptor is almost equally bound by ANP (K_D= 2.6 pM), BNP (K_D = 13 pM), and CNP (K_D = 10.8 pM) [9]. Therefore, GC-A is considered the receptor

for ANP/BNP and GC-B the receptor for CNP. The three natriuretic peptides contain a highly conserved amino acid sequence (CFGXXXDRIXXXXGLGC; X represents any kind of amino acid) in which the two flanking cysteines form a 17 amino acid long disulfide-linked ring. This ring structure defines the binding affinity to the respective receptor [104].

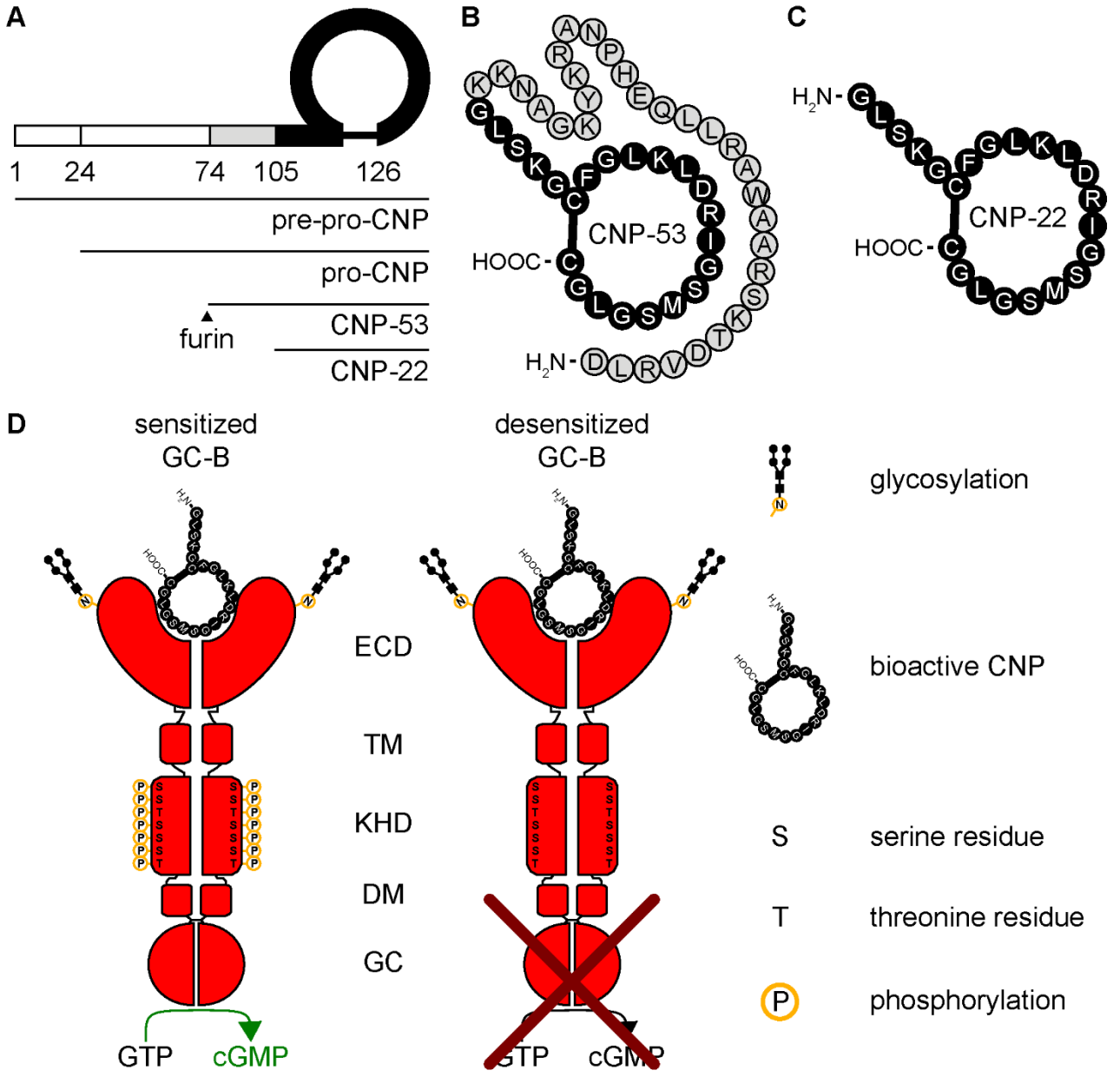

Figure 8: Pre-pro-CNP processing to bioactive CNP and regulation of GC-B activity.

A) CNP is expressed as pre-pro-peptide. The 23 amino acid long N-terminal signal sequence is cleaved of to form pro-CNP. Pro-CNP is intracellularly cleaved by furin to form the biologically activate CNP-53 (B). In some tissue, the N-terminal 31 amino acids long tail of CNP-53 is cleaved of to form CNP-22 (C). The illustrations of CNP-53 (B) and CNP-22 (C) also show the amino acid sequence in the one letter code. D) Active (sensitized) and inactive (desensitized) versions of GC-B. The activity of GC-B is dependent on both, the glycosylation of the extracellular domain and the phosphorylation of the kinase homology domain. Extracellular domain (ECD), transmembrane domain (TD), kinase homology domain (KHD; also termed kinase-like domain), dimerization domain (DM) and the guanylyl cyclase domain (GC). Bioactive CNP refers to either CNP-53 or CNP-22. A-C were adapted from [104] and D was adapted from [119].

Unlike ANP or BNP, CNP is not stored in intracellular granules and its secretion is increased upon stimulation with, for instance, lipopolysaccharide, tumor necrosis factor alpha, transforming growth factor beta, interleukin-1 or sheer stress, however, insulin suppresses CNP secretion [74, 104]. CNP, which is the most conserved natriuretic peptide, is expressed in brain, heart, kidney, lung, testis, uterus, embryonic spinal cord, blood plasma, chondrocytes, endothelial and follicular cells [74, 105, 121]. It is translated as 126 amino acid long pre-pro-CNP with an N-terminal signaling sequence that is proteolytically cleaved off to form the 103 amino acid long pro-CNP. Pro-CNP, in turn, is cleaved by the intracellular serine endoprotease furin into the 53 amino acids long, physiologically active CNP-53. In some tissues, CNP-53 is even further processed to CNP-22 (22 amino acids long) by a so far unknown protease [104]. Although CNP-53 and CNP-22 elicit similar extends of GC-B-mediated cGMP generation [151], the difference between the peptides lies in their tissue distribution (**Figure 8 A - C**). CNP-53 is the major form in brain, endothelial cells, and heart, whereas CNP-22 predominates in the blood plasma and cerebral spinal fluid [104]. Since blood is flushed through all tissues, it has to be considered as a potential source for CNP in every tissue investigated. In mice, the plasma concentration of CNP is 1.1 pM (±0.12 pM, n=5) [91] and its plasma half-life is below 2 minutes [148]. The clearance and degradation of CNP is performed through two mechanisms: 1) binding to the clearance receptor, internalization and intracellular degradation of CNP and 2) extracellular proteolytic cleavage of CNP by the neutral endopeptidase (NEP; also termed neprilysin). NEP is a membrane-bound zinc-dependent metalloprotease which has an extracellular catalytic domain that can be released into the extracellular space. It is considered an ectoenzyme which provides proteolytic cleavage to various peptide hormones like natriuretic peptides, glucagon, or substance P. NEP is expressed in various tissues including the vascular endothelium, blood plasma, lung, kidney, brain, Schwann-cells of the peripheral nervous system, long bones of the limbs, and the intestines [93]. The expression level of both components, the clearance receptor and NEP, defines the tissue and plasma half-life of CNP [103] and is, therefore, crucial for its regulation. Because of the short plasma half-life and concentration, it is thought that CNP exerts its effects in an autocrine and paracrine manner rather than systemically.

The activity of GC-B, in turn, is regulated at multiple levels. It has been shown that the extracellular domain of GC-B has to be glycosylated in order to elicit intracellular cGMP generation upon CNP binding [30]. In addition, the intracellular kinase homology domain of GC-B harbors serine and threonine residues that can be phosphorylated (S489, S513, T516,

S518, S523, S526 and T529). The phosphorylation of these residues sensitizes GC-B allowing for an efficient CNP-induced generation of cGMP. Desensitized GC-B, which is characterized by an unphosphorylated kinase-like domain, only displays a small fraction of the activity of sensitized GC-B (**Figure 8 D**). The kinase and phosphatase mediating the sensitization and desensitization of GC-B are not known [119].

CNP-induced cGMP signaling is crucial for several physiological processes such as bone growth [141], female fertility [4], axon bifurcation [122], homeostasis of arterial blood pressure [134], and proper GI function [128, 129, 131].

In the growth plate of long bones, CNP is secreted from chondrocytes and exerts its effect, in an autocrine and paracrine manner, by binding to GC-B on other chondrocytes. GC-B then generates cGMP and therethrough activates cGKI and cGKII. Downstream of cGKI the fibroblast growth factor signaling pathway is inhibited, whereas cGKII phosphorylates the glycogen synthase kinase-3β which suppresses β-catenin degradation. Both cGKs then regulate the proliferation of chondrocytes, the extracellular matrix production, the number and size of hypertrophic cells, and the rate of differentiation [74]. Dysfunction of this pathway in CNP [23], GC-B [137] and cGKII KO [100] mice inhibits the normal elongation of long bones leading to short limbs and dwarfism. The same phenotype is observed in human LOF mutations of GC-B and is termed AMDM [5, 63]. Gain-of-function mutations of GC-B and an increased secretion of CNP are both known to lead to an overstimulation of the cGMP signaling pathway in chondrocytes. The here through increased elongation of long bones leads to long limbs and gigantism. The corresponding human disease is termed epiphyseal chondrodysplasia type Miura [66, 87, 150]. The investigation of AMDM in human and mouse has already led to the development of promising drugs. For instance, Vosoritide, which is a CNP analog with a longer plasma half-life than CNP-53 or CNP-22, has been shown to be an efficient treatment for the major form of human dwarfism, the so called achondrodysplasia [11, 77]. Whether AMDM patients also suffer from other developmental defects, observed in mouse models of AMDM, like axon bifurcation or GI obstruction (**1.3.3.**), is unknown. But it is known that female AMDM patients, in contrast to the mouse model, do not suffer from infertility [64].

Studies in the developing spinal cord have shown that CNP [121], GC-B [122] and cGKI [123] are crucial for axon bifurcation of the dorsal root ganglion neurons. The axons of these neurons grow into the spinal cord at E12.5 where they undergo bifurcation resulting in caudal and rostral projecting axons. In this process, CNP, which is expressed in the spinal cord,

activates GC-B on the invading axons. GC-B, in turn, generates cGMP which then activates cGKI. Unknown downstream substrates then mediate axon bifurcation. In consequence, mice with an axon bifurcation defect suffer from impaired heat sensation and nociception induced by chemical irritants [34, 140].

In the cardiovascular system, especially in the aorta and other large vessels, ANP, BNP, and NO are the main molecules that induce cGMP-mediated smooth muscle relaxation. CNP, in turn, is secreted by endothelial cells and acts through the clearance receptor in aortic and large vascular SMCs, whereas it acts through GC-B on SMCs and pericytes in precapillary arterioles and capillaries. Therefore, the current opinion in the literature is that the CNP-induced GC-B/cGMP signaling is essential for the maintenance of normal microvascular resistance and blood pressure [134].

A disturbed function of the GIT has previously been observed in young GC-B LOF mutation mice [128, 129, 131]. This disturbed function, and other functional roles of cGMP signaling pathways in the GIT are described in the next chapter (**1.3.**).

1.3. cGMP signaling in the gastrointestinal tract

Studies regarding the cGMP pathway in GIT led to the discovery of multiple different GI mechanisms. The use of KO mice revealed a regulatory role of cGKII in water and electrolyte secretion of intestinal epithelial cells and an essential function of cGKI in GI smooth muscle relaxation.

1.3.1. (Uro)guanylin/GC-C/cGKII-mediated water and electrolyte secretion

Guanylin (5 amino acids long) and uroguanylin (6 amino acids long) are signaling peptides that are expressed by intestinal epithelial cells and Paneth cells along the small and large intestine. Guanylin is highly expressed in the small intestine and colon, whereas uroguanylin is highly expressed all over the jejunum and ileum. Both peptides activate GC-C which itself is found in epithelial cells of the duodenum, jejunum, ileum, and colon [12, 62]. Upon activation, GC-C generates cGMP which, in turn, activates the membrane-bound cGKII. Next, cGKII phosphorylates the cystic fibrosis transmembrane conductance regulator, which is an ATP-driven anion channel that transports Cl^- into the luminal space, leading to the opening of the anion channel. Water and cations like Na^+ are then passively transported through ion channels into the GI lumen. The GC-B-mediated water and electrolyte secretion is essential for the viscosity of the luminal content. The viscosity is supposed to be rather liquid in small intestine (required for maximum distribution and absorption of nutrients) and

more solid in large intestine (formation of rather solid feces). Malfunction of the GC-C-mediated water and electrolyte secretion can lead to diseases like diarrhea. In case of an enterotoxigenic *Escherichia coli* infection, heat-stable enterotoxins (STs),which have a greater affinity for GC-C than guanylin and uroguanylin [74], bind to GC-C and lead to a prolonged activation of the cGMP signaling pathway. Consequently, water and electrolytes are excessively secreted leading to diarrhea. Resistance against STs-induced diarrhea has been observed in guanylin, uroguanylin, GC-C and cGKII KO mice strengthening the suggested mechanism of action [79, 100, 126, 136]. Linaclotide, a drug that has been developed based on STs, stimulates intestinal water and electrolyte secretion. It is used to treat constipation-predominant irritable bowel diseases and has been shown to accelerate colonic transit in healthy patients [15, 74].

1.3.2. NO/NO-GC/cGKI-mediated smooth muscle relaxation

One of the first KO mice generated for a cGMP signaling pathway component was the nNOS KO mouse which, among other non GI phenotypes, developed pyloric stenosis [55, 60]. This phenotype was also observed in NO-GC KO, cGKI KO and IP_3R-associated cGMP kinase substrate (IRAG) LOF mutation mice [40, 47, 95, 100]. IRAG is a downstream substrate of cGKI that mediates smooth muscle relaxation. These studies revealed the following signaling model: nNOS, which is present in neurons of the ENS, generates NO as a signaling molecule for smooth muscle relaxation. NO activates the NO-GC of SMCs. The activated NO-GC generates cGMP which, in turn, activates cGKI. Downstream substrates of cGKI like IRAG, then mediate SMC relaxation by lowering intracellular Ca^{2+} levels [38, 47, 117]. Malfunction of one of these pathway components (e.g. nNOS, NO-GC, cGKI, or IRAG) leads to a higher smooth muscle tone of the pyloric sphincter which then allows less content to travel through. In consequence, pyloric stenosis develops and the area before the sphincter distends. It has been shown that smooth muscle-specific cGKI LOF is responsible for the high lethality of global cGKI KO mice [146]. It has been shown that the nNOS/NO-GC/cGKI signaling pathway regulates GI smooth muscle relaxation in lower esophageal sphincter, forestomach, small and large intestine [7, 50, 51, 143]. NO is the main neurotransmitter mediating the tonic inhibition of the GI SML. Furthermore, it has been shown that NO-GC is also expressed in ICCs and FLCs in various GI segments [7, 51]. ICCs are the pacemaker cells of the GI SML, whereas the function of FLCs is not completely known (**1.3.5.**). NO-GC, expressed in ICCs, seems to aid the pacemaker activity of ICCs and, thereby, contributes to smooth muscle relaxation in coordination with SMCs. Although it has been shown that FLCs express NO-GC, its role in these cells is yet unknown [7, 50, 51].

1.3.3. CNP-induced smooth muscle relaxation in various GI segments

CNP and GC-B have been studied in the GIT of different species like dogs, guinea pigs, rats, mice, and humans. In dog, CNP infusion into the cardiovascular system has been shown to decrease jejunal Na^+, Cl^-, and water absorption from the lumen [65]. Although the expression of GC-B in the GIT has not been conclusively shown so far, epithelial cells, neurons, and SMCs in small intestine seem to produce cGMP in response to excessive CNP concentrations (1 M CNP) [107].

Interestingly, CNP injected into wildtype (WT) mice seems to accelerate gastric emptying and, therefore, pyloric motility [131]. In addition to dwarfism and an early death, GC-B LOF mutation mice displayed GI phenotypes like milk retention in the stomach (due to pyloric stenosis) and a GI distension that was speculated to result from ilei (obstructed intestinal segments) and volvuli (twisted intestinal segments) in the ileum, cecum, and colon [128]. Relaxing effects of CNP on GI smooth muscle have been shown in various tissues including the esophagus [20], stomach [54], pylorus [53, 129], colon [129], and the anal sphincter [61]. Studies on the tissue level have shown that pyloric contractions are inhibited by CNP-induced cGMP signaling, eventually leading to increased cAMP levels in a PDE3-dependent manner [16, 129]. In colon, CNP leads to cGMP generation in a GC-B dependent manner and it also seems to have a contraction inhibiting effect. But, the identity of CNP and GC-B expressing cells in GIT is not known [70, 129, 131].

2. Aims of the study

The CNP-induced cGMP signaling, which is mediated by GC-B, plays a crucial role in several physiological processes including endochondral bone growth [141] and axon bifurcation [122]. Reports have shown that the CNP/GC-B/cGMP signaling pathway leads to pyloric and colonic smooth muscle relaxation. Furthermore, GC-B LOF mutant mice suffer from GI dysfunctions such as pyloric stenosis and intestinal obstruction in the ileum, cecum, and colon. These mice also display an increased lethality and most animals die before weaning [70, 128, 129, 131]. But unfortunately, the underlying cellular and molecular mechanisms are not known and require further elucidation.

In the proposed study, CNP and GC-B reporter and KO mouse lines were employed (CNP-lacZ and GC-B-lacZ; generated by our lab), to address the aims 1-3. Paneth cell-specific (Defensinα6-iCre), neuron-specific (Wnt1-Cre) and SMC-specific (αSMA-CreERT2) Cre driver lines were bred to mouse mutants that carry floxed alleles in either the gene for CNP or GC-B (CNP-flox and GC-B-flox; generated by our lab) to address aim 4. All mouse lines used for the scope of this thesis, as well as corresponding genetic background information, are described in (**3.1.**).

Aim 1: Characterization of GI dysfunction in global GC-B KO mouse lines.

Aim 2: Characterization of CNP and GC-B expression patterns within the GIT using *lacZ*-reporter mouse lines (CNP-lacZ and GC-B-lacZ).

Aim 3: Determination of the identity of CNP and GC-B expressing cells in regions with a GI dysfunction (i.e. small intestine and colon). These analyses are accompanied by *in situ* monitoring of CNP-induced cGMP signals in colonic SMC and neurons of cGi500 cGMP-FRET biosensor mice.

Aim 4: Generation of cell type-specific KO mice for CNP and GC-B using appropriate Cre driver lines and subsequent analysis of colonic segments to further our understanding about the cellular components and mechanisms of CNP-induced cGMP signaling in colonic motility.

3. Materials and methods

The devices and instruments used in this study are specified in the respective protocols. The centrifugation parameters for 1.5 mL and 2 mL reaction tubes are specific for a Heraeus Biofuge Fresco refrigerated benchtop centrifuge with a rotor type Heraeus 3325. Centrifugation parameters for 15 mL and 50 mL reaction tubes are specific for an Eppendorf 5804R centrifuge with a rotor type A-4-44.

Solutions and buffers are prepared with double-distilled purified water (Milli-Q™ Integral Water Purification System from Millipore) which is referred to as ddH_2O or water in this thesis. Solutions are sterilized for 20 minutes at 121 °C using a table autoclave (Ventilab 3000, MMM). The pH of solutions and buffers is measured with a pH meter (pHenomenal® pH 1100 L, VWR) and adjusted with 1 M HCl or 1 M NaOH. Sterile filtration is performed with a polyethersulfone membrane syringe filter (sterile syringe filter, cat.nr.:514-0073, VWR). If not stated otherwise experiments are performed at room temperature (RT, about 22 °C in southern Germany). A detailed list of chemicals as well as a list of common stock solutions is provided in the supplement (**Suppl. table S1 & S2**). A list of pharmacological substances used in various protocols is found in **Table 2**. Antibodies used in western blot and immunofluorescence (IF) staining are listed in **Table 3**.

Table 2: Pharmacologic substances.

substance	company	catalog number	diluent	stock concentration	final dilution
ANP (ANP-28)	Tocris	1912	H_2O	100 µM	various
BNP (BNP-45)	Phoenix	011-23	H_2O	100 µM	250 nM
CNP (CNP-22)	Millipore	05-23-0310	H_2O	100 µM	various
DEA-NO	Axxora	ALX-430-034	10 mM NaOH	100 mM	1 µM
TTX	Axxora	T1878	H_2O	5 mM	1 µM
CCh	Sigma-Aldrich	C4382	H_2O	5 mM	100 nM
IBMX	Sigma-Aldrich	NA	DMSO	500 mM	100 µM
Vinponectin	Biomol	NA	DMSO	5 mM	5 µM
Bay 60-7550	Santa Cruz	NA	DMSO	10 mM	100 nM
EHNA	Axxora	NA	DMSO	10 mM	10 µM
Milrinone	Santa Cruz	NA	DMSO	10 mM	10 µM
Zaprinast	Santa Cruz	NA	DMSO	10 mM	20 µM
Sildenfil	Santa Cruz	NA	H_2O	30 mM	20 µM
Tadalafil	Santa Cruz	NA	DMSO	50 mM	1 µM

Footnote: DEA-NO - 2-(N,N-Diethylamino)-diazenoate-2-oxide. DEA-NO is stable in alkalic pH, but not below a pH of 7.4. Therefore, it is solved in NaOH. TTX – Tetrodotoxin. CCh – Carbachol. IBMX – 3-Isobutyl-1-methylxanthin. EHNA - Erythro-9-(2-hydroxy-3-nonyl) adenine. NA – not available.

Table 3: Antibodies.

target protein (name)	cell type*	antibody (identifier**)	origin	catalog number	use	final dilution
hemagglutinin tag	-	Rb-α-HA	Cell Signaling	3724	WB	1:1000
GC-B	-	gp-α-Npr2	PD Dr. Hannes Schmidt [138]		WB	1:5000
cGKI	-	rb-α-cGKI	PD Dr. Hannes Schmidt [138]		WB	1:2400
Clathrin heavy chain	-	mo-α-Clathrin	BD Pharmingen	610500	WB	1:2000
GAPDH	-	rb-α-GAPDH	Cell Signaling	2118	WB	1:1000
rb-IgG	-	go-α-rb-HRP	Sigma-Aldrich	7074S	WB	1:10000
gp-IgG	-	do-α-gp-HRP	Jackson	706-035-148	WB	1:1000
β-Galactosidase	-	ch-α-βGal	Abcam	ab9361	IF	1:2000
GFP	-	rb-α-GFP	Abcam	ab290	IF	1:1000
GFP	-	ch-α-GFP	Abcam	ab13970	IF	1:2000
RFP	-	rb-α-RFP	Antikoerper-online	ABIN129578	IF	1:2000
PGP9.5	neurons	rb-α-PGP9.5	Dako	Z5116	IF	1:1000
nNOS	nitrergic neurons	rb-α-nNOS	Thermo	61-7000	IF	1:500
c-kit	ICCs	rt-α-c-kit	Linaris	MAK5311	IF	1:1500
PDGFRα	FLCs	rb-α-PDGFRα	Cell Signaling	D1E1E	IF	1:1500
GFAP	glia cells	rb-α-GFAP	Dako	Z0334	IF	1:1000
αSMA	SMCs	mo-α-αSMA	Sigma-Aldrich	A5228	IF	1:500
HuC/D	neurons	mo-α–HuC/D	Thermo	A-21271	IF	1:30
β3Tubulin	neurons	rb-α-β3Tub	Covance	MRB-435P	IF	1:5000
Lysozym	Paneth cells	rb-α-Lyz	Dako	A0099	IF	1:2000
CD3	T-cells	rb-α-CD3	***		IF	1:50
B220	B-cells	r-α-B220	***		IF	1:50
F4/80	macrophages	rb-α-F4/80	***		IF	1:50
CD31	endothelial cells	rt-α-CD31	BD Pharmingen	550274	IF	1:100
Vimentin	fibroblasts	rb-α-vim	Abcam	ab92547	IF	1:250
ch-IgG	-	do-α-ch-AF488	Jackson	703-545-155	IF	1:1000
rb-IgG	-	go-α-rb-AF488	Jackson	111-545-144	IF	1:1000
rb-IgG	-	go-α-rb-Cy3	Jackson	111-165-144	IF	1:10000
rt-IgG	-	go-α-rt-AF488	Jackson	112-545-167	IF	1:1000
rt-IgG	-	do-α-rt-Cy3	Jackson	712-165-153	IF	1:1000
go-IgG	-	do-α-go-AF488	Thermo	A-11055	IF	1:1000
mo-IgG	-	go-α-mo-AF488	Jackson	115-545-146	IF	1:1000
mo-IgG	-	go-α-mo-Cy3	Jackson	115-165-146	IF	1:1000

Footnote: * cell type that can be identified by the expression of the respective marker protein, ** identifier consists of the host abbreviation, an "α" standing for anti, and the antigen name. Host abbreviations: chicken (ch), goat (go), guinea pig (gp), mouse (mo), rabbit (rb), rat (rt). *** antibodies were a donation from Prof. Dr. Leticia Quintanilla-Martinez de Fend (leader of the core facility of the institute for pathology at university Tübingen).

3.1. Laboratory mice

3.1.1. Ethics statement

Animal experiments were performed in accordance with the 3R principle (replace, reduce, refine), the EU Directive 2010/63/EU, and the local authorities (Regierungspräsidium Tübingen; AZ35/9185.81-2).

Global GC-B KO mice were bred in accordance with the approved animal ethics proposal IB1/15. Mice were injected with tamoxifen in accordance with the approved animal ethics proposals IB2/15, IB07/18G and IB02/19G.

The mice sacrificed for organ isolation were reported to the Regierungspräsidium Tübingen in accordance with the §4 registration (notification from 25.11.2016).

3.1.2. Mouse lines

The genetic background of the mouse lines used in this study is C57BL/6N (black 6 mice from Charles River). To increase the survival rate, global GC-B KO mice (homozygous GC-B-lacZ mice) are bred on a mixed background (C57BL/6N and 129/SV). As an example, GC-B KO mice bred on a pure black six background died between three to twelve days after birth whereas GC-B KO mice bred on a mixed background survived up to half a year. The following paragraph describes the mouse lines used in this thesis (**Table 4**).

Table 4: Transgenic mouse lines used in this study.

mouse line	systematic name	promotor	reference
CNP-lacZ	B6Nppc$^{tm1.1Fgr}$	Nppc	[121]
GC-B-lacZ	B6.129Npr2^{tm1Fgr}	Npr2	[138]
GC-B-HA	HA-Npr2	Npr2	[4]
GC-B-CreERT2	B6;129P2-Npr2$^{tm2.1(CreERT2)Fgr}$	Npr2	[138]
Wnt1-Cre	B6.129-Tg(Wnt1-cre)^{11Rth}	Wnt1	[27]
αSMA-CreERT2	B6-Tg(Acta2-cre/ERT2)^{51Pcn}	Acta2	[147]
Defensinα6-iCre	B6-Tg(Defa6-icre)^{1Rsb}	Defa6	[1]
R26-Ai14	B6.Cg-Gt(ROSA)26Sor$^{tm14(CAG-tdTomato)Hze}$	R26	[81]
R26-cGi500(L2)	B6.129-Gt(ROSA)26Sor$^{tm4(ACTB-tdTomato,-cGi-500)Feil}$	R26	[139]
R26-mcGi500(L2)	B6.129-Gt(ROSA)26Sor$^{tm5(ACTB-tdTomato,-mcGi500)Feil}$	R26	unpublished
GC-B-flox	B6;129S7-Npr2$^{tm2.1(flox)Fgr}$	Npr2	[140]

The β-Galactosidase (βGal; gene name: *lacZ*) from *escherichia coli* is a reporter enzyme that cleaves the glycosidic bond of β-galactopyranosides. In this study mouse lines are used where a *NLS-lacZ* (nuclear localization sequence; NLS) fusion gene construct was stably integrated into the mouse genome under the control of either the *Nppc* (protein name: CNP)

or the *Npr2* (protein name: GC-B) promotor. The *NLS* leads to a translocation of the βGal from the cytosol to the nucleus. The knock-in of the fusion gene construct into the respective gene locus also represents a gene KO. Hence, both mouse lines can be used to generate the respective global CNP or GC-B KO mice.

Hemagglutinin (HA; amino acid sequence: YPYDVPDYA) is a small amino sequence (i.e. ~1.1 kDa) that can be fused to a target protein without a high risk of influencing the proteins function. The GC-B-HA mouse has an HA-tag with a small linker (total amino acid sequence YPYDVPDYAGAA) fused to the extracellular N-terminal domain of GC-B.

Cre-inducible reporter lines contain a floxed “stop” cassette (flanked by 2 loxP sites; “flox”) upstream of the reporter protein, which is excised by the Cre-recombinase. Only then the reporter protein is expressed. This allows for cell type-specific reporter protein expression.

The $CreER^{T2}$ is a fusion protein consisting of the Cre-recombinase, which is fused to the T2 mutant of the estrogen receptor (ER^{T2}). This ER^{T2} mutant only recognizes 4-hydroxytamoxifen instead of estrogen. The $CreER^{T2}$ is localized to the cytosol and translocates into the nucleus upon 4-hydroxytamoxifen binding [37]. Therefore, Tamoxifen, which is metabolized to 4-hydroxytamoxifen in the mouse liver, can be administered to induce the activation of the $CreER^{T2}$ recombinase in mice.

The GC-B-flox mouse line contains two LoxP sites which flank exon 17 & 18 of the GC-B gene. Exon 17 & 18 code for the guanylyl cyclase domain and are, therefore, pivotal for the generation of cGMP. The Cre-dependent excision of those exons leads to a premature stop codon in exon 19. In consequence, the expression of GC-B is almost undetectable and allows for the generation of cell type-specific GC-B KO mice.

3.1.3. Caretaking of *mus musculus*

Mice are housed in type-II-short (up to three mice), type-II-long (three to five mice), and type-III (five to eight mice) cages. They are provided with food and water ad libitum, bedding, nest material, and two wooden enrichments per cage (groups of male mice do not get wooden enrichments). Mice are kept in rooms with a repeating day (12 hours; starting at 6 am) and night cycle (12 hours; starting at 6 pm). Male siblings are kept together from weaning to the first time of separation or mating with females. Female siblings are kept in groups also with other not related female mice.

3.1.4. Timed breeding for embryo isolation

For timed breeding, the male parent mouse is kept alone for one day in the breeding cage. Two female parent mice are then added at the start of the night cycle. Successful coitus is indicated by a whiteish plug created by the coagulating and vesicular glands of the male mouse. This kind of plug is visible inside/on top of the vaginal opening of the female mouse and persists for 8-24 hours after breeding. The female mice are checked for whitish vaginal plugs at the start of the next day cycle (12 hours later). Plug positive females are weighed and removed from the breeding. The day of the plug detection is considered as the embryonic day 0.5. One day before the embryo is isolated the mother mouse is weighted again. After about eight days of pregnancy the mother mouse should have gained about 2 g of body weight or more, otherwise a pregnancy is unlikely.

3.1.5. Regular breeding

Pair one male and two female parent mice of the desired genotypes. Check on the appearance of the female mice every week. After about two weeks of pregnancy it can be recognized by the round shape of the mother. For permanent mating arrangements keep male and female mice together after pregnancy is suspected. For one-time mating arrangements remove the male mouse from the cage after pregnancy is suspected.

3.1.6. Weaning and separation of a new litter

After a new litter is born the pups are nursed by the mother for three weeks. At day 21 the young mice are removed from the mother and separated into groups of female and male mice. During separation, mice are earmarked and ear fragments are used for genotyping.

3.1.7. Earmarking of young mice

Mice that are analyzed at a young age (between 5 and 18 days) are earmarked and genotyped two days before the experiment.

3.1.8. Mouse genotyping

The genotype of a transgenic mouse can be identified using standard polymerase chain reaction (PCR) protocols. The primers for these PCRs are designed to recognize the transgenic DNA sequence. The amplified DNA is detected by agarose gel electrophoresis. More elaborate PCR protocols include primers which also recognize the WT DNA sequence. Only if the WT sequence and the transgenic sequence are both amplified and distinguished, it is possible to identify heterozygous and homozygous transgenic mice.

3.1.8.1. DNA extraction

The tissue samples, which are collected during the earmarking of young mice, are used for genotyping. Extraction of the DNA is most successful on the day the tissue is collected.

Materials:

- Tail lysis buffer:
  50 mM KCl, 2 mM $MgCl_2$, 10 mM Tris/Cl pH 8.0, 0.45% (v/v) Triton X-100, 0.45% (v/v) Tween 20 and 0.01 % (w/v) gelatin. Fill up to 500 mL with ddH_2O. Autoclave, prepare 50 mL aliquots and store at 4 °C.
- Proteinase K (PK, 20 mg/mL, cat.nr.: M3036, Genaxxon).

Protocol:

1. Add 1 µL PK per 100 µL Tail lysis buffer.
2. Add 200 µL Tail lysis buffer to each tissue sample.
3. Incubate tissue sample overnight at 56 °C.
4. Vortex reaction tubes thoroughly until tissue samples are disintegrated.
5. Inactivate PK in sample for 7 minutes at 95 °C.
6. Spin down tissue debris at 13.000 g for 5 minutes.
7. Use supernatant as DNA containing fraction for PCR.

3.1.8.2. PCR and PCR product detection

The list of PCR protocols used to genotype the mouse lines of this thesis can be found in the supplement (**Suppl. table S4**). Primers are ordered from Eurofins (**Suppl. table S5**). The thermocycler used for the GC-B-lacZ PCR is the peqSTAR 2X Gradient (PEQLAB). All other PCR protocols can also be performed with the Biometra TAdvanced (AnalytikJena) thermocycler. PCR products are separated with the Kodak BioMax MP1015 (Kodak Biomax) gel electrophoresis system.

Materials:

- Nuclease-free water for molecular biology (cat.nr.: 1058ML500, neoFroxx) is used as H_2O for the PCR protocols.
- *Taq* polymerase (5 unit/µL), 10x RT buffer and 25 mM $MgCl_2$ (cat.nr.: M3001, GENAXXON).
- *Taq* polymerase (5 unit/µL), 10x RT buffer and 50 mM $MgCl_2$ for the GC-B-lacZ PCR (cat.nr.: 10342020, Invitrogen).
- 10 mM dNTPs (cat.nr.: N0447L, NEB).
- Agarose (Biozym LE Agarose, cat.nr.: 840004, Biozym).
- 50 x TAE buffer:
  2 M Tris, 1 M acetic acid, 50 mM EDTA in ddH_2O. Adjust pH to 8.0.

- Midori Green Advance DNA Stain (1 mL stock, cat.nr.: MG04, Genetics).
- 10 x TBE buffer:
  0.5 M Tris, 0.5 M boric acid, 10 mM EDTA in ddH_2O. Adjust pH to 8.3.
- 6 x loading dye:
  0.125% (w/v) bromophenol blue, 0.125% (w/v) xylene cyanole, 30% (v/v) glycerol, 60% (v/v) of 10 x TBE buffer and add up to 100% (v/v) with ddH_2O.

Protocol:

1. Prepare 0.1 mL PCR tubes for all samples, a positive control (positive tested sample), and a water control (lysis buffer without DNA).
2. Pipette master mix, but do not add DNA (**Suppl. table S5**). In case of the GC-B-lacZ PCR, neither add DNA nor *Taq* polymerase.
3. Add master mix to each tube (20 µL for most PCR protocols, 19.75 µL for the GC-B-lacZ PCR protocol and 22 µL for the 100 bp Cre PCR protocol).
4. Add DNA to each tube and lysis buffer without PK to the negative control. Start the PCR program (**Suppl. table S4**).
5. The GC-B-lacZ PCR program is a Hot-start protocol which means that the *Taq* polymerase is only added when the sample reaches the 80 °C step (step 3).
6. Prepare a 2% (w/v) agarose gel for separation of the amplified DNA:
   Assemble agarose gel casting chamber (capacity: 100 mL) and prepare agarose gel in a lockable glass bottle. For one gel, weight in 2 g agarose, add 100 mL 1 x TAE-buffer, and heat in the microwave until solution is clear (keep lit of glass bottle on, but do not screw it tight). Cool solution down to about 50 °C, add 1:25.000 Midori Green Advance, and pure the gel.
7. After the PCR program is completed add 5 µL of 6 x loading dye to each PCR tube.
8. Vortex samples and load 12.5 µL per PCR sample into pockets of agarose gel.
9. Load 7.5 µL of the DNA marker.
10. Run agarose gel at 100 Volts for 50 minutes.
11. Detect PCR products using ultraviolet light at a ChemiDoc (BioRad) imaging system using the settings for UV light transmission (setting: “GelGreen”).

3.1.9. Tamoxifen injection

The translocation of the $CreER^{T2}$ DNA recombinase, from the cytosol to the nucleus of the $CreER^{T2}$ expressing cells, is mediated by 4-hydroxytamoxifen. Tamoxifen, which is injected into the mouse, is converted to 4-hydroxytamoxifen in the liver. If not otherwise stated, mice are injected with 100 µg Tamoxifen per 1 g body weight intraperitoneally, eight, six, five, four, and three days before the experiment.

Materials:

- 10 mg/mL tamoxifen (cat.nr.: T5648-1G, Sigma-Aldrich):
  Heat sunflower oil to 40 °C. Weight in tamoxifen and add to sunflower oil. Sonicate

the mixture at 40 °C until tamoxifen is dissolved. Make 500 µL aliquots and freeze tamoxifen solution at -20 °C in the dark.

- 0.60 x 30 mm 23G x 1 ¼ injection needle (cat.nr.: 4657640, Sterican) and a 1 mL syringe (Inject®-F, cat.nr.: 9166017V, B. Braun).
- Paper towel and disinfectant.

Protocol:

1. Weight mouse and adjust amount of Tamoxifen for injection.
2. Disinfect region of injection using a disinfectant wetted paper towel.
3. Inject tamoxifen.
4. Check mouse behavior directly after injection.
5. Check injection site in the following days to prevent infections.

3.1.10. Isolation of the gastrointestinal tract

Isolation of specific GI segments from mice requires fast action. After sacrificing the mouse, the enzymes and bacteria of the GIT start to digest the tissue itself. Therefore, euthanize the mouse using CO_2 inhalation for 2 minutes. Decapitate the mouse and cut open the mouse belly. For complete isolation and dissection, cut the esophagus in the region where it enters the diaphragm, and the rectum close to the anal sphincter. Before isolation, cut the connection of the mesenteries to the dorsal aorta and place the isolated GIT in ice cold PBS (in case of the *ex vivo* IFM, place tissue in O_2/CO_2 gassed and 37 °C pre-warmed Krebs-Henseleit solution: **3.5.**). Remove the mesenteries and isolate the segments of interest (see **1.1. Figure 1**). Flush the GI segment with a 0.60 x 30 mm 23G x 1 ¼ blunted injection needle and a syringe to free it from any luminal content. In this thesis, as in many other publications, the median and distal colon are isolated and investigated together, and the combined segment is referred to as the distal colon.

3.2. Tissue staining techniques

Tissue staining is performed to detect the expression of a specific protein in the tissue. Two different staining techniques are used in this study. First, Xgal staining utilizes the enzymatic activity of βGal to cleave Xgal (5-bromo-4-chloro-3-indolyl-β-D-galactopyranoside) into galactose and the 5-bromo-4-chloro-3-hydroxaindole. Subsequent oxidation of the 5-bromo-4-chloro-3-hydroxaindole then leads to the formation of an insoluble blue precipitate (5,5'-dibromo-4,4'-dichloro-indigo). Second, IF staining utilizes antibodies to fluorescently label reporter proteins and cell type-specific marker proteins. This also allows for the parallel labeling of multiple proteins within one sample (IF double staining). In all staining techniques, the tissue is fixed on the whole tissue level directly after the isolation

from the mouse (**3.1.10.**). More information about the different staining techniques can be found in this book chapter [73]. The amount of liquid that is filled into one well of a 12 well plate is 2 mL (e.g. for equilibration, wash and staining steps).

Table 5: Staining dyes.

abbreviation	company	catalog number	diluent	stock concentration	final concentration
Xgal	Thermo	15520018	DMF	20 mg/mL	0.5 mg/mL
DAPI	Dianova	NA	ddH_2O	0.5 mg/mL	0.5 µg/mL

Footnote: DAPI (4,6-Diamidine-2-phenylindole), Xgal (5-bromo-4-chloro-3-indolyl-β-D-galactoside). not available (NA).

3.2.1. Fixation

Prior to tissue staining, an appropriate fixation has to be chosen. Tissue fixation crosslinks molecules within the specimen, hence, tissue integrity is conserved. But, it also reduces the enzymatic activity of reporter enzymes like βGal. In this study, two different fixating agents are used, one for IF staining (PFA fixative) and one for Xgal staining (Zambonis fixative). The Zambonis fixative does not influence the βGal activity as strong as the PFA fixative. Whole mount colon, which is used for IF staining, is fixed in a slightly different setup. After isolation and cleaning of the colon, the tube is cut open along the mesenteric border and pinned down, with the mucosa face-up, on a SYLGARD-coated petri dish using insect needles. The tissue is then fixed in this orientation (“open-book preparation”).

Materials:

- PFA fixative (4 % paraformaldehyde):
  Weight in 4% (w/v) paraformaldehyde and add 50% (v/v) ddH_2O. Heat suspension to 50 °C, stir with 100 rpm and add 100 µL of a 1 M NaOH solution. Wait until paraformaldehyde is dissolved, add 10% (v/v) of 10 x PBS and 40 % (v/v) ddH_2O. Adjust pH to 7.4, sterile filter solution, make 50 mL aliquots, and freeze at -20 °C.
- Zambonis fixative [135]:
  Weight in 2% (w/v) paraformaldehyde and add 50% (v/v) ddH_2O. Heat suspension to 50 °C, stir with 100 rpm and add 100 µL of a 1 M NaOH solution. Wait until paraformaldehyde is dissolved, add 10% (v/v) of 10 x PBS, 15% (v/v) picric acid and 25 % (v/v) ddH_2O. Adjust pH to 7.4, sterile filter solution, make 50 mL aliquots, and freeze at -20 °C.
- SYLGARD-coated petri dish:
  Prepare 20 mL of the SYLGARD mixture in 50 mL reaction tube. Add 2 mL of the curing agent to 18 mL of the base agent (SYLGARD™ 184 silicone elastomer kit, SYLGARD ™). Mix thoroughly for several hours. Pure 20 mL of SYLGARD mixture into 100 mm petri dish. Let petri dish rest in incubator at 55 °C for 24 hours.

Protocol:

1. Place freshly isolated tissue in 12 well plate.

2. Wash tissue once in 1 x PBS before fixation.
3. Overlay tissue with ice cold fixating agent and shake at 4 °C or on ice. The fixation time depends on the staining technique, which is performed afterwards, and the genotype of the mouse line used. For IF staining, fix with PFA fixative for 2 hours. For Xgal staining, fix with Zambonis fixative for 30 minutes (tissue from GC-B-lacZ mice) or 2 hours (tissue from CNP-lacZ mice).
4. Wash tissue three times for 30 minutes with 1 x PBS (in case a Xgal staining of whole mount tissue is performed afterwards, wash with Xgal equilibration buffer: **3.2.2**).
5. Continue with staining technique or preparation of cryosections.

3.2.2. Xgal staining of whole tissue

With this protocol whole tissue from *lacZ* reporter mouse lines like the CNP-lacZ or GC-B-lacZ reporter mouse lines can be stained.

Materials:

- 20 mg/mL Xgal reagent (**3.2. Table 5**):
  Weight in Xgal reagent and solve in DMF. Freeze at -20 °C and keep in a box, which is protected from light.
- Xgal equilibration buffer:
  2 mM $MgCl_2$, 0.01% (w/v) sodium deoxycholate, 0.02% (v/v) nonidet-P40 substitute in 1 x PBS.
- Xgal staining solution:
  2 mM $MgCl_2$, 0.01% (w/v) sodium deoxycholate, 0.02% (v/v) nonidet-P40 substitute, 5 mM $K_3[Fe(CN)_6]$ and 5 mM $K_4[Fe(CN)_6]$ in 1 x PBS. Store at 4 °C. Before use, freshly add the Xgal reagent to a final concentration of 0.5 mg/mL (1:40 dilution).
- Xgal wash buffer:
  2 mM $MgCl_2$ in 1 x PBS.

Protocol:

1. Apply Xgal staining solution to the tissue and incubate at 37 °C in the dark. The staining time depends on the genotype of the mouse line used (CNP-lacZ: 2 hours and GC-B-lacZ: 16 hours).
2. Wash tissue three times with Xgal wash buffer for 30 minutes.
3. Fix tissue for 2 hours at room temperature with PFA (**3.2.1.**; Materials).
4. Wash tissue three times with Xgal wash buffer.
5. Store tissue in 1 x PBS at 4 °C.

3.2.3. Tissue clearing and documentation

The native color of GI tissue is yellow. For optimal observation of a stained tissue on the surface, but also in deeper layers of the tissue, the tissue should be transparent. This is achieved using a clearing agent like ScaleA2 where urea intercalates with the tissue and unifies the refraction index. This reaction is based on the high osmotic pressure generated

by the high urea concentration in the ScaleA2 reagent and is rapidly reversible [57]. Therefore, do not remove ScaleA2 from the tissue at any time until documentation of the tissue is done.

Materials:

- ScaleA2 [57]:
  4 M urea, 10% (v/v) glycerol and 0.1% (v/v) Triton X-100 in ddH_2O.
- Documentation setup:
  Upright stereo microscope with camera port (Stemi 2000-CS, Zeiss). A Canon EOS 750D amateur camera (Canon) with a T2-adapter for the Canon EOS 750D (Canon) and a C-mount T2 adapter with a 2x magnification lens (Zeiss) to connect the camera and microscope. A light source (KL 1500 LCD, SCHOTT) with a swan neck optical fiber to focus the light on the sample.

Protocol:

1. Remove 1 x PBS from tissue.
2. Add ScaleA2 to the tissue and incubate in the fridge for 1 week.
3. Document tissue using the documentation setup.

3.2.4. Evaluation and rating of Xgal stained whole tissue

Images taken from the Xgal stained whole mount GI tissue of CNP-LacZ, GC-B-lacZ, and WT mice, at the postnatal days P15, P45, and P75, are evaluated using Fiji. For each GI segment, two images are loaded into Fiji and blue dots are counted using the “Cell Counter” plugin (Fiji/Plugins/Analyze/Cell Counter/). Images of WT Xgal stained GI tissue are used as negative control. The number of cells from the two images are averaged and scored from 0 to 5. Regions without any Xgal stained cells/mm² are scored with 0. Regions with 1 to 100 cells/mm² are scored with 1. Between 101 and 250 cells/mm² score 2 is assigned. Score 3 is assigned for regions with 251 to 500 cells/mm², score 4 for regions with 501 to 1000 cells/mm² and score 5 for regions with more than 1000 cells/mm². Regions with a score below 3 are considered as regions with a low CNP or GC-B gene transcription and regions with a score above 3 are considered as regions with high CNP or GC-B gene transcription.

3.2.5. Immunofluorescence double staining of whole tissue

With this protocol whole tissues like the colon can be stained with IF. The protocol requires long incubation times and well stirring to allow the antibodies to penetrate the tissue. Test the experimental setup (antibodies and tissue, positive and negative controls) on cryosections prior to the whole mount staining to ensure a specific staining with the concentrations used. All steps are performed at 4 °C in a cold room. In this protocol the

volume of all antibody incubation steps is half the volume of any block and wash steps. If the tissue is not covered properly during antibody incubation, increase the volume.

Materials:

- IF wash buffer:
  0.1% (v/v) Triton X-100 in 1 x PBS.
- IF blocking buffer:
  1% (w/v) NGS in IF wash buffer.
- Antibody solution:
  Primary or secondary antibody diluted in IF blocking buffer.
- Immu-Mount (Immu-Mount™, cat.nr.: 9990402, Thermo).
- Nail polish.

Protocol:

1. Transfer tissue to 4 mL scintillation vial.
2. Block tissue with 4 mL IF blocking buffer overnight.
3. Incubate tissue with 2 mL of the first primary antibody solution for 48 hours.
4. Wash tissue seven times for 1 hour with 4 mL wash buffer.
5. Incubate tissue with 2 mL of the first secondary antibody solution for 48 hours.
6. Block tissue with 4 mL IF blocking buffer overnight.
7. Incubate tissue with 2 mL of the second primary antibody solution for 48 hours.
8. Wash tissue seven times for 1 hour with 4 mL wash buffer.
9. Incubate tissue with 2 mL of the second secondary antibody solution for 48 hours. Also add DAPI (**3.2. Table 5**) to the solution.
10. Wash tissue seven times for 1 hour with 4 mL wash buffer.
11. Mount tissue on object slide using Immu-Mount and cover with cover slip:
    - Transfer colon into 35 mm petri dish with Immu-Mount and flatten out the opened colon like a sheet. Add several drops of Immu-Mount to an object slide and hold object slide over petri dish.
    - Pull colon sheet with forceps from the petri dish onto the object slide and cover with cover slip. For imaging of the MP or muscle layers, make sure these layers are facing up towards the cover slip.
12. Dry Immu-Mount for 1 day and seal cover slip with nail polish.

3.2.6. Preparation of tissue cryosections

There are two major sectioning techniques which are used to investigate the tissue microanatomy. Cryosections are performed from frozen tissue and provide the advantage of a native protein conformation. Paraffin sections, in contrast, strongly conserve the tissue structure allowing for thinner sections, but do not conserve the native protein conformation (down to 4 µm with paraffin sections vs. 10 µm with cryosections).

Materials:

- Sucrose cryoprotecting agent:
  30% (w/v) sucrose in 1 x PBS.
- Cryoembedding medium (Sakura Finetek™ Tissue-Tek™ O.C.T. compound, cat.nr.: 4583, Sakura).
- Object slides (Epredia™ SuperFrost PlusTM adhesion slides, cat.nr.: J1800AMNZ, Fisher).

Protocol:

1. Incubate tissue in sucrose cryoprotecting agent overnight in the fridge.
2. Transfer tissue into molds filled with cryoembedding medium and freeze tissue in the desired orientation. The lumen of the GI tissue is filled with cryoembedding medium before freezing and the tissue is embedded in a longitudinal orientation (the tissue-wall faces the bottom of the mold).
3. Freeze tissue for at least 1 hour at -20 °C.
4. Cut tissue with cryotome and a section thickness of 20 µm.
5. Dry tissue for 30 minutes at room temperature.
6. Freeze sections at -20 °C until further use.

3.2.7. Xgal staining and subsequent documentation of cryosections

As opposed to other protocols, where Xgal staining is performed on the whole tissue that is sectioned afterwards, Xgal staining in this thesis is performed on unstained cryosections. The advantage of Xgal staining on unstained cryosections towards whole tissue Xgal staining is that the Xgal staining solution does not has to diffuse through the whole tissue to reach the target cells. Hence, the staining of cell populations at the inner layers of the tissue is as strong as the staining of cells at the outer layers of the tissue. On the downside, over fixation of the unstained tissue leads to signal reduction and should, therefore, be avoided.

Materials:

- Wash cuvette for eight object slides with volumetric capacity of 50 mL.
- Xgal reagent, Xgal equilibration buffer, Xgal staining solution, and Xgal wash buffer (**3.2.2.**; Materials).
- Parafilm (PARAFILM™ M, cat.nr.: CNP8.1, Roth) which is cut to the size of the area covered by the sections on the slide. Curve the Parafilm longitudinally (bring the two long sites of the Parafilm closer together).
- Staining chamber with guide rails to place the slide on (**Figure 9**).
- Nuclear fast red solution (NFR, cat.nr.: N3020-100ML, Sigmal-Aldrich):
  Fresh NFR (up to 3 months) can be used without additional preparations. After 3 months, the NFR solution forms precipitates which cannot be removed from the cryosections afterwards. To remove precipitates, spin down 1 mL of the NFR solution in 1.5 mL reaction tube for 5 minutes at 13.000 g. Transfer supernatant to new 1.5

mL reaction tube. Heat reaction tube to 95 °C for 5 minutes. Spin the NFR supernatant down for 5 minutes at 13.000 g. Transfer the supernatant to a new 1.5 mL reaction tube. Store NFR solution at room temperature.

- Mounting medium:
  Immu-Mount™ (**3.2.5.**; Materials) is used to mount coverslip on stained cryosections. But, be cautious because water containing mounting media like Immu-Mount™ are not optimal for mounting NFR counterstained sections. NFR is water soluble and is washed away if there are only a few, small sections mounted (e.g. the NFR counterstaining of four P15 esophagus cryosection is washed away, whereas four of the much larger P15 colon cryosections keep the NFR counterstaining).
- Documentation setup:
  Inverted microscope (Axiovert 200 with 1.0/1.6x Optovar lens, Zeiss) with fluorescence grade objectives (Plan NeoFluar 10x/0.30 and EC Plan NeoFluar 40x/1.30 Oil, Zeiss). A Canon EOS 750D amateur camera (Canon) with a T2-adapter for the Canon EOS 750D (Canon) and a C-mount T2 adapter with a 2x magnification lens (Zeiss) to connect the camera and microscope.

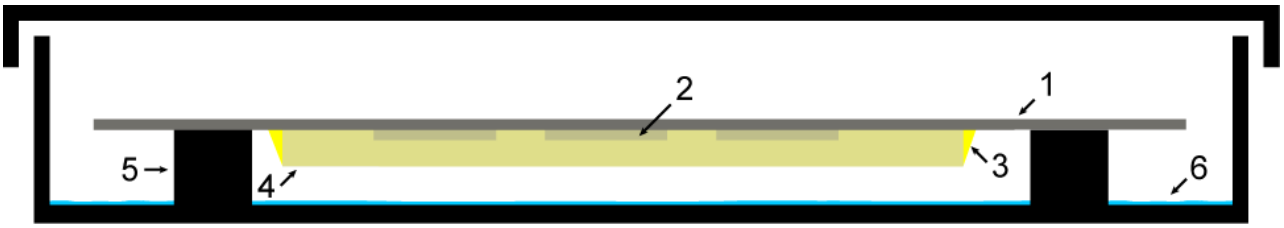

Figure 9: Schematic drawing illustrating the hanging drop Xgal staining of cryosections.

The Xgal staining is performed in a light nontransparent staining chamber that can be closed. With this staining setup, any crystals, which are usually formed during the Xgal staining procedure, will not be sticking to the tissue, but instead to the parafilm. 1) Object slide. 2) Cryosections on object slide. 3) Xgal staining solution covering the cryosections completely. 4) Parafilm which is kept on the object slide by the surface tension of the Xgal staining solution. 5) Guide rails to place the object slide on. 6) Tap water which evaporates, as a result of the warm atmosphere, during the Xgal staining (37 °C).

Protocol:

1. Thaw object slide with cryosections for 10 minutes.
2. Wash object slide for 10 minutes in 1 x PBS.
3. Wash object slide three times for 10 minutes with Xgal wash buffer.
4. Apply 200 µL of Xgal staining solution to the sections and cover them with the curved Parafilm. Place the object slide face down inside the staining chamber. During the staining, keep the staining chamber inside an incubator or heating room with 37 °C. The staining time depends on the genotype of the mouse line (CNP-lacZ: 2 hours and GC-B-lacZ: 16 hours).
5. Remove the Parafilm carefully with tweezers.
6. Wash tissue three times with Xgal wash buffer for 10 minutes.
7. Remove as much liquid as possible from the object slide, but make sure that the sections are still covered.
8. Apply 50 µL of the NFR solution to each section on an object slide. Make sure sections are completely covered.
9. Incubate sections with NFR for 10 minutes.

10. Remove NFR by dipping the complete object slide five times into a wash cuvette filled with ddH_2O.
11. Overlay stained cryosections with mounting medium and place coverslip on top. Dry mounting medium for 1 day.
12. Seal coverslip with nail polish.
13. The stained cryosections should be documented within 2 to 7 days.

3.2.8. Immunofluorescence double staining of cryosections

The design of the IF staining needs to be carefully considered. Newly ordered antibodies have to be tested for optimal staining results by adjusting the antibody dilution and storage temperature (4 °C vs. -20 °C vs. -80 °C) before using. In order to identify the optimal antibody dilution, a dilution row is performed. The signal-to-noise ratio should be calculated and greater than 3 (formula: $\frac{intensity\ (specific\ staining)}{intensity\ (background\ staining)}$). The best staining result is then correlated with a negative control (tissue from a respective KO mouse or secondary antibody control). Use the MOM-Kit (M.O.M.™ Kit, cat.nr.: BMK-2202, Vector Labs) if one of the primary antibodies was generated in mouse. The MOM-Kit provides a “blocking reagent” for blocking steps and a “protein concentrate” for the antibody incubation steps. The MOM-Kit blocking step and the incubation of the mouse antibody should be performed as second antibody staining to prevent unspecific binding of the first antibody staining with the MOM-Kit reagents.

Materials:

- Wash cuvette for object slides with volumetric capacity of 50 mL.
- PAP-Pen (Super PAP Pen Liquid Blocker, cat.nr.: N71310, Science Services).
- Staining chamber with guide rails to place the slide on.
- IF wash buffer:
  0.1% (v/v) Triton X-100 in 1 x PBS.
- IF blocking buffer:
  1% (w/v) NGS in IF wash buffer.
- Antibody solution:
  Primary or secondary antibody diluted in IF blocking buffer.
- MOM-Kit blocking buffer:
  3.6 % (v/v) blocking reagent in IF wash buffer.
- Antibody solution with MOM-Kit:
  Primary and secondary antibody diluted in 8% (v/v) protein concentrate in IF wash buffer.
- Immu-Mount (**3.2.5.**; Materials).

Protocol:

1. Thaw object slide with cryosections for 10 minutes.
2. Wash object slide for 10 minutes in 1 x PBS.
3. Draw a fat border around the area of all sections on the object slide.
4. Block tissue with 300 µL IF blocking buffer for 1 hour.
5. Incubate tissue with 200 µL of the first primary antibody solution overnight at 4 °C.
6. Wash tissue three times with wash buffer for 10 minutes.
7. Incubate tissue with 200 µL of the first secondary antibody solution for 2 hours.
8. Wash tissue three times with wash buffer for 10 minutes.
9. If MOM-Kit is used:
    - Block tissue with 300 µL MOM-Kit blocking buffer for 1 hour
    - Wash tissue three times with wash buffer for 10 minutes.
10. Incubate tissue with 200 µL of the second primary antibody solution overnight at 4 °C (! Dilute mouse primary antibody in “antibody solution with MOM-Kit” !).
11. Wash tissue three times with wash buffer for 10 minutes.
12. Incubate tissue with 200 µL of the second secondary antibody solution for 2 hours. (! Dilute mouse antibody-targeted secondary antibody in “antibody solution with MOM-Kit” !). Also add DAPI (**3.2. Table 5**) to the solution.
13. Wash tissue three times with wash buffer for 10 minutes.
14. Cover stained cryosections with Immu-Mount and cover slip.
15. Dry Immu-Mount for 1 day and seal cover slip with nail polish.
16. Keep at 4 °C until documentation. Antibody staining is usually stable for up to 3 months.

3.2.9. Documentation of IF staining with a laser scanning microscope

The laser scanning microscope (LSM) is a confocal microscope that allows the user to focus on focal planes up to 50 µm to 100 µm inside the tissue. It is used to acquire high-resolution images of IF stained cryosections and confocal high-resolution images of different layers of an IF stained whole mount tissue (e.g. colon).

Materials:

- Microscopy setup:
  Zeiss LSM 710 setup consisting of an inverted Axio Observer.Z1 stand (Zeiss) equipped with a diode laser (405 nm), a multiline Argon laser (25 mW; 458 nm, 488 nm, 514 nm), a diode-pumped solid-state laser (561 nm), a He/Ne laser (633 nm), and an air objective (Plan-APOCHROMAT 20x/0.8; Zeiss). Confocal images are acquired using a Zeiss LSM 710 3-channel spectral detector and the ZEN Black software (Zeiss). DAPI is excited with the 405 nm diode laser, Alexa Fluor 488 with the Argon laser 488 nm line, and Cy3 with the 561 nm solid-state laser.

- The smart setup is used to configure the excitation and emission setup. The channel arrangement for the best signal is chosen.
- Settings
  resolution: 1600 x 1600, scanning: bidirectional, images averaged: 16, averaging method: mean, pinhole size: 1 µm.

Protocol for documenting stained cryosections:

1. Place positive control in the light path of the microscope.
2. Use epifluorescence light source and the oculars to look at all sections on the object slide to compare the equal quality of the staining pattern. Choose a representative region and adjust the laser power and the master gain to the specific staining observed.
3. Acquire image.
4. Place negative control (secondary antibody control) in the light path of the microscope.
5. Use epifluorescence light source and the oculars to look at all section on the object slide to ensure that the staining pattern seen in the positive control is not present on the negative control. Choose the same type of region that is documented for the positive control.
6. Acquire image with the same settings as the positive control:
   If the staining pattern, seen in the image of the positive control, is not present in the negative control, it is a primary antibody-specific staining.
7. Acquire overview images with the 20x objective and magnified images with the 63x oil objective.

Protocol for documenting whole tissue:

1. Use epifluorescence light source and the oculars to look at the staining across the whole tissue. Choose a representative region and adjust the laser power and the master gain to the antibody-specific staining observed.
2. Acquire image with 20x objective and magnified images with the 63x oil objective.
3. Use the tile scan function to image a large part of the tissue for subsequent cell counting. Since the proximal and distal colon are stained together, two tile scans are performed on the proximal and two on the distal part of the colon.

3.2.10. Image editing and preparation of figures

Images taken with the Canon EOS 750D camera are provided in the JPEG format. The images are rotated and cut in Fiji and then converted into the TIFF format. The LSM images are loaded into Fiji, converted from the LSM format to TIFF, and then edited using Photoshop. Only linear editing algorithms, like brightness and contrast adjustments or tonal value corrections, are applied to the images. Figures are prepared with Adobe illustrator. Scalebar sizes are calculated based on the size of the camera chip and the optical aberrations used.

3.2.11. Quantifying cell populations based on immunofluorescence

Cell counting can only be performed if the IF staining is properly established (concentration and blocking is optimized and negative control shows no staining). Images, which are acquired with a confocal microscope like the LSM710, provide a high-level of detail and, thus, aid in identifying positively stained cells. The LSM images are edited in Fiji and cells are counted using the "Cell Counter" plugin (Fiji/Plugins/Analyze/Cell Counter/).

In this study, βGal is probed in IF whole tissue double staining. To identify βGal expressing cells, the nuclear-localized staining, which is seen in tissue of CNP-lacZ or GC-B-lacZ mice, is correlated with the nuclear DNA (DAPI) staining. Cells with an overlapping staining (βGal and DNA) are considered true-positive. βGal positive cells without a DNA staining or a staining in the cytosol are considered false-positive cells. True-negative and false-negative cells cannot be distinguished.

Marker protein specific IF staining is correlated with already published expression patterns to identify true-positive staining patterns in the respective GI segment.

3.3. Western blot-based expression analysis

The identification of proteins in tissue lysates is achieved using discontinued sodium dodecyl sulfate polyacrylamide gel electrophoresis (SDS-PAGE) to separate the proteins, western blot to transfer the proteins to a polyvinylidene fluoride (PVDF) membrane, and antibodies to probe and visualize the protein bands on the PVDF membrane.

3.3.1. Tissue lysis

Two different tissue lysis protocols are used in this thesis. The detection of WT GC-B is performed with an antibody that requires tissue lysis and membrane enrichment. The antibody used for detecting the recombinant, HA-tagged GC-B (GC-B-HA mouse line) does not require membrane enrichment. Hence, the crude tissue lysis protocol is performed.

3.3.1.1. Crude tissue lysis

The crude tissue lysis protocol is performed with tissue from a GC-B-HA mouse. The volumes of this protocol are designed for 40 mg of tissue and will lead to a final protein concentration of about 25-30 µg/µL.

Materials:

- Protease inhibitor 10 x stock (cOmplete™, Mini Protease Inhibitor Cocktail, cat. no. 04693124001, Roche):
  Solve 1 pill in 7 mL ddH_2O.

- PMSF (phenylmethylsulfonylfluoride; cat.no.: 6367.1, Roth):
  100 mM PMSF in ddH_2O.
- Lysis buffer:
  50 mM Tris/Cl pH 8.0, 100 mM NaCl, 5 mM EDTA, 2 % (w/v) SDS, 2.5 mM PMSF and 10 % (v/v) of protease inhibitor 10 x stock.

Protocol:

1. Weight tissue and prepare lysis buffer.
2. Wash tissue once with 1 mL PBS and transfer tissue to a 1.5 mL reaction tube (*note*: make sure washing buffer is completely removed).
3. Add 7.5 µL lysis buffer per 1 mg tissue and homogenize tissue using a pistil for reaction tubes.
4. Incubation homogenized tissue for 5 minutes on ice.
5. Homogenize tissue using a pistil for reaction tubes.
6. Denaturize lysate for 5 minutes at 95 °C.
7. Incubate sample for 5 minutes on ice.
8. Spin down sample (13 000 g, 4 °C, 15 minutes) and collect the supernatant as crude tissue lysate.
9. Proceed with protein quantification (*note*: lysis buffer interferes with protein quantification assays, such as the Lowry assay, at a sample dilution of 1:10. Sample dilution of 1:100 in water does not interfere with the Lowry assay anymore).

3.3.1.2. Tissue lysis and membrane enrichment

Membrane enriched tissue lysates are generated using the Mem-PER™ Plus Kit (Mem-PER™ Plus Membrane Protein Extraction Kit, cat.nr.: 89842, Thermo). The procedure described in this paragraph leads to an enrichment of the membrane fraction which can still be contaminated with high abundant cytosolic proteins. 40 mg of tissue lysed with this protocol will lead to a final membrane protein concentration of about 3-4 µg/µL.

Materials:

- Protease inhibitor 10 x stock (**3.3.1.1.**; Materials)
- PMSF (**3.3.1.1.**; Materials)
- Mem-PER™ Plus Kit:
  - Wash buffer
  - Permeabilization buffer:
    Freshly add 2.5 mM PMSF and 10 % (v/v) of protease inhibitor 10 x stock.
  - Solubilization buffer:
    Freshly add 2.5 mM PMSF and 10 % (v/v) of protease inhibitor 10 x stock.

Protocol:

1. Weight tissue and prepare the buffers.
2. Wash tissue once with 25 µL tissue wash buffer per 1 mg tissue and transfer tissue to a 1.5 mL reaction tube (*note:* make sure washing buffer is completely removed).
3. Add 10 µL permeabilization buffer per 1 mg tissue and homogenize the tissue using a pistil for reaction tubes (*note:* make sure tissue is well homogenized before proceeding to the next step but do not take longer than 3 minutes to do so).
4. Incubate homogenized tissue for 15 minutes on ice.
5. Incubate homogenized tissue for 10 minutes on a spinning wheel in the cold room.
6. Spin down enriched membrane fraction (13 000 g, 4 °C, 15 minutes) and collect the supernatant as cytosol fraction.
7. Mix 5 µL of solubilization buffer per 1 mg tissue with pellet and resuspend the homogenized membrane fraction with a pipette.
8. Incubate the homogenized membrane fraction for 30 minutes on a spinning wheel in the cold room.
9. Spin down homogenized membrane fraction (13 000 g, 4 °C, 15 minutes) and collect the supernatant as membrane fraction.
10. Proceed with protein quantification (*note*: permeabilization buffer and solubilization buffer interfere with protein quantification assays such as the Lowry assay at a sample dilution of 1:10. Sample dilution of 1:100 in water does not interfere with the Lowry assay anymore).

3.3.2. Protein quantification of tissue lysates using Lowry assay

Protein quantification is performed with a Lowry assay-based protein quantification kit (Total Protein Kit, Micro-Lowry, Peterson's Modification, cat.nr.: TP0300-1KT, Sigma-Aldrich). Since the lysis buffers used in both lysis protocols interferes with the Lowry reagent at dilutions of up to 1:10, tissue lysates are prediluted in ddH_2O (1:100). All samples are prepared in duplicate.

Materials:

- BSA protein standard (0, 12.5, 25, 50, 100, 200, 400 µg/mL):
  BSA solved in ddH_2O.
- 5 x SDS-loading buffer:
  50 mM Tris/Cl pH 8.0, 40 % (v/v) glycerol, 15 % (w/v) SDS, 25 % (v/v) 2-mercaptoethanol and 0.1 % (w/v) bromphenol blue in ddH_2O.

Protocol:

1. Mix 5 µL of the diluted tissue lysate (1:10 to 1:100 diluted in ddH_2O) with 95 µL ddH_2O.
2. Mix 5 µL of the blank with 95 µL ddH_2O.
3. Transfer 100 µL of each BSA protein standard to a new reaction tube.
4. Add 100 µL of Lowry reagent to each sample.

5. Mix samples and incubated for 20 minutes at room temperature.
6. Add 50 µL Folin reagent to each sample.
7. Mix samples and incubated for 30 minutes at room temperature in the dark.
8. Transfer 200 µL of each sample to a flat-bottom 96 well plate (*note*: prevent air bubble formation, if air bubbles are present pop bubbles with a lighter).
9. Measure light absorption at 620 nm wavelength with an ELISA plate reader (Multiskan EX, Thermo).
10. Calculate mean of duplicates and subtract the blank corresponding to the respective sample.
11. Correlate sample absorption value with linearly fitted standard curve and interpolate sample protein concentration.
12. Dilute all samples to the same concentration but not below 1 µg/µL using ddH_2O and 5 x SDS-loading buffer.

3.3.3. Discontinuous SDS-PAGE

Proteins are separated using a discontinuous SDS-PAGE. The gel hand casting system and gel electrophoresis chamber are from BioRad (Mini-PROTEAN® Tetra Vertical Electrophoresis Cell, 4-gel, for 1.5 mm thick handcast gels; cat. no. 1658006FC, BioRad).

Materials:

- Rotiphorese (ROTIPHORESE®Gel 30, cat.nr.: 3029.1, Roth)
- 4 x Tris/SDS (pH 8.8):
  15 mM Tris and 4 % (w/v) SDS in ddH_2O. Adjust pH.
- 4 x Tris/SDS (pH 6.8):
  5 mM Tris and 4 % (w/v) SDS in ddH_2O. Adjust pH.
- Tetramethyl ethylene diamine (TEMED, cat.nr.: 2367.3, Sigma-Aldrich)
- APS (20 % stock):
  20 % (w/v) APS in ddH_2O.
- 10 x SDS running buffer:
  250 mM Tris, 14.4 % (w/v) glycine and 1 % (w/v) SDS in ddH_2O.
- Protein ladder (PageRuler™ Prestained Protein Ladder, cat.nr.: 26616, Thermo)

Table 6: Composition of separating and stacking gel.

component	10 % separating gel (v/v)	12 % separating gel (v/v)	4 % stacking gel (v/v)
Rotiphorese	33.4 %	40 %	13.4 %
4 x Tris/SDS (pH 8.8)	25 %	25 %	-
4 x Tris/SDS (pH 6.8)	-	-	25 %
ddH_2O	41 %	34.4 %	61 %
TEMED	0.1 %	0.1 %	0.1 %
APS (20 % stock)	0.5 %	0.5 %	0.5 %
resolving range:	20-300 kDa (GC-B antibody)	10-200 kDa (HA antibody)	-

Protocol:

1. Assemble the gel casting system with 1.5 mm glass plates.
2. Prepare 10 mL of the respective separating gel according to **Table 6**.
3. Pour separating gel between class plates and overlay gel with 2 mL isopropanol.
4. Let separating gel polymerize for 30 minutes at room temperature.
5. Remove isopropanol and prepare 5 mL of the stacking gel (**Table 6**).
6. Pour stacking gel between class plates and place comb inside the stacking gel. Avoid air bubble formation.
7. Let stacking gel polymerize for 30 minutes at room temperature.
8. Remove comb and use gel to assemble the electrophoresis chamber.
9. Fill the inner chamber with 1 x SDS running buffer and wait 2-3 minutes to check for leakage.
10. Fill the outer chamber with 1 x SDS running buffer until the height marked on the outer chamber.
11. Load prepared protein samples (40 µg tissue lysate) and protein ladder (5 µL).
12. Separate proteins:
    - Run gel for approx. 5 minutes at 100 V (until blue border enters separating gel).
    - Run gel for 1 hour at 150 V (until blue border reaches the lower end of the separating gel).
13. Proceed with western blot.

3.3.4. Western blot

After protein separation, the proteins are transferred from the gel to the PVDF membrane using a semi dry western blot aperture (Trans-Blot® SD Semi-Dry Transfer Cell, cat.nr.: 1703940, Bio-Rad).

Materials:

- Whatman papers (blotting paper, cat.nr.: GB46, A. Hartenstein) and PVDF membrane (PVDF-Western-Blot-Membrane, cat.nr.: 03010040001, Roche).
- Anode buffer I (pH 10.4):
  300 mM Tris and 20 % (v/v) methanol in ddH_2O. Adjust pH.
- Anode buffer II (pH 10.4):
  30 mM Tris and 20 % (v/v) methanol in ddH_2O. Adjust pH.
- Cathode buffer (pH 7.6):
  30 mM Tris, 20 % (v/v) methanol and 40 mM 6-aminocapronic acid in ddH_2O. Adjust pH.
- 10 x TBS (pH 8.0):
  100 mM Tris and 1.5 M NaCl in ddH_2O. Adjust pH.

- TBS-T:
  10 % (v/v) of 10 x TBS and 0.1 % (w/v) Tween-20 in ddH_2O.
- Blocking buffer:
  5 % (w/v) powdered milk in TBS-T.
- Primary antibody solution:
  5 % (w/v) BSA and 0.05 % (w/v) NaN_3 in TBS-T.
- Secondary antibody solution:
  1 % (w/v) powdered milk in TBS-T.
- ECL solution (WesternBright® ECL HRP substrate, cat.nr.: K-12045-D20, Advansta):
  Two components, the Luminol/enhancer solution and detection reagent.

Protocol:

1. Prepare 16 Whatman papers (WP) and one PVDF membrane in the shape of the gel.
2. Disassemble electrophoresis chamber, take out the gel, and remove stacking gel.
3. Incubate WPs and PVDF membrane at least 5 minutes in respective buffer and assemble blot sandwich from anode to cathode:
   4x WPs (anode buffer I), 4x WPs (anode buffer II), PVDF membrane (methanol), gel, 8x WPs (cathode buffer)
4. Remove air bubbles with a round object that can be rolled over the blot sandwich.
5. Run semi dry western blot for 1 hour and 20 minutes at 60 mA per gel.
6. Disassemble blot sandwich. For incubation in different antibody solutions, cut the PVDF membrane and label the membrane pieces accordingly.
7. Block membrane with 50 mL blocking buffer for 1 hour at room temperature in a plastic tray shaking on a shaking table at 10-30 rpm.
8. Wash membrane with 50 mL washing buffer in plastic tray.
9. Incubate membrane in 5-10 mL of the primary antibody solution in a 50 mL reaction tube at 4 °C overnight.
10. Wash membrane three times with 50 mL TBS-T.
11. Incubate membrane in 5-10 mL of the secondary antibody solution for 2 hours at room temperature in a 50 mL reaction tube.
12. Wash membrane three times with 50 mL TBS-T.
13. Develop western blot:
    - Mix components of the ECL solution 1:1 and add mixture on top of western blot membrane.
    - Record chemiluminescence reaction using a western blot developer.
    - Also record brightfield image.
14. Cut western blot images together using Fiji.

3.4. cGMP-FRET measurements

Quantitative measurements of intracellular cGMP levels in cell culture or tissue is performed with the cGMP-FRET (Förster resonance energy transfer, abbr.: FRET) biosensor: cGi500. This ratio metric biosensor binds cGMP and changes its emitting fluorescence correspondingly (**Figure 10**). The R26-cGi500(L2) mouse line allows for a Cre-inducible and, therefore, cell type-specific expression of this biosensor. Two versions of the cGi500 biosensor are used in this study. Colonic neurons from the ENS are labeled with a membrane bound version of the sensor (mcGi500) and colonic SMCs are labeled with a cytosolically localized version (cGi500).

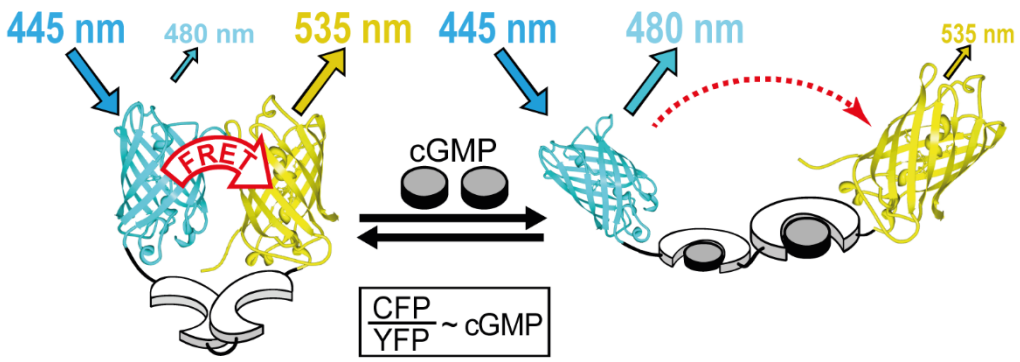

Figure 10: The cGMP-FRET biosensor cGi500.

The cGMP-FRET biosensor cGi500 consists of two fluorophores, cyan fluorescent protein (CFP) and yellow fluorescent protein (YFP) which are interconnected by a linker with a cGMP-binding domain. As long as cGMP is not bound to the linker, CFP and YFP are in close proximity and, therefore, allow energy transfer from CFP (FRET donor) onto YFP (FRET acceptor). The binding of cGMP to the linker then leads to a conformational change that separates CFP from YFP. Hence, the energy transfer decreases. In a cGMP-FRET measurement on cells or tissues that express cGi500, only the CFP fluorophore is excited, but the CFP and YFP emissions are recorded. Division of the CFP by the YFP emission signal results in a ratio metric number that is proportional to the change in intracellular cGMP levels. Figure taken from [139].

3.4.1. Cultivation of colon enteric neurons from the myenteric plexus

After isolation, the colon is cut open along the mesenteric border and the mucosal layer is pulled away from the muscle layer. The muscle layer is then cut down into pieces of 0.2 cm², kept in a 15 mL reaction tube with HBSS, and used for digestion.

Materials:

- 24-well plate
- Coverslips, round, 12 mm Ø (cat.nr.: 631-1577, VWR)
- NaOH/ethanol solution:
  Solve 4 pellets of NaOH in 10 mL ddH_2O and add 25 mL of 96 % (v/v) ethanol.
- Poly-D-lysine stock (Poly-D-Lysine, cat.nr.: A3890401, GIBCO):
  50 µg/mL Poly-D-lysine in ddH_2O.

- Laminin (Natural Mouse Laminin, cat.nr.: 23017-015, invitrogen):
  20 µg/mL in 1 x PBS.
- 10 x HBSS (Hanks balanced salt solution 10 x stock, cat.nr.: 14065056, GIBCO)
- 1 x HBSS:
  Dilute 10 x HBSS 1:10 in ddH_2O.
- Full medium:
  88.8 % (v/v) DMEM/F-12 (DMEM/F-12 (1:1), cat.nr.: 21331020, GIBCO), 2 % (v/v) heat inactivated fetal bovine serum (FBS, cat.nr.: 10270-106, GIBCO), 5 % (v/v) chicken embryo extract (CEE, cat.nr.: C3999, USBio), 1 % (v/v) of 100 x Penn/Strep (Penicillin-Streptomycin 10,000 U/mL, cat.nr.: 15140122, GIBCO), 0.2 % (v/v) of 500 x Gentamicin/Amphotericin (Gentamicin/Amphotericin 500 x stock, cat.nr.: R01510, GIBCO), 1 % (v/v) N2 (N-2 Supplement 100x, cat.nr.: 17502048, Thermo) and 2 % (v/v) B27 (B-27®Supplement 50x, cat.nr.:17504044, GIBCO).
- Collagenase digestion medium:
  1 mg/mL Collagenase IV (cat.nr.: C7926, Sigma-Aldrich), 1 mg/mL Hyaluronidase (cat.nr.: H3506, Sigma-Aldrich), 0.5 mM $CaCl_2$ and 10 mM HEPES (pH 7.4) in DMEM/F12.
- Trypsin digestion medium:
  10 % (v/v) of 10 x Trypsin/EDTA (Trypsin-EDTA 0.5 %, cat.nr.: 15400054, GIBCO) and 10 % (v/v) 10 x HBSS in ddH_2O.
- Neutralizing solution:
  0.5 mg/mL Desoxyribonuclease I (DNase I, cat.nr.: 10104159001, Roche) and 1 mg/mL BSA in DMEM/F-12.
- Trypan blue:
  0.4% (w/v) Trypan blue (Trypan Blue Solution 0.4 %, cat.nr.: 15250061, GIBCO) in ddH_2O.

Protocol:

1. Preparing coverslips for coating:
   - Incubate coverslips in NaOH/ethanol solution overnight.
   - Discard NaOH/ethanol solution and wash coverslips three times with ddH_2O.
   - Incubate coverslips in 50 mL of 1 M HCl solution overnight.
   - Discard 1 M HCl solution and wash coverslips three times with ddH_2O.
   - Wash coverslips for 1 hour in 96 % (v/v) ethanol.
   - Discard 96 % (v/v) ethanol and dry coverslips under the steam hood in a 150 mm petri dish.
2. Coating of coverslips:
   - Load coverslips on 24-well plate.
   - Incubate coverslips with 50 µg/mL Poly-D-lysine overnight.
   - Wash three times with PBS.
   - Incubate coverslips with 20 µg/mL Laminin overnight.
   - Wash three times with PBS.

3. Spin down tissue pieces at 200 g for 5 minutes at 4 °C and discard supernatant.
4. Incubate tissue pieces in 1 mL prewarmed collagenase digestion medium per colon used in preparation at 37 °C for 20 minutes. Shake suspension every 5 minutes (apply shear forces after 12 to 16 minutes using a 1000 µL pipette, do not triturate tissue pieces at this point).
5. Spin down tissue pieces at 200 g for 5 minutes at 4 °C and discard supernatant.
6. Stop digest by adding 2 mL HBSS per 1 mL collagenase digestion medium.
7. Shake tissue pieces in a 10 mm petri dish filled with 20 mL HBSS for 10 minutes at 15 rpm.
8. Transfer tissue pieces with as little as possible HBSS to new 10 mm petri dish filled with 20 mL HSS and shake for 10 minutes at 15 rpm.
9. Transfer tissue pieces to a new 15 mL reaction tube transferring a maximum of 2 mL HBBS with the tissue pieces.
10. Spin down tissue pieces at 200 g for 5 minutes at 4 °C and discard supernatant.
11. Incubate tissue pieces in 1 mL Trypsin digestion medium per colon used in preparation at 37 °C for 12 minutes. Shake suspension every 2 minutes (apply shear forces after 8 minutes using a 1000 µL pipette, do not triturate tissue pieces at this point).
12. Stop digest by adding 2 mL neutralizing solution per 1 mL Trypsin digestion medium.
13. Spin down tissue pieces at 200 g for 5 minutes at 4 °C and discard supernatant.
14. Add 1 mL neutralizing solution per 1 mL Trypsin digestion medium.
15. Triturate tissue pieces starting with a 1000 µL pipette, then use a 100 µL pipette and as a final tool use a Pasteur-pipette to individualize neurons. Use an open flame to reduce the opening of the Pasteur-pipette to an approximate diameter of 0.2-0.5 mm. At the end, individual tissue piece should not be visible by eye.
16. Add 10 mL HBSS.
17. Spin down remaining tissue pieces at 10 g for 1 minute at 4 °C.
18. Transfer supernatant into fresh 15 mL reaction tube, spin down cells at 200 g for 5 minutes at 4 °C and discard supernatant.
19. Add 1 mL full medium.
20. Incubate 18 µL of the cell suspension and 2 µL Trypan blue for 5 minutes in a separate 1.5 mL reaction tube.
21. Transfer Trypan blue stained cell suspension to Neubauer counting chamber and count cells.
22. Seed cell suspension at 100.000 cells/coverslip.
23. Incubate 24-well plate with neuron cultures at 37 °C and 6 % (v/v) CO_2.
24. Cultures are measured after 3 to 5 days in culture.

3.4.2. Cultivation of colonic smooth muscle cells

After isolation of the colon, it is cut open along the mesenteric border and the mucosal layer is pulled away from the muscle layer. The muscle layer is then cut down into pieces of 0.2 cm², kept in a 15 mL reaction tube with Ca^{2+} free medium, and used for digestion.

Materials:

- 24-well plate.
- Coverslips (**3.4.1.**; Materials).
- Ca^{2+} free medium (pH 7.4):
  85 mM L-glutamine, 60 mM NaCl, 10 mM HEPES, 5.6 mM KCl, 1 mM $MgCl_2$ in ddH_2O. Adjust pH, autoclave and store at 4 °C.
- Papain digestion medium:
  0.7 mg/mL Papain (cat.nr.: P4762, Sigma-Aldrich), 1 mg/mL DTT and 1 mg/mL BSA in Ca^{2+} free medium.
- Collagenase digestion medium:
  1 mg/mL Collagenase IV (**3.4.1.**; Materials), 1 mg/mL Hyaluronidase (**3.4.1.**; Materials) and 1 mg/mL BSA in Ca^{2+} free medium.
- Full medium:
  10 % (v/v) FBS (**3.4.1.**; Materials), 1 % (v/v) Penn/Strep (**3.4.1.**; Materials) and 0.2 % (v/v) of 500 x Gentamicin/Amphotericin (**3.4.1.**; Materials) in DMEM (DMEM high glucose GlutaMAX™ Supplement pyruvate, cat.nr.: 31966021, GIBCO).
- Trypan blue (**3.4.1.**; Materials).

Protocol:

1. Spin down tissue pieces at 200 g for 5 minutes at 4 °C and discard supernatant.
2. Incubate tissue pieces in 1 mL prewarmed Papain digestion medium per colon used in preparation at 37 °C for 1 hour. Shake suspension every 15 minutes.
3. Spin down tissue pieces at 200 g for 3 minutes at 4 °C and discard supernatant.
4. Incubate tissue pieces in 1 mL prewarmed collagenase digestion medium per colon used in preparation at 37 °C for 12 minutes. Shake suspension every 2 minutes (apply shear forces after 8 minutes using a 1000 µL pipette and try to triturate tissue pieces at this point).
5. Stop digest by adding 2.5 mL full medium per colon used in preparation.
6. Spin down tissue pieces at 200 g for 8 minutes at 4 °C and discard supernatant.
7. Resuspend cell pellet in 2 mL culture medium per colon used in preparation.
8. Spin down remaining tissue pieces at 10 g for 1 minute at 4 °C.
9. Transfer supernatant into fresh 15 mL reaction tube, spin down cells at 200 g for 5 minutes at 4 °C and discard supernatant.
10. Add 1 mL full medium.
11. Incubate 18 µL of the cell suspension and 2 µL Trypan blue for 5 minutes in a separate 1.5 mL reaction tube.

12. Transfer Trypan blue stained cell suspension to Neubauer counting chamber and count cells.
13. Seed cell suspension at 40.000 cells/coverslip.
14. Incubate 24-well plate with SMC cultures at 37 °C and 6 % (v/v) CO_2.
15. Cultures are measured after 3 days in culture.

3.4.3. *In vitro* cGMP-FRET measurements

Cultivated cells are measured at room temperature.

Materials:

- Microscopy setup (**Figure 11**):
  Inverted microscope (Axiovert 200 with 1.0/1.6x Optovar lens, Zeiss) with fluorescence grade objectives (Plan NeoFluar 10x/0.30 and EC Plan NeoFluar 40x/1.30 Oil, Zeiss) and a light source (Oligochrome, TILL Photonics). The FRET filter set consists of a filter cube with a 445/20 CFP excitation filter and a 470 nm dichroic mirror (CHROMA). The YFP filter set consists of a 497/16 nm excitation filter, a 516 nm dichroic mirror and a 535/22 nm emission filter (CHROMA). The RFP filter set consists of a 543/22 nm excitation filter, a 565 nm dichroic mirror, and a 610/75 nm emission filter (CHROMA). A beam splitter (Micro-Imager DUAL-View, Photometrics) with 05-EM insert (516 nm dichroic mirror, 450/50 nm CFP and 535/40 nm YFP emission filters) is placed between microscope and camera. The camera is a cooled electron-multiplying charge-coupled device camera (Retiga R1, QImaging).
- Superfusion system (**Figure 11**):
  FPLC pump (Pharmacia P-500, GE Healthcare), FPLC injection valves (Pharmacia V-7, GE Healthcare), superfusion chamber (RC-25, Warner instruments), magnetic platform (Warner instruments), and a vacuum pump with adjustable vacuum (Laboport N86, KNF Neuberger). Tubing, connectors, and syringes are from Warner instruments.
- Silicon vacuum grease (KORASILON®, cat.nr.: 0857.1, Roth).
- 30 % ethanol:
  30 % (v/v) ethanol in ddH_2O.
- 70 % ethanol:
  70 % (v/v) ethanol in ddH_2O.
- 250 x stock $_D$-glucose (for imaging buffer):
  2.5 M $_D$-glucose in ddH_2O. Autoclave and aliquot into 2 mL reaction tubes.
- Imaging buffer:
  140 mM NaCl, 5 mM KCl, 1.2 mM $MgCl_2$, 2 mM $CaCl_2$ and 5 mM HEPES in ddH_2O. Aliquot into 500 mL bottles and autoclave bottles. On the day of the experiment freshly add 2 mL of the 250 x $_D$-glucose stock to 500 mL of the imaging buffer.
- Drugs, inhibitors and vehicle controls are diluted in imaging buffer (**3. Table 3**).
- Image acquisition and online analysis are performed with the VisiView software (Visitron).

Protocol:

1. Prepare experimental setup:
    - Turn on all parts of the experimental setup and change the superfusion solvent from 30 % (v/v) ethanol to imaging buffer (“solvent change” button on the FPLC pump). Make sure all tubes are equilibrated and filled with imaging buffer.
    - Thaw drugs and keep them on ice during the measurement.
2. Calibrate split view using a gridded object plate.
3. Assemble imaging chamber:
    - Apply silicon to the magnetic platform and the bottom of the superfusion chamber.
    - Stick coverslip with cells to bottom of the silicon covered superfusion chamber.
    - Place superfusion chamber with the coverslip mounted to it onto the magnetic platform and lock everything into position.
4. Fill imaging chamber with 500 µL imaging buffer, to ensure that cells do not dry out, and clean the coverslip on the down facing site of the chamber with 70 % ethanol.
5. Mount magnetic platform with imaging chamber onto microscope, connect superfusion system to the imaging chamber and establish a steady flow of 60 mL/h.
6. Use the YFP filter set to search for a representative region on the coverslip.
7. Change filter to the FRET filter set and set the following settings:
    - Wavelength series panel: CFP and YFP channels (split view option activated), 300 ms exposure time and 4x4 binning.
    - Time lapse panel: 5 seconds frame time.
8. Make a test run for testing the exposure time with the view loop button. Use the measure line option to estimate the signal-to-noise ratio of cells compared to a background region within the field of view. The signal-to-noise ratio should be 3 or higher.
9. Darken the room, check the superfusion flow, and start the time lapse experiment with an adjusted exposure time:
    a) Record 30 frames for baseline normalization. Prepare drug dilution in imaging buffer and load drug onto loop 2.
    b) Apply cGMP stimulating drug (e.g. ANP, BNP, CNP, DEA-NO) by opening valve 2 which connects loop 2 with the imaging chamber and the FPLC pump. With a flow rate of 60 mL/h (1 mL/min), it takes 24 frames (2 minutes) to empty loop 2 completely. Close valve 2 after 30 frames in total.
    c) Wait until signal from cGMP stimulating drug reaches baseline again. If no signal is observed, wait at least 6 minutes before the next drug application. In the meantime, wash loop 2 three times with imaging buffer.
10. Protocol for drug testing experiments:
    - Repeat drug application (9.b) and waiting period (9.c) until the measurement is done.

11. Protocol for PDE inhibitor experiments:
    - Perform drug application once (9.b and 9.c).
    - Load inhibitor dilution into loop 1 and the dilution for the inhibitor with the drug into loop 2.
    - Open valve 1 to connect loop 1 with the imaging chamber and the FPLC pump.
    - Open valve 2 after 60 frames to connect loop 2 with the imaging chamber and loop 1. This redirects the remaining 2 mL of the inhibitor dilution from loop 1 into loop 2 pushing the drug and inhibitor dilution onto the cells.
    - After a total time of 120 frames both loops are being closed.
    - Wait until signal reaches baseline again, but at least 10 minutes. In the meantime, wash loop 1 and loop 2 three times with imaging buffer.
    - Repeat first drug application again.
12. After the last drug is applied, let signal come back to baseline and stop the measurement.
13. To check the recombination of the culture, deactivate the beam splitter and acquire one image with the YFP filter set and one with the RFP filter set.

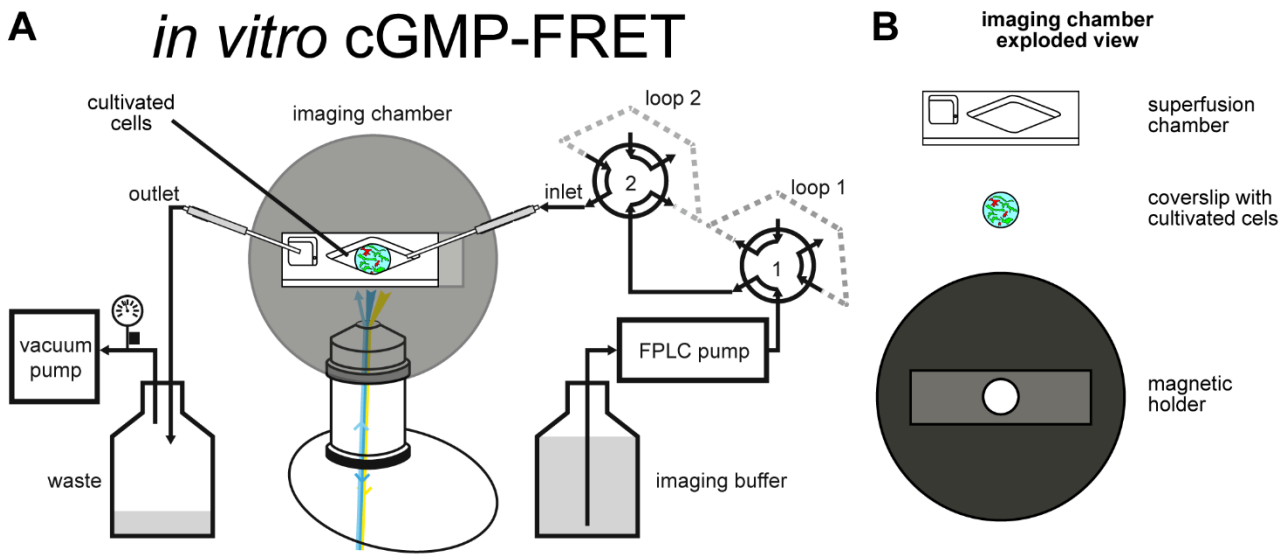

Figure 11: Microscopic setup for *in vitro* cGMP-FRET measurements.

A) Epifluorescence *in vitro* cGMP-FRET setup. The Zeiss Axiovert 200 is an inverted microscope equipped with fluorescence grade objectives and a FRET filter cube. It illuminates and collects light at the bottom of the imaging chamber where the coverslip with the cultivated cells is exposed through a hole in the magnetic holder. On the top site of the coverslip, the superfusion chamber allows for a regular flow. A FPLC (fast protein liquid chromatography) pump controls the inlet flow and pumps the imaging buffer from the stock bottle through two valves (valve 1 and valve 2, harboring loop 1 and loop 2) into the superfusion chamber. Loop 1 of valve 1 is a 7 mL loop used for inhibitor applications. Loop 2 is a 2 mL loop used for the application of cGMP-stimulating drugs like ANP, BNP, CNP, or DEA-NO. The outlet flow is controlled via a vacuum pump which creates a vacuum in the waste bottle (vacuum adjustable). The used imaging buffer is then sucked away from a separate reservoir of the superfusion chamber. The two reservoirs of the superfusion chamber allow for a steady flow, without the development of waves on the surface. Such waves could interfere with the measurement. B) Exploded view of the imaging chamber. Silicon grease is used to clue the superfusion chamber and the coverslip onto the magnetic holder. It also seals the gaps between the superfusion chamber and the coverslip to prevent any leaking.

3.4.4. *Ex vivo* cGMP-FRET measurements

Whole colonic tissue is isolated, cleaned, cut open at the mesenteric border, and then directly measured *ex vivo* with a spinning-disk confocal microscope at room temperature.

Materials:

- Microscopy setup (**Figure 12**):
  Upright microscope (Examiner.Z1, Zeiss), a Yokogawa CSU-X1 spinning disk confocal scanner (YOKOGAWA) with three diode lasers (445 nm, 488 nm and 561 nm) and two fluorescence grade water immersion objectives (W N-Achromat 10x/0.3 and W Plan-Apochromat 20x/1.0 DIC (UV), Zeiss). A Dual-View beam splitter (Photometrics) with a 505 nm dichroic mirror, 470/24 nm CFP and 535/30 nm YFP emission filters is placed between the spinning disk and the camera. The camera is a cooled electron-multiplying charge-coupled device camera (QuantEM 512SC, Photometrics). An additional light source is used for epifluorescence illumination at 400 nm, 450 nm, 500 nm and 561 nm (pE-2; CoolLED).
- Superfusion system (**Figure 12**):
  FPLC pump (Pharmacia P-500, GE Healthcare), FPLC injection valves (Pharmacia V-7, GE Healthcare), superfusion chamber (RC-26, Warner instruments), magnetic platform (Warner instruments), a slice hold-down (SHD-26H/10, Warner instruments), and a vacuum pump with adjustable vacuum (Laboport N86, KNF Neuberger). Tubing, connectors, and syringes are from Warner instruments.
- Silicon vacuum grease, 30 % ethanol, 70 % ethanol, and 250 x stock D-glucose (**3.4.3.**; Materials).
- 100 x Nifedipin stock (Nifedipin, cat.nr.: N7634, Sigma-Aldrich):
  100 µM Nifedipin in ddH_2O.
- 1000 x Hexamethonium stock (Hexamethonium, cat.nr.: H0879, Sigma-Aldrich):
  400 mM Hexamethonium in ddH_2O.
- Imaging buffer with contraction inhibitors:
  Imaging buffer is prepared as described before (**3.4.3.**; Materials). In addition to the D-glucose, 1 % (v/v) of the 100 x Nifedipin stock and 0.1 % (v/v) of the 1000 x Hexamethonium stock are freshly added to the imaging buffer.
- Drugs are diluted in imaging buffer (**3. Table 2**).
- Image acquisition and online analysis are performed with the VisiView software (Visitron).

Protocol:

1. Prepare experimental setup:
   - Turn on all parts of the experimental setup and change the superfusion solvent from 30 % (v/v) ethanol to imaging buffer (“solvent change” button on the FPLC pump). Make sure all tubes are equilibrated and filled with imaging buffer.
   - Thaw drugs and keep them on ice during the measurement.
2. Calibrate split view using a gridded object plate.
3. Assemble imaging chamber:

- Apply silicon to the magnetic platform and the bottom of the superfusion chamber.
- Stick coverslip to bottom of the silicon covered superfusion chamber.
- Place superfusion chamber with the coverslip mounted to it onto the magnetic platform and lock everything into position.

4. Clean the coverslip on the down facing site of the chamber with 70 % ethanol.
5. Fill chamber with imaging buffer and place a piece of the cut-open colon inside the imaging chamber. Use slice hold-down to fix the piece of the cut-open colon into position.
6. Mount magnetic platform with imaging chamber onto microscope, connect superfusion system to the imaging chamber, and establish a steady flow of 60 mL/h.
7. Bring 10x objective into position.
8. Use the 488 nm YFP excitation laser to search for a representative region in the tissue.
9. Change laser to the 445 nm laser and set the following settings:
   - Wavelength series panel: CFP and YFP channels (split view option activated), 300 ms exposure time and 1x1 binning.
   - Time lapse panel: 5 seconds frame time.
   - Laser control panel: 10 % laser power.
   - EMCCD Gain: 500.
10. Make a test run for testing the exposure time with the view loop button. Use the measure line option to estimate the signal-to-noise ratio of cells compared to a background region within the field of view. Adjust laser power, EMCCD Gain and exposure time until the signal-to-noise ratio is higher than 3.
11. Darken the room, check the superfusion flow and start the time lapse experiment with adjusted settings:
    a) Record 30 frames for baseline normalization. Prepare drug dilution in imaging buffer and load drug onto loop 2.
    b) Apply cGMP stimulating drug (e.g. CNP) by opening valve 2 which connects loop 2 with the imaging chamber and the FPLC pump. With a flow rate of 60 mL/h (1 mL/min), it takes 24 frames (2 minutes) to empty loop 2 completely. Close valve 2 after 30 frames in total.
    c) Wait until signal from cGMP stimulating drug reaches baseline again. If no signal is observed, wait at least 6 minutes before the next drug is applied. In the meantime, wash loop 2 three times with imaging buffer.
12. Protocol for drug testing experiments:
    - Repeat drug application (11.b) and waiting period (11.c) until the measurement is done.
13. After the last drug is applied, let signal come back to baseline and stop the measurement.

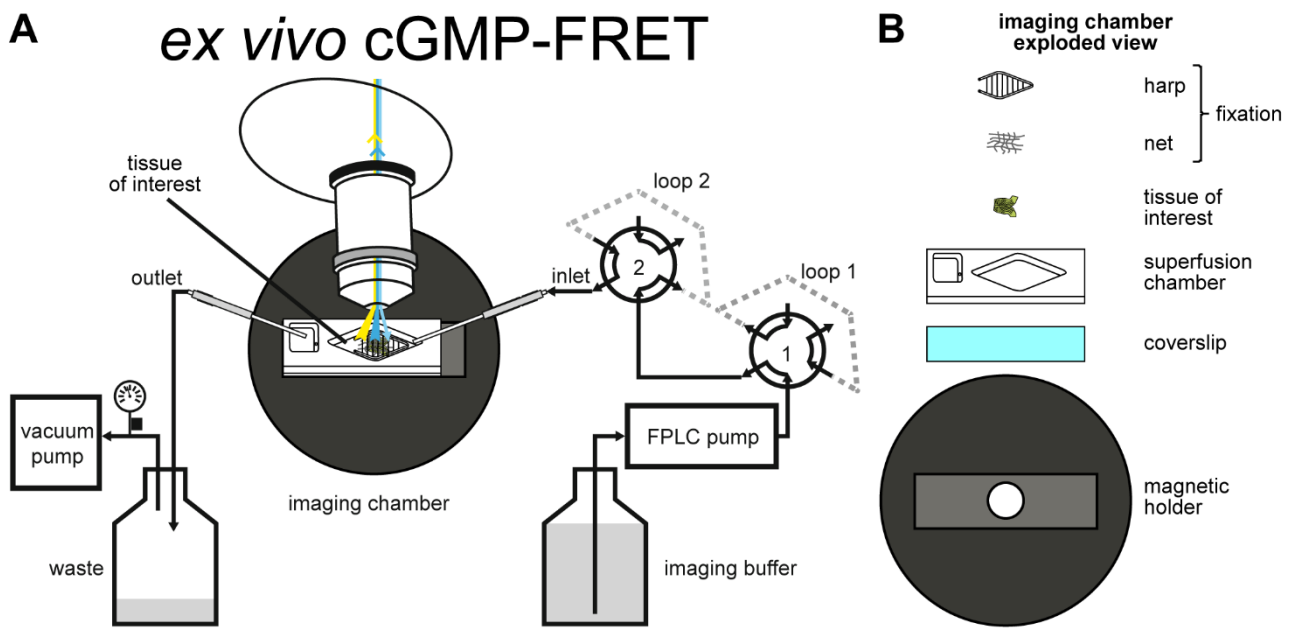

Figure 12: Spinning disk microscope and setup used for *ex vivo* cGMP-FRET measurements.

A) Spinning-disk confocal *ex vivo* cGMP-FRET setup. The Zeiss Examiner.Z1 is an upright microscope equipped with fluorescence grade water objectives, a spinning-disk for confocal imaging, lasers capable of 445 nm and 488 nm excitation, and an EMCCD camera. It illuminates and collects light from the top of the imaging chamber where the tissue is fixed with a slice hold-down (harp) in combination with a net. A FPLC (fast protein liquid chromatography) pump controls the inlet flow and pumps the imaging buffer from the stock bottle through two valves (valve 1 and valve 2, harboring loop 1 and loop 2) into the superfusion chamber. Loop 1 of valve 1 is a 7 mL loop used for inhibitor applications. Loop 2 is a 2 mL loop used for the application of cGMP-stimulating drugs like ANP, BNP, CNP, or DEA-NO. The outlet flow is controlled via a vacuum pump which creates a vacuum in the waste bottle (vacuum adjustable). The used imaging buffer is then sucked away from a separate reservoir of the superfusion chamber. The two reservoirs of the superfusion chamber allow for a steady flow without the development of waves on the surface. Such waves could interfere with the measurement. B) Exploded view of the imaging chamber. Silicon grease is used to clue the superfusion chamber and the coverslip onto the magnetic holder. It also seals the gaps between the superfusion chamber and the coverslip to prevent any leaking.

3.4.5. Evaluation of cGMP-FRET measurements

The cGMP-FRET evaluation is performed with Fiji (open source), Excel (Microsoft) and Origin (OriginLab).

Protocol:

1. Load CFP and YFP dataset into Fiji.
2. Perform a z-stack projection to average all YFP images acquired during the measurement (“Image/Stacks/Z Project…”; project type: average intensity).
3. Use the polygonal selection tool and the ROI manager to draw regions of interest (ROIs) into the averaged YFP image. Draw ROIs close to the cellular border outside the cell.
4. Draw one background at a region where no fluorescence is recognizable by eye.
5. Save the ROI set with the ROI manager.
6. Use the multi measure (“ROI Manager/More/Multi Measure”) option of the ROI manager to measure all ROIs of one dataset at once, but make sure that only the mean gray value is measured (“Analyze/Set Measurements/Mean gray value”).

Perform this step for the CFP and the YFP stack separately. The resulting table is copied into Excel.

7. Using an Excel macro present in the AG Feil (unpublished, programed by Markus Wolters in 2019), the following steps are performed:
    - The intensity value of each frame of the background ROI is subtracted from the corresponding intensity value of each other ROI individually. This is done for the CFP and YFP table.
    - The CFP intensity value of each frame of a ROI is then divided by the corresponding YFP intensity value of the same ROI. The resulting ratio values are then written in a separate table as ratio trace.
    - All values of the ratio trace of one ROI are then divided by the average ratio value of the first 30 frames of that ROI.
8. The criteria, to conclude whether a substance triggers a cGMP-response or not, are:
    - During drug application, the ratio trace has to show a clear increase which also goes back to the baseline.
    - The single traces (CFP and YFP) have to separate (go in opposite directions).
    - The vehicle control does not show an increase in the ratio trace or a separation of the single traces.
9. Load single traces and ratio traces into an origin worksheet for quantitative evaluation:
    - Select ratio trace and evaluate with the peak analyzer (“Analysis/Peaks and Baseline/Peak Analyzer/Open Dialog…”). Choose the following settings:
        - Goal: integrate peaks.
        - Baseline mode: user defined.
        - Baseline treatment: interpolate (add anchor points at start and end of the measurement and before each peak).
        - Find peaks: deactivate auto find and add peaks manually.
        - Integrate peaks: adjust integration window on preview graph and choose the quantities for evaluation (peak area and peak height).
    - Copy the peak area of each peak to a separate table in origin for further calculation.
    - Repeat procedure for all ratio traces of the measurement.

3.5. *Ex vivo* isometric force measurements

Isometric force measurements (IFM) are recordings of tissue originated contraction profiles. In case of the GIT, autonomous contractions are induced and sustained for several hours using a special buffer: the Krebs-Henseleit solution. These measurements can be performed in the presence and absence of tetrodotoxin (TTX). In the absence of TTX, recorded contraction patterns originate from the ENS (**1.1.4.**). The presence of TTX inhibits any communication between neurons of the ENS, hence, contraction patterns originate from the

SML (SMC, ICC and FLC syncytium; **1.1.5.**). For this protocol, the colon is isolated in a fumigated (95 % O_2 and 5 % CO_2) Krebs-Henseleit solution at temperatures close to 37 °C.

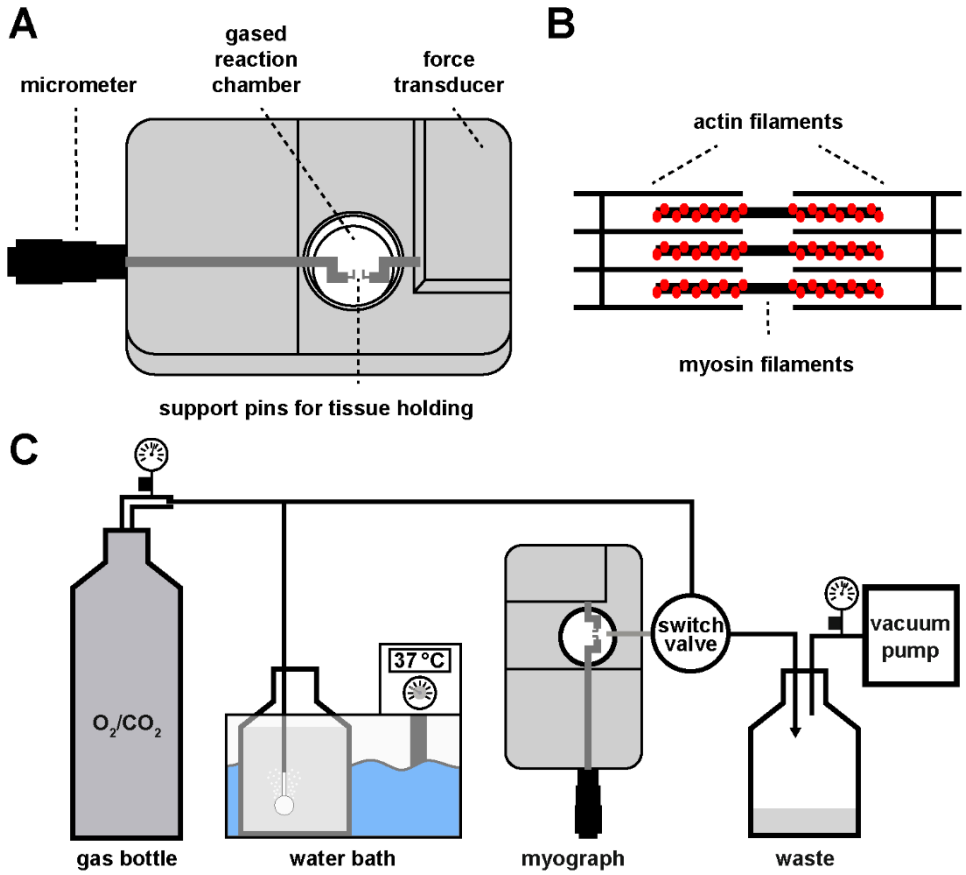

Figure 13: IFM using a multiwire myograph.

A) Different parts of a myograph reaction chamber. B) Illustration of the optimal GI smooth muscle pretension level regarding smooth muscle actin and myosin filaments. By separating the support pins of the myograph reaction chamber, the myosin and actin filaments are placed in a position with maximum overlap. This allows for the strongest possible contraction amplitude. C) Multiwire myograph setup: the gas bottle supplies the Krebs-Henseleit solution, which is warmed inside the water bath and the myograph reaction chamber, with 2 bar of the O_2/CO_2 gas mixture. The myograph has a switch valve which changes between the gas bottle and the vacuum pump (default setting: gas supply). Pressing a button, the switch valve temporarily changes from the gas bottle to the vacuum pump to suck away the liquid from the myograph reaction chamber.

Materials:

- Myograph setup:
  The multi wire myograph system model 610M (ADInstruments) is connected via tubing, valves, and connectors (Mast) to a 95 % O_2 and 5 % CO_2 gas bottle (Westfalen). A water bath is used to keep the Krebs-Henseleit solution at 37 °C (**Figure 13**).
- Krebs-Henseleit solution:
  118 mM NaCl, 4.7 mM KCl, 2.5 mM $CaCl_2$, 1.2 mM KH_2PO_4, 1.2 mM $MgSO_4$, 7.5 mM D-glucose and 25 mM $NaHCO_3$ in ddH_2O.
- Drugs, PDE inhibitors, and vehicle controls are diluted in Krebs-Henseleit solution (**3. Table 2**).
- LabChart (ADInstruments).

Protocol: Part 1 - measurement

1. Start system:
    - Turn on power of the water bath, the myograph, the myograph control unit, the computer, and the vacuum pump.
    - Warm up Krebs-Henseleit solution in a 37 °C water bath and fumigate with O_2/CO_2 gas mixture. Krebs-Henseleit solution should be fumigated for 20 minutes prior to the experiment.
    - Activate the heating of the reaction chamber and set temperature to 37 °C. Fill reaction chamber with 5 mL ddH_2O. Heating takes about 20 minutes until the complete setup reaches 37 °C.
    - Clean reaction chamber three times with 5 mL ddH_2O and cotton swabs. Leave reaction chamber filled with 5 mL ddH_2O until the experiment starts.
    - Clean reaction chamber caps using ddH_2O.
    - Start LabChart and load the template for 8 measurements.
2. Shortly before the measurement is started, activate the myograph fumigation system and calibrate the fumigation rate. The fumigation rate should be the same in all reaction chambers (4-6 bubbles per second).
3. Fill the reaction chambers with 5 mL of the prewarmed and fumigated Krebs-Henseleit solution.
4. Isolate colon and mount colon onto the wire myograph:
    - Sacrifice mouse and isolate colon in Krebs-Henseleit solution.
    - Clean colon, free it from mesenteries and cut the colon into rings with a length of 2-3 mm.
    - Transfer colonic ring into reaction chamber and mount ring onto the support pins.
    - Mount chamber onto multi wire myograph and connect force transducer with the myograph.
    - Start recording the LabChart session by clicking the start button.
5. Calibration of each myograph force transducer:
    - Screw the micrometer clockwise to bring the support pins together. Memorize the force value shown on the myograph display. As soon as the support pins touch each other, the force values go down to a negative value (to a minimum of -60 to -100).
    - Screw the micrometer counterclockwise to the last point where the myograph showed the memorized force value.
    - Go through the myograph menu and set the force value to 0.
6. Start measurement:
    - Screw micrometer counterclockwise until force reaches 2 mN.
    - Wait for 5 seconds for the tissue to adjust the tension.
    - Screw micrometer counterclockwise again until force reaches 2 mN.

      (2 mN is the optimal pretension level for a colonic ring from 15 days old mice).

- Carefully place reaction chamber caps onto the reaction chamber to prevent the Krebs-Henseleit solution from drying out during the 2 hours measurement.
- Now it takes between 5 to 15 minutes until the first contraction patterns occur.
- If no contraction pattern is visible after 30 minutes to 1 hour, the initiation of the measurement failed.

7. Each drug application is annotated using the “add comment” option in LabChart.
8. For measurements with TTX:
   Apply 10 µM TTX directly after the start of the measurement.
9. Drugs are applied through one of the holes in the reaction chamber cap using a pipette. The Krebs-Henseleit solution is not exchanged during the measurement, hence, every drug is applied until the end of the measurement.
10. After all drugs are applied and the last contraction is recorded, apply 100 µM IBMX to show that the tissue can still be relaxed and is, therefore, still alive. The IBMX-induced tissue relaxation also provides a baseline for evaluation.
11. After the measurement is over, press the stop button in LabChart to stop recording.
12. Remove the colon ring from the myograph reaction chamber.
13. Wash reaction chamber three times with 5 mL ddH_2O and use cotton swaps to clean the chamber.

Protocol: Part 2 - evaluation

The evaluation of IFM is performed with LabChart (ADInstruments), Excel (Microsoft) and Origin (OriginLab):

1. Load LabChart file of the respective experiment.
2. Select measurement using the cursor.
3. Copy the selection (Edit/Copy LabChart Reader Data).
4. Use the paste command in Excel:
   - LabChart opens a popup window asking for parameters.
   - Choose: channel for extraction of datapoints, check the “block header” box and down sample by 10.
   - Choose columns that are to be exported: time (always seconds), comments and event markers.
5. Copy columns into an origin worksheet for quantitative evaluation:
   - Select the force trace and evaluate with the peak analyzer (“Analysis/Peaks and Baseline/Peak Analyzer/Open Dialog…”). Choose the following settings:
     - Goal: integrate peaks.
     - Baseline mode: user defined.
     - Baseline treatment: interpolate (add anchor points at start and end of the measurement and at each start/end point of an abnormality that cannot be defined as a peak).

        - Find peaks: activate auto find, set the smoothing window size to 0 and the local points also to 50.
        - Integrate peaks: adjust integration window on preview graph and choose the quantities for evaluation (peak center and peak height).
    - Copy the timestamp, peak center and peak height to a separate table in origin for further calculation.
6. Group measurement into multiple timeframes:
    - The comment column contains one entry at every time point a drug is applied. Copy the column, rename it to “drugs” and replace each entry with 0.25.
    - Change the column type of the comment column into “label”.
    - Select the force trace (y), time trace (x), and comment trace (label) and make a line plot.
    - Use the “select data” tool and group measurement into multiple timeframes. The first timeframe (baseline) starts after the TTX application and ends at the first drug application. Each following timeframe goes from drug application to drug application. The last timeframe starts with the last drug application and ends with the IBMX application.
7. Use timeframes (start and end timestamp) to create average values:
    - Contraction amplitude: the peak height values of each timeframe are averaged and normalized on the baseline timeframe.
    - Time without contraction: a separate column is created where the mathematical difference between peak centers is added. This column is named periodicity. The first entry of the periodicity column of a new drug application timeframe represents the time without contraction and is moved into a separate column.
    - Contraction frequency: the periodicity values of each timeframe are averaged and normalized on the baseline timeframe. At last the reciprocal value of the average periodicity of each timeframe is formed. This value represents the contraction frequency.
    - Normalized time without contraction: the time without contraction is normalized on the average frequency of the timeframe before the time without contraction.

3.6. Assessment and evaluation of the gastrointestinal distention phenotype

To assess a potential phenotype, the respective KO mice are bred. The newly born mice are observed with respect to their social behavior, eating habits and growth rate every day. KO mice and litter matched WT mice at young ages (P5 to P15) are sacrificed by decapitation and an autopsy is performed. The abdominal cavity is carefully opened and an image of the exposed GIT is taken. Then the GIT is carefully isolated, transferred into 1 x PBS and the mesenteries are removed. The GIT is pinned down using insect needles and a SYLGARD-coated petri dish (**3.2.1.**; Materials). Acquire an image of the isolated and

pinned down GIT, focusing on areas with abnormalities in comparison to the WT litter matched sibling. Phenotypes, like the distention phenotype and teeth length, can be quantified with Fiji.

Protocol:

1. Acquire image focusing only on the region of the phenotype. Define start and end point of the phenotype.
2. Load image into Fiji.
3. Use the polygonal selection tool and the ROI manager to draw ROIs around each air bubble that is located inside the GIT. Draw ROIs close to the border of the air bubble.
4. Draw one big ROI (total area) around the whole area of the GIT that harbors the phenotype (from the starting point to the end point) to assess the total area covered in air bubbles.
5. Save the ROI set with the ROI manager.
6. Use the measure (“ROI Manager/Measure”) option of the ROI manager to measure all ROIs of the image at once, but make sure that only the area is measured (“Analyze/Set Measurements/Area”).
7. Copy the area values into Excel. To calculate the distended area, add up all air bubble area values and divide their sum by the value of the total area.

3.7. Statistical evaluation

Statistical evaluations are performed in Origin (OriginLab). A minimum of 3 values is required per group to do statistics. The sequence of testing is performed as followed:

1. Normality test for each group (Shapiro Wilk).
2. Variance test for each group.
3. If two groups are normally distributed, groups are compared with a student t-test.
4. If one of the two groups is not normally distributed, a non-parametric Wilcoxon/Mann-Whitney-test is performed.
5. If one group is used more than once in a statistical comparison, a Bonferroni correction is performed.

Populations are considered significantly different if the error probability is less than 5 %. Significance levels are indicated as followed:

n.s.	$P > 0.05$
*	$P \leq 0.05$
**	$P \leq 0.01$
***	$P \leq 0.001$

4. Results

In this study, the role of CNP-induced cGMP signaling in the GIT was deciphered using transgenic mice. At first GC-B KO mice were used to identify segments of GI abnormalities. Then, the expression of CNP and GC-B was assessed in different segments of the GIT. Special attention was paid to the regions where GI abnormalities had been observed, like the ileum and colon. After identifying the cell types expressing CNP and GC-B, cell type-specific GC-B KO mice were generated to decipher the role of GC-B in colonic motility.

4.1. Gastrointestinal abnormalities of global GC-B KO mice

To characterize potential GI abnormalities of global GC-B KO mice, homozygous GC-B-lacZ mice were generated. These global GC-B KO mice were compared to their litter matched GC-B control siblings (WT or heterozygous global GC-B KO mice). Like in literature, the global GC-B KO mice exhibited a dwarfism phenotype and an early death before weaning (data not shown) [128, 130, 141]. An autopsy performed on sacrificed, global GC-B KO mice at age P25 did not show any obvious GI phenotype (data not shown). To validate the global GC-B KO for GI tissue, lysates of the colon from control and global GC-B KO mice were analyzed with western blot. The GC-B western blot showed that GC-B was expressed in WT colon (**Figure 14 A**: ctr), while the colon from global GC-B KO mice did not show any sign of GC-B expression (**Figure 14 A**: GC-B KO). Focusing on young (P5), global GC-B KO mice before weaning, a GI distension was observed that ranged from the ileum to the transition zone between the median and distal colon (the Cannon-Böhm point). This GI abnormality consisted of many individual, adjacent air bubbles that occupied almost the whole luminal space in that area. Further investigation of global GC-B KO mice at P5, P8, P15, and P20 revealed that the distention was present from P5 until P15, but not at P20 anymore (**Figure 14 B & C**). Although air bubbles were also found in the GI lumen of the respective control mice at P5, P8, and P15 in decreasing amounts, the distention was by far not as strong as for global GC-B KO mice. Another observation was that the two lower frontal teeth of two (out of three) global GC-B KO mice (at P20) were differently long and looked like they had been broken off, whereas the lower frontal teeth of control mice were always of the same size. Although the teeth length ratio (length of the left tooth divided by length of the right tooth) was not significantly different between control and global GC-B KO mice, a trend towards differently long teeth was observed for global GC-B KO mice. The different teeth lengths were only observed in global GC-B KO mice at P20 (**Figure 14 D & E**), never at P5, P8 or P15 (data not shown). It was also never observed in the respective litter

matched control mice. In addition, global GC-B KO mice at P20 exhibited a skinny, malnourished-looking body shape, whereas the litter matched control mice appeared well-fed (data not shown).

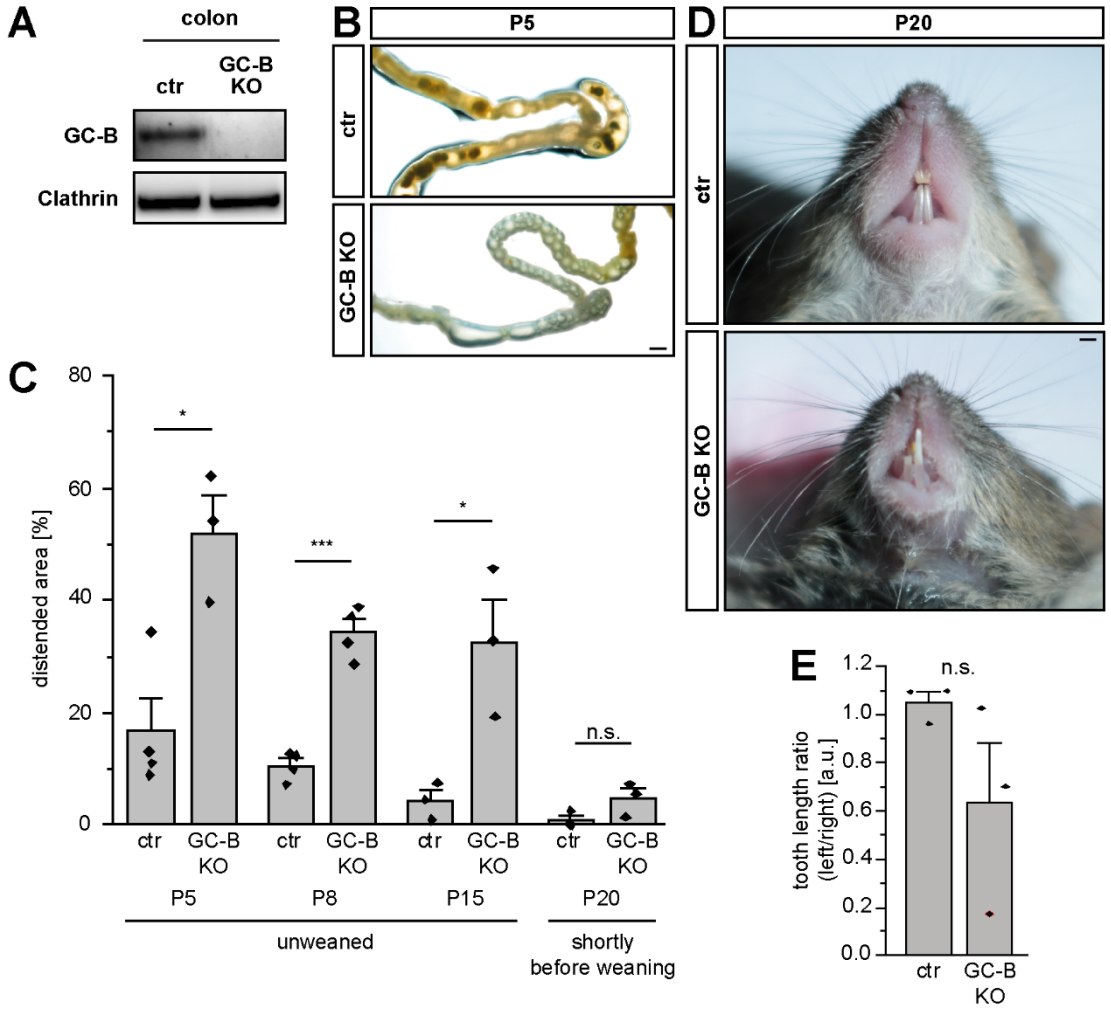

Figure 14: GI and tooth phenotype of global GC-B KO mice.

Global GC-B KO mice were generated using the GC-B-lacZ mouse line. A) Western blot of colon lysates from a control (ctr; genotype: *GC-B* $^{wt/wt}$) and a global GC-B KO mouse (GC-B KO; genotype: *GC-B* $^{wt/lacZ}$) age P21. 10 µg total protein was loaded per lane. GC-B was probed using the gp-α-Npr2 antibody and clathrin was probed using the mo-α-clathrin antibody. B) Representative pictures of the ileum, cecum, and colon from 5 days old control (ctr; genotype: *GC-B* $^{wt/wt}$) and global GC-B KO mice (GC-B KO; genotype: *GC-B* $^{lacZ/lacZ}$). The global GC-B KO mice show a distended lumen filled with air bubbles. C) Quantification of the air bubble filled luminal area from global GC-B KO mice age P5, P8, P15, and P20. For statistical analysis t-tests were performed. D) Pictures of the teeth from a global GC-B KO mouse (genotype: *GC-B* $^{lacZ/lacZ}$) and a litter matched control mouse (genotype: *GC-B* $^{wt/lacZ}$) at P20. E) Tooth length ratio calculated by dividing the length of the left tooth by the length of the right tooth. Tooth length ratio was calculated for global GC-B KO mice and their litter matched control mice at P20 whose intestines were also used to calculate the distended area (C: P20). (Scalebars, 1 mm).

In summary, global GC-B KO mice suffered from a GI distention in the ileum, cecum, and colon at a juvenile age, from P5 until and including P15. Although global GC-B KO mice, transitioning from mother's milk to fiber-rich food at P20, did not suffer from the distention phenotype anymore, they seemed to have differently long frontal teeth.

4.2. Distribution of CNP and GC-B in the gastrointestinal tract

In order to analyze the gene transcription of CNP and GC-B in different GI segments, Xgal staining was performed on the whole GI tissue from heterozygous CNP-lacZ mice, GC-B-lacZ mice and WT mice at different ages (P15, P45, P75). In this setup, the juvenile age is represented by P15, while early and late adult stages are represented by P45 and P75, respectively. Both *lacZ* reporter mouse lines express a nucleus-localized βGal. Any staining procedure employing this βGal leads to a nucleus-localized staining pattern. Thus, Xgal staining on tissue from those *lacZ* mice led to blue dots that highlight *CNP* or *GC-B* transcribing cells. In addition, blurry blue and green background stained areas had also been observed. This background staining was not dot shaped and was found in the small intestine until and including P15 and in the large intestine after P15. Representative images of Xgal stained GI segments at P45 are shown in **Figure 15 A - D**. After Xgal staining of the respective GI segment, βGal positive cells, which transcribe *CNP* or *GC-B*, were counted. The cell number was normalized on the stained area. This normalization allows for the comparison of *CNP* and *GC-B* transcription between GI segments over time (**Figure 15 E**). From all segments stained there were only five with a low CNP and GC-B gene transcription: the stomach, cecum, rectum, mesenteries, and pancreas. The highest *CNP* transcription was found in juvenile esophagus, adult jejunum, and ileum, whereas the highest *GC-B* transcription was found in adult esophagus, ileum, and MLN.

Additional GC-B and cGKI expression was assessed in western blot using lysates of GI segments from the GC-B-HA reporter mouse line (**Figure 15 F**). From all segments blotted, only three showed almost no GC-B and cGKI expression: the proximal duodenum, distal duodenum, and jejunum. MLN showed no cGKI and low GC-B expression. Interestingly, segments with an internal sphincter like the esophagus, pylorus, ileum, and rectum as well as segments with a thick muscle layer like the stomach or colon, exhibited a high expression of cGKI. The highest GC-B expression was observed in the colonic SML and esophagus. Complementarily, the highest cGKI expression was observed in the colonic SML.

Focusing on regions with GI abnormalities in global GC-B KO mice, the ileum, cecum, colon, and rectum were of special interest. Within this group, the cecum displayed the lowest overall transcription and expression of CNP and GC-B. The ileum displayed the highest CNP and GC-B gene transcription at P45 and P75, but only moderate GC-B and high cGKI expression at P25. Almost the same expression level was observed in rectum, but here the CNP and GC-B gene transcription was low. The proximal and distal colon both exhibited a

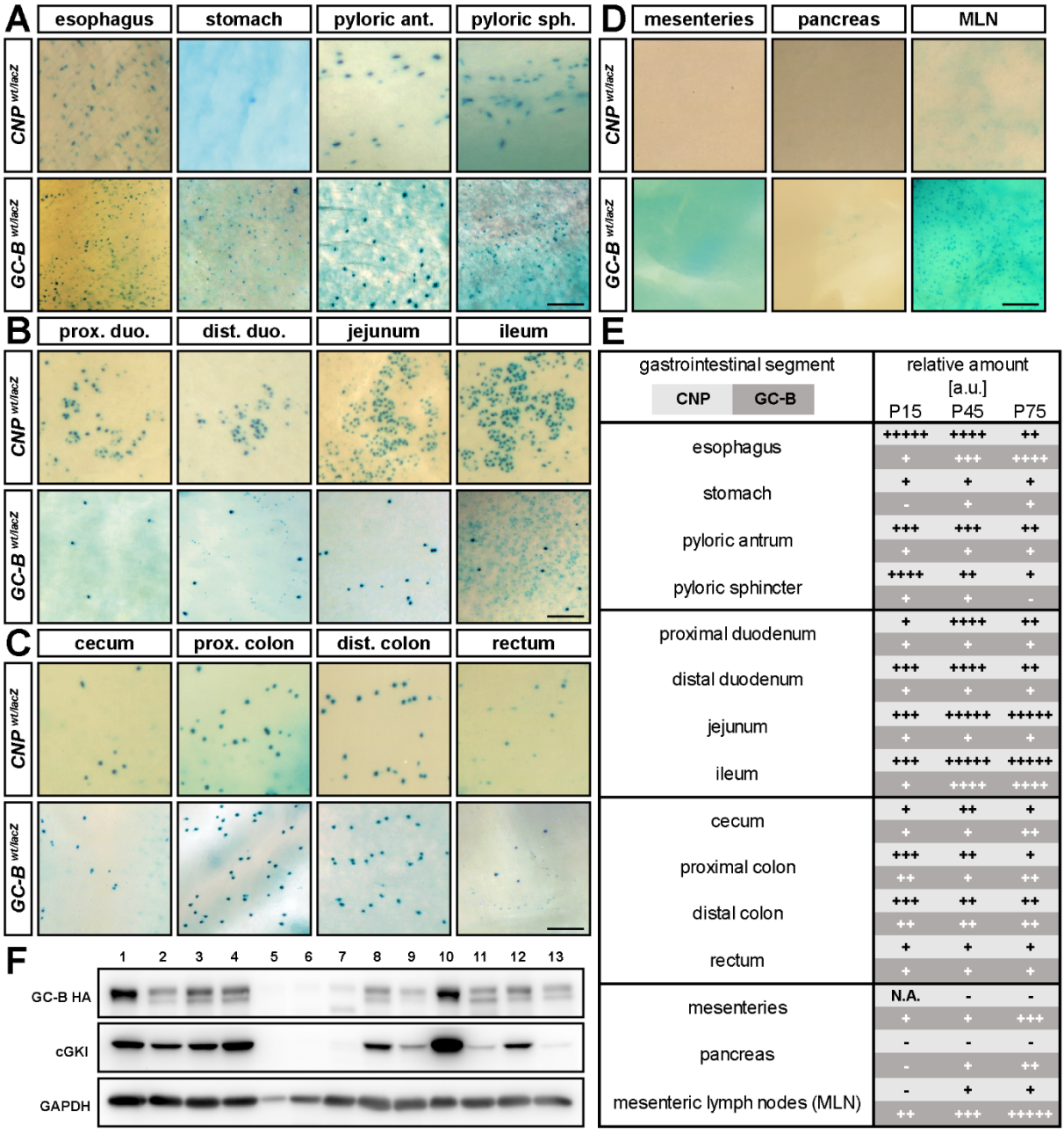

Figure 15: Expression of CNP and GC-B in different parts of the GIT.

A-D) Representative images of whole mount Xgal stained GI tissue from CNP-lacZ and GC-B-lacZ reporter mice age P45 (Scalebar, 100 µm). E) Time course of CNP and GC-B gene transcription based on whole mount Xgal stained GI tissue of three different ages (P15, P45 and P75). The relative amount of Xgal positive cells is represented by a score ranging from 0 to 5. No Xgal positive cells equate to a score of 0 (-). Between 1 and 100 cells/mm² equate to a score of 1 (+), between 101 and 250 cells/mm² equate to a score of 2 (++), 251 to 500 cells/mm² equate to a score of 3 (+++), 501 to 1000 cels/mm² equate to a score of 4 (++++) and >1000 cells/mm² equate to a score of 5 (+++++). The mesenteries of CNP-lacZ mice age P15 were not stained/documented successfully and were, therefore, not available for evaluation (N.A. – not available). F) Western blot of GI tissue lysates from a GC-B-HA reporter mouse (P25). 40 µg of each tissue was loaded onto the SDS-PAGE: esophagus (1), stomach (2), pyloric antrum (3), pyloric sphincter (4), proximal duodenum (5), distal duodenum (6), jejunum (7), ileum (8), cecum (9), colonic SML (10), colonic mucosa layer (11), rectum (12), and MLN (13). The GC-B-HA was probed with the rb-α-HA antibody, cGKI was probed with the rb-α-cGKI antibody and GAPDH was probed with the rb-α-GAPDH antibody (**3. Table 3**).

median CNP and GC-B gene transcription at all three ages. But, the expression of GC-B and cGKI was exceptionally high in the colonic SML as compared to all other GI segments investigated (**Figure 15 F**). These findings identified the ileum (continued in **4.3.**) and colon (continued in **4.4.**) as segments which are, most likely, relevant for GC-B-mediated GI function and dysfunction (e.g. the GI distention phenotype).

Spatial resolution was added to the gene transcription of CNP and GC-B in esophagus (**4.2.1.**), pylorus (**4.2.2.**), and MLN (**4.2.3.**), through Xgal and IF staining on cryosections of tissue from heterozygous CNP-lacZ and GC-B-lacZ mice.

4.2.1. Esophagus

In esophagus, CNP gene transcription was observed in the upper and lower esophagus at a juvenile age (P15), but the number of CNP transcribing cells decreased over time (in P45 and P75). GC-B gene transcription was only found in the lower esophagus in the region of the lower esophageal sphincter. This transcription was not observed at an early age (P15), but it was present in adult mice at age P45 and P75. Hence, it can be concluded that GC-B gene transcription starts between P15 and P45 (**Figure 15 E**). Xgal staining on cryosections of the lower esophagus revealed that *CNP* and *GC-B* transcribing cells were both localized to the CSML and LSML (**Suppl. figure S1**). In addition, high expression of GC-B and cGKI was detected in western blot on the tissue level (**Figure 15 F**).

4.2.2. Pylorus

The pyloric antrum displayed median CNP and low GC-B gene transcription throughout all ages investigated. Although there was a high number of *CNP* transcribing cells observed in pyloric sphincter of juvenile mice, this number decreased until later adult stages. Low GC-B gene transcription was also detected in pyloric sphincter of juvenile and young adult mice at P45 (**Figure 15 A & E**). In order to determine the onset of CNP and GC-B gene transcription, younger (E14.5, P1, P5) and older ages (P300) were also investigated (**Suppl. figure S2**). The resulting time course revealed the first *CNP* transcribing cells between E14.5 and P1 in antrum and sphincter. The *CNP* transcription remained stable until P300 in antrum, while it went down over time in the sphincter.

Due to the nucleus-localized βGal of the lacZ reporter mice used, it is possible to determine the size of the cellular nuclei by the size of the staining. This can be used to distinguish different cell populations by the size of their nucleus. In antrum and sphincter, the first *GC-B* transcribing cells were observed between E14.5 and P1. In the antrum, GC-B gene transcription peaked already at P5 and remained stable until P300. From P45 to P300 a

second cell population, with smaller nuclei than the first population, was observed transcribing GC-B in antrum. The sphincter, in turn, exhibited only low GC-B gene transcription between P1 and P45 which disappeared in later stages of development (**Suppl. figure S2**). Xgal staining on cryosections of the antrum revealed that *CNP* is transcribed in cells of the SML exclusively. In contrast, GC-B gene transcription was first localized only to cells of the MP (at P15), then also to cells of the mucosal layer (at P45) and last to cells of the SML as well (at P75). Xgal staining on cryosections of the sphincter also showed that *CNP* was transcribed in cells of the SML exclusively, while GC-B gene transcription seemed to be restricted to cells of the mucosal layer (**Suppl. figure S3**). Median GC-B expression was observed for the pyloric sphincter and antrum, whereas cGKI was expressed on a high level in both segments (**Figure 15 F**).

4.2.3. Mesenteric lymph nodes

All lymphatic vessels of the GIT converge in the MLN, which represents the center of the GIs immune response. Although CNP gene transcription in MLN was only found in adult stages to a low extent, high GC-B gene transcription was found at P45 and P75 (**Figure 15 E**). The low GC-B gene transcription at P15 matches the also quite low GC-B expression at P25 (**Figure 15 F**). Xgal staining on cryosections of the MLN revealed *GC-B* transcription in cells of the subcapsular sinus. IF double staining was performed to identify the cell type expressing GC-B. It was found that immune cell markers like CD3 (a marker protein for T-cells), B220 (a marker protein for B-cells) or F4/80 (a marker protein for lymph-node specific macrophages) were not expressed in *GC-B* transcribing cells, but marker proteins like CD31 (PECAM; a marker protein for endothelial cells), αSMA (a marker protein for SMCs) or vimentin (a marker protein for fibroblasts, FLCs and other interstitial cells) were expressed in *GC-B* transcribing cells (**Suppl. figure S4**).

4.3. CNP expression in Paneth cells of the small intestine

The previous identification of the GI distention phenotype in the ileum, cecum, and colon of global GC-B KO mice (**4.1.**) led to the question of where this phenotype originates from. Additional investigation of the *CNP* and *GC-B* transcription in those GI segments revealed a high *CNP* transcription in the small intestine and an also high *GC-B* transcription in the ileum at P45 and P75, but it was not possible to determine the onset of transcription with the previous setup (**4.2.**). Therefore, the Xgal staining of whole small intestinal segments was expanded to earlier stages of development (i.e. E14.5, P1 and P5) and also to an older stage (i.e. P300). Tissue clearing was applied to identify Xgal stained cells that were

localized deeper inside the tissue (**Figure 16**). The expanded time course revealed that *CNP* transcription starts between P5 and P15 and increases until age P45. While single *CNP* transcribing cells were present at P15, they were arranged in so far unseen “football-like” patterns (**Figure 16 B & C**) at P45 and later.

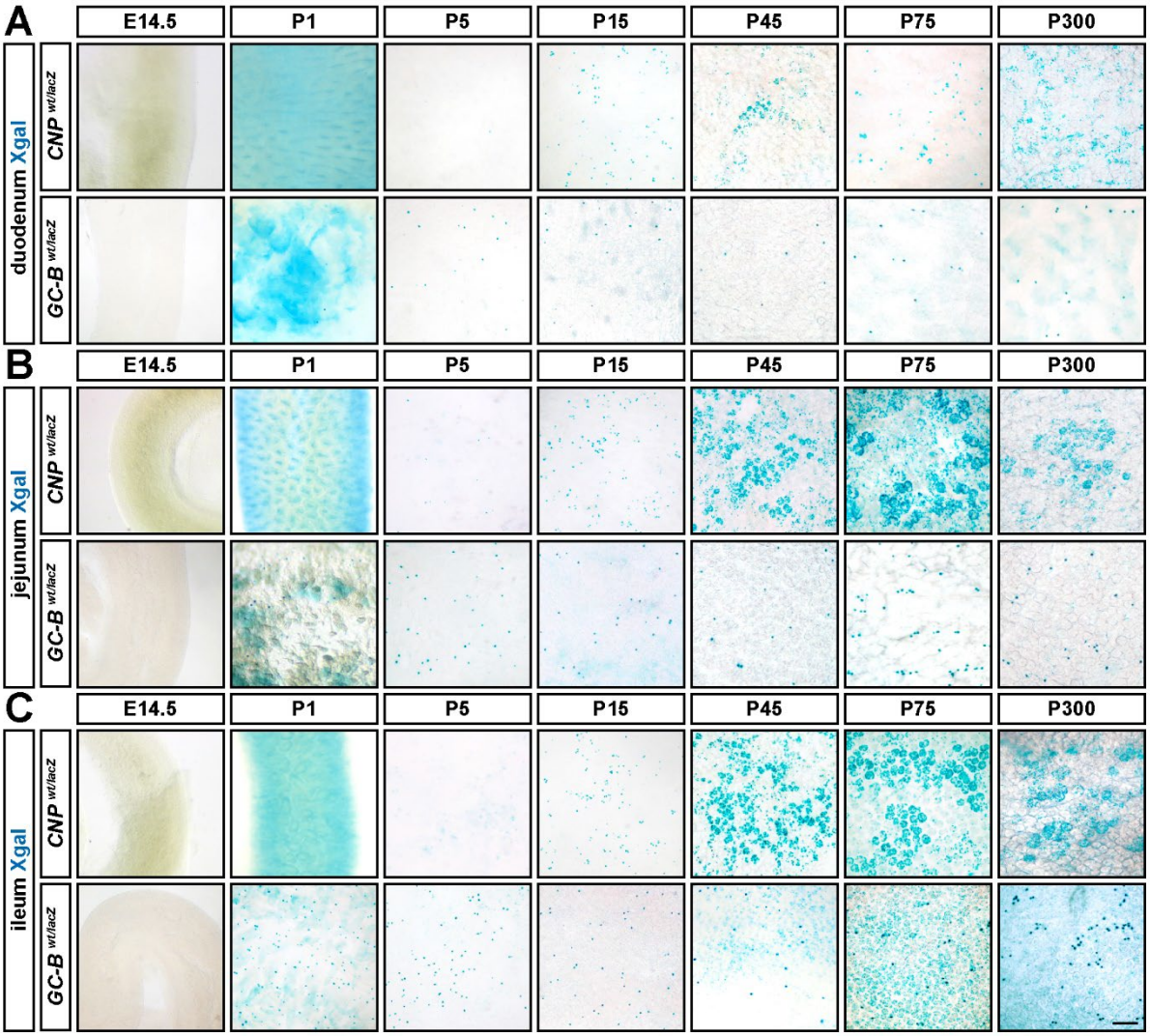

Figure 16: Time course of CNP and GC-B gene transcription in small intestine.

CNP and *GC-B* transcription was investigated over time in duodenum (A), jejunum (B), and ileum (C) based on the CNP-lacZ and GC-B-lacZ reporter mouse lines. The small intestinal compartments were isolated from the respective reporter mouse, stained with Xgal in a whole mount approach, and cleared with ScaleA2 for 1 week before documentation. (Scalebar, 100 µm).

GC-B transcribing cells, in turn, were not arranged in “football-like” patterns and first observed in duodenum and jejunum at P1, but still present at P300 without a visible change in number. In ileum, two populations of GC-B transcribing cells were observed, differentiated by the size of their nuclei. The first population showed the same nucleus size as the *GC-B* transcribing cells in duodenum and jejunum and was observed from age P1 to age P300 without a visible change in number (**Figure 16 C**). At age P45, a second population of *GC-B* transcribing cells emerged and remained present until P300 (**Figure 16 C**). This second

population was characterized by a smaller nucleus size than the first population and they were also localized in another focal plane, deeper inside the tissue (recognizable by a blurry appearance in the whole mount Xgal staining).

Xgal staining on jejunal and ileal cryosections from lacZ reporter mice showed that *CNP* was mainly transcribed in cells of the small intestinal crypts, whereas the *GC-B* transcribing cell population with the larger nuclei was localized to the MP and the cell population with the smaller nuclei was found in the epithelial layer (**Figure 17 A:** ileum).

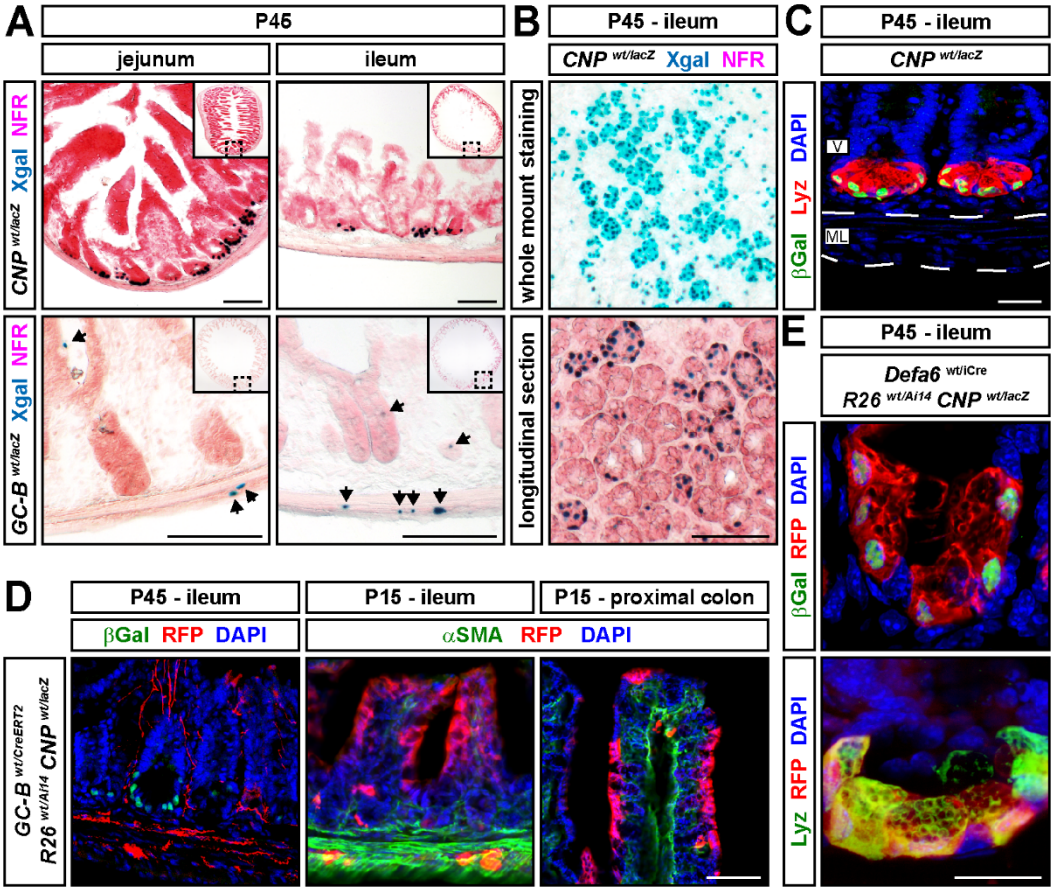

Figure 17: Localization of *CNP* and *GC-B* transcribing cells in the small intestine.

A) 20 µm cryosections from the jejunum and ileum of 45 days old CNP-lacZ (genotype: *CNP* $^{wt/lacZ}$) and GC-B-lacZ (genotype: *GC-B* $^{wt/lacZ}$) reporter mice were stained with Xgal and counter stained with NFR. (Scalebar, 100 µm). B) Xgal staining of ileum from 45 days old CNP-lacZ reporter mice in whole mount and in longitudinal cryosections (cut through the crypt layer). (Scalebar, 100 µm). C-E) IF staining of sections from mice of different genotypes. The reporter protein βGal was probed with ch-α-βGal and tdTomato was probed with rb-α-RFP. The Paneth cell marker lysozyme was probed with rb-α-Lyz antibodies, the SMC marker αSMA was probed with mo-α-αSMA antibodies and DNA was probed with DAPI. (Scalebar, 25 µm).

Further Xgal staining on longitudinal ileum cryosections revealed that the “football-like” *CNP* transcription pattern observed in whole mount came from the crypt cells themselves (**Figure 17 B:** whole mount staining vs. longitudinal section). IF staining on ileum cryosections from 45 days old CNP-lacZ mice showed that *CNP* is transcribed in Paneth cells of the small intestinal crypts (**Figure 17 C**: lysozyme is a marker protein for Paneth

cells). In addition to the lacZ reporter mice, the GC-B-CreERT2 reporter mouse line was combined with the R26-Ai14 reporter mouse line and used to identify *GC-B* transcribing cells in ileum. While the first *GC-B* transcribing cell population was localized to the MP, the second one was localized to the epithelial layer. This localization was observed in ileum and proximal colon (**Figure 17 D**: ileum and proximal colon - αSMA, RFP and DAPI staining). It was also observed that *GC-B* transcribing neurons project their axons and dendrites alongside the *CNP* transcribing Paneth cells into the villi (**Figure 17 D**: ileum – βGal, RFP and DAPI staining).

At last, a Paneth cell-specific Cre-mouse line was established, the Defα6-iCre mouse line. By crossing this mouse line to the R26-Ai14 and the CNP-lacZ reporter mouse line, it was shown that the Paneth cell-specific Cre line does recombine in Paneth cells (**Figure 17 E**: Lyz, RFP and DAPI staining) and covers *CNP* transcribing cells (**Figure 17 D**: βGal, RFP and DAPI staining).

Regarding actual protein expression, GC-B and cGKI expression were not detected in duodenum. Only GC-B, but not cGKI expression was detected in jejunum, whereas the ileum displayed high expression of cGKI and median expression of GC-B (**Figure 15 B**). These findings confirmed the low GC-B gene transcription observed in duodenum and jejunum as well as its median transcription in ileum.

In summary, GC-B was transcribed in two cell populations. The first population with large nuclei was localized to the MP and it was found in all segments of the small intestine from P1 to P300. The second population with smaller nuclei was observed in the epithelial layer of the ileum from P45 to P300. CNP transcription, in turn, was found in Paneth cells of the small intestine. The highest *CNP* transcription rate was, hereby, observed at P75 in jejunum and ileum. Considering that the GI distention phenotype of global GC-B KO mice was observed between P5 and P15 (**4.1.**), the question was whether the origin of this phenotype lays within the ileum, cecum or colon. Unfortunately, due to the timing of the CNP and GC-B gene transcription in ileum, it appears to be very unlikely that *GC-B*, transcribed in either of the two cell populations, is connected to the GI distention phenotype. Therefore, this study did not continue to focus on any segment of the small intestine.

4.4. CNP-induced cGMP signaling in colon

The GI distension phenotype was located to the ileum, cecum, and colon. Investigation of the GC-B expression pattern eliminated the ileum and cecum as potential origin, whereas the high expression of GC-B and cGKI in the colonic SML suggested that the CNP/GC-B/cGKI signaling pathway holds a critical role in colon.

4.4.1. CNP-induced circular smooth muscle relaxation in proximal and distal colon

Previous research has already shown that CNP inhibits the colonic motility that is primarily regulated by the functional syncytium of the SML. To study colonic motility *ex vivo*, the colon was isolated and segmented into 2 mm long rings (3 rings for the proximal colon and 3 rings for the distal colon). Each of these rings was placed in an organ bath multiwire myograph to measure circular smooth muscle movements.

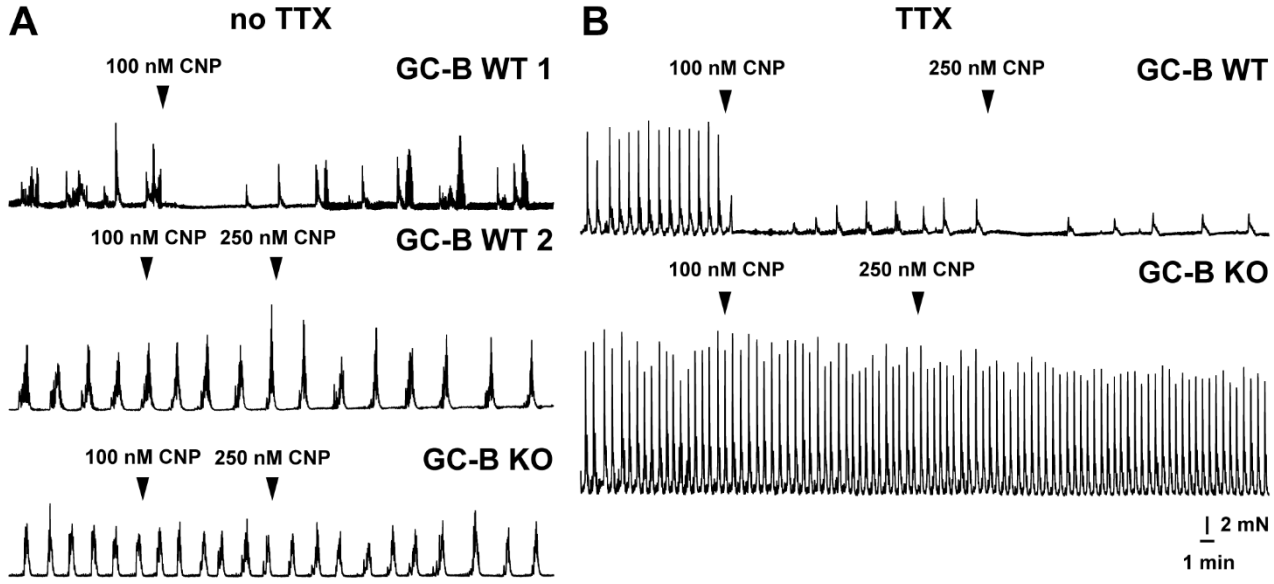

Figure 18: CNP-induced colonic circular smooth muscle relaxation with and without TTX.

Colonic rings of GC-B WT (genotype: *Npr2*$^{wt/wt}$) and global GC-B KO (GC-B KO, genotype: *Npr2*$^{lacZ/lacZ}$) mice were measured in IFM at age P15. A) IFM without application of TTX showing low frequency long-lasting large contractions of GC-B WT and GC-B KO colonic rings. In GC-B WT, CNP application led to two different reaction patterns. Reaction pattern 1 (GC-B WT 1) showed an inhibition of autonomous colonic contractions with 100 nM CNP, while reaction pattern 2 (GC-B WT 2) did not react on any concentration of CNP. The observed difference between the two patterns was the peak shape. A typical peak observed in pattern 1 consists of multiple peaks of different amplitudes in a time period of 1-2 minutes. A typical peak of pattern 2 consists of one defined peak over a time period of up to 1 minute, but not longer. Thus, the peak shape of pattern 2 is the same as the GC-B KO pattern. B) IFM in presence of 10 µM TTX shows high frequency large contractions of GC-B WT and GC-B KO colonic rings. Contractions of GC-B WT colonic rings were inhibited by 100 nM and 250 nM CNP, while both concentrations did not inhibit contractions of GC-B KO colonic rings. The GC-B WT reaction on CNP in presence of TTX was highly reproducible among all colonic rings measured.

In the first set of experiments, 100 nM CNP and 250 nM CNP were applied to colonic segments. Although WT colonic contraction patterns were inhibited by CNP (**Figure 18 A**: GC-B WT 1), the effect was not very reproducible (**Figure 18 A**: GC-B WT 2). Some colonic contractions were inhibited and some were not inhibited by CNP. Reproducible were only the measurements of colonic rings from global GC-B KO mice which never showed any response to CNP (**Figure 18 A**: GC-B KO). Since the ENS induces long-lasting large contractions via neurotransmitters that act on SMCs, ICCs, and FLCs, TTX was used to inhibit signals from the ENS. Thus, the application of TTX at the beginning of the measurement completely changed the frequency of the contraction pattern. Additional application of 100 nM and 250 nM CNP led to a highly reproducible inhibition of the colonic contraction pattern. This contraction inhibiting effect of CNP was only observed in colonic rings from GC-B WT mice (**Figure 18 B**: GC-B WT), but never observed in colonic rings from global GC-B KO mice (**Figure 18 B**: GC-B KO). Hence, the contraction inhibiting effect of CNP might not be mediated by neurons of the ENS, but it is most certainly GC-B dependent. To decipher the role of CNP in colonic motility, further IFM studies were performed in presence of TTX.

Comparing the basal parameters of TTX-treated proximal and distal colon from GC-B WT and KO mice only revealed minor differences between colonic rings of either segment. First, the distal colon showed a general trend (in WT and KO) towards a higher basal contraction amplitude and, second, also displayed a significantly lower basal contraction frequency (**Suppl. figure S5 A & B**).

To characterize the contraction inhibiting effect of CNP in proximal and distal colon, dose-response curves were recorded in the absence (**Figure 19 A**: CNP) and presence of carbachol (CCh) (**Figure 19 B**: CNP + CCh). Half maximal effective concentrations (EC50) were calculated for the contraction amplitude and frequency. The effect of CNP was observed to be dose dependent in the proximal and distal colon as well as in the absence and presence of CCh. In the absence of CCh, the EC50 of the contraction amplitudes was similar between both segments (**Figure 19 C**: EC50 of about 15 nM CNP without CCh). But, the EC50 of the contraction frequency was significantly lower in distal colon (**Figure 19 D**: EC50 of about 12.5 nM CNP in distal colon without CCh). As opposed to the EC50 values, the last two endpoints of the dose-response curves for the contraction amplitude were significantly different (**Figure 19 E**: i.e. 50 nM and 100 nM CNP application). The contraction amplitude after 100 nM CNP application was reduced by 75 % in proximal colon and reduced by almost 100 % in distal colon.

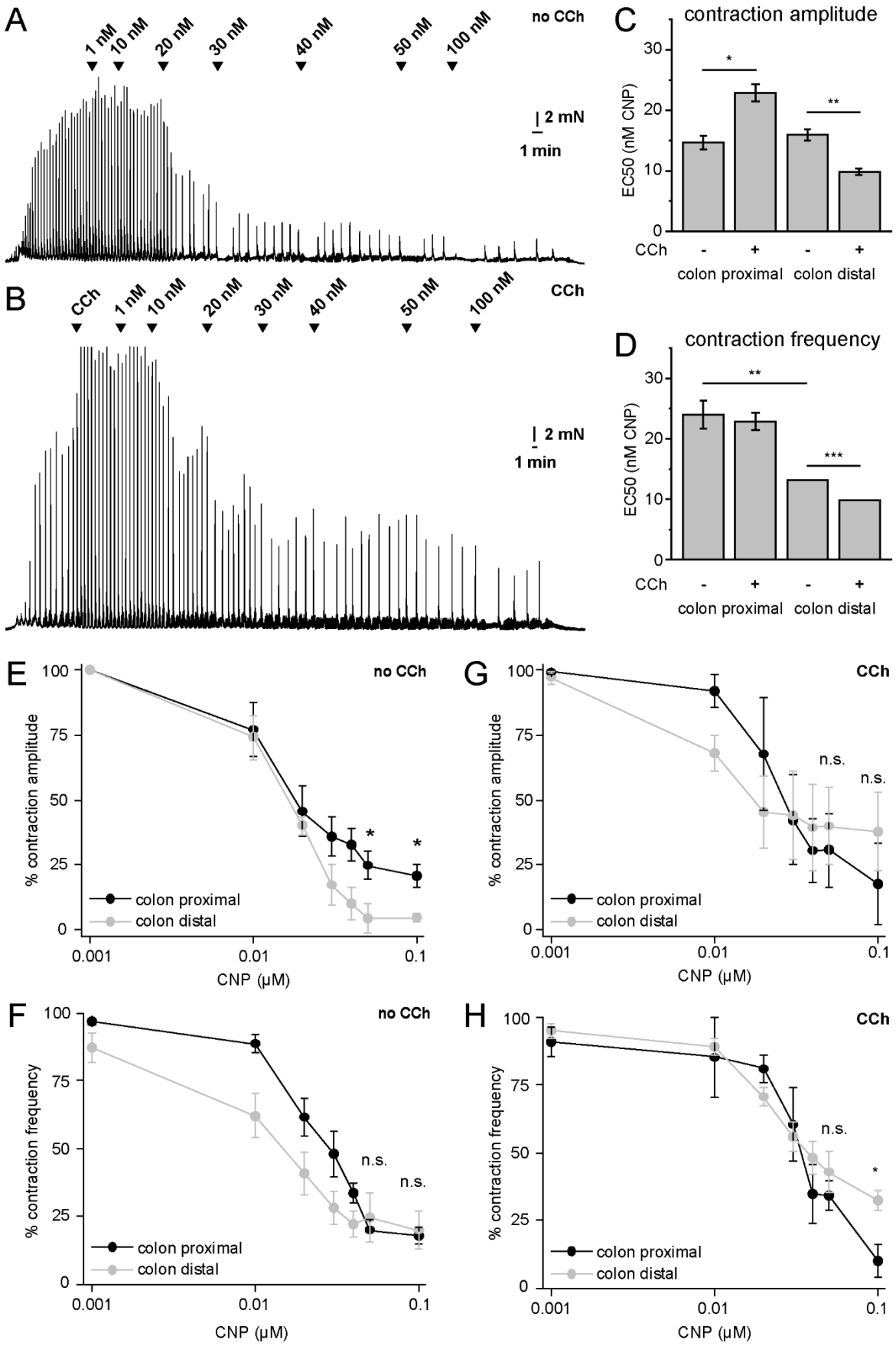

Figure 19: CNP-induced circular smooth muscle relaxation in proximal and distal colon.

IFM was performed on colonic rings from the proximal and distal colon of GC-B WT mice in the presence of TTX. CNP was applied in increasing concentrations from 1 nM to 100 nM CNP in the absence and presence

Figure 19: CNP-induced circular smooth muscle relaxation in proximal and distal colon.
of 100 µM CCh. The measurements were evaluated and the change in contraction amplitude, contraction frequency and time without contraction was quantified. Representative IFM traces from segments of the distal colon in the absence (A) and presence (B) of 100 µM CCh. Mean EC50 values of the contraction amplitude (C) and contraction frequency (D) without and with CCh. Development of contraction amplitudes after different concentrations of CNP in proximal and distal colon without (E) and with CCh (G). Development of contraction frequency after different concentrations of CNP in proximal and distal colon without (F) and with CCh (H). Figure is continued in the supplement (Suppl. figure S6).

Albeit, the mean EC50 values of the contraction frequency were different between both colonic segments, the last two endpoints of the respective dose-response curves were not significantly different (**Figure 19 F**: 50 nM and 100 nM CNP application). These experiments showed that the distal colon is in general more susceptive to CNP application. This susceptibility was even stronger in the presence of CCh. Although the application of 100 nM CCh affected the baseline contraction amplitude and frequency similarly in proximal and distal colon (**Suppl. figure S6 A & B**), inverse effects were observed in combination with CNP. Regarding the contraction amplitude, the application of CCh led to a reduced sensitivity to CNP in proximal colon (**Figure 19 C**: significantly increased EC50 in proximal colon with CCh) and opposed to that to an increased sensitivity to CNP in the distal colon (**Figure 19 C**: significantly decreased EC50 in distal colon with CCh). This increased sensitivity to CNP was also observed for the contraction frequency in distal colon (**Figure 19 D**: significantly decreased EC50 in distal colon with CCh). CCh did not change the EC50 of the contraction frequency in proximal colon. The endpoints of the contraction amplitude for the proximal and distal colon dose-response curves (i.e. 50 nM and 100 nM CNP application) were not significantly different anymore (**Figure 19 G**), while the endpoint of the dose-response curves for the distal colon contraction frequency was significantly higher than the respective endpoint of the proximal colon (**Figure 19 H**).

The time without contraction was also calculated and normalized to the average contraction frequency of the time period right before the respective CNP application. The time without contraction was not significantly different between the proximal and distal colon at any CNP concentration applied, neither in the absence nor presence of CCh. Hence, it was concluded that CCh does not influence the CNP-induced time without contraction (**Suppl. figure S6 C & D**).

Additional motility measurements were performed on both colonic segments to compare the contraction inhibiting effect of CNP with the effects of ANP and DEA-NO. Thus, dose-response curves were recorded with increasing concentrations of ANP and DEA-NO (**Suppl. figure S7 A & B**) in proximal and distal colon. It was found that ANP, much like CNP, induced a stronger contraction inhibiting effect in the distal colon with respect to

contraction amplitude and frequency (**Suppl. figure S7 C & D**). DEA-NO, in turn, led to an equally strong contraction inhibiting effect in both segments (**Suppl. figure S7 E & F**). EC50 values were calculated to estimate the sensitivities. In comparison, the contraction amplitude in proximal colon was more sensitive to CNP than to ANP (**Suppl. figure S7 G**: EC50 around 28 nM for ANP & 15 nM for CNP), but equally sensitive to both in distal colon (**Suppl. figure S7 G**: EC50 around 15 nM for ANP & CNP). The contraction frequency in proximal colon was equally sensitive to ANP and CNP (**Suppl. figure S7 H**: EC50 around 25-28 nM for ANP & CNP), but more sensitive to CNP in distal colon (**Suppl. figure S7 H**: EC50 around 18 nM for ANP & 12 nM for CNP). Both, contraction amplitude and frequency, were similarly sensitive to DEA-NO in proximal and distal colon with an EC50 of about 300 nM (**Suppl. figure S7 G & H**).

This set of experiments demonstrated that the contraction inhibiting effect of CNP has a much greater impact on the distal colon as it has on the proximal colon. It was shown that small concentrations (between 10-20 nM) of ANP and CNP already lead to circular smooth muscle relaxation. Furthermore, tissue from global GC-B KO mice confirmed that the CNP-induced contraction inhibiting effect is mediated by GC-B, and not GC-A or the clearance receptor. Considering that the distention phenotype probably originates in the distal colon makes this segment a very interesting candidate for further investigations.

4.4.2. Identity of CNP and GC-B expressing cells and time course of expression in the distal colon

In order to generate cell type-specific GC-B KO mice, it was required to discover the identity of CNP and GC-B expressing cells in distal colon. To do so, the CNP-lacZ, GC-B-lacZ and GC-B-CreERT2 reporter mouse lines were employed. The time course of transcription was assessed using the *lacZ* reporter systems. A representative Xgal staining of the colon from 45 days old mice showed a gradient of *CNP* and *GC-B* transcribing cells in the proximal colon which reached the maximum number of cells at the boarder to the distal colon (**Figure 20 A**: dashed line). The number of cells transcribing *CNP* or *GC-B* did also not change along the distal colon. For the time course of transcription, Xgal stainings were performed on the distal colon of CNP-lacZ and GC-B-lacZ mice at different ages. The first *CNP* transcribing cells were detected between P5 and P15, and the first *GC-B* transcribing cells were detected between E14.5 and P1 (**Figure 20 B**). After the onset of transcription, the number of Xgal positive cells did not change over time, until P300 (**Figure 20 B**: number of *CNP* transcribing cells remain constant after P15 and number of *GC-B* transcribing cells remain constant after P1).

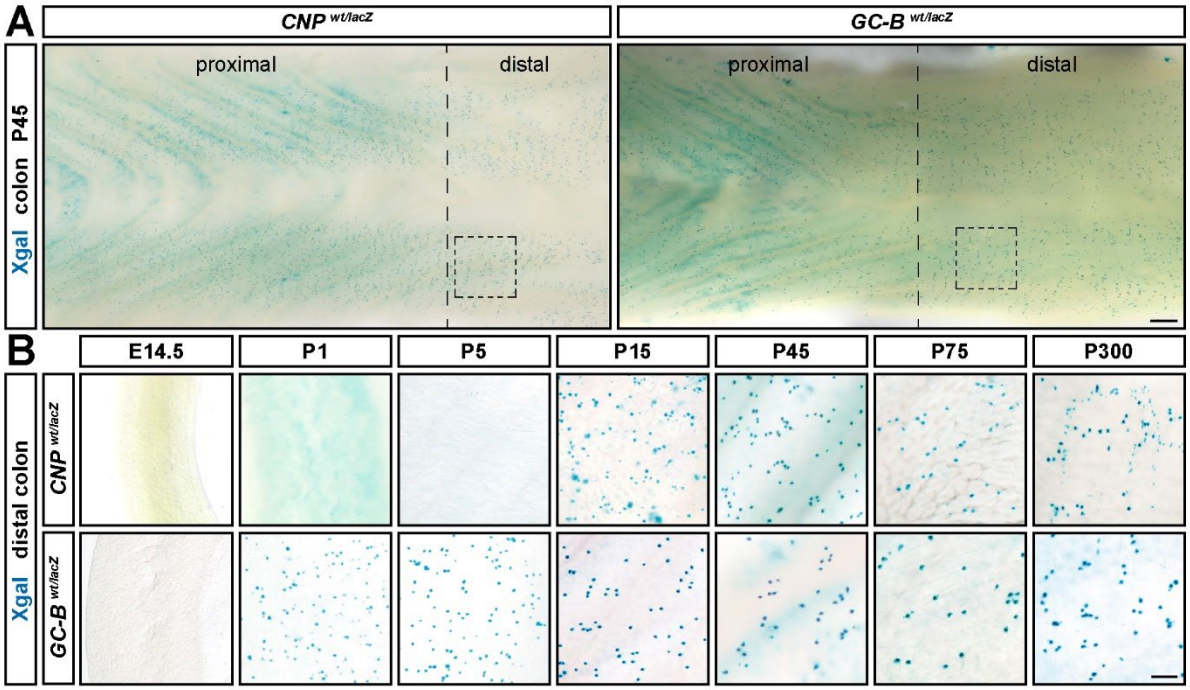

Figure 20: Time course of CNP and GC-B gene transcription in distal colon.

A) Xgal stained colon from 45 days old CNP-lacZ (genotype: *Nppc* $^{wt/lacZ}$) and GC-B-lacZ (genotype: *Npr2* $^{wt/lacZ}$) reporter mice. The colon was cut open at the mesenterial border and the images were taken with the SML facing up (mucosal layer facing down). The dashed line represents the border between the proximal and distal colon. The rectangle represents the size of the region observed in the transcription time course (B). (Scalebar, 200 µm). B) Time course of *CNP* and *GC-B* transcription in distal colon. The Xgal stained distal colon was cleared with ScaleA2 for 1 week before documentation (Scalebar, 100 µm).

To decipher the cellular identity of *CNP* and *GC-B* transcribing cells, Xgal and IF stainings were performed on distal colon cryosections. Xgal stained cryosections from CNP-lacZ and GC-B-lacZ mice showed that *CNP* and *GC-B* transcribing cells were located in the MP of the distal colon (**Figure 21 A**). The MP harbors different cell types such as neurons (marker protein: protein gene product 9.5, abbr.: PGP9.5), ICCs (marker protein: tyrosine-protein kinase kit, abbr.: c-kit) and glia cells (marker protein: glial fibrillary acidic protein, abbr.: GFAP). Based on the lacZ reporter lines, CNP and GC-B gene transcription was neither detected in ICCs, glia cells, FLCs (marker protein: platelet-derived growth factor receptor alpha, abbr.: PDGFRα) nor SMCs (marker protein: alpha smooth muscle actin, abbr.: αSMA) (**Figure 21 B**). But in IF staining, *CNP* and *GC-B* transcribing cells were immunoreactive for the neuronal marker protein PGP9.5 (**Figure 21 C**). Further characterization showed that these neurons are in part nitrergic (**Figure 21 C**). To assess the proportion of neurons that transcribe *CNP* or *GC-B*, whole mount IF double staining was performed on the distal colon from CNP-lacZ and GC-B-lacZ mice (P45). The amount of *CNP* and *GC-B* transcribing neurons (βGal positive cells divided by HuC/D positive cells) was quantified. From 4095 neurons counted, about 15 % transcribed *CNP* and from 2938 neurons about 7 % transcribed *GC-B* (**Figure 21 D & E**). LacZ positive nuclei were never

observed in the SML, neither with tissue from CNP-lacZ nor tissue from GC-B-lacZ reporter mice. Although *CNP* transcribing cells were not found anywhere in the colon at P5, there were Xgal positive nuclei observed in the inferior mesenteric ganglion of five days old CNP-lacZ mice (**Suppl. figure 8**).

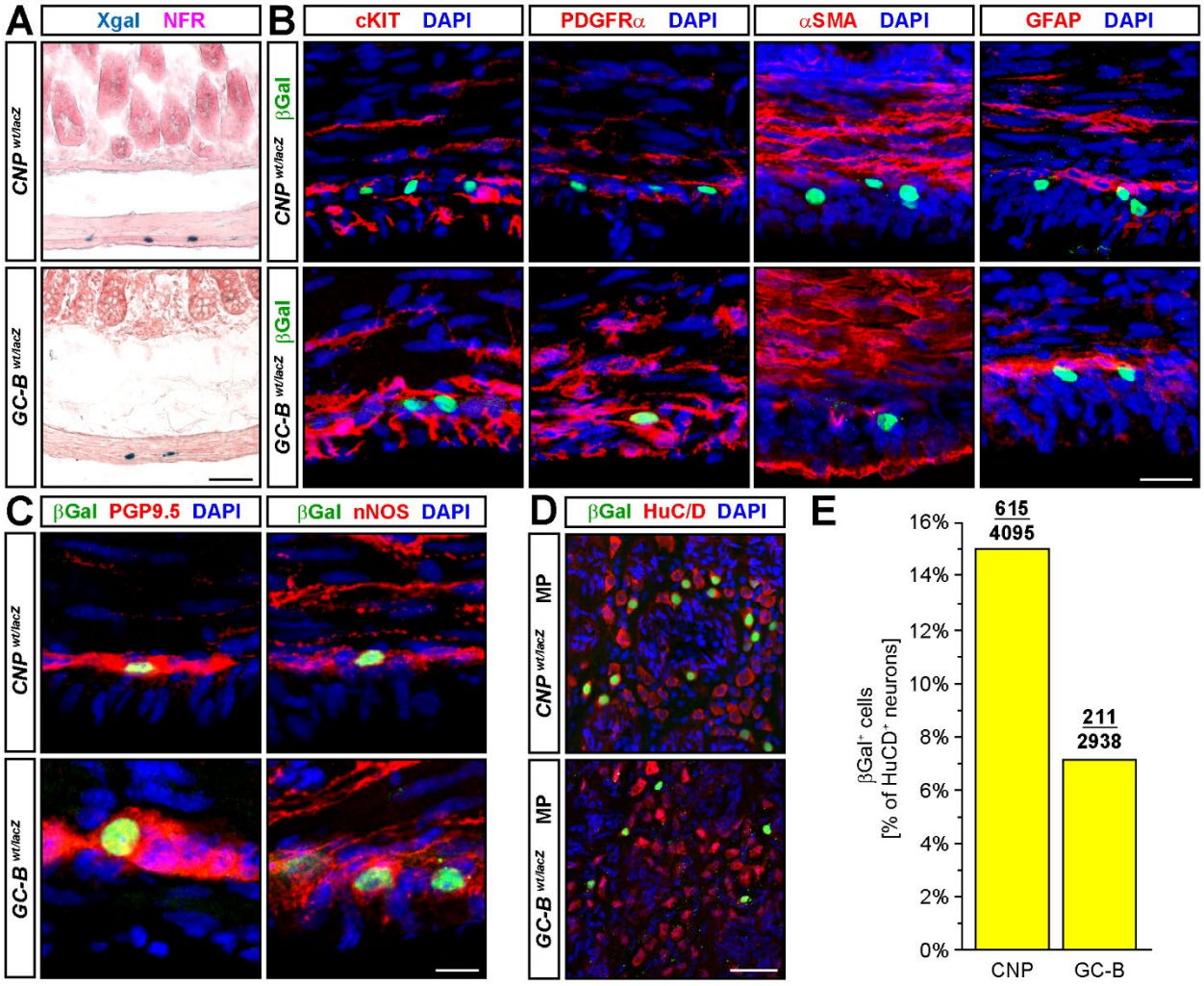

Figure 21: Identity of CNP and GC-B transcribing cells in distal colon.

A-C) 20 µm cryosections from the distal colon of 45 days old CNP-lacZ (genotype: *Nppc* $^{wt/lacZ}$) and GC-B-lacZ (genotype: *Npr2* $^{wt/lacZ}$) reporter mice were stained with Xgal (A) and with different antibodies for IF detection (B, C). The βGal reporter protein, which represents *CNP* and *GC-B* transcription, was probed with the ch-α-βGal antibody. DAPI was used to stain nuclei allowing for the clear identification of a positive βGal staining. ICCs were probed with ra-α-c-kit (B), FLCs were probed with Rb-α-PDGFRα (B), SMCs were probed with mo-α-αSMA (B), glia cells were probed with rb-α-GFAP (B), neurons were probed with Rb-α-PGP9.5 (C) and nitrergic neurons were probed with Rb-α-nNOS (C). (Scalebar, 25 µm). D-E) Whole mount IF staining of the distal colon from 45 days old CNP-lacZ (genotype: *Nppc* $^{wt/lacZ}$) and GC-B-lacZ (genotype: *Npr2* $^{wt/lacZ}$) reporter mice. The tissue was probed with a ch-α-βGal antibody, mo-α-HuC/D antibody and DAPI. The staining was performed 3 times per genotype and the different cell populations were counted. D) Representative image of the MP recorded with the LSM showing neuronal cell bodies in red (HuC/D expression) and the nucleus of *CNP* or *GC-B* transcribing cells in green (dots of nuclear localized βGal) respectively (Scalebar, 100 µm). E) Percentage of neurons transcribing *CNP* or *GC-B*.

To validate the results of the GC-B-lacZ reporter mouse line, the GC-B-CreERT2 mouse line was crossed with the Cre-inducible tomato reporter mouse line: R26-Ai14. This combination allows the labeling of *GC-B* transcribing cells and daughter cells in a Tamoxifen-induced

manner. In addition to the *GC-B* transcription in neurons, this reporter mouse line also showed *GC-B* transcription in another cell type present in the LSML and CSML. IF staining against marker proteins revealed that these cells are SMCs (**Figure 22 B**), but neither ICCs, FLCs nor glia cells (**Figure 22 C**).

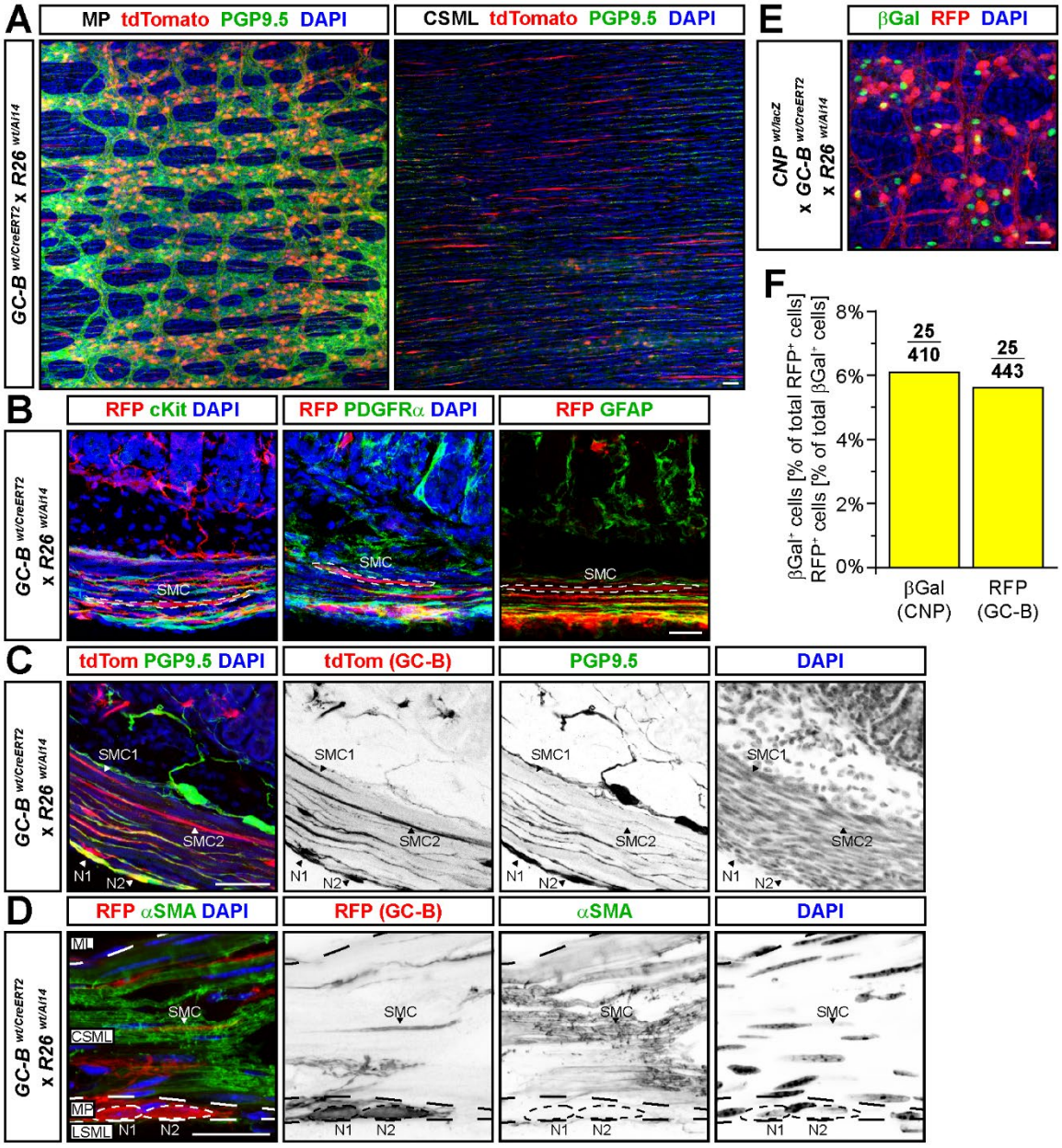

Figure 22: GC-B gene transcription in distal colonic neurons and SMCs.

IF staining of the distal colon from *GC-B* $^{wt/CreERT2}$ x *R26* $^{wt/Ai14}$ mice age P21 in whole mount (A) and cryosections (B-D). The CreER^{T2} activity was induced two times at age P15 and age P18 with 0.1 mg/g body weight Tamoxifen. The cytosolic tdTomato reporter protein, which represents *GC-B* transcription, was probed with the rb-α-RFP antibody. DAPI was used to stain nuclei (DNA). Neurons were probed with Rb- α-PGP9.5 (A & C), ICCs were probed with rt-α-c-kit (B), FLCs were probed with rb-α-PDGFRα (B), glia cells were probed with rb-α-GFAP (B) and SMCs were probed with mo-α-αSMA (D). E-F) Whole mount IF staining of the distal colon from *GC-B* $^{wt/CreERT2}$ x *R26* $^{wt/Ai14}$ x *CNP* $^{wt/lacZ}$ mice age P15. The reporter protein βGal representing *CNP* transcription was probed with ch-α-βGal (green nuclei) and the reporter protein tdTomato representing *GC-B* transcription was probed with Rb-α-RFP (red cell body). DAPI was used to stain nuclei (DNA). E) Confocal image of the MP. F) Percentage of *CNP* and *GC-B* transcribing cells relative to the total population of *CNP* or *GC-B* transcribing cells. Abbr.: Mucosal layer (ML), circular smooth muscle layer (CSML), myenteric plexus (MP) and longitudinal smooth muscle layer (LSML).

In order to estimate the number of cells that transcribe both CNP and GC-B, the CNP-lacZ reporter mouse line was crossed to the GC-B-CreERT2 and the R26-Ai14 mouse lines. The subsequent whole mount IF staining of the distal colon revealed that about 6 % of the *CNP* transcribing neurons also transcribe *GC-B* and vice versa (**Figure 22 E & F**).

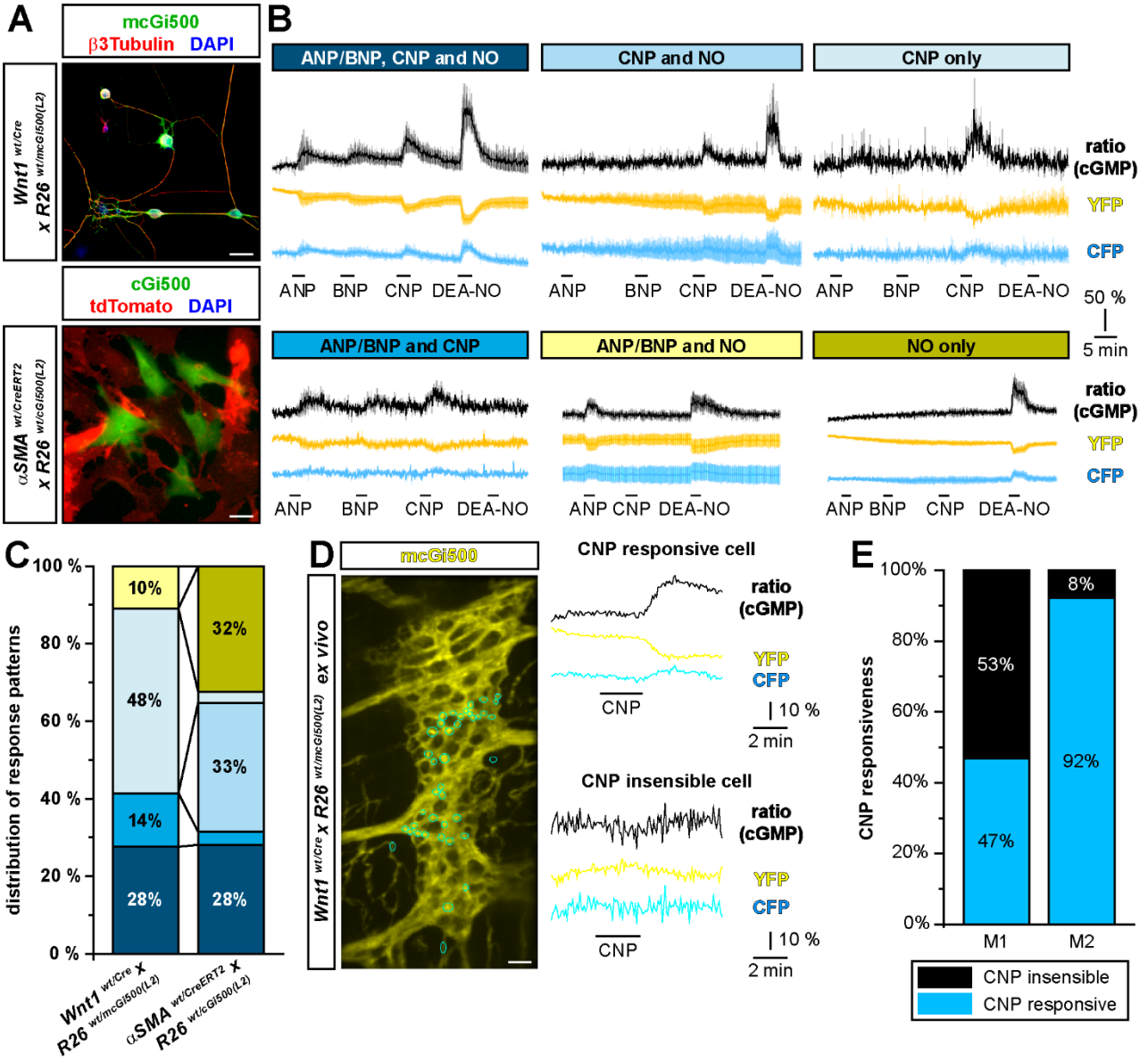

Figure 23: cGMP generation in colonic neurons and colonic SMCs.

ENS cell culture was performed with 5 to 7 weeks old mice that express the membrane bound cGMP sensor mcGi500 in neurons (genotype: *Wnt1* $^{wt/Cre}$ x *R26* $^{wt/mcGi500(L2)}$). The neurons were measured after 3 to 5 days in cell culture (n = 65 cells in 9 measurements from 2 mice). SMC culture was performed with 5 to 10 weeks old mice that express the cytosolic cGMP sensor cGi500 in SMCs (genotype: Acta2 $^{wt/CreERT2}$ x R26 $^{wt/cGi500(L2)}$). The CreER^{T2} activity was induced with 0.1 mg/g body weight Tamoxifen (5 consecutive days of injection, 9 days break, 5 consecutive days of injection). The SMC culture was measured after 3 days in cell culture (n = 102 cells in 9 measurements from 3 mice). Neuron and SMC cultures were stimulated with 250 nM ANP, 250 nM BNP, 250 nM CNP and 1 µM DEA-NO, in that sequence, for 2 minutes each. A) Representative region of a neuron culture and a SMC culture measured in cGMP-FRET measurements. B) Single cell response patterns to GC-stimulating drugs showing single traces (CFP and YFP) and the ratio trace. The ratio is proportional to intracellular cGMP levels. C) Distribution of single cell response patterns (shown in B) within the respective cell culture. D) Representative YFP image and cGMP response patterns to CNP application (single and ratio trace) of neurons in the colon MP, measured *ex vivo*. E) Distribution of neuron response patterns (shown in D; n= 2 from 1 mouse termed M1 and M2).

Since *GC-B* transcription was only shown based on the GC-B-CreERT2 mouse line, and not based on the GC-B-lacZ mouse line, an additional layer of confirmation for GC-B expression in SMCs was required. Therefore, cell type-specific cGMP-FRET measurements were performed to validate the expression of GC-B, and actual CNP-induced cGMP generation, in neurons and SMCs. Cell type-specific sensor expression was achieved by crossbreeding of the respective Cre-mouse line (Wnt1-Cre for neurons and αSMA-CreERT2 for SMCs) with the Cre-inducible R26-cGi500(L2) cGMP-FRET sensor mouse line. Different cell culture protocols for neurons and SMCs in combination with the respective crossbreeding (neuron- or SMC-specific cGMP-FRET sensor mice) ensured the purity of the cultures (**Figure 23 A**). Comprehensive characterization of colonic neurons and SMCs in cell culture showed that CNP application leads to a rise of intracellular cGMP concentrations in about 90 % of the neurons and about 68 % of the SMCs (**Figure 23 B & C**: blue shaded response patterns). Both cell types were subclassified into different response profiles reacting on ANP/BNP and/or CNP and/or DEA-NO application (**Figure 23 B & C**). Additional *ex vivo* cGMP-FRET measurements of the colon from a neuron-specific sensor mouse showed that not only cultivated neurons, but also the neurons in the tissue context generate cGMP upon CNP application (**Figure 23 D & E**).

In summary, neurons of the MP and SMCs of the CSML both express GC-B in distal colon and generate cGMP in response to CNP stimulation. Additionally, CNP transcription has only been found in neurons of the MP. This information can now be used to generate neuron-specific and SMC-specific GC-B KO mice for further investigations.

4.4.3. CNP-induced smooth muscle relaxation in distal colon is mediated by SMCs and not neurons

In the last part of this study, it was tested whether the CNP-induced distal colonic circular smooth muscle relaxation is mediated through GC-B in neurons or SMCs. Knowing that 100 nM CNP reproducibly inhibits colonic contractions to a maximum of more than 90 % relaxation, the distal colon of neuron-specific and SMC-specific GC-B KO mice was investigated in *ex vivo* IFM. Neuron-specificity was achieved with the Wnt1-Cre mouse line. The Wnt1 Cre-driver line is highly specific for neurons and leads to a recombination of “floxed” genes in neurons of the ENS. Recombination of the cGi500(L2) sensor in colonic neurons has been shown qualitatively in the cGMP-FRET experiments (**Figure 23**). To show that this Cre-driver line can potentially recombine *CNP* and *GC-B* in neurons, the Wnt1 Cre-driver line was crossbred with a Cre-inducible tomato reporter line (R26-Ai14) and the

respective CNP-lacZ or GC-B-lacZ reporter lines (**Figure 24 A & B**). An IF staining of the distal colon from these mice showed that about 8.6 % of the Wnt1 positive neurons did transcribe *CNP* and about 3.6 % of the Wnt1 positive neurons did transcribe *GC-B* (**Figure 24 C**). Assuming that the lacZ reporter line covers all CNP and GC-B expressing neurons, the possible recombination rates for *CNP* and *GC-B* were calculated. According to this calculation about 98.2 % of *CNP* transcribing cells and about 98.5 % of *GC-B* transcribing cells were covered by the Wnt1 Cre-driver line (**Figure 24 D**). The missing 1.8 % and 1.5 % of this coverage can probably be explained by technique-based fluctuations in the evaluation of the IF staining (a weak tomato staining below the threshold for positive stained cells is

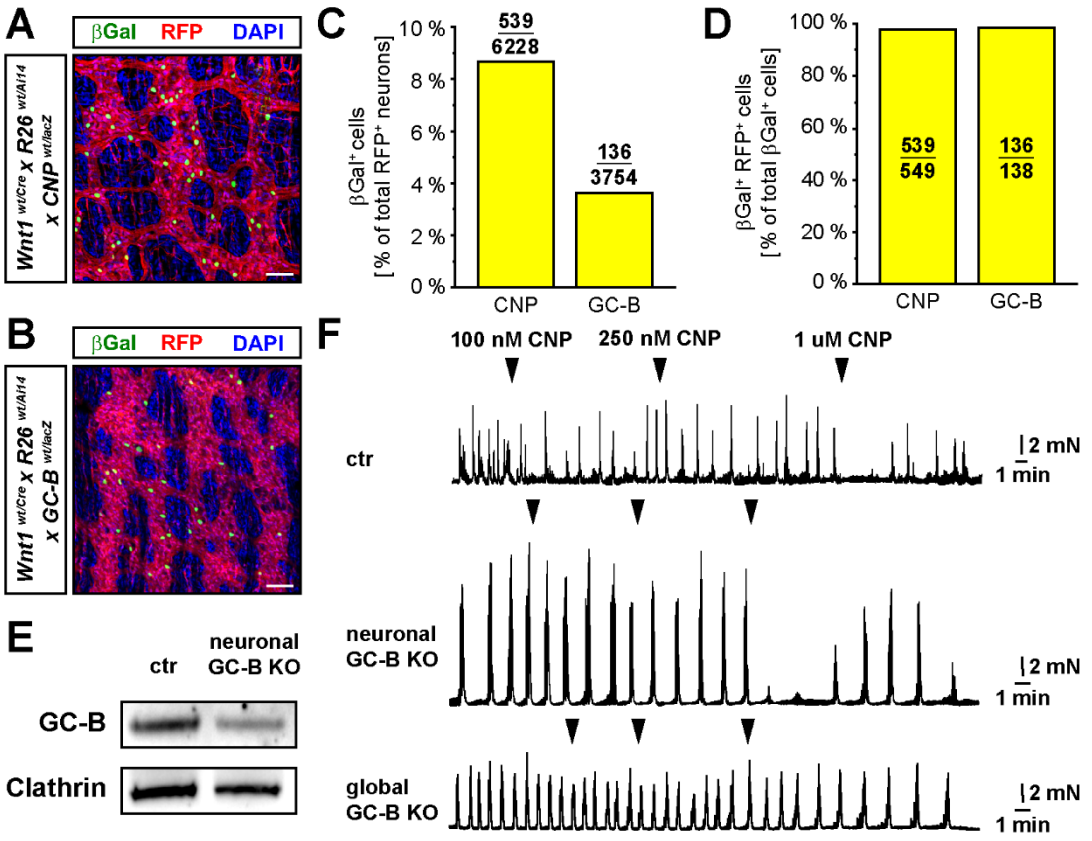

Figure 24: Contraction inhibiting effect of CNP on the distal colon of neuronal GC-B KO mice without TTX.

IF staining of the colon MP from neuronal reporter mice, which harbor either the CNP-lacZ (genotype: *Wnt1* $^{wt/Cre}$ x *R26* $^{wt/Ai14}$ x *Nppc* $^{wt/lacZ}$; A) or GC-B-lacZ (genotype: *Wnt1* $^{wt/Cre}$ x *R26* $^{wt/Ai14}$ x *Npr2* $^{wt/lacZ}$; B) gene was performed with antibodies against the βGal reporter (antibodies: ch-α-βGal and do-α-ch-AF488), antibodies against the tomato reporter (antibodies: rb-α-RFP and go-α-rb-Cy3) and DAPI. The IF staining was performed three times per genotype and the staining in the MP was recorded with a confocal microscope (LSM). Representative whole mount images of the thereby stained MP are shown in A & B. The herein stained cell populations (CNP, GC-B and Wnt-1 stained neuronal cells) were counted and the percentage of *CNP* or *GC-B* transcribing neurons were plotted in (C). The percentage of total *CNP* or *GC-B* transcribing cells that were also neurons was plotted in (D) and represents the recombination rate. E) Western blot of lysates from the distal colon of ctr (genotype: *Npr2* $^{flox/flox}$) and neuronal GC-B KO (genotype: *Wnt1* $^{wt/Cre}$ and *Npr2* $^{flox/flox}$) mice. 50 µg of protein was loaded per lane. GC-B was probed using the gp-α-Npr2 antibody and clathrin was probed using the mo-α-clathrin antibody. F) Representative IFM recordings of colonic rings (distal colon) from ctr (genotype: *Wnt1* $^{wt/wt}$ x *Npr2* $^{wt/wt}$), neuronal GC-B KO (genotype: *Wnt1* $^{wt/Cre}$ x *Npr2* $^{lacZ/flox}$) and global GC-B KO (genotype: *Wnt1* $^{wt/wt}$ x *Npr2* $^{lacZ/lacZ}$) mice at P15 without TTX application. CNP was applied at three different concentrations (100 nM CNP, 250 nM CNP and 1 µM CNP).

not counted as a Wnt1 positive cell, although the cell might show a strong lacZ staining) or the acquired image (sometimes the focal plane of the confocal microscope only includes the nucleus and, therefore, the cell body is not in the focal plane or vice versa). The neuron-specific GC-B KO mouse line was then generated by crossbreeding of the Wnt1-Cre mouse line with the GC-B-flox and the GC-B-lacZ mouse lines. The combination of these transgenic GC-B mouse lines leads to offspring with a global GC-B KO on one allele whereas the other GC-B allele is only knocked-out in neurons. This strategy only requires half as much Cre-lox recombination events and is, therefore, less error prone and more successful in generating a neuron-specific GC-B KO mouse. To confirm the neuron-specific GC-B KO, protein lysates of the distal colon were generated, membrane enriched, and a GC-B western blot was performed. The neuron-specific GC-B KO colon lysate exhibited a visible reduction in GC-B expression in comparison to the control condition (**Figure 24 E**). If quantified, normalization on the respective loading controls showed a GC-B band reduction of about 15 % comparing the neuron-specific GC-B KO colon with the control condition. The remaining GC-B band is probably explained by the expression of GC-B in SMCs which are far more abundant than neurons (the size of the SML is about two to five times the size of the MP in colon). At next, it was tested whether the GC-B expressing neurons are responsible for the smooth muscle relaxing effect of CNP in distal colon. Therefore, IFM was performed on the distal colon of neuron-specific GC-B KO mice in absence of TTX to enable communication between neurons of the ENS. The poor reproducibility of the CNP-induced relaxation without TTX (4.4.1. **Figure 18 A**: GC-B WT 1 and GC-B WT 2) made it very difficult to get similarly looking and, thereby, comparable traces. The highest CNP concentration applied in this experiment was 1 µM CNP which led to a contraction inhibiting effect in colonic rings from control and neuron-specific GC-B KO mice, but not in global GC-B KO mice. Since 1 µM CNP was applied to colonic rings of global GC-B KO mice, in more than three independent experiments, and never led to a contraction inhibiting effect (or other effects), it was still concluded that 1 µM CNP mediates a contraction inhibiting effect via GC-B. Since the colon from neuron-specific GC-B KO mice showed the same reaction pattern as the colon from WT mice, it was also concluded that CNP-induced cGMP signaling in neurons is not responsible for the contraction inhibiting effect of CNP in distal colon. However, this finding has to be confirmed in the presence of TTX where the colonic rings showed a more reproducible CNP-response pattern. Interestingly, the distention phenotype was never observed in any neuron-specific GC-B KO mouse investigated (data not shown).

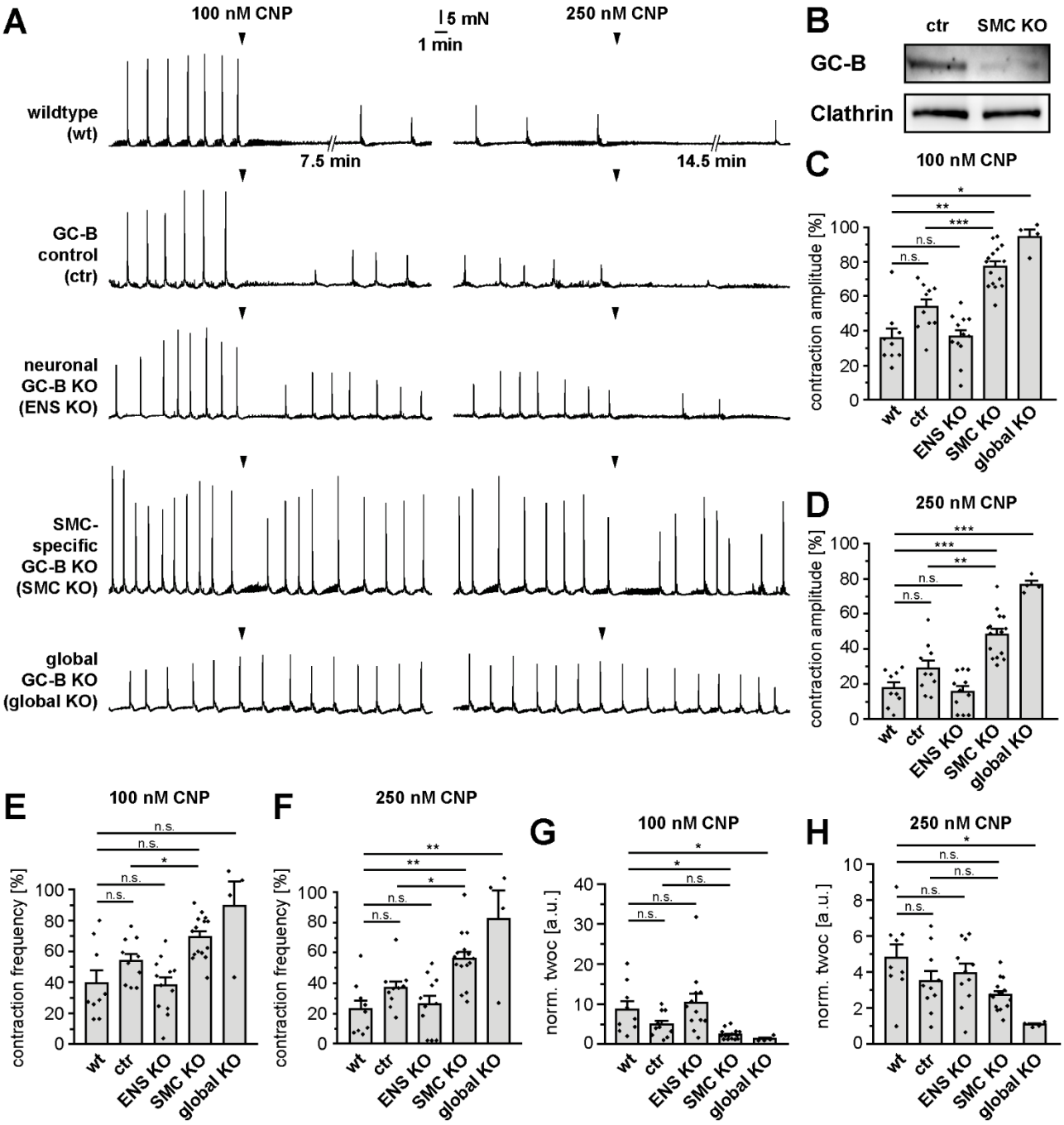

Figure 25: Contraction inhibiting effect of CNP on the distal colon from cell type-specific GC-B KO mice.

IFM was performed on rings of the distal colon from different genetically modified mice age P15. The measurements were performed in the presence of 1 µM TTX. CNP was applied twice (100 nM and 250 nM) within one measurement. WT mice (genotype: *Acta2* $^{wt/wt}$ *x Npr2* $^{wt/wt}$; n = 9 from 4 mice) represent the litter matched control group for global GC-B KO mice (genotype: *Npr2* $^{lacZ/lacZ}$; n = 4 from 3 mice) and the GC-B control mice (genotype: *Acta2* $^{wt/wt}$ *x Npr2* $^{lacZ/flox}$; n = 10 from 3 mice) represent the control group for the litter matched SMC-specific GC-B KO mice (genotype: *Acta2* $^{CreERT2/wt}$ *x Npr2* $^{lacZ/flox}$; n = 15 from 6 mice) and the not litter matched neuronal GC-B KO mice (genotype: *Wnt1* $^{Cre/wt}$ *x Npr2* $^{lacZ/flox}$; n = 12 from 3 mice). A) Representative IFM traces showing the effect of 100 nM and 250 nM CNP on the TTX-induced contraction pattern of the CSML in distal colon. B) Western blot of the distal colon from GC-B control and SMC-specific GC-B-KO mice. 50 µg of protein lysate was loaded per lane. GC-B was probed using the gp-α-Npr2 antibody and clathrin was probed using the mo-α-clathrin antibody. Baseline normalized contraction amplitude after the addition of 100 nM CNP (C) and 250 nM CNP (D). Baseline normalized contraction frequency after the addition of 100 nM CNP (E) and 250 nM CNP (F). Frequency normalized time without contraction (norm. twoc) after the addition of 100 nM CNP (G) and 250 nM CNP (H).

The next set of motility measurements was performed in the presence of TTX on distal colonic rings from global GC-B KO, neuron-specific GC-B KO and SMC-specific GC-B KO mice, as well as the respective control animals. To achieve SMC-specificity, the tamoxifen inducible Cre-driver mouse line (αSMA-CreERT2) was used. Recombination of the cGi500(L2) sensor in colonic SMCs has been shown qualitatively in the cGMP-FRET experiments (4.4.2. **Figure 23**). To confirm the identity of these colonic SMCs, the distal colon from SMC-specific cGMP-FRET sensor mice was analyzed in IF double staining of cryosections. The IF staining showed that the cGMP-FRET sensor was expressed in SMCs of the distal colon, but not in ICCs, FLCs or neurons (**Suppl. figure S9**). This confirmed that the αSMA-CreERT2 mouse line specifically recombines in SMCs of the distal colon, but neither in one of the other cell types. Hence, this mouse line was used to generate distal colon SMC-specific GC-B KO mice by crossbreeding the αSMA-CreERT2 mouse line to the GC-B-flox and the GC-B-lacZ mouse lines. Here again, the combination of these transgenic GC-B mouse lines was used to decrease the amount of recombination events needed to successfully generate a SMC-specific GC-B KO mouse. To confirm the SMC-specific GC-B KO in distal colon, protein lysates were generated and a GC-B western blot was performed. The SMC-specific GC-B KO lysate showed a visible reduction in GC-B expression in comparison to the control lysate (**Figure 25 B**). If quantified, normalization on the respective loading controls showed a reduction of 50 % comparing the SMC-specific GC-B KO with the control condition. Note, that the distention phenotype was also not observed in SMC-specific GC-B KO mice (data not shown). The impact of GC-B in neurons and GC-B in SMCs, on the contraction inhibiting effect of CNP in colon, was then quantified by IFM in the presence of TTX. In WT distal colon (**Figure 25 A**: wt), a long-lasting contraction inhibiting effect was observed upon application of 100 nM CNP. After reoccurrence of the contraction pattern, 250 nM CNP was applied leading to another long-lasting contraction inhibiting effect. This effect was also observed in the heterozygous GC-B-lacZ-flox control which was not combined with any Cre-driver line, but CNP application did not inhibit the contraction pattern by far as long as in WT (**Figure 25 A**: ctr). This discrepancy is explained by the genotype of all GC-B-lacZ-flox crossbreeding's (GC-B control, neuron-specific GC-B KO and SMC-specific GC-B KO). GC-B, which is knocked-out by the *lacZ* mutation in the GC-B gene on one allele globally, is still expressed on the other allele. Hence, GC-B expression is cut in half. In addition, GC-B is knocked-out in neurons (for the neuron-specific GC-B KO mouse), in SMCs (for the SMC-specific GC-B KO mouse) and in all cells (for the global GC-B KO mouse). A comprehensive quantification of both control conditions did not

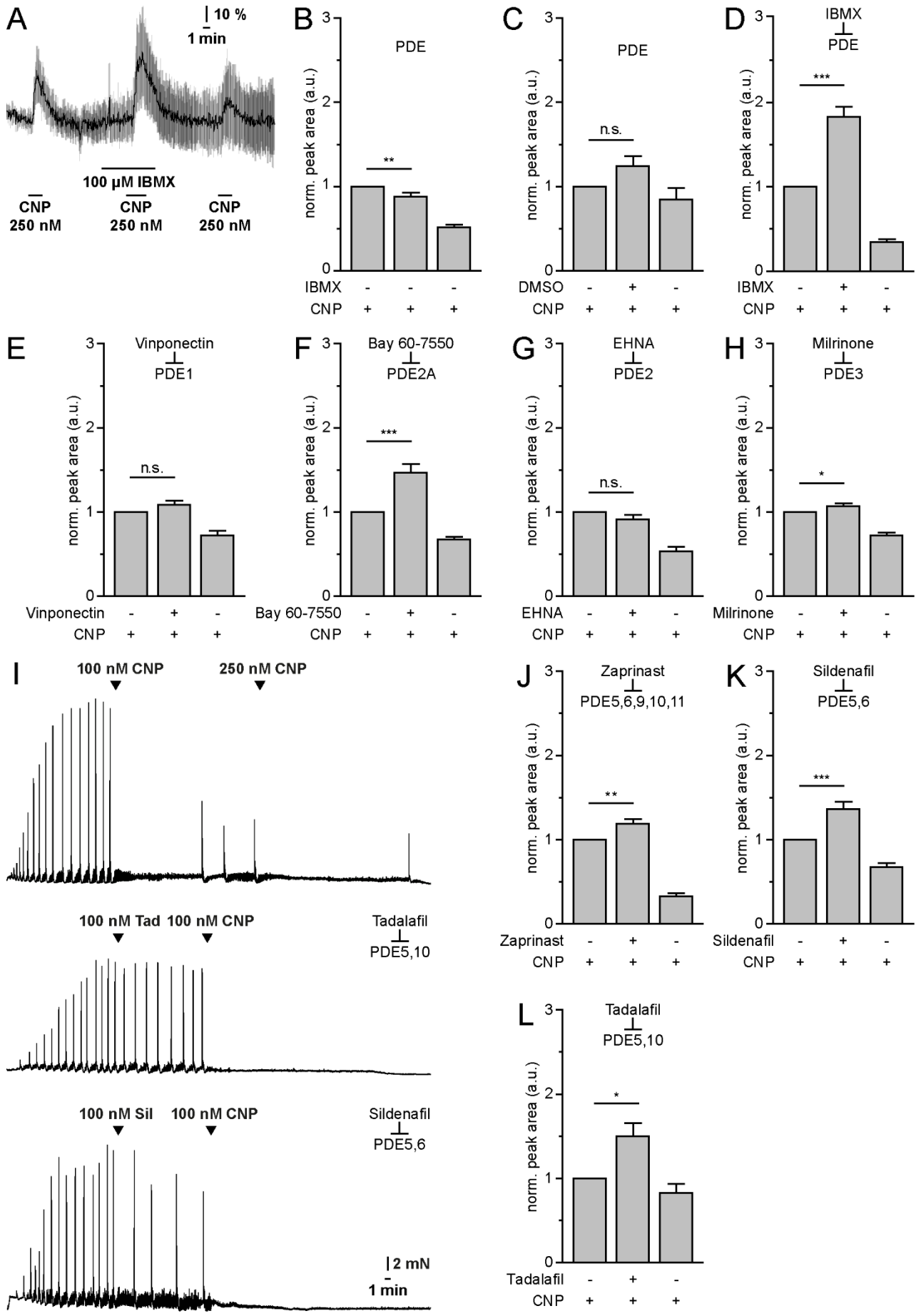
A
10 %
1 min
100 µM IBMX
CNP 250 nM
CNP 250 nM
CNP 250 nM
B
PDE
norm. peak area (a.u.)
**
IBMX - - -
CNP + + +
C
PDE
n.s.
DMSO - + -
CNP + + +
D
IBMX
PDE
***
IBMX - + -
CNP + + +
E
Vinponectin
PDE1
n.s.
Vinponectin - + -
CNP + + +
F
Bay 60-7550
PDE2A
***
Bay 60-7550 - + -
CNP + + +
G
EHNA
PDE2
n.s.
EHNA - + -
CNP + + +
H
Milrinone
PDE3
*
Milrinone - + -
CNP + + +
I
100 nM CNP
250 nM CNP
100 nM Tad
100 nM CNP
Tadalafil
PDE5,10
100 nM Sil
100 nM CNP
Sildenafil
PDE5,6
2 mN
1 min
J
Zaprinast
PDE5,6,9,10,11
**
Zaprinast - + -
CNP + + +
K
Sildenafil
PDE5,6
***
Sildenafil - + -
CNP + + +
L
Tadalafil
PDE5,10
*
Tadalafil - + -
CNP + + +

Figure 26: PDEs counteracting CNP-induced cGMP generation in colonic SMCs.

SMC culture was performed with 5 to 10 weeks old mice that express the cytosolic cGMP sensor cGi500 in SMCs (genotype: α*SMA* $^{wt/CreERT2}$ x *R26-cGi500(L2)* $^{wt/tg}$). The SMC culture was measured after 3 days in cell culture. SMC cultures were stimulated three times with 250 nM CNP during the cGMP-FRET measurement. The second time, CNP was co-applied with the respective PDE-inhibiting drug or vehicle control. An example of the drug application scheme for the co-application of 100 µM IBMX with 250 nM CNP is shown in (A). Mean cGMP-FRET ratio trace (black) with SEM (gray) showing an average cellular response. B) Control experiment with imaging buffer (n = 29, 2 measurements, 2 mice), which serves as vehicle control for Bay60-7550, Sildenafil and Tadalafil. C) Control experiment with DMSO (final concentration 1:500; (n = 23, 4 measurements, 3 mice), which serves as vehicle control for IBMX, Vinponectin, Milrinone, EHNA, and Zaprinast. Co-application of 250 nM CNP with 100 µM IBMX (D; n = 37, 4 measurements, 3 mice), 5 µM Vinponectin (E; n = 28, 3 measurements, 3 mice), 100 nM Bay60-7550 (F; n = 22, 2 measurements, 3 mice), 10 µM EHNA (G; n = 27, 3 measurements, 3 mice), 10 µM Milrinone (H; n = 27, 3 measurements, 3 mice), 20 µM Zaprinast (J; n = 22, 3 measurements, 3 mice), 20 µM Sildenafil (K; n = 28, 3 measurements, 3 mice) or 1 µM Tadalafil (L; n = 11, 3 measurements, 1 mice). I) Effect of CNP on the contraction patter of the distal colon from WT mice in the presence of 1 µM TTX. Without any PDE-inhibitor, CNP suppresses the contraction pattern only for a short time until the contraction pattern reoccurs. The contraction pattern in completely inhibited and does not reoccur again in the presence of 100 nM Tadalafil or 100 nM Sildenafil.

yield in a significant difference between the contraction amplitude, frequency or normalized time without contraction after 100 nM or 250 nM CNP application (**Figure 25 C - H**). In the next measurement, the neuron-specific GC-B KO (**Figure 25 A**: ENS KO) led to a similar level of CNP-induced relaxation as the GC-B control and WT (**Figure 25 C - H**). This confirmed the previous finding that GC-B in neurons does not mediate the contraction inhibiting effect of CNP in distal colon. In turn, the SMC-specific GC-B KO exhibited a visibly smaller contraction inhibiting effect than both controls after the application of 100 nM and 250 nM. The contraction amplitude and frequency, after both CNP applications, were significantly higher in SMC-specific GC-B KO than in the GC-B control, but not significantly different from the global GC-B KO (**Figure 25 C - F**). Although the mean normalized time without contraction of the SMC-specific GC-B KO was not significantly different from the GC-B control, a trend towards a smaller normalized time without contraction was observed for the SMC-specific GC-B KO (**Figure 25 G - H**). This trend appeared strong after the first application of CNP (100 nM), but was clearly damped after the second CNP application (250 nM). Overall the global GC-B KO was not affected by any concentration of CNP (**Figure 25 A**: global KO), neither with respect to the contraction amplitude, frequency nor the normalized time without contraction (**Figure 25 C - H**).

With these findings, the conclusion can be drawn that GC-B in SMCs, but not GC-B in neurons, is responsible for the contraction inhibiting/smooth muscle relaxing effect of CNP on the distal colon.

To further the knowledge about CNP-induced cGMP signaling in SMCs, the involvement of PDEs was investigated. PDEs, which degrade cyclic nucleotides, prolong or shorten the duration of CNP-induced smooth muscle relaxation in distal colon. Therefore, PDE inhibitors

were employed in SMC-specific cGMP-FRET cell culture measurements. After IBMX showed a significant increase of the CNP-induced cGMP response by two-fold (**Figure 26 A - D**), various PDE-specific inhibitors were tested (**Figure 26 E - H, J - L**). It was found that PDE2A-specific and PDE5-specific inhibitors both increase the cGMP response in cell culture. To identify the impact of PDE5 on the contraction inhibiting effect of CNP, Tadalafil and Sildenafil were coapplied with 100 nM CNP in IFM of the distal colon (**Figure 26 I**). These experiments showed that the autonomous contraction pattern, which reoccurs several minutes after CNP application, does neither reoccur in the presence of Sildenafil nor in the presence of Tadalafil. Therefore, SMC-expressed PDE2A and PDE5 seem to counteract the CNP-induced cGMP production and the CNP-induced smooth muscle relaxation in distal colon.

In summary, CNP, which is expressed by nitrergic neurons of the distal colon, induces GC-B-mediated cGMP generation in colonic neurons and SMC. The smooth muscle relaxing effect of CNP is mediated by GC-B on SMCs, but not by GC-B on neurons. The here through generated cGMP in SMCs, is degraded by PDE2A and PDE5. This novel signaling model might help to understand the GI distension phenotype and the early death observed in global GC-B KO mice.

5. Discussion

Studies in the last 30 years have shown that cGMP signaling is pivotal for proper GI function. Most of these studies were focusing on nNOS and NO-GC, (uro)guanylin and GC-C, or cGKs. The few studies investigating CNP-induced cGMP signaling in the GIT were performed at the tissue level and did not identify the respective cell types expressing CNP or GC-B. Therefore, the present study aimed at the identification of cell type-specific and functionally relevant CNP and GC-B expression in the GIT.

5.1. Gastrointestinal abnormalities of global GC-B KO mice

The first step to decipher CNP-induced cGMP signaling in the GIT was to identify regions where GC-B is functionally relevant. To do so, the GC-B-lacZ mouse line was used to generate global GC-B KO mice and investigate potential GI abnormalities.

It was found that global GC-B KO mice suffer from a GI distention phenotype that is located to the ileum, cecum, and colon. This distension phenotype was observed at P5, P8, and P15, but not at P20 (**4.1. Figure 14 B**). In addition to the GI phenotype, the teeth of P5, P8 or P15 mice did not appear to be different between WT and GC-B KO mice, but there was a difference in teeth appearance at P20. The teeth of P20 WT mice were all of the same size, whereas the lower incisors of the global GC-B KO mice were differently long (in two out of three cases) and appeared to be broken off (**4.1. Figure 14 D**). This observation suggested that GC-B KO mice at P20 are prone to get longer lower incisors than WT mice which then break off at some point. In general, the front teeth of mice erupt between P10-P12 and grow continuously throughout their life. The upper incisors grow 2 mm/week, whereas the lower incisors grow 2.8 mm/week [145]. Due to this growth rate, mice have to use and wear off their teeth by chewing on solid food (food pellets) or other hard objects (e.g. cage bedding). Since weaning happens around P21, young mice have about 1 week to learn this process. Broken of teeth usually imply that the teeth were already too long to use them properly. This can only happen if the teeth were not worn off for multiple days which also usually means that the respective mice did also not eat solid food during that time either. Malnutrition is the consequence and explains the skinny, malnourished-looking appearance of global GC-B KO mice at P20. Nakao and coworkers [92] have shown that CNP KO mice, which like GC-B KO mice suffer from dwarfism, tend to have longer teeth at weaning. They observed that CNP KO mice, which were fed with pulverized food instead of the whole food pellets, have a significantly higher survival rate around weaning (70 % with pulverized food

pellets and 40 % with whole food pellets). This led to the conclusion that the reason why the mice die around weaning is that they cannot eat whole food pellets as soon as their teeth are too long and, therefore, they eventually starve to death. But why do CNP and GC-B KO mice not wear off their teeth properly before weaning? Regarding the global GC-B KO mice of this study, the not worn off lower incisors could be explained through the distention phenotype. This GI complication must cause a lot of pain and suffering between P5 and P15 and might prevent the mice from eating solid food or even just wearing off their teeth. Although the distention phenotype was not observed at P20, it is possible that the respective mice had already suffered from it before. Consistently, the distention phenotype has been observed by us in all global GC-B KO mice dissected between the age of P5 and P15. Signs of malnourishment are usually observed in global GC-B KO mice before weaning, ultimately resulting in the premature death of approximately 74 % of the global GC-B KO mice [128]. Therefore, it can be hypothesized that the overgrown incisor phenotype is only a secondary effect resulting from a lack of solid food consumption due to GI distention and pain, and is not the consequence of an increase in tooth growth per se.

To identify the underlying mechanisms, it is important to understand where the distention phenotype is coming from and why it was not observed at P20 in this thesis. Assuming that P20 global GC-B KO mice lose the GI distention due to the consumption of solid food pellets between P15 and P20, the diet itself seems to be responsible for this phenotype somehow. The two major diets, which young mice get, are the fiber-free mother's milk from P0 to P21 and the fiber-rich solid food pellets from P10-12 to the end of their life. Interestingly, motility patterns also change once during the first 21 days after birth. Immature motility patterns are in place from E18.5 to P10-14 and specialized on the digestion of mother's milk. They are in general weaker, more frequent, not migrating, and only under limited ENS control. Mature motility patterns in turn take over from P10-14 and are designed to support the digestion of fiber-rich food. They are strong, less frequent, migrating throughout large segments of the GIT, and entirely controlled by the ENS [14, 142]. Therefore, complete MMCs (peristaltic waves that propagate from the beginning to the end of the colon) are only observed with mature motility patterns after P10-14. The GI distention observed in global GC-B KO mice starts at the Cannon-Böhm point which is known for its luminal narrowing due to decreased tonic inhibition of the CSML. It is possible that the CNP/GC-B signaling pathway is involved in the tonic inhibition of immature motility patterns which then cause a more narrowed and, thereby, an obstructed Cannon-Böhm point. The obstruction then blocks the passage for fiber-free mother's milk. While immature motility patterns are too weak to open this

obstruction, mature motility patterns (like complete MMCs) need to be evoked by stimulating the sensory neurons of the mucosal layer. The fiber-rich food then provides enough solidity to stimulate motility patterns which open the obstruction, thereby, mitigating the distention phenotype. Validation of this hypothesis requires the characterization of the cellular expression profiles of CNP and GC-B in the GIT, to rule out the involvement of other compartments (**5.2.** & **5.3.**). After that, cell-type specific gene KO mice have to be established for CNP and GC-B to analyze their function in the colon (**5.4.**).

Previous studies by Sogawa and coworkers, using the GC-B-slw (short-limbed dwarfism) mouse line which harbors a spontaneous GC-B LOF mutation, revealed a complex GI phenotype [128-131] that was only in part observed in the experiments of this thesis. Besides the dwarfism phenotype [130] and an early death before weaning (survival chance of 26 %) [128], juvenile GC-B-slw mice were reported to suffer from pyloric [129] and colonic stenosis [128] with milk retention in the stomach and distended intestines due to ilei (obstructed intestinal segments) and volvuli (twisted intestinal segments) in the ileum and large intestine [128, 129, 131]. These GI phenotypes were found in pylorus and colon which both showed smooth muscle relaxation in response to CNP application *ex vivo.* Therefore, it was speculated that GC-B in SMCs might be responsible for the phenotypes observed in these regions, however, the expression of GC-B in pyloric and colonic SMCs has never been convincingly shown (discussed in **5.2.**) [131]. Sogawa and coworkers also discovered the GI distension phenotype in their global GC-B LOF mutation mice before P20, but they could not identify the underlying mechanism or cell types involved [128]. The reappearance of the distention phenotype in various GC-B LOF mutation mouse lines of different genetical backgrounds (mouse line in this thesis: GC-B-lacZ, mouse line used by Sogawa and coworkers: GC-B-slw) indicates a high reproducibility of this phenotype in mice. Similar observations were reported for other GC-B LOF-specific defects like axon bifurcation or oocyte maturation (**1.2.3.**). In human, homozygous LOF or compound inactivating mutations of the GC-B gene lead to an achondroplasia called AMDM (**1.2.3.**) that is characterized by a short stature (dwarfism). Human AMDM patients only suffer from the short stature and subsequent tertiary effects, but no other medical issues have been reported to date. Whether the GI distention also occurs in newborn AMDM patients is unknown and requires further investigations.

5.2. Distribution of CNP and GC-B in the gastrointestinal tract

To find the origin and a possible explanation for the GI distention phenotype, we used Xgal staining of *lacZ*-reporter mouse lines to assess the expression patterns of CNP and GC-B in the GIT. *CNP* was found to be notably transcribed in esophagus, pylorus, small and large intestine, whereas *GC-B* transcription was found in esophagus, pylorus, ileum, colon, and MLN. GC-B expression was then confirmed in esophagus, pylorus, ileum, colon, and MLN. Co-expression of GC-B and cGKI were found in esophagus, pylorus (antrum and sphincter), ileum, colon, and rectum. Interestingly, the expression of GC-B and cGKI was especially high in the colonic SML.

Notable co-expression of GC-B and cGKI were found in segments with internal GI sphincters and valves, namely the lower esophageal sphincter, the pyloric antrum (also called pyloric valve), the pyloric sphincter, and the ileo-cecal sphincter. In addition, both proteins were expressed in GI segments with a storage function like the stomach, pyloric antrum, colon, and rectum. It is known that cGKI is expressed in SMCs of the LSML and CSML where it mediates smooth muscle relaxation [146]. Since all these regions have a high SML to mucosa ratio, it is plausible that more cGKI is present in the respective segments. The small intestinal segments have a very small SML in comparison to the mucosal layer which is probably the reason for the weak cGKI detection. GC-B expression, in turn, has been investigated before using antibodies. Sogawa and coworkers employed western blot and immunohistochemistry to identify GC-B expression in pylorus, jejunum, ileum, colon, and rectum [131]. They observed a similar expression pattern on western blot as shown in this thesis. That is a high expression of GC-B in pylorus, colon, and rectum and a rather low expression in duodenum and jejunum. In contrast to our data, they observed a low expression of GC-B in ileum, whereas we observe high *GC-B* transcription and GC-B expression (**4.2. Figure 15 B & Figure 15 F lane 8**). Although Sogawa and coworkers observed similar distributions of GC-B in immunohistochemistry and western blot, their GC-B immunohistochemistry antibody stained a great quantity of the tissue. Such staining patterns usually include unspecific binding to the tissue. To confirm the respective antibody staining, the GC-B antibody has to be validated with tissue from GC-B KO mice. This has not been done for the anti-GC-B antibody (Abcam; ab37620) used in the study of Sogawa and coworkers [131]. In general, the most common problem of antibodies is their specificity. The generation of a GC-B-specific antibody is more successful if it is generated against the extracellular domain (43 % sequence homology to GC-A), because the sequence identity of the other GC-B domains to GC-A is quite high (78 % for the intracellular domains) [74].

Although the western blot antibody used by Sogawa and coworkers was directed against the N-terminal domain of GC-B (extracellular domain), their immunohistochemistry antibody was directed against the C-terminal domain (intracellular domain) and was, consequently, more prone to cross-reactivity with other pGCs. Cross-reactivity would also explain why ab37620 was retracted from the fabricator's homepage with a letter of excuses. In turn, the reliability of their immunohistochemistry results is unclear. Such ambiguities were avoided in the current study by using βGal-based reporter mice to investigate *CNP* (CNP-lacZ) and *GC-B* (GC-B-lacZ) promotor activity. Both reporter mouse lines express a nuclear-localized βGal that produces a nucleus-confined Xgal and IF staining. The subcellular localization of the staining then enables the user to distinguish between neighboring, individual cells inside the tissue. A major advantage of the *lacZ*-reporter mice used in this study is the possible differentiation of true-positive (e.g. nucleus-confined staining) and false-positive staining results (e.g. not nucleus-confined staining). The major source of false-positive staining results in the intestines are bacteria contained in the luminal space. Intestinal Bacteria also express βGal and, therefore, produce a strong blue Xgal staining. This is especially problematic in the large intestine where bacteria make up for a prominent portion of the luminal content. However, the staining pattern produced by nuclear-localized βGal is clearly distinguishable from any bacterial staining. Other unavoidable sources of false-positive staining results are the endogenous, non-bacterial βGals. Lactase, for instance, is expressed in epithelial cells along the small intestine in young mice before weaning (**1.1.6.**) [73]. Xgal staining performed on Lactase-expressing GI segments then leads to a prominent blue staining in epithelial cells. This unspecific staining pattern was observed in the small intestine at P1 and cannot be avoided at that age (**4.3. Figure 16**: P1). But, the true power of the two βGal-based reporter systems is revealed in combination with the high sensitivity of the Xgal staining. It allows to identify even small traces of *CNP* or *GC-B* promotor activity while being certain about their trueness. The only uncertainty left is the rate of true-negative to false-negative staining results. Since the histochemical staining efficiency is based on the reporter enzyme activity, some conditions (like fixative agents or a high concentration of digestive enzymes) can destroy this activity and prevent successful Xgal staining. Hence, it is still possible that βGal-expressing (*CNP* or *GC-B* transcribing) cell populations are overlooked with this reporter system.

Protein lysates, for the detection of GC-B by western blot, were generated using tissue preparations from transgenic mice where the N-terminal domain of GC-B harbors the hemagglutinin-tag (HA-tag). This allows a highly specific and reliable detection of GC-B

through HA-tag antibodies [4]. CNP, in turn, is more difficult to analyze. Due to its highly conserved nature throughout all mammals [105], it is very difficult to generate antibodies that are specific for CNP. Previous studies, however, identified *CNP* transcription and CNP expression at the tissue level using RT-PCR and different chromatography-based approaches, respectively. Minamino and coworkers were able to detect *CNP* transcription and CNP expression in rat stomach, jejunum, ileum, colon, and rectum [86]. Another study focusing on rabbit colon identified *CNP* and *GC-B* transcription as well as CNP expression in colon [70]. These studies show that other species also express CNP in the same GI segments as observed in the experiments of this thesis.

5.2.1. Esophagus

The highest number of *CNP* transcribing cells within the GIT has been detected in the developing esophagus. This number declined from P15 to P75, whereas *GC-B* transcription seemed to increase from P15 to P75. Xgal stainings on cryosections showed that both the *CNP* and *GC-B* transcribing cells were localized within the circular and longitudinal muscle layers. Future experiments will have to focus on the identification of those cell types and the subsequent generation of cell type-specific CNP and GC-B KO mice. Since the esophagus consists of skeletal muscle cells (marker protein: sarcomeric actin) as well as SMCs (marker protein: αSMA), marker protein staining against both muscle types are required [108]. In addition, transcription of *CNP* and *GC-B* in interstitial cells like ICCs (marker protein: c-kit) or FLCs (marker protein: PDGFRα) also has to be clarified. A previous study from Groneberg and coworkers, about NO-GC-mediated cGMP signaling in lower esophageal sphincter, showed that NO-GC is expressed in SMCs, ICCs, and FLCs where NO-induced cGMP signaling mediates lower esophageal sphincter relaxation [51]. This leads to the question of which role the CNP-induced cGMP signaling plays in healthy lower esophageal sphincter. The observation that the number of *CNP* transcribing cells decreases, whereas the number of *GC-B* transcribing cells increases over time is rather enigmatic. One would expect a similar relation of transcription over time, if it is assumed that the cells producing CNP secret it to signal to the GC-B expressing cells. However, the gradually decreasing pattern of *CNP* transcription rather indicates that the respective cells might be relevant for esophageal development. Hence, one potential cell type could be the skeletal muscle cell precursor called satellite cell (marker protein: paired box 7). These cells differentiate into skeletal muscle cells, thereby, forming and regenerating skeletal muscle tissue in the esophagus [22]. Future experiments should clarify the identity of *CNP* and *GC-B* expressing cells. Cell type-specific GC-B KO mice should be used to identify the function of GC-B in

those cell types on the tissue level. Functional assays could include IFM of the esophagus to investigate CNP-induced esophageal SML relaxation as well as H&E staining of esophagus paraffin sections to assess any developmental impairment.

5.2.2. Pylorus

The pylorus as part of the stomach is pivotal for proper digestion. The pyloric antrum serves as a valve that engulfs a part of the chyme from the stomach and gates it through the pyloric sphincter into the duodenum. Previous studies performed on the tissue level have already revealed that 100 nM and 1 µM CNP inhibit the contraction profile of the pyloric CSML in a GC-B dependent manner. It has also been shown that CNP induces the generation of cGMP in pyloric tissue and GC-B LOF mutation mice develop a pyloric stenosis in early life [129, 131]. Another study, which was performed on the tissue level in rat pylorus, confirmed the generation of cGMP upon CNP stimulation and suggested a PDE3-mediated cAMP crosstalk [17]. But after all these studies, the cell type-specific expression of CNP, GC-B, and other signaling components is still not known. In order to change that, this thesis provides detailed insights into the time course of transcription and the localization of the cells involved. Cells transcribing *CNP* in the pyloric antrum were first observed at E14.5 and strongly increased in number until P1. The onset of *CNP* transcription in pyloric sphincter seemed to be around P1. From that point on the number of *CNP* transcribing cells in pyloric antrum and sphincter seemed to remain stable until P300. Looking into cryosections, the nuclei of *CNP* transcribing cells in pyloric antrum and sphincter were localized almost exclusively within the CSML. This suggests that these cells are either SMCs, ICCs or FLCs. Although the *GC-B* transcribing cells in pyloric antrum were also observed from P1 on, their number increased until P5. At P15 and later it was observed that a second type of cell, which was characterized by a smaller nuclear Xgal staining, emerged. This staining pattern remained until P300. In cryosections, the largest Xgal stained nuclei were localized to the MP and were already observed at P15. At P45 a second population of Xgal stained nuclei was observed which seemed to be localized to the mucosal layer. In addition to cells observed in the whole mount staining, cryosection staining revealed a third cell type localized to the CSML at P75. In pyloric sphincter, *GC-B* transcription was only faintly observed in some conditions (**Suppl. figure S2 - sphincter – *Npr2* $^{wt/lacZ}$ - P45**), but a closer look into cryosections revealed that this population was localized to the mucosal layer and, therefore, probably not easily seen in whole mount. *GC-B* transcribing cells localized to the MP could be neurons (marker protein: PGP9.5), cells localized to the SML could be SMCs, ICCs or FLCs, and cells localized to the mucosal layer could be parietal cells (marker protein:

H^+/K^+-ATPase alpha subunit), chief cells (marker protein: pepsinogen), enteroendocrine cells (marker protein: chromogranin A), G-cells (marker protein: gastrin), surface mucus cells (foveolar cells; marker protein: mucin 5AC), mucus neck cells (marker protein: trefoil factor 2) or stem cells (marker protein: leucine-rich repeat containing G-protein coupled receptor 5) [113]. In future experiments, IF staining should be performed to clarify the cell types transcribing *CNP* and *GC-B*. In addition, cell type-specific GC-B KO mice should be generated to identify the function of GC-B in the different cell types. Functional assays could include IFM of the pylorus to investigate CNP-induced pyloric SML relaxation as well as H&E staining of pyloric paraffin sections to assess any degree of pyloric stenosis.

5.2.3. Mesenteric lymph nodes

A major difference between gene transcription and expression of GC-B has been observed in the MLN. It was observed that a lot of cells in the subcapsular sinus transcribe *GC-B* (**Suppl. figure S4 A & B**) in later stages (P45 and P75), but the GC-B expression in the whole tissue on western blot was quite low as compared to the pylorus, esophagus, ileum, and the colonic SML (**4.2. Figure 15 F – lane 13 vs. lane 1, 8 & 10**). This discrepancy could originate from the different ages investigated. *GC-B* transcription was observed at P15 already, but increased strongly over time until P75. The rather faint GC-B western blot band of the MLN from 25 days old GC-B-HA mice is only comparable to the Xgal stained MLNs of 15 days old GC-B-lacZ mice, and not any older stage (**4.2. Figure 15 E**). Later ages were not confirmed on the protein level via western blot. The subcapsular sinus, where *GC-B* transcription was localized to, harbors three major cell types: the lymphatic endothelial cells (LEC), marginal reticular cells, and subcapsular macrophages. It was observed that *GC-B* transcribing cells in the subcapsular sinus express the endothelial cell marker CD31, the SMC marker αSMA, and the fibroblast marker vimentin, but neither of them expressed the T-cell marker CD3, the B-cell marker B220, nor the macrophage marker F4/80 (**Suppl. figure S4 A & B**). According to literature, only the endothelial cells express CD31 in MLN. From the two different endothelial cells present in MLN, LECs line the subcapsular sinus, whereas blood endothelial cells line the high endothelial venules inside the paracortex [153]. Therefore, it can be concluded that *GC-B* transcribing cells in MLN are LECs. *CNP* transcription was only found in adult stages in a very small number of cells. Future experiments should be focusing on the origin of CNP in MLN. The question is whether CNP is produced by cells of the MLN, produced by cells that are present in the lymph juice, or whether CNP is a component of the lymph juice itself. In addition, a LEC-specific GC-B KO

mice could reveal potential phenotypes such as, for instance, an altered MLN perfusion, leucocyte recruitment, or tissue regeneration.

5.3. CNP expression in Paneth cells of the small intestine

The Xgal screening approach performed to identify *CNP* transcription in whole mount preparations of the small intestine revealed “football-like” staining patterns. These staining patterns were successfully deciphered as *CNP* transcribing Paneth cells (**4.3. Figure 17 A - C**). Paneth cells lay in the crypts of Lieberkühn and have two very important functions. The first is to maintain the stem cell niche and the second is to release antimicrobial peptides which act against microorganisms. Paneth cells are abundantly present in the small intestine where microorganisms are a natural competitors for the chyme that is supposed to be absorbed by the mucosal layer [24]. *CNP* transcription was observed as early as P15, therefore, showing that transcription starts between P5 and P15 in duodenum, jejunum, and ileum. The number of *CNP* transcribing Paneth cells increases until P45 and remains stable until P75, still being observed at P300 (**4.3. Figure 16**). Whether *CNP* is transcribed by the same Paneth cells throughout their lifetime, or if they transcribe it only temporarily, needs to be clarified in future experiments. Paneth cells degranulate into the small intestinal lumen in response to Toll-like receptor (TLR) activation and cholinergic agonists [24]. Early Paneth cell degranulation (3 hours after ingestion) is mediated via DNA binding to TLR9, whereas late Paneth cell degranulation (up to 18 hours after ingestion) is mediated by lipopolysaccharide binding to TLR4 in a tumor necrosis factor alpha-mediated manner [109]. Interestingly, CNP production and secretion is also stimulated in the presence of lipopolysaccharides [74]. This suggests that CNP secretion and Paneth cell degranulation could happen through a similar or even the same stimulus. Further experiments are required to clarify this question. The expression of GC-B, in turn, has previously been investigated by Rambotti and coworkers in rat small intestine [107]. Their study suggested the expression of GC-B in neurons and epithelial cells of the small intestine even though they used excessive amounts of CNP (1 M) to stimulate GC-B activity. Such high concentrations of CNP or ANP (in the molar range) always bear the risk of GC-A/GC-B cross activation as we know from *in vitro* studies [9]. Anyhow, we also observed *GC-B* transcription in neurons (**4.3. Figure 17 D**) and epithelial cells (**4.3. Figure 17 E**) which suggests two possible modes of CNP secretion: (1) CNP secretion into the lumen of the small intestine or (2) CNP secretion into the interstitial mucosal layer.

In hypothesis (1), CNP is secreted into the lumen of the small intestine where it mixes with the liquid present in the crypt. It is flushed out eventually and binds to GC-B on epithelial

cells in the ileum and proximal colon. The cGMP generated by GC-B would then activate the same downstream signaling cascade as GC-C normally does. That is cGKII activation which in turn reduces the absorption potential of the cystic fibrosis transmembrane conductance regulator. Thereby, it would be possible for CNP to reduce electrolyte and water absorption of ileal and colonic epithelial cells. Reduced absorption would also lead to a more liquid chyme which is known to increase bacterial activity, hence, gas is produced. This could be a possible explanation for the distension phenotype observed in early life.

In hypothesis (2), CNP is secreted into the interstitial space inside the mucosal layer. In this scenario it either binds to GC-B on the axons and dendrites of neurons, or it is collected with the interstitial liquid and transported away through the lymphatic vessel. In the latter case CNP could serve as a signaling molecule for the LECs in the MLN. In the first case, CNP could be a signaling molecule for neurons. The current knowledge about the role of CNP and GC-B in axon bifurcation of dorsal root ganglion neurons and cranial sensory neurons [121, 138] suggests a similar mechanism for the small intestine. CNP released by freshly formed crypt Paneth cells could trigger axon bifurcation in GC-B expressing neurons and, therefore, aid in proper small intestinal villus innervation. Alternatively, it is also possible that CNP serves as a neurotransmitter between Paneth cells and GC-B expression neurons, but with an unknown response.

Evidence supporting either of those hypotheses will have to be collected with future experiments. Since the Defα6-iCre mouse line seems to cover CNP-expressing Paneth cells, it should be used to generate Paneth cell-specific CNP KO mice. These KO mice could then be investigated in terms of any phenotypic alterations like the distention phenotype or ileal/colonic stenosis.

5.4. CNP-induced cGMP signaling in colon

Interestingly, the distension phenotype, observed in the ileum, cecum, and colon of global GC-B KO mice, has always been started at the Cannon-Böhm point which lies in the colonic segment referred to as distal colon. It was also hypothesized that mature motility patterns in combination with fiber-rich food mitigate the distention phenotype. To strengthen this hypothesis, the impact of CNP-induced cGMP signaling on colonic motility was assessed. Next, the respective cell types of transcription were identified and ultimately GC-B was knocked-out in a cell type-specific manner.

5.4.1. CNP-induced circular smooth muscle relaxation in proximal and distal colon

To find the colonic segment where CNP had the highest impact on motility patterns, the proximal and distal colon were investigated in IFM. In general, it was observed that autonomic contraction patterns, with a defined peak shape, never showed a contraction inhibiting effect of CNP, but irregularly shaped, autonomic contraction peak patterns were inhibited by CNP. This was changed in the presence of TTX where the peak shape in all segments had the same appearance (including a change in contraction frequency) and CNP always induced a contraction inhibiting effect in WT. The GC-B KO measurements never showed a reaction to CNP, indicating that the contraction inhibiting effect of CNP in proximal and distal colon is mediated by GC-B.

The smooth muscle syncytium of the GIT consists of SMCs performing the contraction, ICCs and FLCs, which aid in SMCs membrane de- and hyperpolarization, and neurons of the ENS. The ENS controls the tonic inhibition of the SML and also coordinates contractile stimuli [32]. Coordinated release of excitatory neurotransmitters leads to a strong circular contraction of the respective GI segment. In *ex vivo* IFM, the amplitude (strength) of the autonomous contraction pattern depends on the length, cutting point, and basal tension of the respective colonic ring. Although the cutting is always performed at the same positions, not all contraction patterns develop in the same way. The two contraction patterns observed in this thesis differ mainly in their peak shape and reaction to CNP. A peak of the GC-B WT pattern 1 reacts on CNP and consists of multiple smaller and one or two stronger peaks (**4.4.1. Figure 18 A**; GC-B WT 1), whereas the peak of the GC-B WT pattern 2 does not react on CNP and consists of more or less one strong peak (**4.4.1. Figure 18 A**; GC-B WT 2). The different peak shapes could be explained by the ENS which probably coordinates an excitatory contraction signal in pattern 1 less successful as in pattern 2. In

consequence, the peak shape of pattern 2 is more defined and indicates a higher level of ENS coordination than the peak shape of pattern 1. Hence, we hypothesize that colonic rings, which behaved like pattern 1, were either cut at the wrong position or the length of the segment was too short. Both would lead to a colonic ring that harbors an insufficient amount of intact/functional ENS ganglions and is, thus, unable to properly coordinate motility. Since autonomic contractions are only inhibited by CNP in pattern 1, which probably lacks proper ENS functionality, it is very likely that the ENS somehow suppresses CNP-induced relaxation. To confirm this, colonic rings were treated with TTX. TTX inhibits voltage gated sodium ion channels of neurons, thereby, preventing axonal firing. This disturbs the communication of ENS neurons with each other and prevents the coordinated release of neurotransmitters from excitatory and inhibitory motor neurons. In consequence, the tonic inhibition of the SML, which happens under normal conditions all the time, is now deactivated. Instead, the slow-wave contraction pattern, which is elicited by ICCs, can now be observed in the motility pattern as slow phasic contractions (**4.4.1. Figure 18 B**). Consequently, CNP reproducibly induced a contraction inhibiting effect in TTX-treated colonic rings, whereas the same effect was only sometimes observed in TTX-untreated colonic rings. These results, therefore, demonstrated that the contraction inhibiting effect of CNP is suppressed by the ENS in TTX-untreated colon and is probably not mediated via the ENS network itself, but rather via other cells of the functional smooth muscle syncytium of the colon (SMCs, ICCs or FLCs).

The comparison between the proximal and distal colon showed that the contraction inhibiting effect of CNP is stronger in the distal colon than in the proximal colon (**4.4.1. Figure 19 C & E**). Although the contraction frequency did not seem to be different at the end of the dose-response curves (**4.4.1. Figure 19 F**: 50 nM and 100 nM CNP), the respective EC50 value was significantly lowered (**4.4.1. Figure 19 D**). Both results show that the distal colon reacts stronger to the application of CNP. The additional application of CCh, which is an ACh receptor agonist, showed variable results. In proximal colon, CCh increased the amount of CNP required to reach the half maximal concentration, whereas the inverse effect was observed in distal colon. This might be explained by the presence of ICCs which, besides SMCs, also express the muscarinic ACh receptor M3 [72]. It has been shown that there are more ICCs present in the proximal colon as there are in the distal colon. Therefore, it may be possible that the influence of ICCs on the motility pattern is higher in the proximal colon. This was also indicated by a higher basal contraction frequency and, in consequence, lower basal contraction amplitude in proximal colon (**Suppl. figure S5**).

Altogether it appears that the distal colon reacts stronger to CNP application. Since this is also the colonic segment where the Cannon-Böhm point is located in, the distal colon became the major focus of subsequent experiments.

5.4.2. Identity of CNP and GC-B expressing cells and time course of expression in the distal colon

Although CNP and GC-B expression in colon has been shown before in various species, their time course of expression had never been investigated. The first set of experiments was performed with tissue from the CNP-lacZ and GC-B-lacZ mouse lines. A Xgal screening on whole colon revealed the onset of *CNP* transcription between P5 and P15, whereas *GC-B* transcription already started before birth. The transcription of both genes was observed until late in life (i.e. P300). IF staining of distal colon cryosections from CNP-lacZ and GC-B-lacZ reporter mice showed that both genes are transcribed in neurons, but not in ICCs, FLCs, SMCs or glia cells. Closer investigations showed the transcription of *CNP* and *GC-B* in a subpopulation of nitrergic neurons, but also non-nitrergic neurons (**4.4.2. Figure 21 C**). Most nitrergic neurons of the MP are inhibitory motor neurons (~18 % of MP neurons) which contribute to the tonic inhibition of smooth muscle contraction in mature motility. Under basal conditions, tonic inhibition keeps the SML in a relaxed state that can be excited, hence, contracted upon a coordinated excitatory signal from the ENS. Any imbalance regarding the tonic inhibition of the SML could lead to motility disturbances like a narrowed Cannon-Böhm point. The other type of nitrergic neurons present in the ENS are descending interneurons which mediate local reflexes (~ 5 % of MP neurons). Much like IPANs (~ 26 % of MP neurons), the descending interneurons (mainly cholinergic) sense local stimuli like SML stretch or luminal chyme composition/viscosity and integrate their resulting activation state into the local ENS ganglion. In consequence, these sensory neurons can elicit a motility response like peristaltic waves or segmentation movements. A previous single cell transcriptome study of the small intestinal ENS revealed *GC-B* transcription in IPANs [88]. Since IPANs are cholinergic, it is very likely that the non-nitrergic *CNP* and *GC-B* transcribing neurons, which were observed with the *lacZ* reporter mice in this thesis, are IPANs as well. The nitrergic neurons, in turn, are either inhibitory motor neurons or local reflex-mediating descending interneurons (**1.1.4. Figure 4 & Table 1**). But, evidence for the suggested cell types has to be collected in future studies.

An additional set of experiments, utilizing another GC-B reporter mouse line (GC-B-CreERT2), confirmed the transcription of *GC-B* in colonic neurons, but also exposed *GC-B* transcribing SMCs (**4.4.2. Figure 22 C & D**). Looking at whole mount IF staining of

the distal colon (**4.4.2. Figure 22 A**), it appears that there are much less *GC-B* transcribing SMCs as there are *GC-B* transcribing neurons. This could be a true observation, but it could also be that the Tamoxifen induction of the CreER^{T2}, which is expressed under control of the GC-B promotor, was less successful in SMCs as it was in neurons. In contrast to the lacZ reporter system, where we observe the promotor activity at a very specific time point, the CreER^{T2} reporter system labels cells which display the respective promotor activity within the time frame of Tamoxifen injection. In addition, the staining intensity of the lacZ reporter system strongly depends on the respective promotor activity. Low levels of promotor activity might not produce enough βGal to be detected in Xgal or IF staining. The CreER^{T2} reporter system, in comparison, functions as an on/off switch. In theory, there is only one molecule of Tamoxifen-activated CreER^{T2} required to recombine the genome of the cell. The Cre-inducible tomato reporter (R26-Ai14), which was combined with the GC-B promotor-mediated CreER^{T2} expression (GC-B-CreERT2), has a defined expression level as soon as it is recombined. Therefore, a low level of GC-B promotor-mediated CreER^{T2} expression can already be enough to generate a very easily detectable and relatively strong tomato expression. To induce CreER^{T2} activity, Tamoxifen was injected 2 times over a total time frame of 4 days. This means that cells transcribing *GC-B* in that time frame, as well as their daughter cells, were labeled through the tomato reporter. In conclusion, a low *GC-B* transcription level might not produce enough βGal to be directly detected via IF or Xgal staining, but it might produce enough CreER^{T2} to recombine the R26-A14 transgene which, in turn, leads to a strong tomato expression in GC-B transcribing cells and their daughter cells. This would explain why *GC-B* transcription in SMCs was only detected with the GC-B-CreERT2 reporter system.

The expression and activatability of GC-B in neurons and SMCs was then shown in cGMP-FRET measurements. 90 % of cultivated neurons as well as 68 % of cultivated SMCs did respond to CNP stimulation with a rise of the intracellular cGMP concentration (**4.4.2. Figure 23 A - C**). In addition, ENS neurons were also measured *ex vivo* in the isolated colon where CNP also led to intracellular cGMP generation (**4.4.2. Figure 23 D & E**). These findings showed that the neurons and SMCs, labeled with the respective Cre-driver line, indeed generate cGMP in response to CNP application. Although it can be argued that the concentration of CNP used in the cGMP-FRET measurements (i.e. 250 nM) might have also stimulated GC-A to a low degree, such cross reactivity was not observed here. Most colonic neurons and SMCs reacted on CNP, and not

on ANP, suggesting that GC-A was not present. Therefore, it can be concluded that CNP-activatable GC-B is expressed in neurons and SMCs of the colon.

Sogawa and coworkers also claimed to have seen GC-B expression in SMCs, but not in neurons. The major limitation of their studies was the immunohistochemistry antibody which they used to detect GC-B (ab37620; discussed in **5.2.**). The ab37620 antibody binds GC-B at the C-terminus and, therethrough, provides a high probability for GC-A cross-reactivity. They also did not back up their immunohistochemistry staining with tissue from GC-B KO mice which would have validated their antibody and strengthened their conclusions [131]. We know today that this core result of Sogawa and coworkers, which is the foundation of all their speculations regarding GC-B in SMCs, is uncertain. Therefore, this thesis adds genetical and functional evidence for GC-B expression in neurons and SMCs of the colon as well as *CNP* transcription in colonic neurons.

5.4.3. CNP-induced smooth muscle relaxation in distal colon is mediated by SMCs and not neurons

The last part of this thesis focuses on the question whether the CNP-activatable GC B, which is present in neurons and SMCs, also contributes to the contraction-inhibiting effect of CNP in distal colon. Thus, neuron-specific GC-B KO mice were analyzed in *ex vivo* IFM showing that the contraction inhibiting effect of CNP was still present. There are two possible ways to explain why the distal colon of neuron-specific GC-B KO mice behaved similar to the WT and control condition in response to CNP application. First, it is possible that the Wnt1-Cre line does not cover all GC-B expressing colonic neurons. In consequence, GC-B would still be expressed in some neurons of the colonic ENS. Although this was not disproven, the whole mount IF staining suggested that the Wnt1-Cre line covers all *GC-B* transcribing neurons (**4.4.3. Figure 24 A - D**). Additional protein expression analysis showed a reduction of GC-B in the colon of neuron-specific GC-B KO mice. Therefore, it is more likely that neuronal GC-B does not mediate the contraction inhibiting effect of CNP in distal colon. Additional experiments, performed in the presence of TTX, showed that the distal colon from SMC-specific GC-B KO mice behaved similar to the distal colon of global GC-B KO mice in terms of contraction amplitude and frequency (**4.4.3. Figure 25**). On the protein level, the SMC-specific GC-B KO showed a much stronger reduction of GC-B than the neuron-specific GC-B KO. Hence, it can be concluded that GC-B in SMCs, and not GC-B in neurons, mediates the contraction inhibiting effect of CNP in distal colon. Noticeably, the behavior of the distal colon from SMC-specific GC-B KO mice was not identical to the behavior of the distal colon from global GC-B KO mice, but very close to it. The contraction amplitude and

frequency were both slightly lower and there was still a small time without contraction present in the SMC-specific GC-B KO. Furthermore, SMC-specific GC-B KO mice did not experience the GI distention phenotype of the global GC-B KO mice. Both observations are probably explained by the necessity of the $CreER^{T2}$ recombinase to be activated with Tamoxifen. This activation, which is performed by injecting the respective mice with tamoxifen, needs to be done multiple times to ensure a high recombination rate. Thus, we hypothesize that the recombination of *GC-B* was limited to a subset of GC-B expressing SMCs and, therefore, some SMCs still expressed functional GC-B. Future experiments could use a non-inducible SMC-specific Cre line that ensures recombination in all SMCs. The resulting SMC-specific GC-B KO might then behave just like the global GC-B KO and maybe even develops the distention phenotype.

Another interesting question concerns the target receptor of CNP in colon. Besides GC-B, CNP could also bind to the clearance receptor which guides signaling peptides (like natriuretic peptides) to their intracellular degradation [94]. Although the clearance receptor was not investigated directly in this study, it does not mediate the contraction inhibiting effect of CNP in colon. This was shown through IFM on distal colonic rings from global GC-B KO mice which did not react to CNP at all. But, it is still possible that the clearance receptor is present in colon and responsible for the degradation of CNP inside the tissue compound.

Additional experiments were performed to identify the PDEs that act downstream of GC-B in colonic SMCs. It was shown that PDE2A and PDE5 both degrade GC-B-generated cGMP in SMCs. The PDE5 inhibitors Tadalafil and Sildenafil were also used in *ex vivo* IFM on distal colonic rings to demonstrate a sustained, contraction inhibiting effect of CNP in their presence. PDE5 can, therefore, be considered as a major key player in degrading cGMP in colonic SMCs upon CNP stimulation. The role of PDE2A, in turn, is less certain. Although PDE2A has previously been associated with CNP-induced cGMP signaling in dorsal root ganglion neurons [120], it has not been associated with GI SMCs so far. Confusingly, SMCs did not respond to the PDE2 inhibitor EHNA (applied concentration: 10 µM), but to the PDE2A inhibitor Bay60-7550 (applied concentration: 100 nM). Like Bay60-7550, EHNA also binds and inhibits PD2A. Hence, this different outcome might be explained by a technical issue. The applied concentrations of EHNA (10 µM) and Bay60-7550 (100 nM) were chosen based on the respective half maximal inhibitory concentrations (IC50) multiplied by a number. EHNA was applied at a 10-times higher concentration than its IC50 suggests (IC50 1 µM), whereas Bay60-7550 was applied at a 20-times higher concentration than its IC50 suggests (IC50 4.7 nM) [8]. Maybe this difference led to an effect with Bay60-7550 that

was not observed with EHNA. Another possible explanation could be that EHNA, which also inhibits adenosine deaminases (IC50: 2 nM), elicits other intracellular responses which counteract any PDE2A-inhibiting effects [13]. Taken together, it can still be concluded that PDE2A degrades the cGMP that is generated by GC-B in colonic SMCs, but future studies might focus on this discrepancy between EHNA and Bay60-7550.

Finally, we aimed to determine the cellular origin of CNP. What we observed in our experiments was that *CNP* is transcribed in nitrergic neurons of the ENS. But this transcription starts between P5 and P15. The distention phenotype, however, was already present at P5, suggesting an earlier onset of CNP expression and secretion in that region. Therefore, CNP is either expressed at P5, but cannot be detected with the methods used in this study, or it comes from another source. A potential other source could be the blood vessels which run through the GI tissue. Although CNP is present in the blood plasma, studies have shown that its blood plasma concentration is in the pM range (1.1 pM ±0.12 pM, n=5; [91]). In comparison, the CNP dose-response curves of this thesis showed that 1 nM CNP is not enough to elicit a contraction inhibiting effect in colon (**4.4.1. Figure 19**). Therefore, it can be concluded that the concentration of CNP in the blood plasma is not high enough to influence colonic motility. A more plausible source of CNP could be, for instance, sympathetic neurons which are localized outside the GIT, but project they nerve endings into the ENS. Indeed, *CNP* transcription was found in cells of the inferior mesenteric ganglion at P5. The sympathetic neurons of this ganglion project to the cecum and colon, up to the Cannon-Böhm point where they exert inhibitory actions (e.g. inhibition of GI motility) [14, 133, 142]. So far it can only be speculated whether CNP is expressed and released from these neurons, but it would explain why the distension phenotype was already observed at P5 and vanished after the occurrence of mature motility patterns (first occurrence between P10 and P14) around P15. Unfortunately, it is not known whether CNP is expressed in sympathetic neurons or other cells of the inferior mesenteric ganglion. This should be investigated in future studies.

The analysis of CNP, GC-B, cGKI and also NO-GC (β1 subunit) KO mice revealed a general trend towards GI problems and deprecated survival curves. Depending on the genetic background (usually black 6), the survival rate of CNP and GC-B KO mice can drop to 30 % - 40 % before weaning, but remains rather constant afterwards [23, 128]. In comparison, around 40 % of NO-GC KO mice survive until weaning, but die until P40. Around 50 % of cGKI KO mice survive weaning itself, but they continue to die until they reach a maximum age of one year [40, 146]. It is obvious that most mice die before weaning,

but the reasons are not clear. Weber and co-workers have generated SMC-specific cGKI rescue mice which express cGKI only in SMCs. These rescue mice showed a survival curve similar to WT until the age of one year. Although rescue mice still died earlier than the WT control mice (maximum age of 2 years), they survived weaning without major complications [146]. This is a strong indication for the importance of cGKI-mediated cGMP signaling in SMCs of young mice before weaning. However, it has to be considered that the SMC-specific cGKI rescue mice, generated by Weber and co-workers, do not only rescue cGKI in GI SMCs, but also in vascular SMCs [146]. To extend the experiments of this thesis, a GI SMC-specific GC-B rescue mouse could clarify the impact of GC-B in GI SMCs on the GI distention phenotype and, thereby, the corresponding survival rate at weaning.

Future experiments should include *in vivo* force measurements of the Cannon-Böhm point in global GC-B KO mice, to show the luminal narrowing in the living animal. It should also be tested whether supplementation of mother's milk with fibers, already mitigates the distention phenotype. This could be done at P5 and P8 to investigate immature motility and at P15 to investigate mature motility. Furthermore, the gastrointestinal transit time should be assessed in WT and GC-B KO mice to identify potential transit time delays. Alternatively, the duration of meconium (first feces) excretion after birth should be assessed in WT and GC-B KO mice. This could give information about the transit time without staining of the feces.

5.4.4. Model of CNP-induced cGMP signaling in colonic smooth muscle motility

In summary, we propose the following model for the role of CNP-induced cGMP signaling in GI motility: CNP is released by sympathetic neurons in immature motility and inhibitory motor neurons in mature motility. This CNP then contributes to the tonic inhibition of the distal colon CSML by binding to GC-B on SMCs. GC-B then generates cGMP which activates cGKI, but is also degraded by PDE2A and PDE5 to limit the amount of cGMP produced. The activated cGKI then phosphorylates its downstream substrates leading to SMC relaxation, membrane hyperpolarization, and a reduced excitability of the SMC through excitatory neurotransmitters like ACh (**Figure 27**). A strong tonic inhibition is very important in the median and distal colon, because the only motility pattern wanted here is the peristaltic wave (colonic mass movement that pushes the content into the aboral direction), but not any segmentation movement (motility pattern that distributes content over a large surface area). Without GC-B expressed in SMCs, the baseline colonic smooth muscle tone might be slightly elevated leading to a significant luminal narrowing at the Cannon-Böhm point. The

combination of fiber-free food (i.e. mother's milk), which is digested by pups until weaning, and immature motility patterns does not develop enough pressure to keep the narrowed passage at the Cannon-Böhm point open. Therefore, the distal colon constipates and the backlog of bacteria, which accumulate before the constipation at the Cannon-Böhm point, leads to gas development and colonic distension. This distension also affects the cecum and ileum. The consumption of fiber-rich food shortly before weaning, in turn, helps to elicit mature motility patterns which then open up the constipated Cannon-Böhm point. The subsequent reestablishment of normal contraction patterns in the large intestine then allow for a mother-independent diet after weaning.

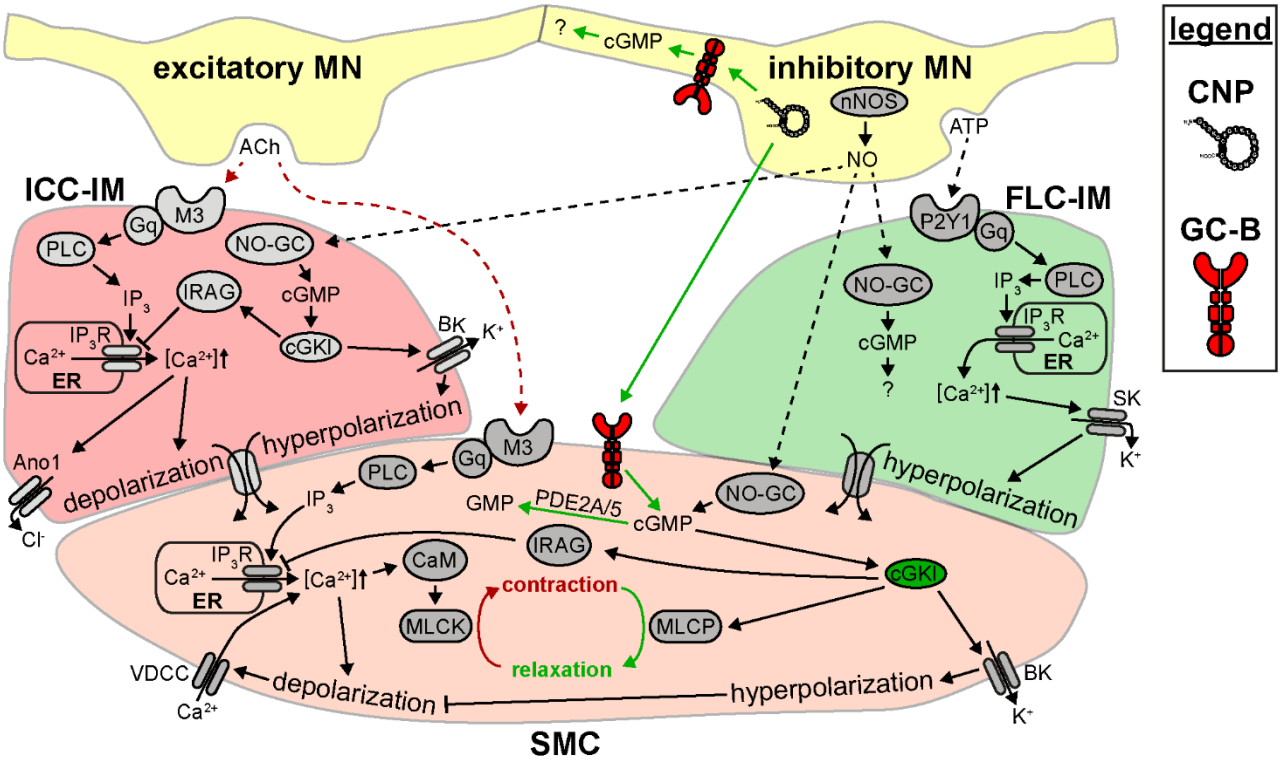

Figure 27: Schematic depiction of the role of CNP and GC-B in colonic smooth muscle contraction and relaxation.
The figure description of **1.1.5. Figure 6** also applies here. All pathways not investigated for the scope of this thesis are depicted in gray. Green pathways lead to relaxation and red pathways lead to contraction. **Abbr.:** muscarinic ACh receptor M3 (M3), $G_{\alpha q}$ subunit (Gq), beta-type phospholipase C (PLC), inositol trisphosphate (IP_3), IP_3-receptor (IP_3R), endoplasmic reticulum (ER), L-type voltage-dependent calcium channels (VDCC), calmodulin (CaM), myosin light chain kinase (MLCK), anoctamin-1 (Ano1), IP_3R-associated cGMP kinase substrate (IRAG), large conductance calcium-activated potassium channels (BK channel), myosin light chain phosphatase (MLCP), G_{qa}-protein coupled P2Y1 ATP-receptor (P2Y1), small conductance calcium-activated potassium channels (SK channel). Adapted from [7, 32, 33, 46, 75, 78, 114]. **What is new in this schematic:** CNP is produced by inhibitory motor neurons (MN) in mature motility. It binds to GC-B on inhibitory MN and GC-B on SMCs, thereby inducing cGMP generation. The downstream protein kinase cGKI, which is present in GI SMCs [146], can now be activated by cGMP to phosphorylate substrates like IRAG, BK channels, and MLCP, thereby, leading to membrane hyperpolarization and SMC relaxation. PDE2A & PDE5, which are also present in SMCs, degrade the CNP-induced cGMP to GMP. Downstream substrates of cGMP in neurons are unknown. Enteric inhibitory MN did not display any obvious changes or effects that could be attributed to cGMP generation.

6. Conclusions of the study

The questions addressed in this study were answered as followed:

Aim 1: Characterization of GI dysfunction in global GC-B KO mouse lines.

Conclusion 1: Juvenile GC-B KO mice suffer from a distension phenotype as compared to litter-matched controls.

Aim 2: Characterization of CNP and GC-B expression patterns within the GIT using *lacZ*-reporter mouse lines (CNP-lacZ and GC-B-lacZ).

Conclusion 2: High CNP or GC-B gene transcription was observed in esophagus, pylorus, small and large intestine. High GC-B, but almost no CNP gene transcription was observed in MLN.

Aim 3: Determination of the identity of CNP and GC-B expressing cells in regions with a GI dysfunction (i.e. small intestine and colon). These analyses are accompanied by *in situ* monitoring of CNP-induced cGMP signals in colonic SMC and neurons of cGi500 cGMP-FRET biosensor mice.

Conclusion 3: CNP gene transcription was found in Paneth cells of the small intestine and nitrergic neurons of the colon. GC-B gene transcription was localized to neurons and SMCs of the colon which both displayed CNP-induced cGMP generation *in situ*.

Aim 4: Generation of cell type-specific KO mice for CNP and GC-B using appropriate Cre driver lines and subsequent analysis of colonic segments to further our understanding about the cellular components and mechanisms of CNP-induced cGMP signaling in colonic motility.

Conclusion 4: GC-B was knocked-out in neurons (Wnt1-Cre) and SMCs (αSMA-CreERT2). It was found that GC-B on SMCs, but not neurons of the distal colon, mediates the contraction-inhibiting effect of CNP on the CSML in a PDE2A- and PDE5-regulated manner.

7. References

1. Adolph, T.E., et al., *Paneth cells as a site of origin for intestinal inflammation.* Nature, 2013. **503**(7475): p. 272-6.
2. Anand-Srivastava, M.B., *Natriuretic peptide receptor-C signaling and regulation.* Peptides, 2005. **26**(6): p. 1044-59.
3. Andreas, N.J., B. Kampmann, and K. Mehring Le-Doare, *Human breast milk: A review on its composition and bioactivity.* Early Human Development, 2015. **91**(11): p. 629-635.
4. Baena, V., et al., *Cellular heterogeneity of the luteinizing hormone receptor and its significance for cyclic GMP signaling in mouse preovulatory follicles.* Endocrinology, 2020. **161**(7): p. 1-18.
5. Banapurmath, C.R., et al., *Acromesomelic dysplasia of the Maroteaux type.* Indian J Pediatr, 1990. **57**(6): p. 803-5.
6. Bartels, C.F., et al., *Mutations in the transmembrane natriuretic peptide receptor NPR-B impair skeletal growth and cause acromesomelic dysplasia, type Maroteaux.* American journal of human genetics, 2004. **75**(1): p. 27-34.
7. Beck, K., A. Friebe, and B. Voussen, *Nitrergic signaling via interstitial cells of Cajal and smooth muscle cells influences circular smooth muscle contractility in murine colon.* Neurogastroenterol Motil, 2018. **30**(6): p. 1-12.
8. Bender, A.T. and J.A. Beavo, *Cyclic nucleotide phosphodiesterases: molecular regulation to clinical use.* Pharmacol Rev, 2006. **58**(3): p. 488-520.
9. Bennett, B.D., et al., *Extracellular domain-IgG fusion proteins for three human natriuretic peptide receptors. Hormone pharmacology and application to solid phase screening of synthetic peptide antisera.* J Biol Chem, 1991. **266**(34): p. 23060-7.
10. Bharucha, A.E., J.H. Pemberton, and G.R. Locke, 3rd, *American Gastroenterological Association technical review on constipation.* Gastroenterology, 2013. **144**(1): p. 218-238.
11. BioMarin. *The first and only therapy approved to increase linear growth in children with achondroplasia aged 5 years and over with open growth plates*. 2021 2022 [cited 2022 18.02.2022]; Available from: https://www.biomarin.com/our-treatments/products/voxzogo/.
12. Birbe, R., et al., *Guanylyl cyclase C is a marker of intestinal metaplasia, dysplasia, and adenocarcinoma of the gastrointestinal tract.* Hum Pathol, 2005. **36**(2): p. 170-9.
13. Boess, F.G., et al., *Inhibition of phosphodiesterase 2 increases neuronal cGMP, synaptic plasticity and memory performance.* Neuropharmacology, 2004. **47**(7): p. 1081-92.
14. Burns, A.J., et al., *Development of the enteric nervous system and its role in intestinal motility during fetal and early postnatal stages.* Semin Pediatr Surg, 2009. **18**(4): p. 196-205.
15. Busby, R.W., et al., *Linaclotide, through activation of guanylate cyclase C, acts locally in the gastrointestinal tract to elicit enhanced intestinal secretion and transit.* Eur J Pharmacol, 2010. **649**(1-3): p. 328-35.

16. Cai, Y.-L., et al., *cGMP–PDE3–cAMP signal pathway involved in the inhibitory effect of CNP on gastric motility in rat.* Regulatory Peptides, 2013. **180**: p. 43-49.

17. Cai, Y.L., et al., *CNP-pGC-cGMP-PDE3-cAMP signal pathway upregulated in gastric smooth muscle of diabetic rats.* Gastroenterol Res Pract, 2015. **2015**: p. 1-9.

18. Cannon, W.B., *The movements of the intestines studied by means of the Rontgen rays.* American Journal of Physiology-Legacy Content, 1902. **6**(5): p. 251-277.

19. Casteleyn, C., et al., *Surface area assessment of the murine intestinal tract as a prerequisite for oral dose translation from mouse to man.* Lab Anim, 2010. **44**(3): p. 176-83.

20. Chang, B.S. and S.C. Huang, *Natriuretic peptides cause relaxation of human esophageal mucosal muscle.* Regul Pept, 2008. **146**(1-3): p. 224-9.

21. Cheung, W.Y., *Cyclic 3',5'-nucleotide phosphodiesterase. Demonstration of an activator.* Biochem Biophys Res Commun, 1970. **38**(3): p. 533-8.

22. Chihara, D., et al., *PAX7 is required for patterning the esophageal musculature.* Skelet Muscle, 2015. **5**: p. 39.

23. Chusho, H., et al., *Dwarfism and early death in mice lacking C-type natriuretic peptide.* Proc Natl Acad Sci U S A, 2001. **98**(7): p. 4016-21.

24. Clevers, H.C. and C.L. Bevins, *Paneth cells: maestros of the small intestinal crypts.* Annu Rev Physiol, 2013. **75**: p. 289-311.

25. Conti, M. and J. Beavo, *Biochemistry and physiology of cyclic nucleotide phosphodiesterases: essential components in cyclic nucleotide signaling.* Annu Rev Biochem, 2007. **76**: p. 481-511.

26. Costa, M., et al., *Characterization of alternating neurogenic motor patterns in mouse colon.* Neurogastroenterol Motil, 2021. **33**(5): p. e14047.

27. Danielian, P.S., et al., *Modification of gene activity in mouse embryos in utero by a tamoxifen-inducible form of Cre recombinase.* Curr Biol, 1998. **8**(24): p. 1323-6.

28. Degerman, E., P. Belfrage, and V.C. Manganiello, *Structure, localization, and regulation of cGMP-inhibited phosphodiesterase (PDE3).* J Biol Chem, 1997. **272**(11): p. 6823-6.

29. Degerman, E., et al., *Purification of the putative hormone-sensitive cyclic AMP phosphodiesterase from rat adipose tissue using a derivative of cilostamide as a novel affinity ligand.* J Biol Chem, 1987. **262**(12): p. 5797-807.

30. Dickey, D.M., et al., *Catalytically active guanylyl cyclase B requires endoplasmic reticulum-mediated glycosylation, and mutations that inhibit this process cause dwarfism.* J Biol Chem, 2016. **291**(21): p. 11385-93.

31. Drokhlyansky, E., et al., *The human and mouse enteric nervous system at single-cell resolution.* Cell, 2020. **182**(6): p. 1606-1622.e23.

32. Drumm, B.T., et al., *Tonic inhibition of murine proximal colon is due to nitrergic suppression of Ca(2+) signaling in interstitial cells of Cajal.* Sci Rep, 2019. **9**(1): p. 4402.

33. Drumm, B.T., et al., *Excitatory cholinergic responses in mouse colon intramuscular interstitial cells of Cajal are due to enhanced Ca(2+) release via M(3) receptor activation.* Faseb j, 2020. **34**(8): p. 10073-10095.

34. Dumoulin, A., et al., *Molecular analysis of sensory axon branching unraveled a cGMP-dependent signaling cascade.* Int J Mol Sci, 2018. **19**(5): p. 1-14.

35. Eroglu, E., et al., *Real-time visualization of distinct nitric oxide generation of nitric oxide synthase isoforms in single cells.* Nitric Oxide, 2017. **70**: p. 59-67.

36. Feil, R. and B. Kemp-Harper, *cGMP signalling: from bench to bedside. Conference on cGMP generators, effectors and therapeutic implications.* EMBO Rep, 2006. **7**(2): p. 149-53.

37. Feil, S., et al., *Genetic inducible fate mapping in adult mice using tamoxifen-dependent Cre recombinases.* Methods Mol Biol, 2014. **1194**: p. 113-39.

38. Frei, E., et al., *Calcium-dependent and calcium-independent inhibition of contraction by cGMP/cGKI in intestinal smooth muscle.* Am J Physiol Gastrointest Liver Physiol, 2009. **297**(4): p. G834-9.

39. Friebe, A. and D. Koesling, *The function of NO-sensitive guanylyl cyclase: what we can learn from genetic mouse models.* Nitric Oxide, 2009. **21**(3-4): p. 149-56.

40. Friebe, A., et al., *Fatal gastrointestinal obstruction and hypertension in mice lacking nitric oxide-sensitive guanylyl cyclase.* Proceedings of the National Academy of Sciences, 2007. **104**(18): p. 7699-7704.

41. Furchgott, R.F., *Endothelium-derived relaxing factor: discovery, early studies, and identifcation as nitric oxide (Nobel lecture).* Angew Chem Int Ed Engl, 1999. **38**(13-14): p. 1870-1880.

42. Furness, J.B., *Types of neurons in the enteric nervous system.* J Auton Nerv Syst, 2000. **81**(1-3): p. 87-96.

43. Furness, J.B., *The enteric nervous system and neurogastroenterology.* Nat Rev Gastroenterol Hepatol, 2012. **9**(5): p. 286-94.

44. Furness, J.B., et al., *The enteric nervous system and gastrointestinal innervation: integrated local and central control.* Adv Exp Med Biol, 2014. **817**: p. 39-71.

45. Furuya, S. and K. Furuya, *Subepithelial fibroblasts in intestinal villi: roles in intercellular communication.* Int Rev Cytol, 2007. **264**: p. 165-223.

46. Gallego, D., et al., *Mechanisms responsible for neuromuscular relaxation in the gastrointestinal tract.* Rev Esp Enferm Dig, 2016. **108**(11): p. 721-731.

47. Geiselhöringer, A., et al., *IRAG is essential for relaxation of receptor-triggered smooth muscle contraction by cGMP kinase.* The EMBO Journal, 2004. **23**(21): p. 4222-4231.

48. Gekle, M., *Funktion des Magen-Darm-Trakts, Energiehaushalt und Ernährung*, in *Physiologie*, R. Klinke, H.-C. Pape, and S. Silbernagel, Editors. 2005, Georg Thieme Verlag. p. 407-483.

49. Gerbe, F., C. Legraverend, and P. Jay, *The intestinal epithelium tuft cells: specification and function.* Cell Mol Life Sci, 2012. **69**(17): p. 2907-17.

50. Groneberg, D., et al., *Cell-specific deletion of nitric oxide–sensitive guanylyl cyclase reveals a dual pathway for nitrergic neuromuscular transmission in the murine fundus.* Gastroenterology, 2013. **145**(1): p. 188-196.

51. Groneberg, D., et al., *Dominant role of interstitial cells of Cajal in nitrergic relaxation of murine lower oesophageal sphincter.* J Physiol, 2015. **593**(2): p. 403-14.

52. Gross-Langenhoff, M., et al., *cAMP is a ligand for the tandem GAF domain of human phosphodiesterase 10 and cGMP for the tandem GAF domain of phosphodiesterase 11.* J Biol Chem, 2006. **281**(5): p. 2841-6.

53. Guo, H.S., et al., *Inhibitory effect of C-type natriuretic peptide on spontaneous contraction in gastric antral circular smooth muscle of rat.* Acta Pharmacol Sin, 2003. **24**(10): p. 1021-6.

54. Guo, H.S., et al., *Comparative study in the effect of C-type natriuretic peptide on gastric motility in various animals.* World J Gastroenterol, 2003. **9**(3): p. 547-52.

55. Gyurko, R., S. Leupen, and P.L. Huang, *Deletion of exon 6 of the neuronal nitric oxide synthase gene in mice results in hypogonadism and infertility.* Endocrinology, 2002. **143**(7): p. 2767-74.

56. Hall, J.E., *Guyton and Hall textbook of medical physiology*. Thirteenth edition. ed. 2016, Philadelphia, PA: Elsevier. xix, 1145 pages.

57. Hama, H., et al., *Scale: a chemical approach for fluorescence imaging and reconstruction of transparent mouse brain.* Nat Neurosci, 2011. **14**(11): p. 1481-8.

58. Herrmann, P. and D. Mauer, *Nobelpreis Medizin 1998*, in *Notfall & Rettungsmedizin*. 1998. p. 324-324.

59. Hofmann, F., *The biology of cyclic GMP-dependent protein kinases.* J Biol Chem, 2005. **280**(1): p. 1-4.

60. Huang, P.L., et al., *Targeted disruption of the neuronal nitric oxide synthase gene.* Cell, 1993. **75**(7): p. 1273-86.

61. Huang, S.-C., *C-type atriuretic peptide causes relaxation of the internal anal sphincter through natriuretic peptide receptor B.* Tzu Chi Medical Journal, 2015. **27**(2): p. 65-70.

62. Ikpa, P.T., et al., *Guanylin and uroguanylin are produced by mouse intestinal epithelial cells of columnar and secretory lineage.* Histochem Cell Biol, 2016. **146**(4): p. 445-55.

63. Irfanullah, et al., *Homozygous sequence variants in the NPR2 gene underlying acromesomelic dysplasia Maroteaux type (AMDM) in consanguineous families.* Annals of Human Genetics, 2015. **79**(4): p. 238-244.

64. Jaffe, L.A. and J.R. Egbert, *Regulation of mammalian oocyte meiosis by Intercellular communication within the ovarian follicle.* Annu Rev Physiol, 2017. **79**: p. 237-260.

65. Kagawa, K., et al., *Relationship between the suppressive actions on intestinal absorption and on cGMP production for the natriuretic peptide family in dogs.* Clin Exp Pharmacol Physiol, 1994. **21**(2): p. 83-92.

66. Kake, T., et al., *Chronically elevated plasma C-type natriuretic peptide level stimulates skeletal growth in transgenic mice.* Am J Physiol Endocrinol Metab, 2009. **297**(6): p. E1339-48.

67. Kaupp, U.B. and R. Seifert, *Cyclic nucleotide-gated ion channels.* Physiol Rev, 2002. **82**(3): p. 769-824.

68. Kessmann, J., *Hirschsprung's disease: diagnosis and management.* Am Fam Physician, 2006. **74**(8): p. 1319-22.

69. Kiela, P.R. and F.K. Ghishan, *Physiology of intestinal absorption and secretion.* Best Pract Res Clin Gastroenterol, 2016. **30**(2): p. 145-59.

70. Kim, J.H., et al., *C-type natriuretic peptide system in rabbit colon.* Peptides, 2001. **22**(12): p. 2061-8.

71. Koldovský, O., et al., *Postnatal changes in beta-galactosidase activity in the jejunum and ileum of mice, rabbits, and guinea pigs.* Can J Biochem, 1966. **44**(5): p. 523-7.

72. Kondo, T., et al., *Muscarinic receptor subtypes involved in regulation of colonic motility in mice: functional studies using muscarinic receptor-deficient mice.* Eur J Pharmacol, 2011. **670**(1): p. 236-43.

73. Krämer, M.S., R. Feil, and H. Schmidt, *Analysis of gene expression using lacZ reporter mouse lines.* Methods Mol Biol, 2021. **2224**: p. 29-45.

74. Kuhn, M., *Molecular physiology of membrane guanylyl cyclase receptors.* Physiol Rev, 2016. **96**(2): p. 751-804.

75. Kurahashi, M., et al., *Platelet-derived growth factor receptor-α-positive cells and not smooth muscle cells mediate purinergic hyperpolarization in murine colonic muscles.* Am J Physiol Cell Physiol, 2014. **307**(6): p. C561-70.

76. Lafontan, M., et al., *Adrenergic regulation of adipocyte metabolism.* Hum Reprod, 1997. **12 Suppl 1**: p. 6-20.

77. Legeai-Mallet, L., *C-type natriuretic peptide analog as therapy for achondroplasia.* Endocr Dev, 2016. **30**: p. 98-105.

78. Lies, B., D. Groneberg, and A. Friebe, *Toward a better understanding of gastrointestinal nitrergic neuromuscular transmission.* Neurogastroenterol Motil, 2014. **26**(7): p. 901-12.

79. Lorenz, J.N., et al., *Uroguanylin knockout mice have increased blood pressure and impaired natriuretic response to enteral NaCl load.* J Clin Invest, 2003. **112**(8): p. 1244-54.

80. Lu, C., et al., *Different distributions of interstitial cells of Cajal and platelet-derived growth factor receptor-α positive cells in colonic smooth muscle cell/interstitial cell of Cajal/platelet-derived growth factor receptor-α positive cell syncytium in mice.* World J Gastroenterol, 2018. **24**(44): p. 4989-5004.

81. Madisen, L., et al., *A robust and high-throughput Cre reporting and characterization system for the whole mouse brain.* Nat Neurosci, 2010. **13**(1): p. 133-40.

82. Malone, J.C. and A. Thavamani, *Physiology, gastrocolic reflex*, in *StatPearls*. 2021, StatPearls Publishing Copyright © 2021, StatPearls Publishing LLC.: Treasure Island (FL).

83. Mane, N., et al., *Inverse gradient of nitrergic and purinergic inhibitory cotransmission in the mouse colon.* Acta Physiol (Oxf), 2016. **216**(1): p. 120-31.

84. Martins, T.J., M.C. Mumby, and J.A. Beavo, *Purification and characterization of a cyclic GMP-stimulated cyclic nucleotide phosphodiesterase from bovine tissues.* J Biol Chem, 1982. **257**(4): p. 1973-9.

85. McKnight, S.T., et al., *A functional colonic obstruction: Cannon's point.* Radiol Case Rep, 2011. **6**(4): p. 557.

86. Minamino, N., et al., *Distribution of C-type natriuretic peptide and its messenger RNA in rat central nervous system and peripheral tissue.* Biochem Biophys Res Commun, 1993. **197**(1): p. 326-35.

87. Miura, K., et al., *Overgrowth syndrome associated with a gain-of-function mutation of the natriuretic peptide receptor 2 (NPR2) gene.* Am J Med Genet A, 2014. **164a**(1): p. 156-63.

88. Morarach, K., et al., *Diversification of molecularly defined myenteric neuron classes revealed by single-cell RNA sequencing.* Nat Neurosci, 2021. **24**(1): p. 34-46.

89. Mowat, A.M. and W.W. Agace, *Regional specialization within the intestinal immune system.* Nat Rev Immunol, 2014. **14**(10): p. 667-85.

90. Moyes, A.J., et al., *Endothelial C-type natriuretic peptide maintains vascular homeostasis.* Journal of Clinical Investigation, 2014. **124**(9): p. 4039-4051.

91. Nakao, K., et al., *Endothelium-derived C-type natriuretic peptide contributes to blood pressure regulation by maintaining endothelial integrity.* Hypertension, 2017. **69**(2): p. 286-296.

92. Nakao, K., et al., *The local CNP/GC-B system in growth plate is responsible for physiological endochondral bone growth.* Sci Rep, 2015. **5**: p. 10554.

93. Nalivaeva, N.N., I.A. Zhuravin, and A.J. Turner, *Neprilysin expression and functions in development, ageing and disease.* Mech Ageing Dev, 2020. **192**: p. 111363.

94. Nussenzveig, D.R., J.A. Lewicki, and T. Maack, *Cellular mechanisms of the clearance function of type C receptors of atrial natriuretic factor.* J Biol Chem, 1990. **265**(34): p. 20952-8.

95. Ny, L., et al., *Impaired relaxation of stomach smooth muscle in mice lacking cyclic GMP-dependent protein kinase I.* Br J Pharmacol, 2000. **129**(2): p. 395-401.

96. Okada, D. and S. Asakawa, *Allosteric activation of cGMP-specific, cGMP-binding phosphodiesterase (PDE5) by cGMP.* Biochemistry, 2002. **41**(30): p. 9672-9.

97. Omori, K. and J. Kotera, *Overview of PDEs and their regulation.* Circ Res, 2007. **100**(3): p. 309-27.

98. Orstavik, S., et al., *Characterization of the human gene encoding the type I alpha and type I beta cGMP-dependent protein kinase (PRKG1).* Genomics, 1997. **42**(2): p. 311-8.

99. Padmanabhan, P., et al., *Gastrointestinal transit measurements in mice with 99mTc-DTPA-labeled activated charcoal using NanoSPECT-CT.* EJNMMI Res, 2013. **3**(1): p. 60.

100. Pfeifer, A., et al., *Intestinal secretory defects and dwarfism in mice lacking cGMP-dependent protein kinase II.* Science, 1996. **274**(5295): p. 2082-6.

101. Pfeifer, A., et al., *Defective smooth muscle regulation in cGMP kinase I-deficient mice.* EMBO J, 1998. **17**(11): p. 3045-51.

102. Plimmer, R.H., *On the presence of lactase in the intestines of animals and on the adaptation of the intestine to lactose.* J Physiol, 1906. **35**(1-2): p. 20-31.

103. Potter, L.R., *Natriuretic peptide metabolism, clearance and degradation.* Febs j, 2011. **278**(11): p. 1808-17.

104. Potter, L.R., S. Abbey-Hosch, and D.M. Dickey, *Natriuretic peptides, their receptors, and cyclic guanosine monophosphate-dependent signaling functions.* Endocrine Reviews, 2006. **27**(1): p. 47-72.

105. Potter, L.R., et al., *Natriuretic peptides: their structures, receptors, physiologic functions and therapeutic applications.* Handb Exp Pharmacol, 2009(191): p. 341-66.

106. Radomski, M.W., R.M. Palmer, and S. Moncada, *Glucocorticoids inhibit the expression of an inducible, but not the constitutive, nitric oxide synthase in vascular endothelial cells.* Proc Natl Acad Sci U S A, 1990. **87**(24): p. 10043-7.

107. Rambotti, M.G., I. Giambanco, and A. Spreca, *Detection of guanylate cyclases A and B stimulated by natriuretic peptides in gastrointestinal tract of rat.* Histochem J, 1997. **29**(2): p. 117-26.

108. Romer, A.I., et al., *Smooth muscle fascicular reorientation is required for esophageal morphogenesis and dependent on Cdo.* J Cell Biol, 2013. **201**(2): p. 309-23.

109. Rumio, C., et al., *Induction of Paneth cell degranulation by orally administered Toll-like receptor ligands.* J Cell Physiol, 2012. **227**(3): p. 1107-13.

110. Russwurm, M., N. Wittau, and D. Koesling, *Guanylyl cyclase/PSD-95 interaction: targeting of the nitric oxide-sensitive alpha2beta1 guanylyl cyclase to synaptic membranes.* J Biol Chem, 2001. **276**(48): p. 44647-52.

111. Rybalkin, S.D., et al., *Regulation of cGMP-specific phosphodiesterase (PDE5) phosphorylation in smooth muscle cells.* J Biol Chem, 2002. **277**(5): p. 3310-7.

112. Rybalkin, S.D., et al., *PDE5 is converted to an activated state upon cGMP binding to the GAF A domain.* Embo Journal, 2003. **22**(3): p. 469-478.

113. Samuelson, L.C., *Genetically engineered mouse models of gastric physiology*, in *Physiology of the Gastrointestinal Tract (Fourth Edition)*, L.R. Johnson, Editor. 2006, Academic Press: Burlington. p. 1293-1312.

114. Sanders, K.M. and S.M. Ward, *Nitric oxide and its role as a non-adrenergic, non-cholinergic inhibitory neurotransmitter in the gastrointestinal tract.* Br J Pharmacol, 2019. **176**(2): p. 212-227.

115. Sanders, K.M., S.M. Ward, and S.D. Koh, *Interstitial cells: regulators of smooth muscle function.* Physiol Rev, 2014. **94**(3): p. 859-907.

116. Sands, W.A. and T.M. Palmer, *Regulating gene transcription in response to cyclic AMP elevation.* Cell Signal, 2008. **20**(3): p. 460-6.

117. Schlossmann, J., et al., *Regulation of intracellular calcium by a signalling complex of IRAG, IP3 receptor and cGMP kinase Ibeta.* Nature, 2000. **404**(6774): p. 197-201.

118. Schlossmann, J., R. Feil, and F. Hofmann, *Insights into cGMP signalling derived from cGMP kinase knockout mice.* Front Biosci, 2005. **10**: p. 1279-89.

119. Schmidt, H., et al., *Regulation of the natriuretic peptide receptor 2 (Npr2) by phosphorylation of juxtamembrane serine and threonine residues is essential for bifurcation of sensory axons.* J Neurosci, 2018. **38**(45): p. 9768-9780.

120. Schmidt, H., et al., *Dorsal root ganglion axon bifurcation tolerates increased cyclic GMP levels: the role of phosphodiesterase 2A and scavenger receptor Npr3.* Eur J Neurosci, 2016. **44**(12): p. 2991-3000.

121. Schmidt, H., et al., *C-type natriuretic peptide (CNP) is a bifurcation factor for sensory neurons.* Proc Natl Acad Sci U S A, 2009. **106**(39): p. 16847-52.

122. Schmidt, H., et al., *The receptor guanylyl cyclase Npr2 is essential for sensory axon bifurcation within the spinal cord.* J Cell Biol, 2007. **179**(2): p. 331-40.

123. Schmidt, H., et al., *cGMP-mediated signaling via cGKIalpha is required for the guidance and connectivity of sensory axons.* J Cell Biol, 2002. **159**(3): p. 489-98.

124. Schmidt, H.H., et al., *Ca2+/calmodulin-regulated nitric oxide synthases.* Cell Calcium, 1992. **13**(6-7): p. 427-34.

125. Schuijers, J. and H. Clevers, *Adult mammalian stem cells: the role of Wnt, Lgr5 and R-spondins.* The EMBO Journal, 2012. **31**(12): p. 2685-2696.

126. Schulz, S., et al., *Disruption of the guanylyl cyclase-C gene leads to a paradoxical phenotype of viable but heat-stable enterotoxin-resistant mice.* J Clin Invest, 1997. **100**(6): p. 1590-5.

127. Shabb, J.B., *Physiological substrates of cAMP-dependent protein kinase.* Chem Rev, 2001. **101**(8): p. 2381-411.

128. Sogawa-Fujiwara, C., et al., *Defective development and microcirculation of intestine in Npr2 mutant mice.* Sci Rep, 2020. **10**(1): p. 14761.

129. Sogawa, C., et al., *Gastrointestinal tract disorder in natriuretic peptide receptor B gene mutant mice.* Am J Pathol, 2010. **177**(2): p. 822-8.

130. Sogawa, C., et al., *Short-limbed dwarfism: slw is a new allele of Npr2 causing chondrodysplasia.* J Hered, 2007. **98**(6): p. 575-80.

131. Sogawa, C., et al., *C-type natriuretic peptide specifically acts on the pylorus and large intestine in mouse gastrointestinal tract.* Am J Pathol, 2013. **182**(1): p. 172-9.

132. Spencer, N.J., et al., *Identification of a rhythmic firing pattern in the enteric nervous system that generates rhythmic electrical activity in smooth muscle.* J Neurosci, 2018. **38**(24): p. 5507-5522.

133. Spencer, N.J. and H. Hu, *Enteric nervous system: sensory transduction, neural circuits and gastrointestinal motility.* Nat Rev Gastroenterol Hepatol, 2020. **17**(6): p. 338-351.

134. Spiranec, K., et al., *Endothelial C-type natriuretic peptide acts on pericytes to regulate microcirculatory flow and blood pressure.* Circulation, 2018.

135. Stefanini, M., C. De Martino, and L. Zamboni, *Fixation of ejaculated spermatozoa for electron microscopy.* Nature, 1967. **216**(5111): p. 173-4.

136. Steinbrecher, K.A., et al., *Targeted inactivation of the mouse guanylin gene results in altered dynamics of colonic epithelial proliferation.* Am J Pathol, 2002. **161**(6): p. 2169-78.

137. Tamura, N., et al., *Critical roles of the guanylyl cyclase B receptor in endochondral ossification and development of female reproductive organs.* Proc Natl Acad Sci U S A, 2004. **101**(49): p. 17300-5.

138. Ter-Avetisyan, G., F.G. Rathjen, and H. Schmidt, *Bifurcation of axons from cranial sensory neurons is disabled in the absence of Npr2-induced cGMP signaling.* J Neurosci, 2014. **34**(3): p. 737-47.

139. Thunemann, M., et al., *Transgenic mice for cGMP imaging.* Circ Res, 2013. **113**(4): p. 365-71.

140. Troster, P., et al., *The absence of sensory axon bifurcation affects nociception and termination fields of afferents in the spinal cord.* Front Mol Neurosci, 2018. **11:19**: p. 1-18.

141. Tsuji, T. and T. Kunieda, *A loss-of-function mutation in natriuretic peptide receptor 2 (Npr2) gene is responsible for disproportionate dwarfism in cn/cn mouse.* J Biol Chem, 2005. **280**(14): p. 14288-92.

142. Uesaka, T., et al., *Development of the intrinsic and extrinsic innervation of the gut.* Dev Biol, 2016. **417**(2): p. 158-67.

143. Voussen, B., et al., *Comparison of nitrergic signaling in circular and longitudinal smooth muscle of murine ileum.* Neurogastroenterol Motil, 2018. **30**(3).

144. Wang, Y., et al., *Over-expression of human lipoprotein lipase in mouse mammary glands leads to reduction of milk triglyceride and delayed growth of suckling pups.* PLOS ONE, 2011. **6**(6): p. e20895.

145. Wasco, S. *Malocclusion in the laboratory mouse*. JAX Notes 2003 [cited 2021 27.08.2021]; Available from: https://www.jax.org/news-and-insights/2003/april/malocclusion-in-the-laboratory-mouse.

146. Weber, S., et al., *Rescue of cGMP kinase I knockout mice by smooth muscle specific expression of either isozyme.* Circ Res, 2007. **101**(11): p. 1096-103.

147. Wendling, O., et al., *Efficient temporally-controlled targeted mutagenesis in smooth muscle cells of the adult mouse.* Genesis, 2009. **47**(1): p. 14-8.

148. Wendt, D.J., et al., *Neutral endopeptidase-resistant C-type natriuretic peptide variant represents a new therapeutic approach for treatment of fibroblast growth factor receptor 3-related dwarfism.* J Pharmacol Exp Ther, 2015. **353**(1): p. 132-49.

149. Wu, A.Y., et al., *Molecular determinants for cyclic nucleotide binding to the regulatory domains of phosphodiesterase 2A.* J Biol Chem, 2004. **279**(36): p. 37928-38.

150. Yamamoto, K., et al., *CREB activation in hypertrophic chondrocytes is involved in the skeletal overgrowth in epiphyseal chondrodysplasia Miura type caused by activating mutations of natriuretic peptide receptor B.* Hum Mol Genet, 2019. **28**(7): p. 1183-1198.

151. Yeung, V.T., et al., *Binding of CNP-22 and CNP-53 to cultured mouse astrocytes and effects on cyclic GMP.* Peptides, 1996. **17**(1): p. 101-6.

152. Zhang, Y.W. and G. Rudnick, *Myristoylation of cGMP-dependent protein kinase dictates isoform specificity for serotonin transporter regulation.* J Biol Chem, 2011. **286**(4): p. 2461-8.

153. Zou, M., C. Wiechers, and J. Huehn, *Lymph node stromal cell subsets-Emerging specialists for tailored tissue-specific immune responses.* Int J Med Microbiol, 2021. **311**(3): p. 151492.

8. Supplement

Suppl. table S1: Chemicals.

name	chemical formula	supplier	cat. nr.
2-mercaptoethanol (99 %)	C_2H_6OS	Roth	4227.1
6-aminocapronic acid	$C_6H_{13}NO_2$	Roth	3113.2
acetic acid (>99.8 %)	$C_2H_4NO_2$	Sigma-Aldrich	33209
APS	$(NH_4)_2S_2O_8$	Roth	9592.2
boric acid	BH_3O_3	CHEMSOLUTE	2563
bromophenol blue	$C_{19}H_{10}Br_4O_5S$	Roth	T116.1
BSA (Albumin Fraction V)	-	Roth	8076.4
calcium chloride	$CaCl_2$	Roth	A119.1
D-glucose	$C_6H_{12}O_6$	Fischer	G/0500/60
DMF (>99.8 %)	C_3H_7NO	Roth	T921.1
DTT	$C_4H_{10}O_2S_2$	Roth	6908.3
EDTA	$C_{10}H_{16}N_2O_8$	Roth	X986.2
ethanol (>99.8 %)	C_2H_6O	Sigma-Aldrich	34852-M
gelatin	-	Roth	4582.1
glycerol	$C_3H_8O_3$	Roth	3783.2
glycine	$C_8H_9NO_3$	Sigma-Aldrich	33226
hydrochloric acid (>37 %), fuming	HCl	Sigma-Aldrich	30721
HEPES	$C_8H_{18}N_2O_4S$	Roth	HN78.3
L-glutamine	$C_5H_{10}N_2O_3$	Sigma-Aldrich	G7513
magnesium chloride	$MgCl_2$	Roth	2189.1
magnesium sulfate	$MgSO_4$	Roth	0261.1
methanol (>99.8 %)	CH_4O	Sigma-Aldrich	32213-M
monopotassium phosphate	KH_2PO_4	Merck	1.04873
NGS	-	Merck	S26
nonidet-P40 substitute	$(C_2H_4O)_nC_{14}H_{22}O$ (n = 9 - 10)	Merck	11754599001
PBS	-	Biochrom	L182-50
PFA	$OH(CH_2O)_nH$ (n = 8 - 100)	Roth	0335.3
picric acid (1.3 % in H_2O)	$C_6H_3N_3O_7$	Sigma-Aldrich	P6744
potassium ferricyanide	$K_3[Fe(CN)_6)]$	Merck	1.04973
potassium ferrocyanide	$K_4[Fe(CN)_6)]$	Roth	7974.2
potassium chloride	KCl	Roth	P017.3
powdered milk	-	Roth	T145.2
sodium azide	NaN_3	Roth	K305.1
sodium bicarbonate	$NaHCO_3$	Honeywell	S8875
sodium chloride	NaCl	Merck	1.06404
SDS	$C_{12}H_{25}NaSO_4$	Roth	4360.2
sodium deoxycholate	$C_{24}H_{39}NaO_4$	Roth	3484.1
sodium hydroxide (>99 %)	NaOH	Roth	6771.1
sucrose	$C_{12}H_{22}O_{11}$	Roth	4621.1
Tris: Trizma® base (>99.9 % Tris)	$C_4H_{11}NO_3$	Sigma-Aldrich	T1503
Triton X-100	$C_{14}H_{22}O(C_2H_4O)_n$ (n = 9-10)	Roth	3051.2
Tween® 20	$C_{58}H_{114}O_{26}$	Roth	9127.1

name	chemical formula	supplier	cat. nr.
urea	CH_4N_2O	Merck	1.08487
xylene cyanole	$C_{25}H_{27}N_2NaO_6S_2$	Roth	A513.1

Footnotes: APS – ammonium persulfate, bovine serum albumin (BSA), N,N-dimethylformamide (DMF), dithiothreitol (DTT), ethylenediaminetetraacetic acid (EDTA), hydrochloric acid (HCl), 4-(2-hydroxyethyl)-1-piperazine ethane sulfonic acid (HEPES), normal goat serum (NGS),phosphate buffered saline (PBS), paraformaldehyde (PFA), sodium dodecyl sulfate (SDS), 2-amino-2-(hydroxymethyl)propane-1,3-diol (Tris).

Suppl. table S2: Buffers, solutions and media.

solution	composition	storage
$CaCl_2$, 0.5 M	solve in ddH_2O	RT
HCl, 1 M	dilute in ddH_2O	RT
KCl, 1 M	solve in ddH_2O	RT
KH_2PO_4, 1 M	solve in ddH_2O	RT
$MgCl_2$, 1 M	solve in ddH_2O	RT
$MgSO_4$, 1M	solve in ddH_2O	RT
NaCl, 4 M	solve in ddH_2O	RT
NaN_3, 20 % (w/v)	solve in ddH_2O	4 °C
NaOH, 1 M	solve in ddH_2O	RT
PBS, 10 x	weight in 45 g/L PBS and dilute in ddH_2O	RT
PBS, 1 x	dilute 1/10 of PBS (10 x) in ddH_2O	RT
PMSF, 100 mM	solve in ddH_2O	- 20 °C
Tris/Cl, 1 M, pH 8.0	weight in Trizma® base, fill up with ddH_2O and adjust pH	RT
Triton X-100, 10 % (v/v)	dilute in ddH_2O	RT, ITD
Tween 20, 10 % (v/v)	dilute in ddH_2O	RT, ITD

Footnote: RT – room temperature, ITD – in the dark

Suppl. table S3: Brand affiliations.

brand	company
A. Hartenstein	A. Hartenstein GmbH, Würzburg, Germany
Abcam	Abcam plc, Cambridge, MA, USA
ADInstruments	ADInstruments Ltd, Dunedin, New Zealand
Advansta	Advansta Inc., San Jose, CA, USA
Antikoerper-online	antibodies-online GmbH, Aachen, Germany
AnalytikJena	Analytik Jena AG, Jena, Germany
Axxora	Enzo Biochem Inc., Farmingdale, NY, USA
B. Braun	B. Braun Melsungen AG, Melsungen, Germany
Bayer	Bayer AG, Wuppertal, Germany
BD Pharmingen	Becton, Dickinson and Company, San Jose, CA, USA
Biochrom	Biochrom GmbH, Berlin, Germany
Bio-Rad	Bio-Rad Laboratories Inc., Hercules, CA, USA
Biozym	Biozym Scientific GmbH, Hessisch Oldendorf, Germany
Canon	Canon Inc., Tokyo, Japan
Cell Signaling	Cell Signaling Technology Inc., Danvers, MA, USA
Charles River	Charles River Laboratories International Inc., Wilmington, MA, USA
CHEMSOLUTE	Th. Geyer GmbH & Co. KG, Renningen, Germany
CHROMA	Chroma Technology Corp., Bellows Falls, VT, USA
CoolLED	CoolLED Ltd., Andover, UK
Covance	BioLegend Inc., San Diego, CA, USA

brand	company
Dako	Agilent Technologies Inc., Santa Clara, CA, USA
Eppendorf	Eppendorf AG, Hamburg, Germany
eurofins	Eurofins Scientific SE, Luxembourg, Luxembourg
Fisher	Thermo Fisher Scientific Inc., Waltham, MA, USA
Heraeus	Heraeus Holding GmbH, Hanau, Germany
GE Healthcare	General Electric Corp., Chicago, IL, USA
GENAXXON	GENAXXON bioscience GmbH, Ulm, Germany
Genetics	NIPPON Genetics EUROPE GmbH, Düren, Germany
GIBCO	Thermo Fisher Scientific Inc., Waltham, MA, USA
Honeywell	Honeywell International Inc., Charlotte, NC, USA
Instech	Instech Laboratories Inc, Plymouth Meeting, PA, USA
invitrogen	Thermo Fisher Scientific Inc., Waltham, MA, USA
Jackson	Jackson ImmunoResearch Europe Ltd, Ely, UK
KNF Neuberger	KNF Neuberger GmbH, Freiburg im Breisgau, Germany
Kodak Biomax	Carestream Health, Inc., Rochester, NY, USA
Mast	Hans Mast GmbH, Tübingen, Germany
Merck	Merck KGaA, Darmstadt, Germany
Microsoft	Microsoft Corp., Redmond, WA, USA
Millipore	Merck KGaA, Burlington, MA, USA
MMM	MMM Münchener Medizin Mechanik GmbH, Planegg, Germany
NEB	New England Biolabs Inc., Ipswich, MA, USA
neoFroxx	neoFroxx GmbH, Einhausen, Germany
OriginLab	OriginLab Corp., Northampton, MA, USA
PEQLAB	Avantor Inc., Radnor, PA, USA
Phoenix	Phoenix Pharmaceuticals Inc., Burlingame, CA, USA
Photometrics	Teledyne Photometrics Inc., Tucson, AZ, USA
QImaging	QImaging Corp., Surrey, BC, Canada
Roche	F. Hoffmann-La Roche AG, Basel, Switzerland
Roth	Carl Roth GmbH + Co. KG, Karlsruhe, Germany
Sakura	Sakura Finetek Japan Co. Ltd, Koto-Ku, Tokyo, Japan
Santa Cruz	Santa Cruz Biotechnology Inc., Dallas, TX, USA
SCHOTT	SCHOTT AG, Mainz, Germany
Science Services	Science Services GmbH, Munich, Germany
Sigma-Aldrich	Merck KGaA, Burlington, MA, USA
ssniff	ssniff Spezialdiäten GmbH, Soest, Germany
Sterican	B. Braun Melsungen AG, Melsungen, Germany
SYLGARD™	The Dow Chemical Company, Midland, MI, USA
Thermo	Thermo Fisher Scientific Inc., Waltham, MA, USA
TILL Photonics	TILL Photonics GmbH, Gräfeling, Germany
Tocris	Bio-Techne Corp., Minneapolis, MN, USA
USBio	United States Biological Inc., Salem, MA, USA
Vector Labs	Vector Laboratories Inc., Burlingame, CA, USA
Visitron	Visitron Systems GmbH, Puchheim, Germany
Warner Instruments	Harvard Bioscience Inc., Hamden, CT, USA
Westfalen	Westfalen AG, Westfalen, Germany
YOKOGAWA	Yokogawa Electric Corp., Musashino, Tokyo, Japan
ZEISS	Carl Zeiss AG, Oberkochen, Germany

Suppl. table S4: PCR protocols and programs.

mouse line (PCR name)	primer name	components (pipetting scheme for 25 µL)		program	cycles
CNP-lacZ	P1: Fwd	14.55 µL	H_2O	03:00 min 95 °C	
	P2: Rev WT	2.5 µL	10 x RT buffer	00:35 min 94.5 °C	
	P3: Rev KO	1.5 µL	25 mM $MgCl_2$	00:25 min 60 °C	
		0.5 µL	dNTPs	00:25 min 68 °C	=> 35
		0.25 µL	Primer 1 & 2 & 3	10:00 min 68 °C	
		0.2 µL	*Taq*	HOLD 4 °C	
		5 µL	DNA		
GC-B-lacZ	P1: Fwd	15.1 µL	H_2O	03:00 min 94 °C	
	P2: Rev WT	2.5 µL	10 x RT buffer	HOLD 80 °C	
	P3: Rev KO	0.75 µL	50 mM $MgCl_2$	00:30 min 94 °C	
		0.5 µL	dNTPs	00:30 min 57 °C	
		0.3 µL	Primer 1 & 2 & 3	00:30 min 72 °C	=> 35
		0.25 µL	*Taq*	10:00 min 72 °C	
		5 µL	DNA	HOLD 4 °C	
GC-B-HA	P1: Fwd	14.8 µL	H_2O	03:00 min 95 °C	
	P2: Rev	2.5 µL	10 x RT buffer	00:30 min 94.5 °C	
		1.5 µL	25 mM $MgCl_2$	00:30 min 62 °C	
		0.5 µL	dNTPs	00:30 min 72 °C	=> 35
		0.25 µL	Primer 1 & 2	10:00 min 72 °C	
		0.2 µL	*Taq*	HOLD 4 °C	
		5 µL	DNA		
GC-B-flox LP1	P1: Fwd	14.8 µL	H_2O	03:00 min 95 °C	
	P2: Rev	2.5 µL	10 x RT buffer	00:30 min 94.5 °C	
		1.5 µL	25 mM $MgCl_2$	00:30 min 59 °C	
		0.5 µL	dNTPs	00:30 min 72 °C	=> 35
		0.25 µL	Primer 1 & 2	10:00 min 72 °C	
		0.2 µL	*Taq*	HOLD 4 °C	
		5 µL	DNA		
R26-Ai14	P1: Fwd WT	14.8 µL	H_2O	03:00 min 94 °C	
	P2: Rev WT	2.5 µL	10 x RT buffer	00:20 min 94 °C	
	P3: Fwd TG	1.5 µL	25 mM $MgCl_2$	00:15 min 65 °C	
	P4: Rev TG	0.5 µL	dNTPs	00:25 min 68 °C	=> 10
		0.25 µL	Primer 1 & 2	00:15 min 94 °C	
=> Prepare separate reaction mixes for WT and TG PCR	=> Run WT & TG reaction mix with same PCR program	0.2 µL	or Primer 3 & 4	00:15 min 50 °C	
		5 µL	*Taq*	00:25 min 72 °C	=> 28
			DNA	05:00 min 72 °C	
				HOLD 4 °C	
R26-cGi500(L2) & **R26-mcGi500(L2)**	P1: Fwd (BB01)	14.4 µL	H_2O	03:00 min 95 °C	
	P2: Rev WT (BB02)	2.5 µL	10 x RT buffer	00:10 min 95 °C	
		1.5 µL	25 mM $MgCl_2$	00:30 min 61 °C	
	P3: Rev TG (BB03)	0.5 µL	dNTPs	00:30 min 72 °C	=> 35
		0.3 µL	Primer 1 & 2 & 3	10:00 min 72 °C	
		0.2 µL	*Taq*	HOLD 4 °C	
		5 µL	DNA		

mouse line (PCR name)	primer name	components (pipetting scheme for 25 µL)		program	cycles
GC-B-CreERT2	P1: Fwd	14.55 µL	H_2O	03:00 min 94 °C	
	P2: Rev WT	2.5 µL	10 x RT buffer	00:30 min 94 °C	
	P3: Rev KO	1.5 µL	25 mM $MgCl_2$	00:30 min 57 °C	
		0.5 µL	dNTPs	00:30 min 72 °C	=> 35
		0.25 µL	Primer 1 & 2 & 3	10:00 min 72 °C	
		0.2 µL	*Taq*	HOLD 4 °C	
		5 µL	DNA		
Wnt1-Cre	P1: Fwd	17.05 µL	H_2O	04:00 min 94 °C	
	P2: Rev	2.5 µL	10 x RT buffer	00:30 min 94 °C	
		1.5 µL	25 mM $MgCl_2$	00:30 min 55 °C	
		0.5 µL	dNTPs	01:00 min 72 °C	=> 40
		0.1 µL	Primer 1 & 2	07:00 min 72 °C	
		0.25 µL	*Taq*	HOLD 4 °C	
		3 µL	DNA		
αSMA-CreERT2	P1: Fwd TG	16.25 µL	H_2O	04:00 min 94 °C	
	P2: Rev TG	2.5 µL	10 x RT buffer	00:30 min 94 °C	
	P3: Fwd ctr	1.5 µL	25 mM $MgCl_2$	01:00 min 51.7 °C	
	P4: Rev ctr	0.5 µL	dNTPs	01:00 min 72 °C	=> 40
		0.25 µL	Primer 1 & 2 & 3 &	02:00 min 72 °C	
		0.25 µL	4	HOLD 4 °C	
		3 µL	*Taq*		
			DNA		
Defensinα6-iCre	P1: Fwd TG	15.2 µL	H_2O	03:00 min 94 °C	
	P2: Rev TG	2.5 µL	10 x RT buffer	00:30 min 94 °C	
	P3: Fwd ctr	1.5 µL	25 mM $MgCl_2$	01:00 min 60 °C	
	P4: Rev ctr	0.5 µL	dNTPs	01:00 min 72 °C	=> 35
		1 µL	Primer 1 & 2	02:00 min 72 °C	
		0.5 µL	Primer 3 & 4	HOLD 4 °C	
		0.1 µL	DMSO		
		0.2 µL	*Taq*		
		2 µL	DNA		

Suppl. table S5: Primers used in PCR protocols.

mouse line (PCR name)	primer name	primer sequences (5' to 3')	primer stock conc.	PCR products size
CNP-lacZ	Fwd	AAG ATG ACA TCA GCG GCA G	50 µM	WT 393 bp
	Rev WT	GCT TTG AGG GAG CAA GTC C	50 µM	TG 347 bp
	Rev KO	CCT CTT CGC TAT TAC GCC AG	50 µM	
GC-B-lacZ	Fwd	TGC CAC CCT ATC CTT AGT CC	50 µM	WT 348 bp
	Rev WT	GTG TTC TGG CAG CAC CAC	50 µM	TG 398 bp
	Rev KO	TCG CTA TTA CGC CAG CTG	50 µM	
GC-B-HA	P1: Fwd	CCT GGC CCT CTT CCC CAG GCT C	50 µM	WT 270 bp
	P2: Rev	GTG CCT CCA CAG CCA GTG CCA C	50 µM	TG 307 bp
GC-B-flox LP1	P1: Fwd	GCC ACT TTT GCA CCC GGA TG	50 µM	WT 231 bp
	P2: Rev	GTG ACG CTG TCG AAG GCC TC	50 µM	TG 334 bp
R26-Ai14	Fwd WT	AAG GGA GCT GCA GTG GAG TA	50 µM	
	Rev WT	CCG AAA ATC TGT GGG AAG TC	50 µM	WT 297 bp
	Fwd TG	GGC ATT AAA GCA GCG TAT CC	50 µM	TG 196 bp
	Rev TG	CTG TTC CTG TAC GGC ATG G	50 µM	
R26-cGi500(L2) & **R26-mcGi500(L2)**	P1: Fwd (BB01)	CTC TGC TGC CTC CTG GCT TCT	100 µM	WT 330 bp TG 250 bp
	P2: Rev WT (BB02)	CGA GGC GGA TCA CAA GCA ATA	100 µM	
	P3: Rev TG (BB03)	TCA ATG GGC GGG GGT CGT T	100 µM	
GC-B-CreERT2	P1: Fwd	CTC AGA TTC CTC CCT TCT CG	50 µM	WT 456 bp
	P2: Rev WT	GGC ATA GCT CAG GTT GTG TT	50 µM	TG 356 bp
	P3: Rev KO	TTG GAC ATG GTG GAA TTC AT	50 µM	
Wnt1-Cre	P1: Fwd	TAA GAG GCC TAT AAG AGG CGG	100 µM	WT -
	P2: Rev	AGC CCG GAC CGA CGA TGA A	100 µM	TG 550 bp
αSMA-CreERT2	P1: Fwd TG	GCG GTC TGG CAG TAA AAA CTA TC	10 µM	
	P2: Rev TG	GTG AAA CAG CAT TGC TGT CAC TT	10 µM	ctr 324 bp
	P3: Fwd ctr	CTA GGC CAC AGA ATT GAA AGA TCT	10 µM	TG 100 bp
	P4: Rev ctr	GTA GGT GGA AAT TCT AGC ATC ATC C	10 µM	
Defensinα6-iCre	P1: Fwd TG	AGG ATA ACA GCA TCT CCC AGT TC	10 µM	
	P2: Rev TG	ACT TCA TCA GAG GTG GCA TCC	10 µM	ctr 324 bp
	P3: Fwd ctr	CTA GGC CAC AGA ATT GAA AGA TCT	10 µM	TG 222 bp
	P4: Rev ctr	GTA GGT GGA AAT TCT AGC ATC ATC C	10 µM	

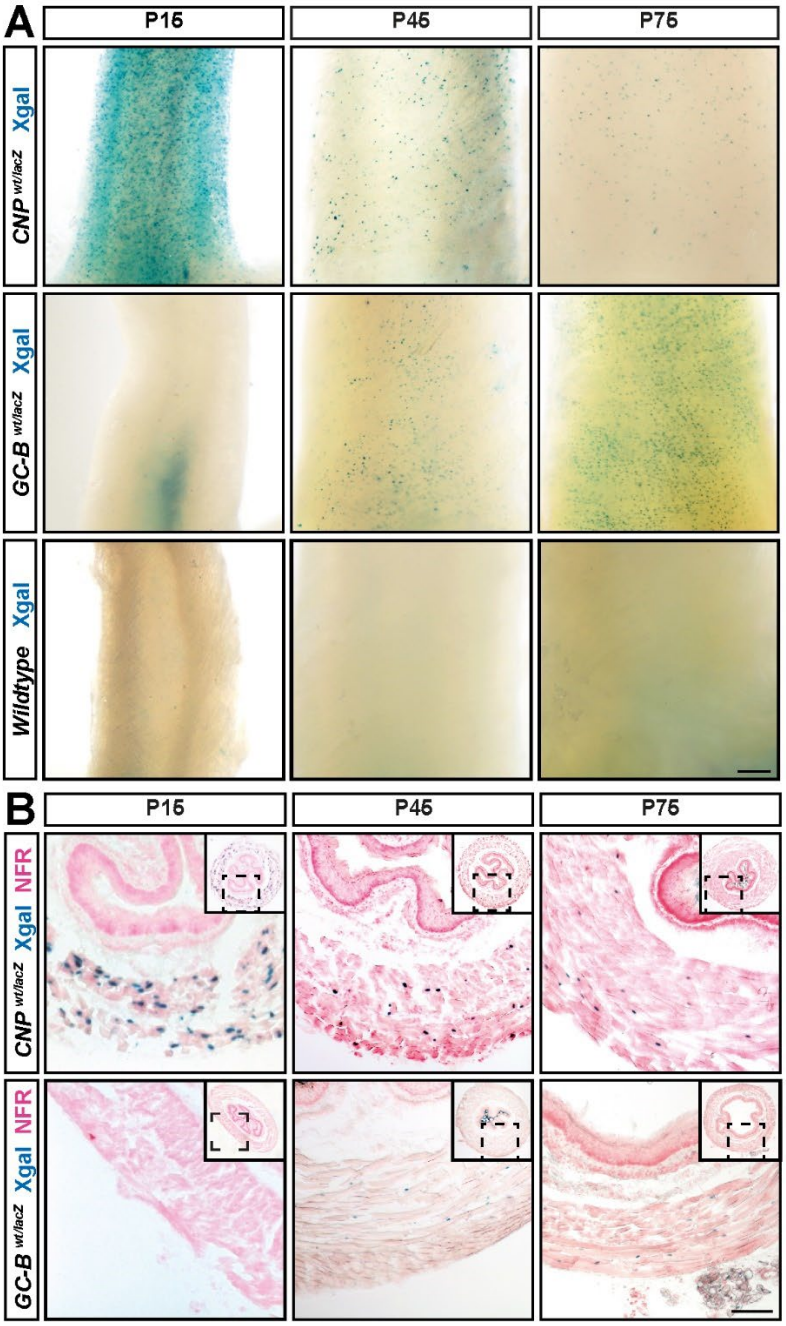

Suppl. figure S1: CNP and GC-B gene transcription in esophagus.

A) Xgal staining of the whole esophagus from CNP-lacZ, GC-B-lacZ and WT mice at P15, P45 and P75. (Scalebar, 200 µm). B) Xgal staining of lower esophagus cryosections from CNP-lacZ and GC-B-lacZ mice at P15, P45 and P75 counterstained with NFR. (Scalebar, 100 µm).

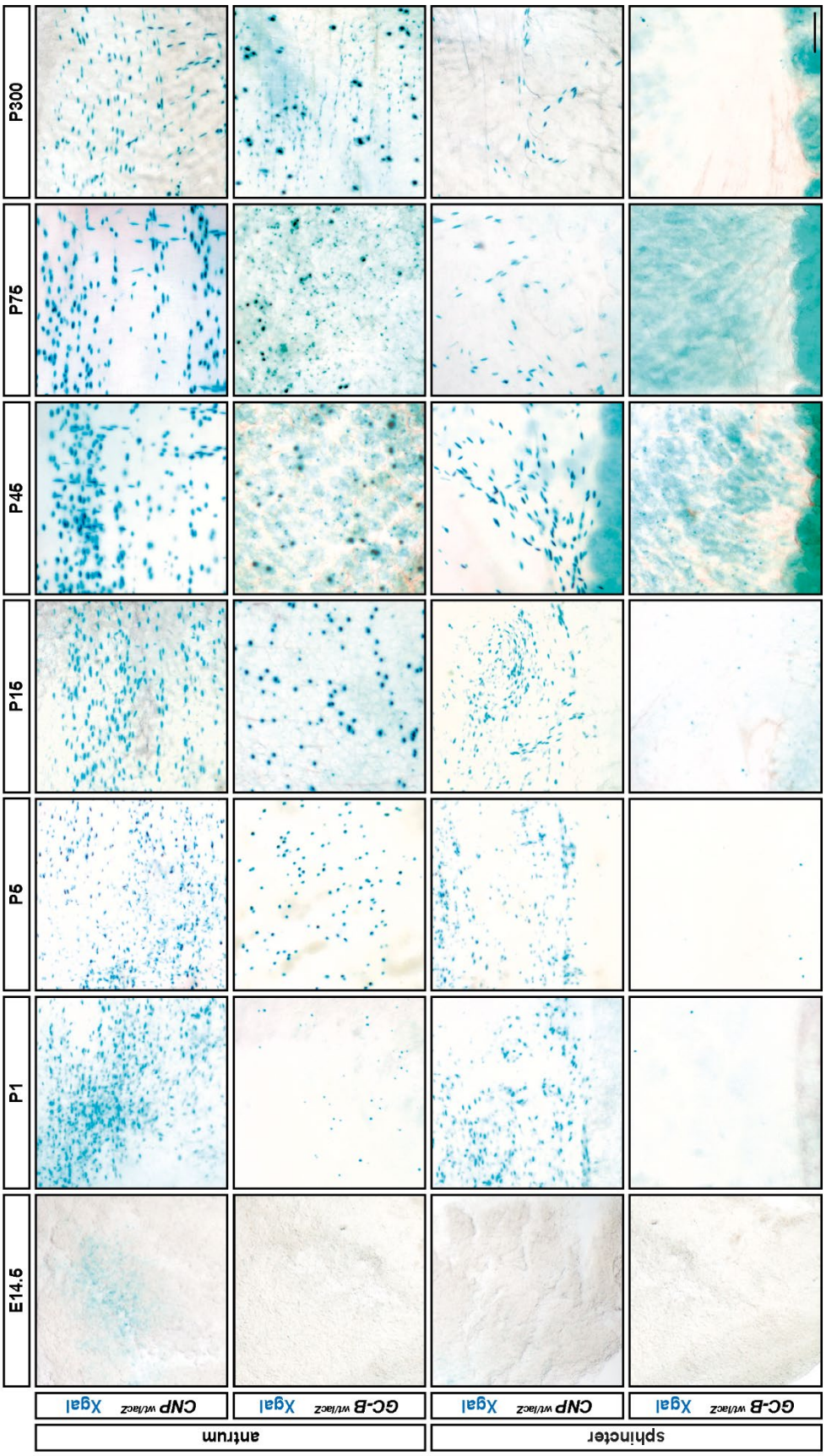

Suppl. figure S2: Time course of CNP and GC-B gene transcription in pyloric antrum and sphincter.

Whole mount Xgal staining of the pyloric antrum and sphincter from CNP-lacZ and GC-B-lacZ mice at different ages. The Xgal stained tissue was cleared with ScaleA2 for one week prior to documentation. Each image has the same scaling. (Scalebar, 200 µm).

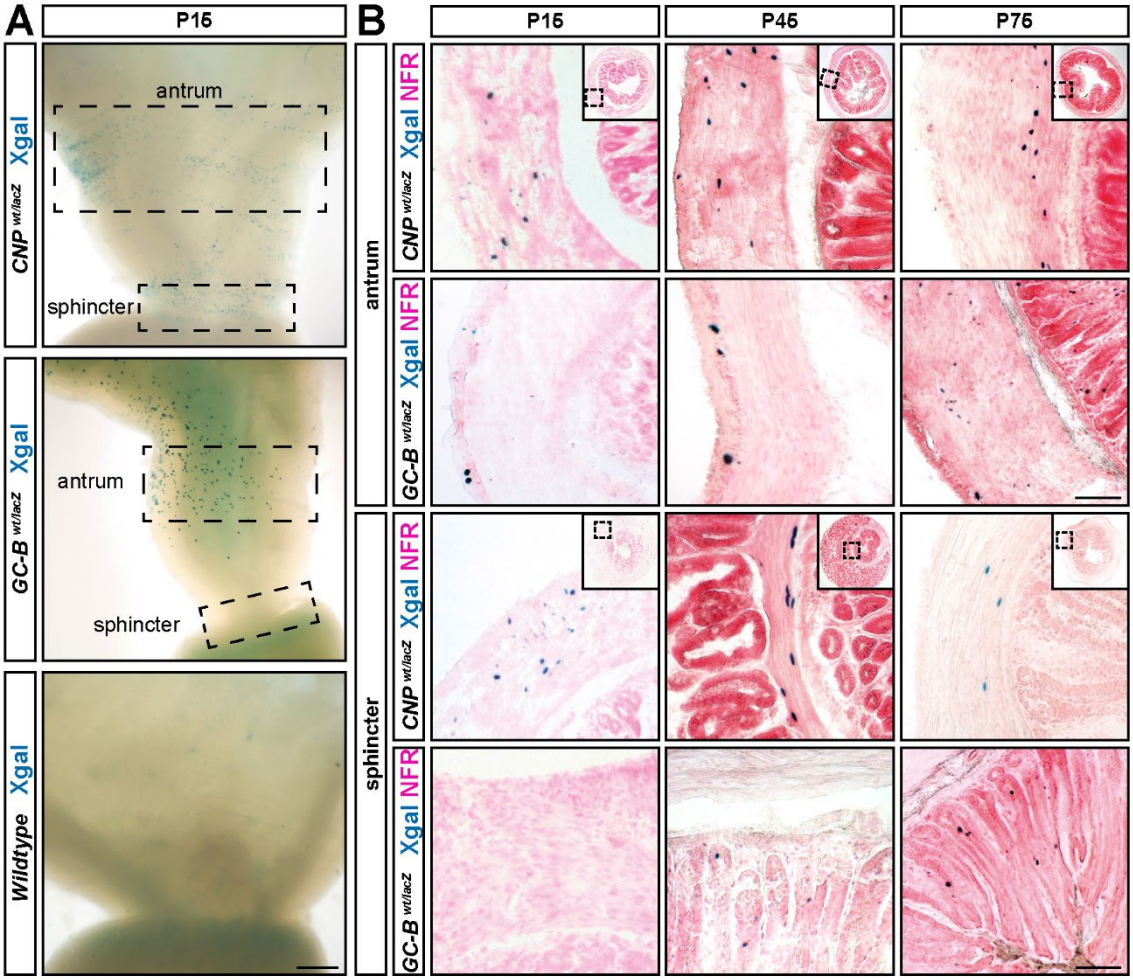

Suppl. figure S3: CNP and GC-B gene transcription in pyloric antrum and sphincter.

A) Xgal staining of the whole pylorus from CNP-lacZ, GC-B-lacZ and WT mice at P15. The dashed rectangle represents the regions where the antrum and the sphincter were investigated, respectively. (Scalebar, 400 µm). B) Xgal staining of pylorus (antrum and sphincter) cryosections from CNP-lacZ and GC-B-lacZ mice at P15, P45 and P75 counterstained with NFR. (Scalebar, 100 µm).

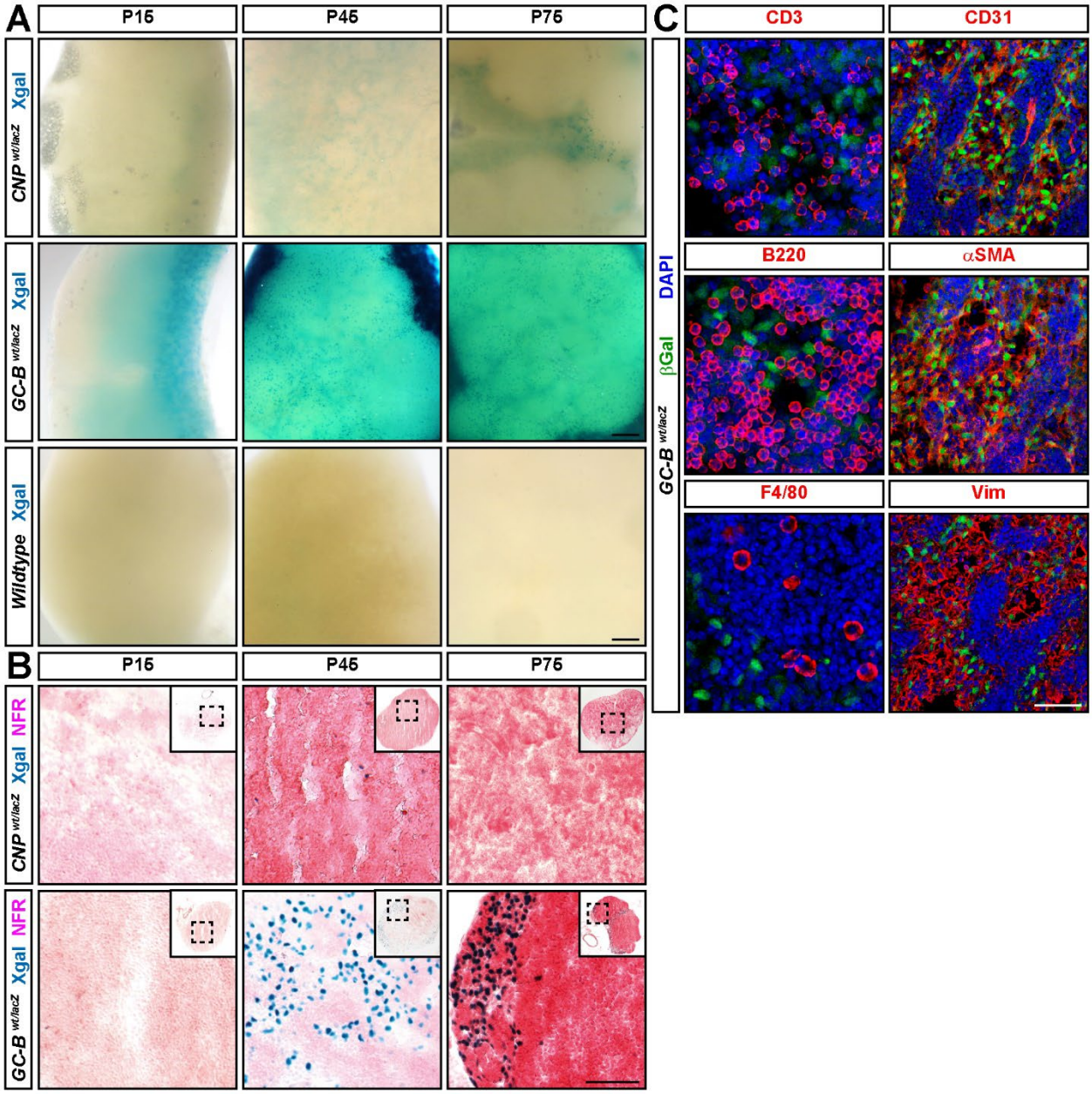

Suppl. figure S4: CNP and GC-B gene transcription in MLN.

A) Xgal staining of MLN from 15, 45 and 75 days old CNP-lacZ, GC-B-lacZ and WT mice. (Scalebar, 200 µm). B) Xgal staining of MLN cryosections from CNP-lacZ and GC-B-lacZ reporter mice showing *GC-B* transcription in the subcapsular sinus of the lymph nodes at P45, but no *CNP* transcription. (Scalebar, 100 µm). C) IF staining of MLN cryosections from P45 GC-B-lacZ mice with antibodies against the βGal enzyme (green) and different marker proteins (CD3 for T-cells, B220 for B-cells, F4/80 for macrophages, CD31/αSMA/vim for lymphatic endothelial cells). (Scalebar, 50 µm).

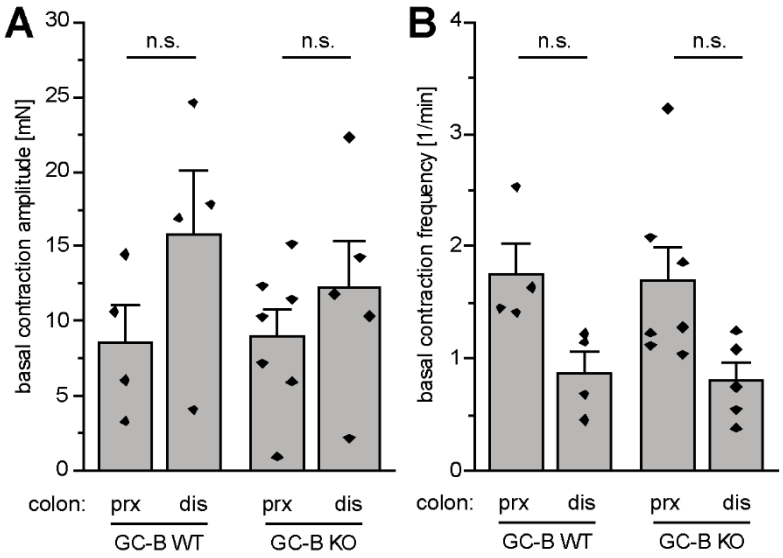

Suppl. figure S5: Basal colonic contraction amplitude and frequency comparing GC-B WT with KO.

Colonic rings of GC-B WT (genotype: *GC-B $^{wt/wt}$*) and global GC-B KO (GC-B KO, genotype: *GC-B $^{lacZ/lacZ}$*) mice were measured in IFM at age P15 in the presence of 1 µM TTX. A) Mean basal contraction amplitude before CNP application. B) Mean basal contraction frequency before CNP application.

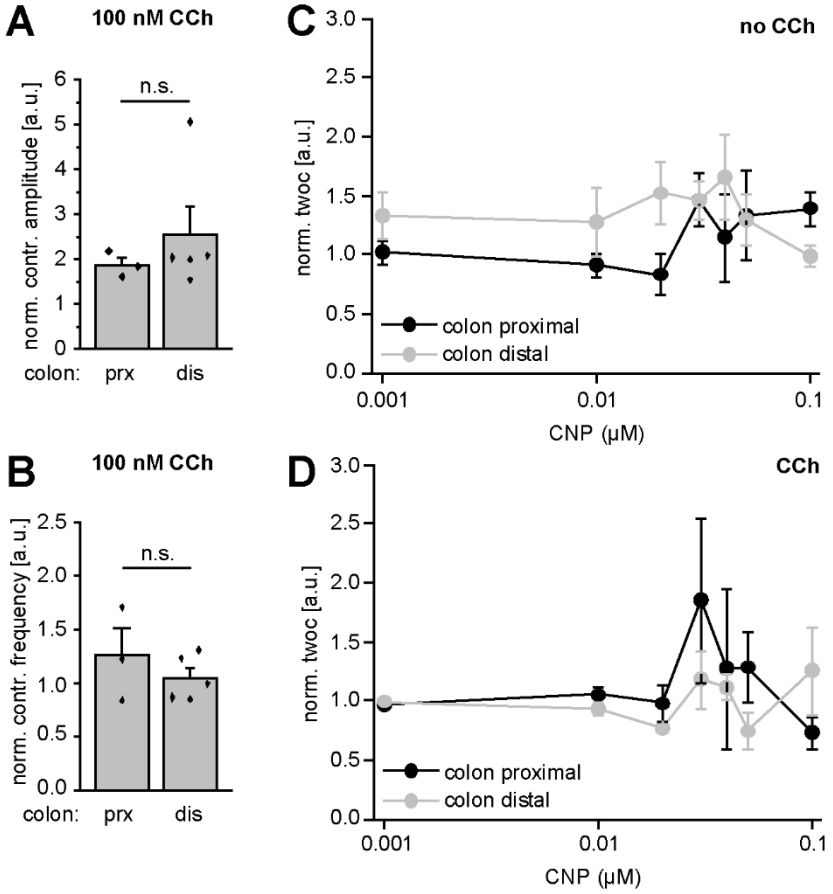

Suppl. figure S6: CNP-induced circular smooth muscle relaxation in proximal and distal colon.

Continued from figure 19. Change of baseline contraction amplitude (A) and frequency (B) due to 100 nM CCh application in proximal and distal colon. The time without contraction was normalized on the mean frequency of the time period before the respective CNP application. Frequency normalized time without contraction (norm. twoc) without CCh (C) and with CCh (D).

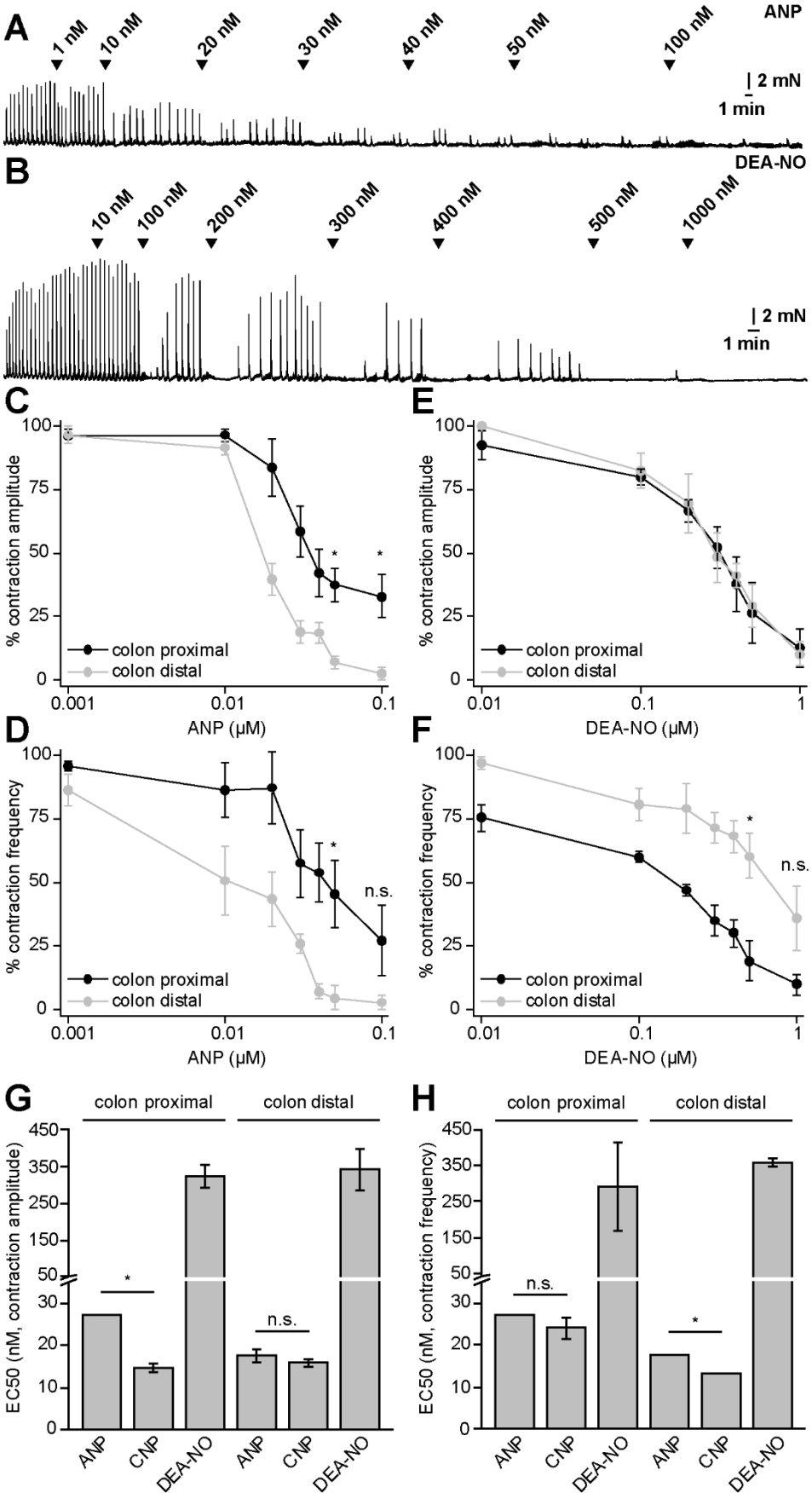

Suppl. figure S7: ANP- and DEA-NO-induced colonic circular smooth muscle relaxation.

Suppl. figure S7: ANP- and DEA-NO-induced colonic circular smooth muscle relaxation.
IFM was performed on colonic rings from the proximal and distal colon of WT mice in the presence of TTX. ANP was applied in increasing concentration from 1 nM to 100 nM and DEA-NO was applied in increasing concentration of 10 nM to 1000 nM.. A) shows a representative IFM trace for the ANP concentration series and B) for the DEA-NO concentration series. The measurements were evaluated and the change in contraction amplitude (C-D) and contraction frequency (E-F) were quantified for the proximal and distal colon. Mean EC50 values of the ANP, DEA-NO but also CNP concentrations series were blotted in bar graphs for the contraction amplitude (G) and contraction frequency (H). The error bars represent the SEM (n = 3, measurements are from 3 different mice).

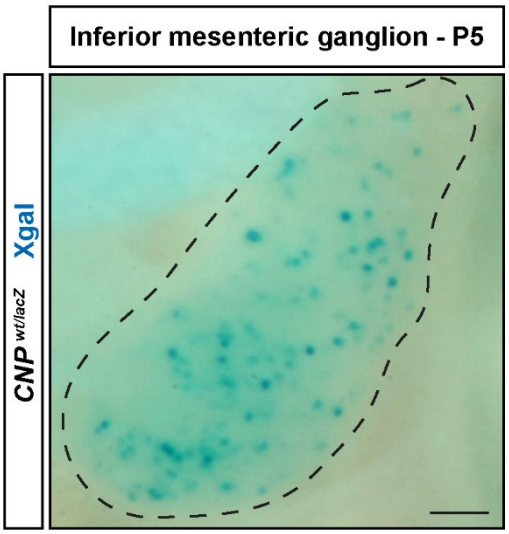

Suppl. figure S8: *CNP* transcription in the inferior mesenteric ganglion at P5.

The inferior mesenteric ganglion (surrounded by dashed line) was isolated from a heterzygous CNP-lacZ mouse at P5 and a Xgal staining was performed. The blue dots display *CNP* transcribing cells. (Scalebar, 200 µm).

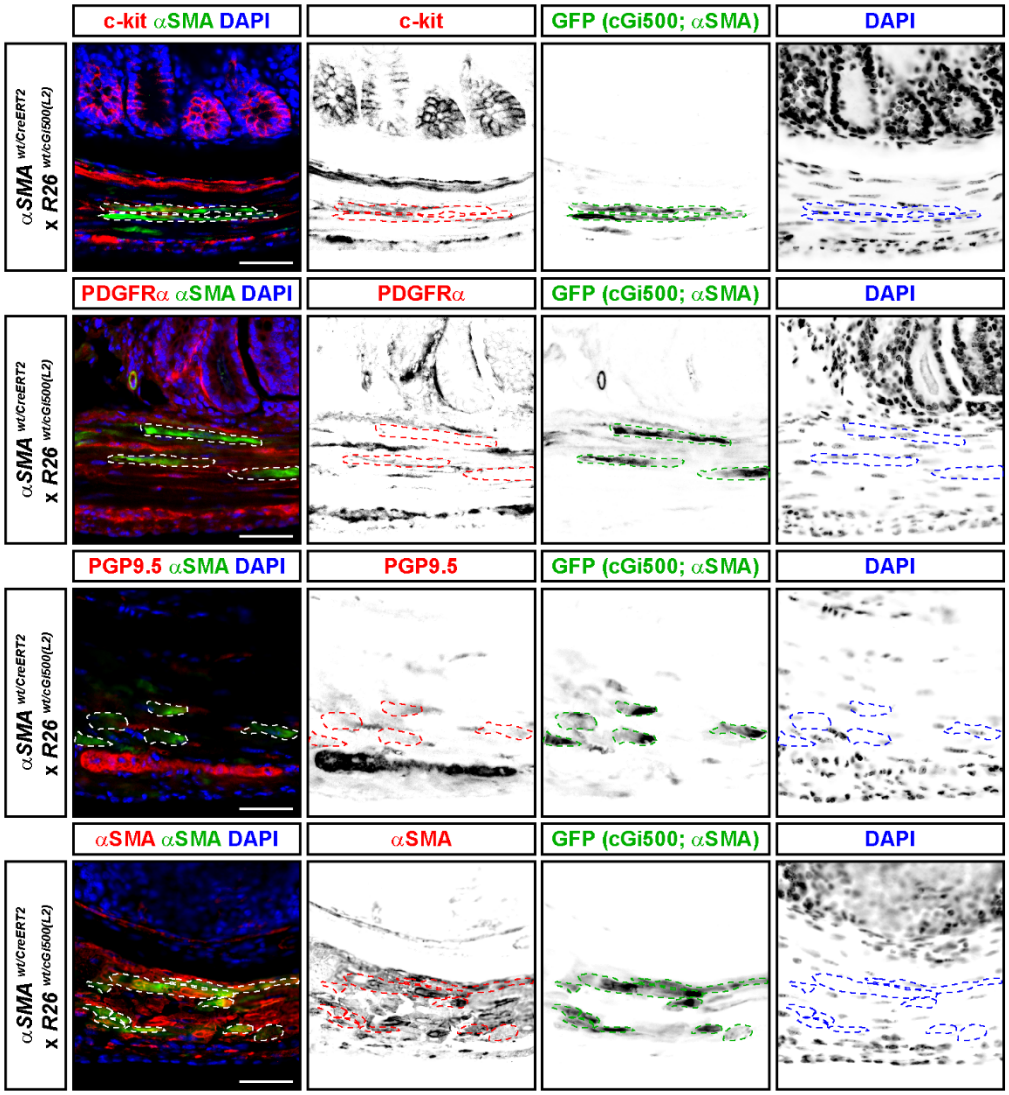

Suppl. figure S9: Identification of cells labeled by the αSMA-CreERT2 mouse line.

IF staining of cryosections were performed on distal colon from 10 weeks old SMC-specific cGMP-FRET sensor mouse (genotype: *Acta2* $^{wt/CreERT2}$ *x R26-cGi500(L2)* $^{w/tg}$). The CreER^{T2} activity was induced for 5 consecutive days in week 5 and another 5 days in week 9 using Tamoxifen. The YFP fluorophore of the cGi500 sensor was probed with a ch-α-GFP antibody, ICCs were probed with rt-α-c-kit, FLCs were probed with rb-α-PDGFRα, neurons were probed with rb-α-PGP9.5 and SMCs were probed with mo-α-αSMA antibodies.

Index of figures

Index of tables

Acknowledgement

First, I want to thank Prof. Dr. Robert Feil for the chance to make my PhD thesis in his laboratory, his great support and mentoring during the PhD time and before that in my masters. It has been 7 years since I joined the lab and I have learned a lot.

Second, I am very grateful for the great support and supervision from PD Dr. Hannes Schmidt who invested a lot of time, money and effort in supervising me and my work. I have learnt a lot about science, professionalism and culture from him. Thank you, Hannes.

I also want to thank Prof. Dr. Andreas Friebe who provided me with the multiwire myograph to perform the IFM of the colon. In addition, I want to thank Dr. Dieter Groneberg who introduced me to the myograph methodology. They have provided a very friendly working atmosphere which I greatly enjoyed. Furthermore, I learnt a lot about my own project from both.

I also would like to thank Dr. Susanne Feil who supported me and my work wherever possible.

I want to thank Barbara Birk for always supporting the people in the lab with whatever is necessary (e.g. a helping hand during an experiment, organizing of materials, or backing of food).

High gratitude also goes to the current and former coworkers of the Feil lab who always provided a friendly, comradely, but if necessary also professional working atmosphere. Namely I want to thank: Moritz Lehners, Daniel Stehle, Frank Regler, Dr. Angelos Vachaviolos, Stefani Peters, Dr. Jatzek Dobrowinski, Dr. Michael Paolillo, Krithika Rajeth, Alexandra Böttcher, Maria-Giovanna Barresi, Malte Roessing, Dr. Kristina Zaldivia, Eduarda Streit Morsch and Stefanie Mendes Bader.

Especially, I would like to thank Moritz Lehners for all the work he always invests in explaining methodologies (e.g. FRET or statistics, the use of Fiji or origin) and other stuff to people in the lab, including me.

I want to thank Carolin Warnecke and Sarah Merz for their hard work as my interns. I also want to thank Stefanie Mendes Bader for helping me to establish the neuron cell culture approach in the lab.

I want to thank Astrid Große and Jana Speidel for taking special care of my mice, but also for always lightening my mood. You both provided a very friendly, funny, and relaxing atmosphere which I always enjoyed.

And I want to thank all the other members of the Feil lab and the IFIB who provided comradeship and support in the last years.

I also want to thank my girlfriend Jana Speidel who always supported me and my work. She endured even the longest working hours of mine.

A very special thanks goes to my family who were always there for me if I needed them. My brother Stefan Ralf Krämer who I can always count on no matter what. My mother Susanne Krämer who would always comfort me, and my father Ralf Eugen Krämer who would always provide a reasonable solution for my problems.

I want to thank Jana Speidel, Rubina Rönnfeld, Nabila, Courtney, and Sabrina for comradeship and all the nice long walks and hikes which we did in the last half year. The adventures we experienced were amazing and I am really grateful for that.

At last, I want to thank my friends, Pascal Reis, Matthias Golla, Sören Kirchgässner, Gerd Berger, Dajena Toebes, Daniel Stehle and Moritz Lehners for providing comradeship and relaxing, fun evenings.

All the above-mentioned people have inspired me, my professional and personal life. I am eternally grateful for knowing all of them.